

NOTE TO USERS

Page(s) not included in the original manuscript and are unavailable from the author or university. The manuscript was scanned as received.

101

This reproduction is the best copy available.

UMI[®]

**Circum-Troodos Limestone Succession
of South and West Cyprus:
A magnetic fabric and magnetic mineralogical study**

**by
Thomas Hamilton**

Submitted as partial fulfillment of
the requirements for the degree of

Master of Science

Supervisor: Dr G. J. Borradaile

Department of Geology
Lakehead University
Thunder Bay, ON
April, 2005



Library and
Archives Canada

Bibliothèque et
Archives Canada

Published Heritage
Branch

Direction du
Patrimoine de l'édition

395 Wellington Street
Ottawa ON K1A 0N4
Canada

395, rue Wellington
Ottawa ON K1A 0N4
Canada

Your file *Votre référence*
ISBN: 978-0-494-15619-3
Our file *Notre référence*
ISBN: 978-0-494-15619-3

NOTICE:

The author has granted a non-exclusive license allowing Library and Archives Canada to reproduce, publish, archive, preserve, conserve, communicate to the public by telecommunication or on the Internet, loan, distribute and sell theses worldwide, for commercial or non-commercial purposes, in microform, paper, electronic and/or any other formats.

The author retains copyright ownership and moral rights in this thesis. Neither the thesis nor substantial extracts from it may be printed or otherwise reproduced without the author's permission.

AVIS:

L'auteur a accordé une licence non exclusive permettant à la Bibliothèque et Archives Canada de reproduire, publier, archiver, sauvegarder, conserver, transmettre au public par télécommunication ou par l'Internet, prêter, distribuer et vendre des thèses partout dans le monde, à des fins commerciales ou autres, sur support microforme, papier, électronique et/ou autres formats.

L'auteur conserve la propriété du droit d'auteur et des droits moraux qui protègent cette thèse. Ni la thèse ni des extraits substantiels de celle-ci ne doivent être imprimés ou autrement reproduits sans son autorisation.

In compliance with the Canadian Privacy Act some supporting forms may have been removed from this thesis.

Conformément à la loi canadienne sur la protection de la vie privée, quelques formulaires secondaires ont été enlevés de cette thèse.

While these forms may be included in the document page count, their removal does not represent any loss of content from the thesis.

Bien que ces formulaires aient inclus dans la pagination, il n'y aura aucun contenu manquant.


Canada

Abstract

Calcite petrofabrics align easily with weak strains, possibly being the most sensitive classical petrofabric indicator. Thus, calcareous sediments may reveal stress trajectories in neotectonic environments. Calcite aligns by crystal-plastic deformation and pressure solution to produce corresponding alignments in accessory clay minerals and magnetite (possibly fossil-bacterial). Their alignments are rapidly and precisely detected by anisotropy of low field magnetic susceptibility (AMS). These net magnetic fabrics blend diamagnetic contributions from matrix calcite (diamagnetic bulk susceptibility $\kappa \sim -14 \mu\text{SI}$), accessory clay minerals ($\kappa = 100$ to $500 \mu\text{SI}$) and trace magnetite ($\kappa > 2 \text{ SI}$). Considering their relative abundances and different anisotropies, their orientation distributions of AMS axes are sensibly interpreted as paleostress trajectories in Neogene and Quaternary strata at the regional and sub-area level (each $\sim 400\text{km}^2$ and $\sim 30\text{km}^2$ respectively). The AMS axes may be correlated with the orientation of faults, plate-motion vectors and seismic solutions. A large sample (1090 specimens from 419 sites) was treated by different statistical approaches (“standardization”) to emphasize or suppress the contribution of sub-fabrics with anomalous mean susceptibility. A subsample of 254 specimens from 219 sites, from different sub-areas was also investigated by anisotropy of anhysteretic remanence (AARM), which isolates the orientation distributions of magnetite. AMS and AARM magnetic fabrics are mostly of the L-S kind with the magnetic lineations compatible with gravitational stretching of the sedimentary cover away from the Troodos massif and orthogonal to the strike of principal faults and graben. The L-direction (k_{MAX}) shows a smooth variation in orientation, through the sub-areas, directed radially from the Troodos massif and the S-components of the magnetic

fabrics are inclined gently to the bedding, compatible with vergence toward the Cyprean Arc that lies offshore to the South and South-West of Cyprus.

From the original set of 1090 specimens, two smaller sets of samples were further studied using different magnetic techniques to examine differences in magnetic mineralogy and granulometry in different lithologies and through time.

The first set of 100 specimens was divided into pelagic and non-pelagic sub-sets and microhysteresis showed that these samples contained magnetite in the appropriate size ranges for simply interpretable AMS fabrics (“normal fabrics”) and also exhibited possible contributions from titanomagnetite (TM_{60}) in the non-pelagic samples.

A sub-set of 55 samples in stratigraphic sequence with approximately known age determinations (54-6 Ma) shows systematic variations in bulk susceptibility (κ), anhysteretic susceptibility (κ_{ARM}), saturation isothermal remanence (SIRM), and thermal demagnetization unblocking temperatures (T_{UB}). Some combinations of these magnetic parameters have demonstrated that TM_{60} is present in appreciable amounts in the youngest of the Cyprus limestones (due to uplift and early erosion of the Troodos massif), and in some of the oldest rocks (due to distal submarine volcanism). Furthermore, the lack of TM_{60} in the middle of the sequence and the magnetic granulometry shows that magnetotactic bacteria dominate the chalk units of Cyprus.

ACKNOWLEDGEMENTS

This research was financially supported by NSERC grants to Dr. Graham Borradaile and all laboratory work was performed in his rock magnetism laboratory, funded by NSERC and Sapphire Instruments. The fieldwork was greatly assisted logistically and encouraged by the Geological Survey Department of Cyprus, in particular through its Director Dr. G. Petrides and by Dr. I. Panayides and by Panicos Emilianou (CyCar Rentals, Larnaca) provided invaluable logistical support.

Special thanks to: Dr. Borradaile, Anne Hammond, Sam Spivak, France Lagroix, Dave Gauthier, Mike Jackson and Becky Rogala for technical and conceptual assistance in this project.

TABLE OF CONTENTS

ABSTRACT.....	ii
ACKNOWLEDGMENTS.....	iv
TABLE OF CONTENTS.....	v
LIST OF FIGURES.....	vi
LIST OF TABLES.....	vii
LIST OF APPENDICES.....	viii
1. Introduction.....	1
1.1 - The purpose of this study.....	2
1.2 - Background.....	4
1.2.1 - Background Limestone Magnetic Mineralogy.....	5
1.2.2 - Theoretical Background Magnetics.....	6
2. Magnetic Fabric Studies (AMS & AARM).....	8
2.1 - Anisotropy of Magnetic Susceptibility (AMS).....	8
2.2 - Tectonic Background.....	9
2.3 - Neotectonic interpretation of AMS.....	12
2.4 - Interpreting AMS.....	19
2.5 - Processing AMS data from low-κ specimens.....	21
2.6 - AMS measurements.....	23
2.7 - AARM: Anisotropy of Anhysteretic Remanent Magnetization.....	23
2.8 - Sampling Strategy.....	24
2.9 - Localized sampling: Polis Rift Region (subareas I, II, III).....	27
2.10 - Localized sampling: Southern slopes of Troodos (subareas IV, V, VI).....	28
2.11 - Regional scale AMS.....	29
2.12 - Regional scale AARM.....	30
3. Magnetic Mineralogy.....	31
3.1 - Introduction.....	31
3.2 - Purpose.....	33
3.3 - Hysteresis.....	35
3.4 - Sedimentary sequence and Sampling Strategy.....	42
3.5 - Methods for Magnetic Mineralogy.....	45
3.6 - Methods for Magnetic Granulometry.....	49
3.7 - Stratigraphic Interpretation of Magnetic Mineralogy and Granulometry.....	52
4. Conclusions.....	60
5. Discussion: Paleomagnetism and Tectonic Implications for Cyprus.....	62
6. References.....	65

LIST OF FIGURES

1-1	Cyprus from Space.....	3
1-2	Troodos in snow.....	4
1-3	Types of Magnetization.....	7
2-1	Geology of Cyprus.	10
2-2	Frequency-distribution of bulk magnetic susceptibility.....	15
2-3	Polar plots.....	17
2-4	Idealized symmetry of confidence cones.....	22
2-5	Sub-areas of Cyprus (I-VI) and their magnetic fabrics.....	25
2-6	Regional domains of Cyprus (I-V) and their magnetic fabrics.....	26
3-1	An example of a hysteresis loop.....	36
3-2	Day Plots.....	37
3-3	Squareness (M_{RS}/M_S) versus coercive force (B_C).....	39
3-4	Geological map of Cyprus and stratigraphic sampling sites.....	43
3-5	Circum Troodos Sedimentary Succession	44
3-6	κ ARM and κ versus stratigraphic sequence.....	46
3-7	SIRM versus stratigraphic sequence	46
3-8	SIRM TD_{2000C} /SIRM versus stratigraphic sequence.....	48
3-9	King et al. (1982) Plot. κ ARM versus κ	50
3-10	κ ARM/ κ versus stratigraphic sequence.....	50
3-11	SIRM/ κ versus stratigraphic sequence.....	53
3-12	κ ARM/ SIRM versus stratigraphic sequence.....	53
3-13	Lefkara Lower Marl Unit.....	54
3-14	Amalgamation of Figures 3-7, 3-8, and 3-10 for ease of comparison.....	55
3-15	Lefkara Chalk and Chert Unit.....	56
3-16	Lefkara Chalk Unit.....	56
3-17	Pakhna Formation.....	58

LIST OF TABLES

Table 2-1	The major tectonic events of Cyprus.....	11
Table 3-1	Different Magnetic Techniques	31

LIST of APPENDICES

APPENDIX 1- Magnetic and Tectonic Fabric Glossary.....	73
APPENDIX 2- AMS Local Samples (location, age, formation).....	77
APPENDIX 3- AMS Local Samples (AMS Data).....	80
APPENDIX 4- Regional Samples (location, formation).....	88
APPENDIX 5- Regional Samples (AMS Data).....	91
APPENDIX 6- Hysteresis Samples Data.....	107
APPENDIX 7- Stratigraphic Samples (magnetic data)	109

Chapter 1 - Introduction

Originally, basalts were the first choice of rock types for paleomagnetic studies, but with the advent of equipment like the high sensitivity spinner-magnetometer and SQUID (super-conducting quantum interference device) magnetometer, the equally precise measurement of weakly magnetized rocks like limestones, has been possible. Although limestones have $< 0.02\%$ of the remanence intensity of basalts (a common target for paleomagnetists), limestones have many other attributes that make them appealing.

First, calcite petrofabrics are sensitive to weak strains, possibly being the most sensitive classical petrofabric indicator. Thus, calcareous sediments may reveal stress trajectories in neotectonic environments. Calcite aligns by crystal-plastic deformation and by pressure solution that produces corresponding alignments in accessory clay minerals and magnetite (possibly fossil-bacterial). Their alignments are rapidly and precisely detected by anisotropy of low field magnetic susceptibility (AMS) with net magnetic fabrics, which blend diamagnetic contributions from matrix calcite (diamagnetic bulk susceptibility $\kappa \sim -14 \mu\text{SI}$), accessory clay minerals ($\kappa = 100$ to $500 \mu\text{SI}$) and sometimes trace magnetite ($\kappa > 2 \text{ SI}$).

Second, limestones are of wide-spread stratigraphic importance accounting for approximately 10% of the sedimentary record exposed on land (Blatt et al., 1980) and limestone sequences may have excellent temporal continuity. Therefore, in places of thick limestone sequences one can take numerous samples and have a continuous set of data covering many millions of years.

Third, limestones are common in the biostratigraphically documented part of the Geological Time Column, which may be bracketed geochronologically and by different paleontological techniques. Furthermore, the precision of age determination using geochronologically calibrated paleontological techniques is quite refined, for example <1 Ma in the Mesozoic and Cenozoic eras. This attribute makes the correlation of paleomagnetic vectors and paleopoles between sites easier and more significant. It also permits a chronological assessment of rock magnetic properties.

1.1 - The purpose of this study

1. The main goal of this study was to examine a large sample of anisotropy of magnetic susceptibility (AMS), and anisotropy of anhysteretic remanent magnetism (AARM) data from post-Palaeogene strata in Cyprus. These should correlate with the orientations of neotectonic structures or events such as faults, rifts, Tertiary uplift, and even recent seismic events. This allows a investigation as to whether AMS/AARM fabric axes are consistent with stress trajectories inferred from those structures and from recent plate motion trajectories. Sampling at two density-levels has the potential to verify the homogeneity of the regional domains and the validity of the regional conclusions. Local sub-areas (I-VI) were structurally homogenous and sampled with as little lithological variation as possible over areas $\leq 30 \text{ km}^2$. The regional-scale domains (I- V) have an average area of $\sim 400 \text{ km}^2$.
2. The second objective of this study was to determine different magnetic contributions of minerals in Cyprus limestones by comparing the magnetic

properties of Cyprus limestones through time. Given the proximity and location of the Troodos ophiolite on Cyprus in relation to the overlying limestones (Fig. 1-1 and Fig. 1-2), it is likely that the ophiolite contributed some clastic material to the limestones in the form of titanomagnetite, titanomaghemite or magnetite.

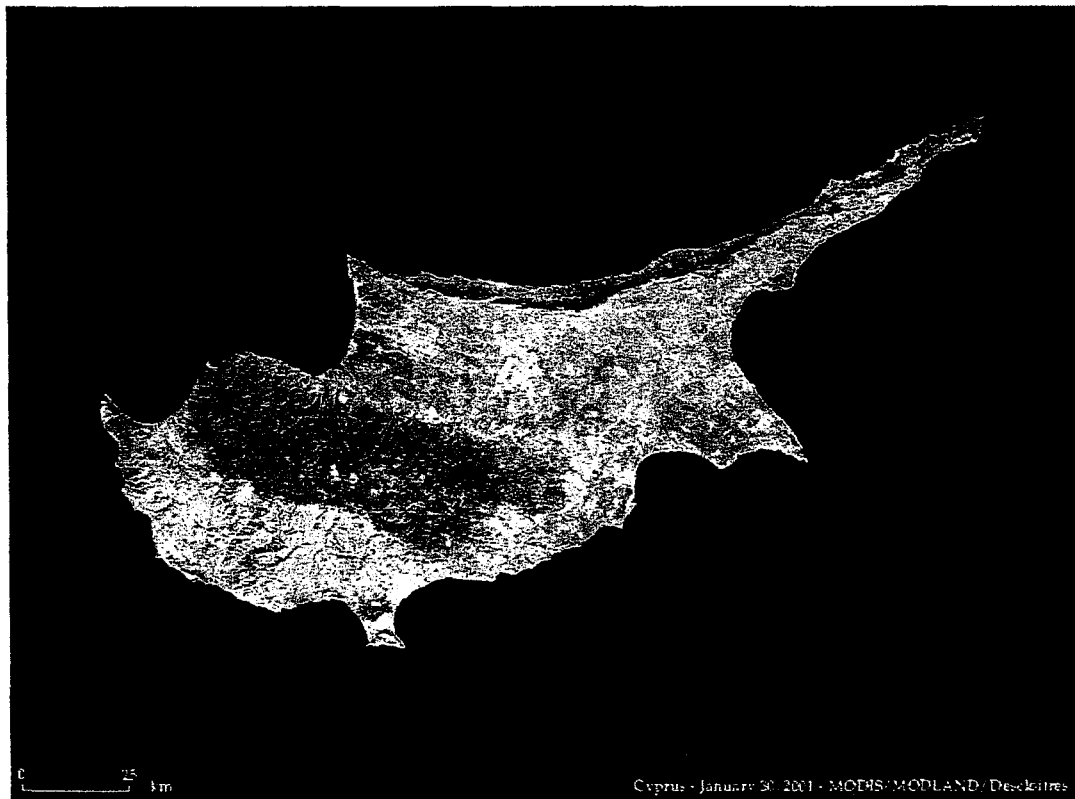


Figure 1-1. Cyprus from Space. Satellite photo of Cyprus demonstrating lithological and topographical changes. Note the dark ophiolite sequence emerging through the limestone cover. Small white spot in ophiolite sequence is snow on Mt. Olympus.



Figure 1-2. Troodos in snow. Although situated in the Mediterranean, Cyprus weather can fluctuate greatly due to dramatic changes in elevation (0-1951m) over short distances .

1.2 - Background

To understand the topic of magnetic mineralogy and fabrics in Cyprus limestones and their relation to Cyprus tectonism and stratigraphy, there are some necessary background topics that have to be covered: basic limestone magnetic mineralogy, and a cursory theoretical background in magnetics. More detailed examination of specific magnetic methods and procedures will be covered in the later chapters, together with a

review of Cyprus tectonics. For the non-paleomagnetist, a glossary of some of the magnetic and tectonic terminology can be found in Appendix 1.

1.2.1 - Background Limestone Magnetic Mineralogy

Limestone primarily consists of calcite with minor clay and trace amounts of numerous other minerals including ferromagnetic minerals. The most common ferromagnetic minerals found in limestone include magnetite, goethite, hematite, maghemite, and Fe-Ti oxides. These ferromagnetic minerals may have various provenances but can be grouped basically into one of six main groups: biogenic, clastic, exhalative (in the broadest sense), extraterrestrial, chemical-authigenic, and some derived from seafloor-metamorphosed basalt. Biogenic sources include (in order of importance): magnetotactic bacteria, dissimilatory iron reducing bacteria, and in rare circumstances chiton teeth. Clastic sources are more varied but are predominantly present as a fine-grained wind blown fraction from different continental sources or as inclusions in fluvial clay minerals. Exhalative processes may also contribute a significant fraction of mostly fine-grained material from terrestrial and submarine volcanic sources. Extraterrestrial and chemical authigenic sources are minor and difficult to verify in most instances.

Distinguishing different minerals and phases of magnetic minerals in limestone can be difficult using traditional mineralogical techniques such as optical mineralogy or SEM analysis because of small grain sizes, low abundances, and similar characteristics of some ferromagnetic minerals. The best way to look at magnetic mineralogy is to measure, examine and compare different magnetic properties of different samples. This is possible because every mineral has different magnetic properties and even the magnetic properties of the same mineral may differ due to grain size, shape, or internal stress.

Moreover, magnetic properties have a wider range of values than most other physical properties.

1.2.2 - Theoretical Background Magnetics

All materials have common fundamental magnetic properties due to electrons rotating around their spin axis and also around a nucleus. Materials can be classified as diamagnetic, paramagnetic, or ferromagnetic (*sensu lato*) depending on how they react in the presence of a magnetic field and after subsequent removal of the applied magnetic field (Fig. 1-3).

Diamagnetic materials will acquire a small negatively induced magnetization when in the presence of an applied field, and lose their induced magnetism once the applied field is removed. All substances possess a diamagnetic response but may be masked by their paramagnetic or ferromagnetic properties.

Paramagnetic materials will acquire a small positively induced magnetization in the presence of an applied field, and lose their induced magnetism once the applied field is removed.

Ferromagnetism can be defined in two ways: ferromagnetic *sensu lato* (*s.l*) and ferromagnetic *sensu stricto* (*s.s*). Ferromagnetic (*s.l*) materials will acquire a small to large positively induced magnetization in the presence of an applied field, and retain an amount of their induced magnetism once the applied field is removed. Ferromagnetic (*s.l*) include ferromagnetic (*s.s*), antiferromagnetic, and ferrimagnetic materials. Ferromagnetic (*s.s*) materials will acquire a large positively induced magnetization in the presence of an applied field and retain its induced magnetism once the applied field is removed.

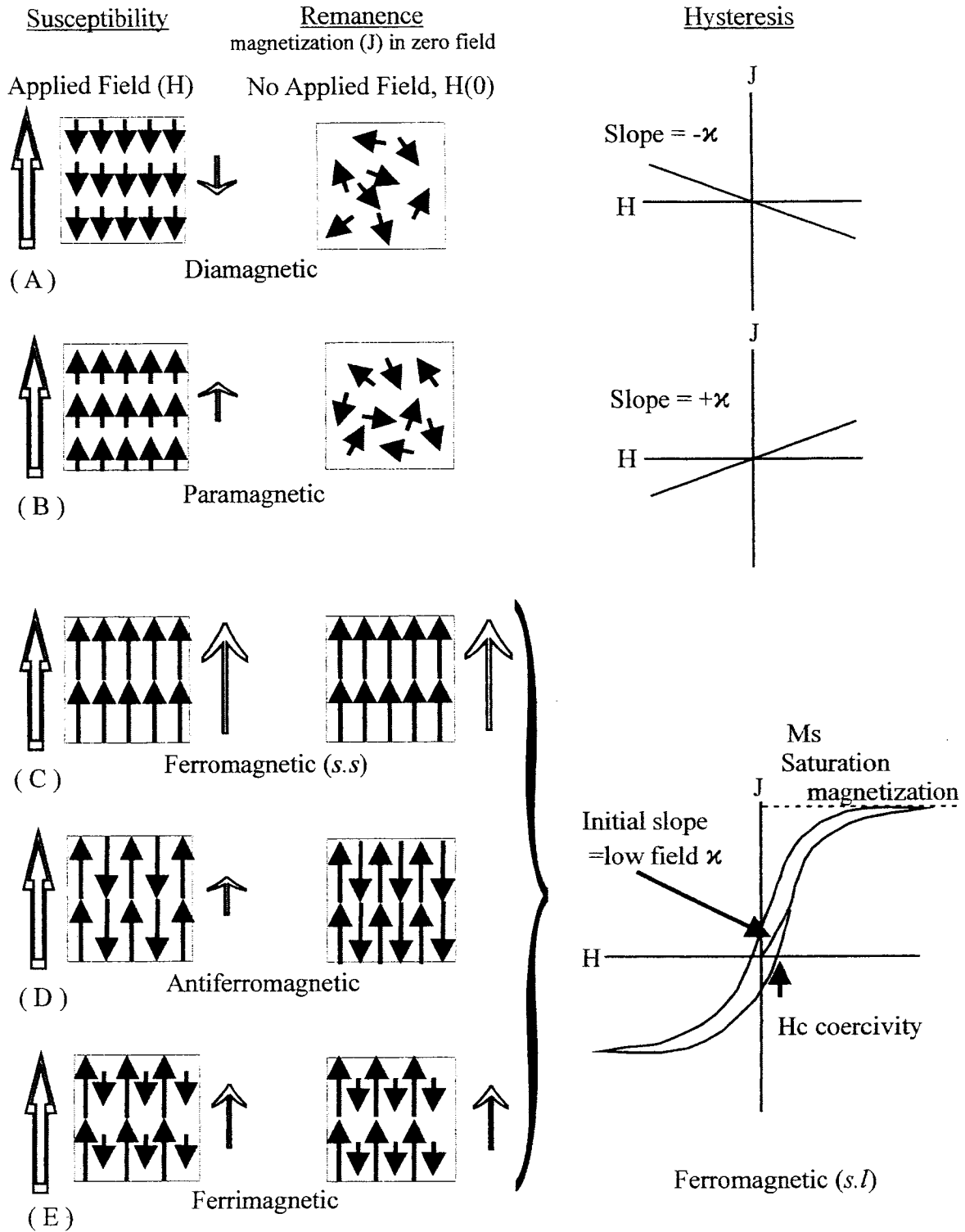


Figure 1-3. Types of Magnetization showing alignments of spin moments schematically. Different responses of (A) diamagnetic, (B) paramagnetic. (C-E) shows hysteresis during cycling through large fields $-H$ to $+H$, initial slope κ is the low field susceptibility. (Slope κ = magnetic susceptibility)

Chapter 2 – Magnetic Fabric Studies (AMS & AARM)

2.1 – Anisotropy of Magnetic Susceptibility (AMS)

Magnetic fabric analysis, most commonly using anisotropy of low-field magnetic susceptibility (AMS), is now well established as a non-destructive technique to isolate the mean orientation-distribution of crystals in an anisotropic rock. AMS blends contributions from different minerals that have different magnetic responses, i.e., paramagnetic, diamagnetic or “ferro”-magnetic (Rochette et al., 1992). In turn, the principal AMS axes may proxy for the principal axes of the orientation distribution ellipsoid of crystals (Borradaile, 2001; Henry, 1989), which, in turn, may reveal the finite strain axes in tectonically deformed rock (Borradaile & Henry, 1997; Tarling & Hrouda, 1993). In deformed calcite matrices, interpretation is somewhat complicated by an intrinsic counterintuitive arrangement of crystallographic and AMS axes, a so-called “inverse fabric” (Rochette, 1988), which nevertheless still permits sensible interpretations of their finite strain axes (Ihmlé et al., 1989; de Wall et al., 2000).

However, recent studies show that in neotectonic environments, with imperceptible penetrative strain, AMS axial orientations may be sensibly related to the orientations of joints or faults, for which stress-axes are reliably inferred (Sagnotti, et al. 1994, 1998; Mattei et al., 1999; Cifelli et al., 2004). In some instances, AMS axes may correlate with modern seismic solutions and plate movements (Kissel et al., 1986; Mattei et al., 1999; Borradaile & Hamilton, 2004). Thus, AMS may proxy for stress trajectories under limited circumstances.

2.2 - Tectonic Background

This study concentrates on the limestone and marl sedimentary cover to the Cretaceous Troodos ophiolite. Excluded from this discussion are the juxtaposed older allochthonous Mamonia and Kyrenia Terranes, which include exotic formations as old as Triassic and perhaps even Carboniferous (Robertson, 1990) (Fig. 2-1a). The Troodos Terrain exposes an integral ophiolite sequence with mantle harzburgite and lherzolite at the base overlain by layered gabbros and dunite, sheeted dykes, a transitional sheeted-dike-to pillowed unit and a thick pillow basalt sequence (Malpas et al., 1990). Supra-Troodos sedimentation commenced in the Maastrichtian (~ 68 Ma) with a pelagic chalk blanket, and forms a relatively continuous sequence to the present (Lord et al., 2000). Northwards subduction stalled in the Eocene, with southward thrusting of the Kyrenia Range. Subduction then retreated southwards to its present location off the south shore of Cyprus in the Miocene, initiating the present stress regime (Fig. 2-1b). Miocene extensional basins, most prominently the Polis graben, formed in response to changing stress trajectories during the retreat of the subduction zone's hinge away from the Troodos microplate. Subduction continued during the Pliocene, until the Eratosthenes Seamount reached the trench in the Pleistocene when serpentitization-driven diapirism continued to uplift the Troodos dome (Robertson, 2000). These events drastically changed the neotectonic regime in the last 5 Ma, which is evident from studies of structure (Robertson et al., 1995), earthquake distribution and fault systems (Arvidsson et al., 1998; Ben-Avraham et al., 1988; Borradaile & Hamilton, 2004; Papazachos & Papaioannou, 1999) and geodetically determined plate motion (Reilinger et al., 1997).

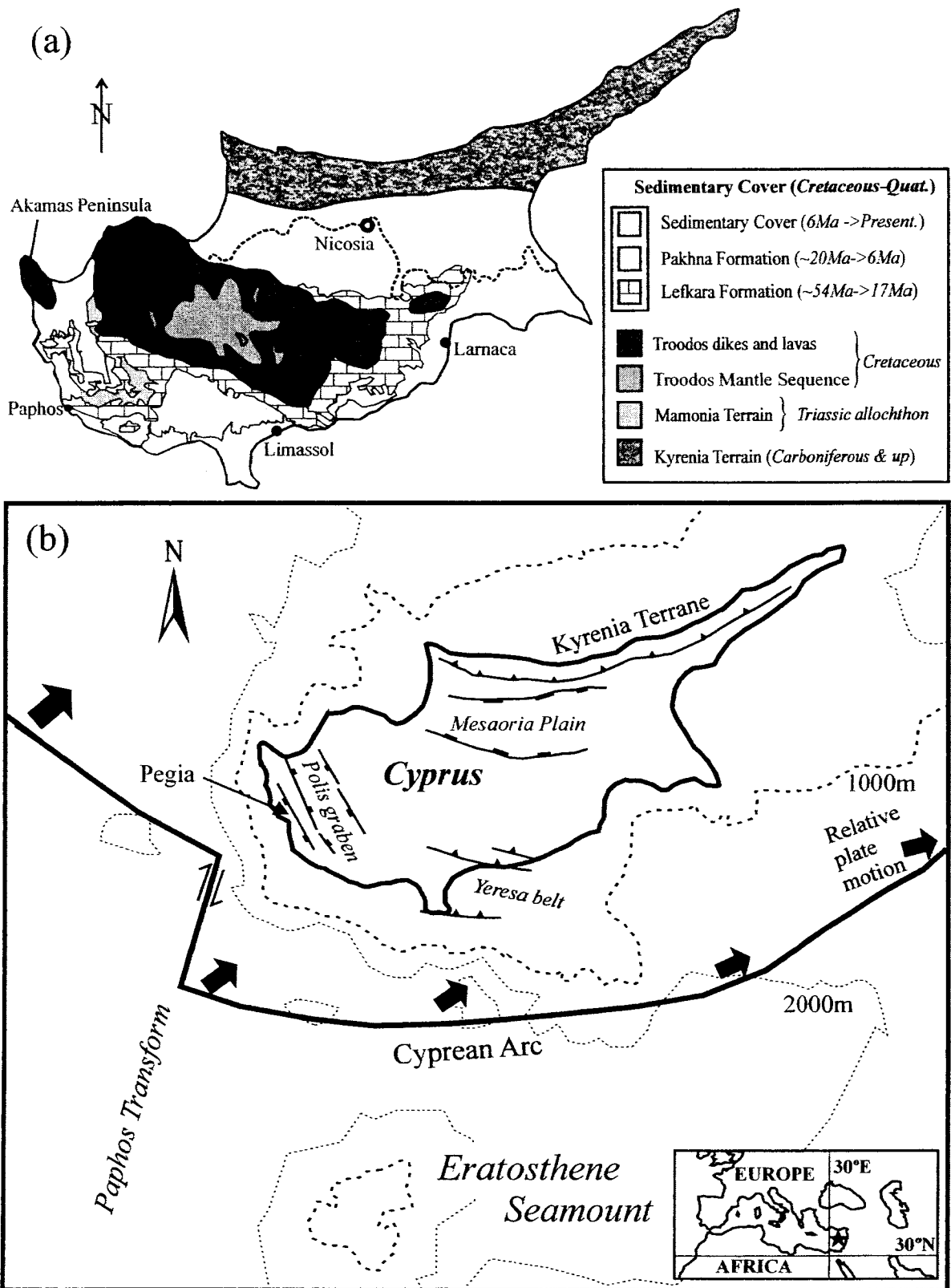


Figure 2-1 Geology of Cyprus. (a) Major lithological units of Cyprus (Geological Survey Department, Cyprus, 1979). (b) Major Tectonic features of Cyprus (Robertson, 1990; Arvidsson et al, 1998; Borradaile & Hamilton, 2004)

The tectonic events, their principal plate-geometrical consequences and the reasonably inferred principal tensile or compressive stress trajectories are summarized in Table 2-1.

Table 2-1. The major tectonic events of Cyprus through time and formations.

Age	Periods	Formations	Tectonic Events					
			Principal Stresses	Troodos Microplate Rotations				
0.01	Holocene	Alluvium		<p>Final ~30° slow rotation (50 Ma - 10 Ma) distant rotation-axis</p>				
	Pliocene	Terrace Deposits						
Fanglomerate								
2.0	Pliocene		Athalassa					
		Nicosia						
5.2	Messinian Tortonian Serravallian Langhian Burdigalian	Kalavassos						
		Koronia						
		Pakhna						
		Terra						
23.3		Oligocene	Lefkara					
					35.4	Eocene		
							56.5	
65.0		Maastrichtia Campanian	Moni					
	Kannaviou							
	Perapedhi							
	88.0		Troodos Ophiolite					

Previous studies indicated the potential for AMS (anisotropy of low field magnetic susceptibility) to indicate very weak strains and weak orientation distributions of minerals, like those accompanying calcite-crystal plastic mechanisms in neotectonic environments (Borradaile & Jackson, 2004; Borradaile & Henry, 1997; Rochette et al, 1992). AMS shows neotectonic potential in the limestone cover from the Palaeogene Lefkara Formation through the Neogene Pakhna Formation to the localized Pleistocene cover. Without regard to detailed stratigraphic level within the Troodos Cover sequence, Lagroix and Borradaile (2000) showed that the AMS principal axes correspond to kinematic patterns. k_{MAX} defines down-slope gravitational stretching away from the Troodos dome and locally into tectonic/depositional basins. In the Polis Rift Valley, AMS and AARM (anisotropy of anhysteretic remanent magnetization) axes correlate with principal stress trajectories inferred from Miocene and younger fault-orientations and from modern seismic fault-plane solutions (Borradaile & Hamilton, 2004; their fig. 6).

2.3 - Neotectonic interpretation of AMS

The presence of consistently oriented AMS axes unrelated to depositional fabrics in young sedimentary rocks, itself argues for some subtle tectonic imprint (e.g., Sagnotti et al., 1994). In such environments, AMS axes may be oriented consistently and simply with respect to faults or joints. These structures have orientations uniquely associated with their co-genetic stress trajectories and thus by induction, the AMS axes may proxy as *stress* trajectories. Of course, AMS axes may proxy for stress trajectories in ancient rocks too, but their recognition requires fortunate circumstances (e.g., Borradaile &

Kehlenbeck, 1996). Usually, in ancient or severely deformed rocks, the association of AMS with finite strain axes with earlier tectonic events will mask any young and feeble AMS overprint associated with late stress increments. *Note that this study uses Flinn's L-S scheme (1965) equally to describe tensor magnitude ellipsoid shapes, whether they are for strain, AMS, stress, or mineral ODs (Orientation-Distributions or "petrofabrics").*

Calcite twinning and other crystal-plastic deformation have long been used in petrofabrics as sensitive indicators of *incremental* strain axes, which are essentially parallel to the causative *palaeostress*-axes. Indeed, the association of calcite petrofabrics, their causative stress axial orientations and magnetic fabrics have been shown in some other studies (Jackson et al., 1989; Borradaile et al., 1989; Owens & Rutter, 1978; Owens & Bamford, 1976). The Neogene and Quaternary limestone and marl that covers the Troodos microplate shows evidence of weak to moderate strain, expressed by calcite twinning and, rarely, a feeble stylolitic cleavage. Calcite, accessory clay and magnetite-traces are aligned and readily detectable in the AMS signal (Lagroix & Borradaile, 2000). These minerals contribute quite differently to AMS and to bulk susceptibility. Calcite is diamagnetic (usually quoted as $\kappa \sim -14 \mu\text{SI}$) but it has a large anisotropy and comprises >97% of the rocks' volumes. Its crystal-plastic deformation aligns the paramagnetic accessory clay minerals ($100\text{-}500 \mu\text{SI}$, $\leq 3\%$ by rock volume) and the scarce traces of magnetite. However, the latter may contribute significantly to AMS due to magnetite's high bulk susceptibility (~ 1.0 to 5.7 SI) (Hunt et al., 1995); and the grains may align either as overgrowths or inclusions associated with clay grains or as independent grains. Magnetite grains may be of clastic or bacterial origins; their hysteresis properties are

compatible with the latter hypothesis (Borradaile & Hamilton, 2003; Borradaile & Lacroix, 2000). Specific hysteresis data for these rocks will be discussed in later sections.

The specimen's bulk susceptibilities [$\kappa = \sqrt[3]{(k_{MAX}k_{INT}k_{MIN})}$] are a first guide to the mineralogical controls on AMS. These are presented in rather homogenous sub- areas ($\sim 40\text{km}^2$) (Fig. 2-2a), which justifies the subsequent interpretation of larger sampling schemes in regional domains ($\sim 400\text{km}^2$) (I-V) (Fig. 2-2b). The positive susceptibility sections of the histograms are scaled logarithmically and, to a first approximation, it appears that the weakly positive κ specimens have susceptibilities with a lognormal distribution, with most sub- areas and regional domains having modal κ in the range $+15 \mu\text{SI} \leq \kappa \leq +35 \mu\text{SI}$. Very low concentrations of accessory clay ($\leq 1000 \mu\text{SI}$) and trace magnetite ($>2.0 \text{ SI}$) suffice to raise the specimens' κ from the level of a pure calcite diamagnetic matrix ($\sim -14 \mu\text{SI}$) to the levels of the positive κ specimens shown in Fig.2-2a,b. In the complete absence of magnetite, only 3% by volume of clay would be required to justify the positive κ values. Many specimens are truly diamagnetic and the linear scale for the diamagnetic part of the histogram clarifies the frequency distributions. For calcite, κ is commonly quoted at $\sim -14 \mu\text{SI}$ (Voight & Kinoshita, 1907) or -7.5 to $-39 \mu\text{SI}$. (Hunt et al., 1995). Whereas there are fairly modern high precision torque measurements for anisotropy (i.e., $k_{MAX}-k_{MIN}$; Hellwege & Hellwege, 1967; Owens & Rutter, 1978) there are apparently no recent high-precision measurements for the bulk value (κ), which hinders modelling and interpretation of AMS. Values for synthetic calcite would be preferable for modelling work whereas measurements from natural calcite are contaminated by non-diamagnetic impurities. Our instrument has a low-drift environment ($<0.05 \mu\text{SI}$) and is calibrated with MnO_2 ($\sim 1654 \mu\text{SI}$). Due to the small range of

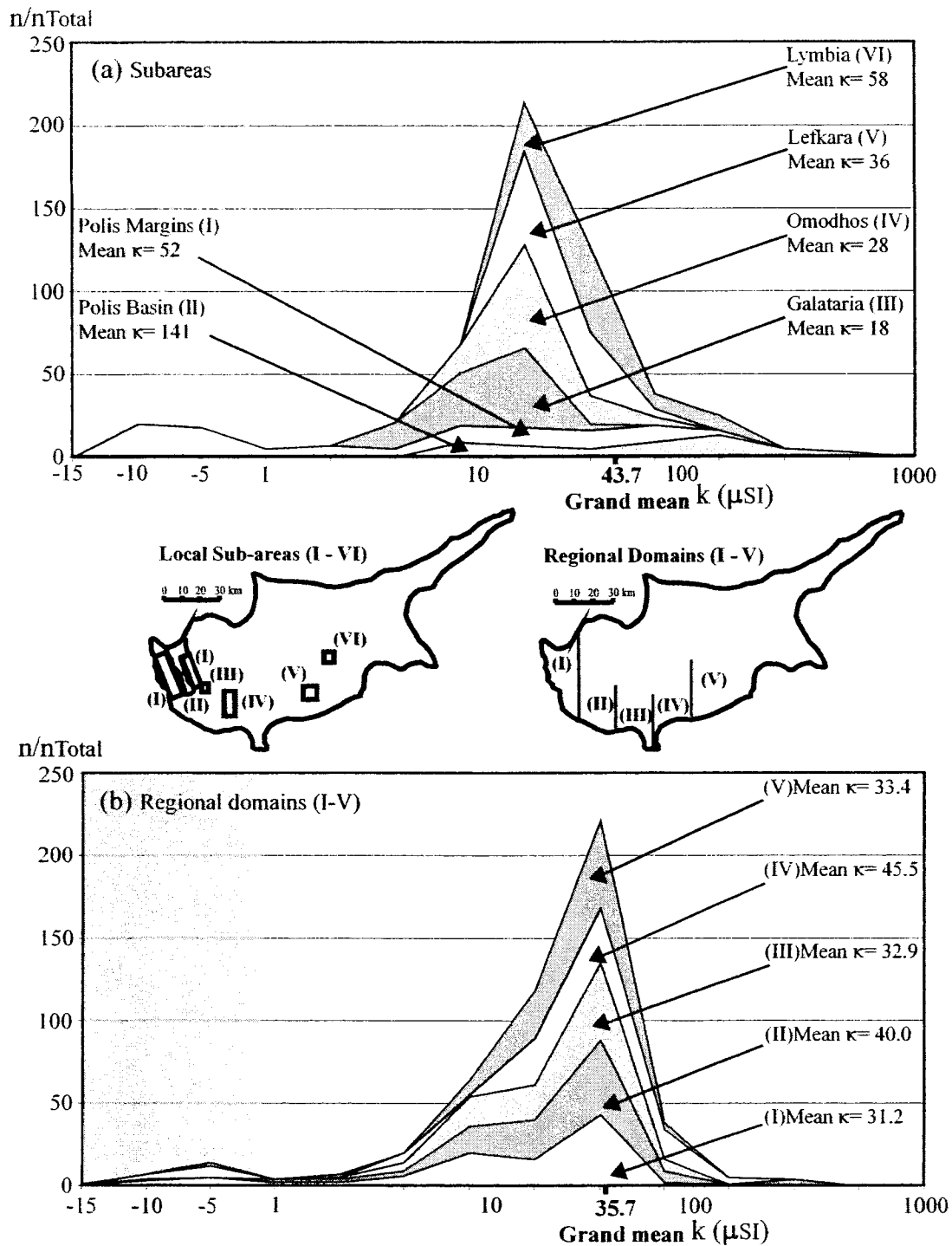


Figure 2-2. Frequency-distribution of bulk magnetic susceptibility (κ) for (a) sub-areas (each $\sim 30 \text{ km}^2$) and (b) regional domains (each $\sim 400 \text{ km}^2$). Data in the shaded box on the left represent diamagnetic specimens and their scale is linear. Data with $\kappa > 0$ represent paramagnetic specimens and are shown with a logarithmic scale. κ is calculated as the mean of the seven measurements made in 7 different directions during AMS determination.

diamagnetic susceptibilities there may be some slight bin boundary bias in that part of the histogram.

The susceptibility frequency-distribution indicates that paramagnetic limestone is more common and it confirms that the rocks' susceptibilities, whether paramagnetic or diamagnetic are mostly bi-mineralic in origin. Interpreting AMS axes in such rocks necessitates the evaluation of the balance between weak paramagnetism and weak diamagnetism in the same specimens, and between weakly dia/paramagnetic specimens within a sample of several different specimens, for example from a sub-area.

A new plot of fabric anisotropy parameters, introduced by Borradaile & Jackson (2004), simplifies the interpretation in this context. Jelinek's (1981) anisotropy parameters (P_j , T) are usually presented on Cartesian axes. Consequently, for weak degree of anisotropy (low-eccentricity ellipsoids with $P_j \sim 1.0$) the difference between T -values that describe ellipsoid shape is exaggerated. In the extreme case, the sphere (isotropic case, $P_j=1.0$), which should plot at *one point* on the diagram actually spread along the entire axis from $T=+1$ (prolate) to $T=-1$ (oblate). This biases the presentation and interpretation of all low- P_j anisotropies that are essentially near-isotropic, a matter of considerable relevance here where specimens straddle the diamagnetic-paramagnetic boundary. The new polar plot presents P_j radially and T along arcs; thus, all spheres plot uniquely at the origin and the difference in shape between weak anisotropies is not exaggerated. Moreover, the plot facilitates the simultaneous presentation and comparison of positive and diamagnetic susceptibilities (Fig. 2-3).

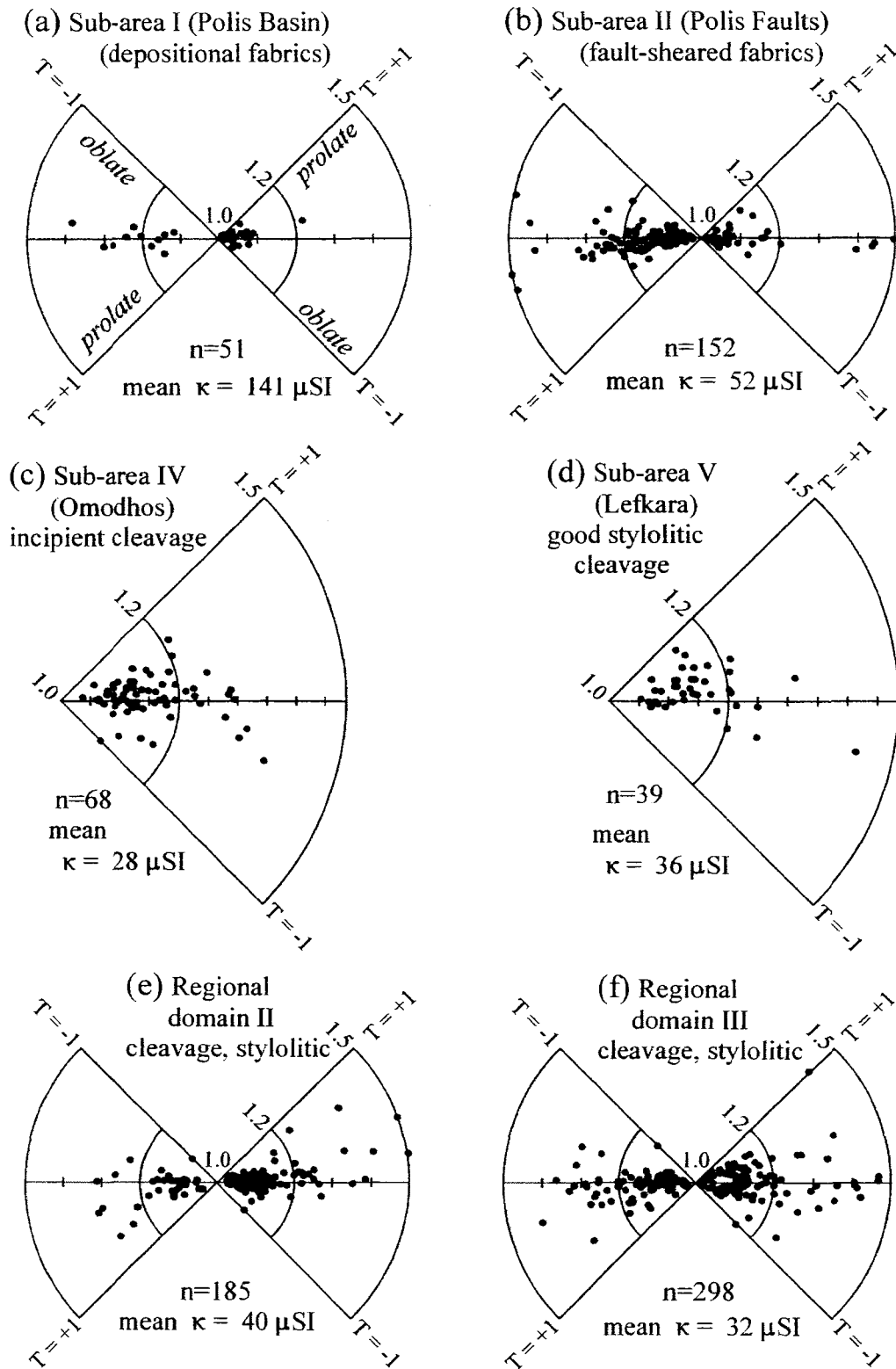


Figure 2-3. Polar plots (see Borradaile & Jackson, 2004) of four select sub-areas (a-d) and two select regional domains (e-f). Shaded area represents diamagnetic specimens and white area represents paramagnetic specimens. Fabrics are apparent from Jelinek's (1981) P_j (radial) and T (arc) parameters calculated from the principal susceptibilities. Different patterns reflect the degree and type of deformation. (T =shape, P_j =eccentricity)

When working with anisotropies of diamagnetic rocks and weakly paramagnetic rocks it is also important not to overlook some non-trivial issues, which software must be carefully manage:

- (1) Anisotropy is indeterminate for a specimen if some axes have positive susceptibility and others have negative susceptibility (Borradaile, 2003). This occurs in some limestone specimens.
- (2) k_{MAX} is obviously the largest absolute value for a paramagnetic material but for a diamagnetic material the most negative value represents the long axis of the magnitude ellipsoid.
- (3) Regardless of the convention for defining the ellipsoid in (2) above, the common diamagnetic minerals, quartz and calcite have the idiosyncrasy that under most metamorphic conditions their c-axes tend to align parallel to the shortening axis (however, see Borradaile & Jackson, 2004). Thus, c-axes are parallel to the most negative susceptibility, which may be perpendicular to the rock's S-fabric. Calcite exhibits a strong prolate diamagnetic anisotropy with ($\kappa_{MAX} - \kappa_{MIN}$) estimated at 1.39 μSI (Krishnan et al., 1933; Hellwege & Hellwege, 1967, p.143) or $1.172 \pm 0.028 \mu\text{SI}$ (Owens & Rutter, 1978). If we accept the much less certain but commonly quoted bulk susceptibility $\kappa \sim -14 \mu\text{SI}$, these precise anisotropy determinations indicate a large anisotropy of $\sim 10\%$.
- (4) Since most deformation mechanisms align calcite with its c-axis (most negative susceptibility) parallel to shortening it produces an "inverse fabric" (Rochette, 1988; Ihmlé, 1989).

Examples of the anisotropies of both local-scale samples (Fig. 2-3a-d) and regional domains (Fig. 2-3e, f) indicate that the anisotropy degree (P_j) is similar for diamagnetic and paramagnetic limestones and that ellipsoid shape tends slightly toward the oblate case ($T > 0$) for both diamagnetic and paramagnetic specimens. Anisotropies are remarkably similar for the diamagnetic and paramagnetic fields and diamagnetic limestones are only absent in marl Formations in the Omodhos and Lefkara subareas (Fig. 2-3c, d).

2.4 - Interpreting AMS

AMS orientations and magnitudes would reflect the orientation distribution of a monomineralic rock with a unique petrofabric. However, for rocks with multiple minerals with similar contributions to the net susceptibility or with multiple subfabrics some care is required in evaluating the influence of mineral abundances and subfabrics (Borradaile, 1988; Borradaile & Henry, 1997). For rocks of high mean susceptibility (κ), AMS axes may be controlled by one of two or a few minerals (Borradaile & Mothersill, 1984; Borradaile & Kehlenbeck, 1996; Borradaile & Lagroix, 2001; Henry, 1983; 1990; 1992; Nakamura & Borradaile, 2001). In these limestones however, sub-equal competition from the diamagnetic matrix and paramagnetic clay complicate the issue. To illustrate the argument with hypothetical but not unrealistic values chosen for arithmetic simplicity; disperse a concentration of 5% clay (assume $\kappa = 266 \mu\text{SI}$) in a calcite matrix (assume $\kappa = -14 \mu\text{SI}$). The limestone's net susceptibility is approximately zero and the specimen may also be isotropic. It is for this reason that some AMS data from limestone must be examined carefully because the AMS directions are simply too unstable; their anisotropy

is too low to define stable orientations of principal axes as itemized in the list above (Borradaile & Jackson, 2004). In worse cases, the principal susceptibilities may not all be of the same sign so that the AMS tensor may not be represented by any magnitude ellipsoid.

Although it is now realized that the magnitude ellipsoids of individual specimen tensors have little kinematic significance due to the complex blend of multiple mineralogical responses, specimen magnitudes do affect the calculation of the orientation of the mean-tensor. The mean-tensor's orientation may be strongly deflected toward the orientation of a few large-magnitude specimen tensors. However, high susceptibility specimens need not be considered as outliers in the disparaging statistical sense. They may provide useful information from a subfabric or second population of grains with a different orientation-distribution. That is the case in this study where specimens with larger concentrations of paramagnetic accessory clay minerals may strongly influence the orientation of the mean tensor for a sub-sample. By recalculating the mean tensor using standardized specimen-tensors, the influence of high susceptibility specimens and kinematically distinct subfabrics may be isolated, or emphasized (Borradaile, 2001; 2003). Specimen-tensors are standardized by dividing each of the principal magnitudes for a specimen (k_{MAX} , k_{INT} , k_{MIN}) by κ ; this weights all specimens equally, regardless of their bulk susceptibility. Consequently the contribution high- κ subfabrics to the orientation-distribution will be subdued in the net-AMS. On the other hand, the mean-tensor for non-standardized specimens emphasizes the role of such subfabrics (Borradaile, 2001; 2003).

The following comparison of mean-tensors for standardized *versus* non-standardized specimens in regional-scale and local-scale samples, display different AMS axes that reveal a rapidly changing tectonic regime, especially in the last 5 Ma. Sample mean-tensors for standardized and non-standardized specimens are also compared profitably to previously determined AARM tensors.

2.5 - Processing AMS data from low- κ specimens

The tectonic significance of AMS data in limestone having weak susceptibilities depends on a careful assessment of the mineralogical origins of AMS and the effects of specimen-variation within the sample-suite. Jelinek (1978) showed that the orientation distribution (OD) of a suite of tensors (“AMS ellipsoids”) must be treated by a special statistical procedure so that the sample’s mean tensor retains orthogonal axes, just like individual specimen-tensors. Applying Jelinek statistics permits us to characterize a sample of AMS tensors much more effectively than with density contours, although the latter still have their use (Borradaile, 2001; 2003). The shape and symmetry of the 95% confidence regions around the mean-tensor’s principal axes define the orientation-distribution of specimen tensors in the L-S fabric scheme (Flinn, 1965); thus regional suites of AMS ellipsoids define the regional variation from S through L tectonites (Fig. 2-4).

Confidence cones for the mean-tensor’s principal axes reflect the shape of the orientation-distribution (OD) ellipsoid for the sample, not of individual tensors. For example, individual prolate ellipsoids scattered with their long axes in a plane define a sample with an orientation-distribution described by an oblate ellipsoid (e.g., Borradaile,

2003; p.286-287). Thus in AMS studies, if the mean $T_j > 0$ for specimens, it does not necessarily mean that their orientation distribution, described by the mean-tensor is also prolate (Borradaile, 2001).

The sample's mean tensor and its confidence cones may be biased toward the orientation of specimens of anomalous κ . In this study, the anomalous specimen may be a diamagnetic one or a paramagnetic one in a contrasting matrix. The standardization technique described (dividing k_{MAX} , k_{INT} , and k_{MIN} each by κ , etc.) suppresses this bias. Whereas it may change the orientation of the mean tensor, it may also change the shape of the confidence regions about the mean tensor's axes. Thus one may re-evaluate the OD of the mean tensor as an $L > S$ rather than $S > L$ fabric.

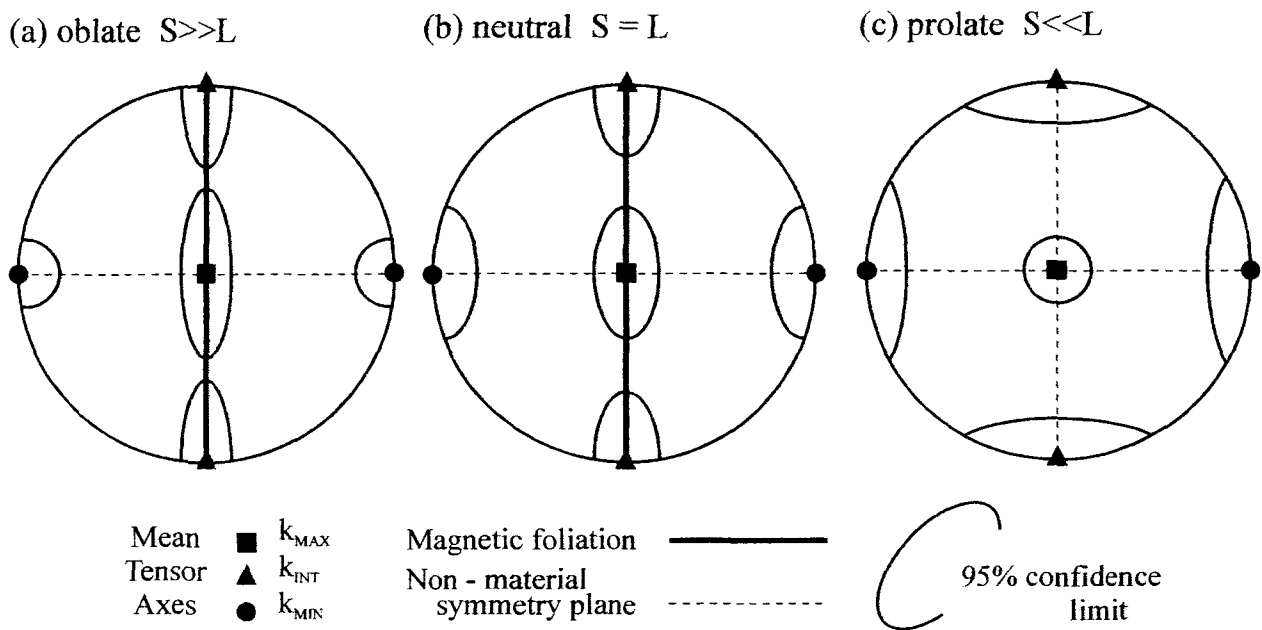


Figure 2-4. Idealized symmetry of confidence cones about the mean orientations of the principal axes of the mean tensor for a petrofabrically homogeneous group of specimens. The shapes of confidence cones for tensor-mean principal axes may be used for other petrofabrically significant axes (as in orientation-distributions of crystals), for finite strain axes and for principal stresses. The shape of the confidence cones may also related to the relative magnitudes of the three principal mean-axes: (a) elongate confidence ellipses in the maximum-intermediate plane define an ellipsoid with oblate symmetry ($S > L$) whereas (c) elongate confidence ellipses in the plane perpendicular to the maximum axis are associated with prolate symmetry ($L > S$). Flinn's (1965) L-S notation was initially introduced to describe finite strain ellipsoids or fabric ellipsoids but it is a useful shorthand for any anisotropy

2.6 - AMS measurements

AMS was determined using a Sapphire Instruments SI2B device operating at 19,200 Hz and ~ 0.1 mT. The anisotropy measurement utilized the seven-orientation system (Borradaile & Stupavsky, 1995), which includes four body-diagonal measurements, improving precision over the more commonly used orientations confined to coordinate axes and their symmetry-planes (e.g., Girdler, 1961). Instrument control and real-time data processing were performed using the SI2B01 software package developed by G.J.B. A complete AMS determination and analysis requires less than four minutes per core. The low-field AMS was determined on 360 cores from 121 specimens of the local sampling campaign (Appendix 2 & 3) and remeasured on 730 cores from 298 specimens of the regional sampling campaign (Appendix 4 & 5) of Lagroix and Borradaile (2000). Sample holder correction is particularly critical in the case of specimens with near-zero susceptibility. In the seven orientations of measurement, the holder calibrates approximately -18, -18, -18, +30, +30, +30, and +30 μSI , respectively.

2.7 - AARM: Anisotropy of Anhysteretic Remanent Magnetization

AARM was determined using the same seven-axis anisotropy scheme as for AMS measurements. The specimen is fully demagnetized and then the seven differently oriented ARMs are applied and measured, in a sequence such that each ARM is inclined at 45° or 35.3° to the previous one. For many rock types, this effectively cleans the ARM acquired in each preceding treatment. This tested technique greatly reduces the measurement time because 3-axis AF cleaning between each ARM application is no longer necessary (Werner & Borradaile, 1996). However, the success of this short-cut

must be verified with each new measurement campaign and each new lithology. ARMs were imposed with a Sapphire Instruments three-axis Alternating Field (AF) demagnetizer outfitted with a supplementary DC coil applying a bias field of 0.05mT. The AF decayed from a peak field of 80 or 100 mT to zero while the DC bias field was turned on from 60 mT to zero. The imposed ARM was measured in a JR5a automatic spinner magnetometer (sensitivity 0.03 mA/m). Instrument control, measurement and simultaneous data-reductions were performed using the SPIN01 software package developed by Borradaile. Complete AARM determination and analysis requires 18 minutes per core. We have only included AARM results from regional scale sampling suite in this study. Of the original sample (n = 1170, Lagroix & Borradaile, 2000), 201 cores were rejected for AARM determination. The criteria for accepting or rejecting the AARM results occur during measurement; results were rejected if intensities were < 1 mA/m when measured in position 1 of the AARM scheme or if the AMS ellipsoid for the sample had a negative κ . In the present study, for AARM we selected and re-measured 254 cores from 229 specimens from the original suite published by Lagroix and Borradaile (2000).

2.8 - Sampling Strategy

The first level of sampling focussed on structurally and lithologically homogenous subareas $\leq 30 \text{ km}^2$ that were densely sampled (Fig. 2-5). They include the Polis Rift Margins, Polis Basin, Galataria, Omodhos-Pakhna, Lefkara, and Lymbia, designated subareas I – VI, respectively, yielding n = 360 cores from N = 121 sites. These areas include Formations from the Lefkara up to the Athalassa Formation.

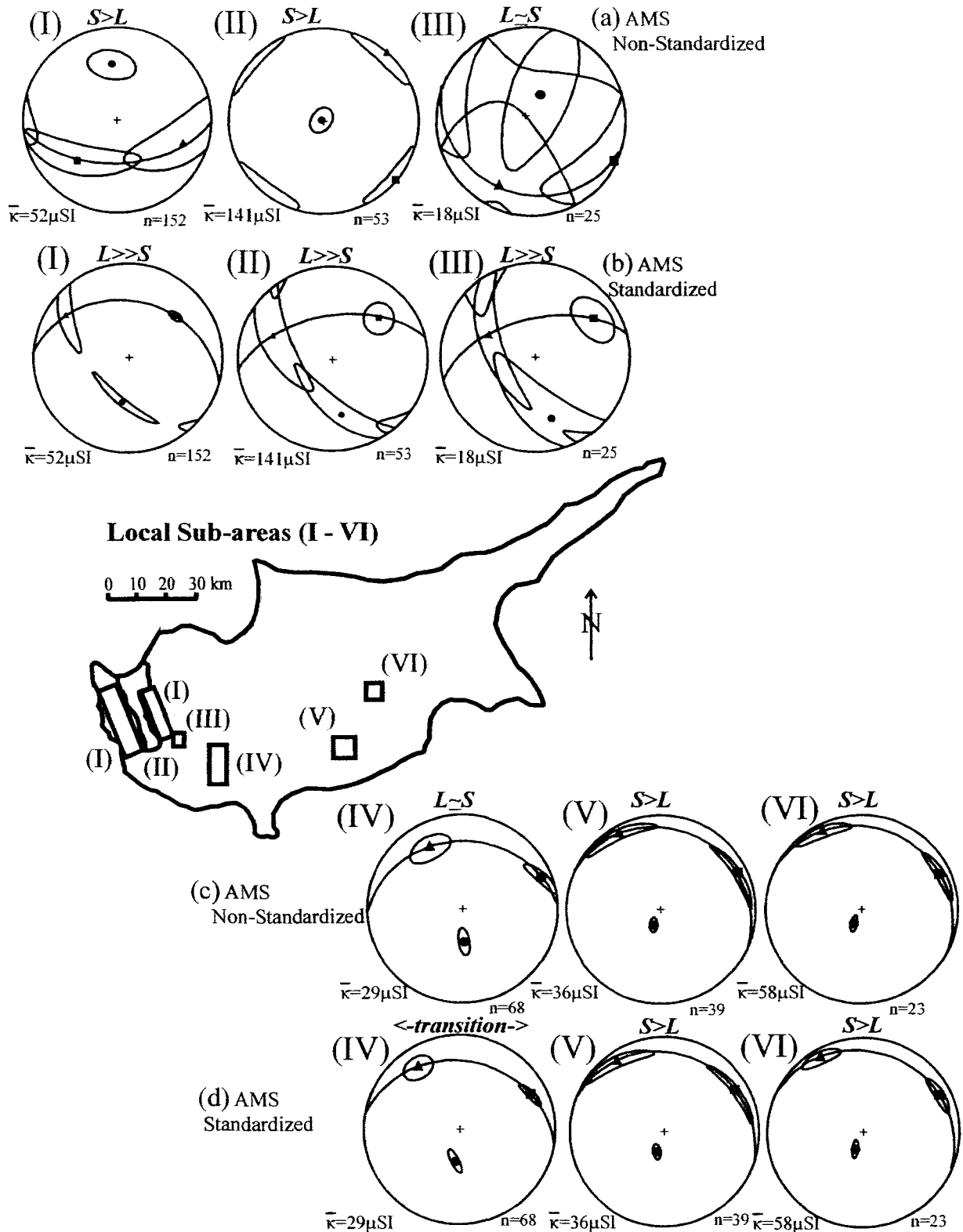


Figure 2-5. Sub-areas of Cyprus (I-VI) and their magnetic fabrics as discriminated by standardization (specimen tensors standardized dividing by each specimen's $\bar{\kappa}$). (a) Non-standardized AMS orientation distributions are biased by anomalously oriented subfabrics, especially with anomalously high- $\bar{\kappa}$. (b) Standardized AMS fabrics usually suppress the contribution of specimens with anomalous orientations.

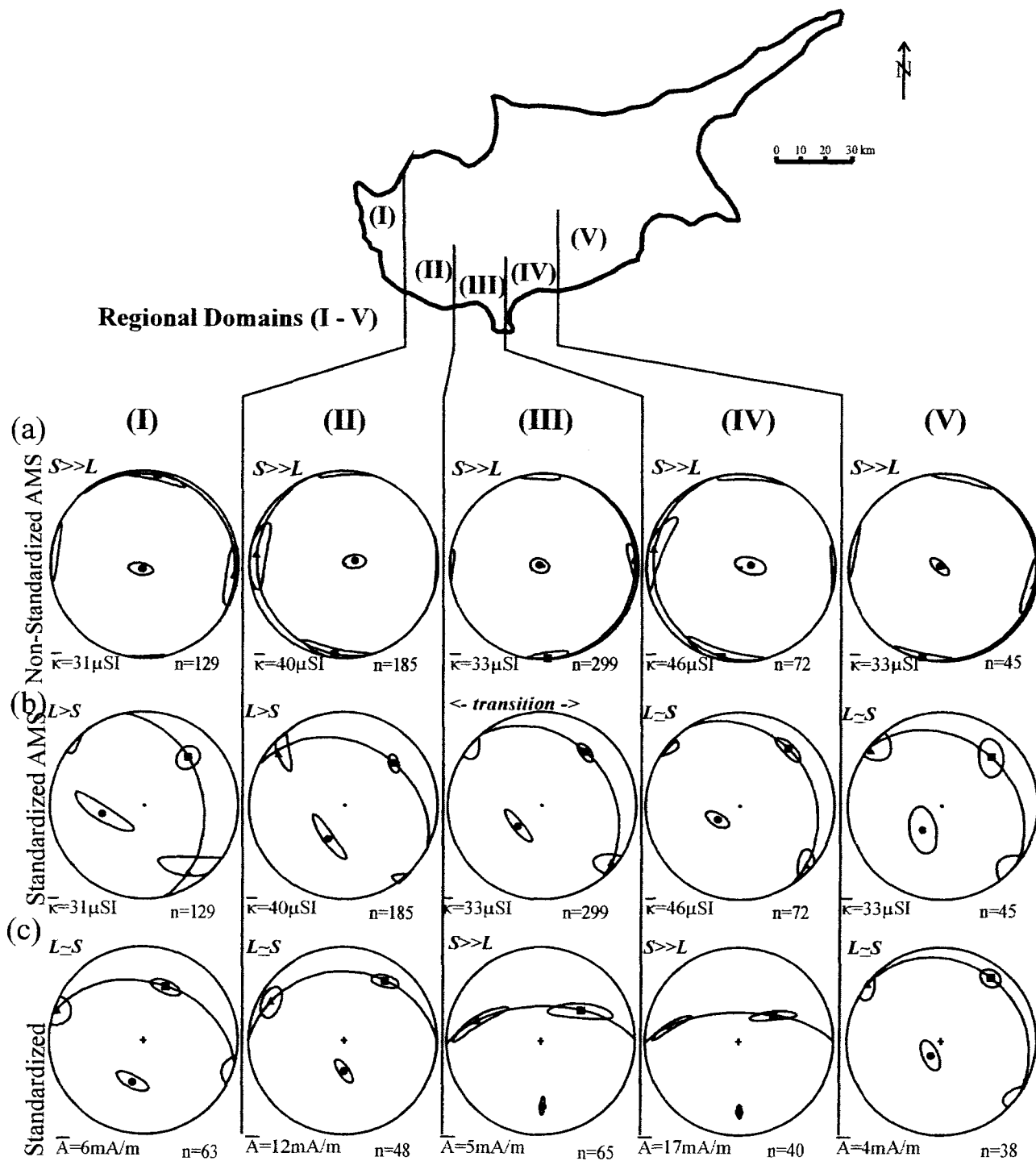


Figure 2-6. Regional domains of Cyprus (I-V) and their magnetic fabrics. (a) Non-standardized AMS. (b) Standardized AMS. (c) Standardized AARM. AARM isolates the magnetite sub-fabric and when standardized, and standardization subdues the contribution of anomalously oriented specimens.

The homogeneity of fabrics in these subareas justified the larger scale interpretation from the next level of sampling.

The second level of sampling was a diluted regional-scale campaign. The limestone specimens covered a wide age-range of the sedimentary cover, from the Lefkara Formation up to the Nicosia Formation (Lagroix & Borradaile, 2000). Of the original sample suite (cores $n = 1170$, sites $N = 434$), a sub-sample ($n = 730$, $N = 298$) was analyzed in five regional domains of similar tectonic style and trend (Fig. 2-6), each with an area of $\sim 400 \text{ km}^2$.

All hand-specimens were oriented in the field and three to six cores (25 mm in diameter and 22 mm high) were drilled in the laboratory from each specimen, restored to geographic coordinates.

2.9 - Localized sampling: Polis Rift Region (subareas I, II, III)

Non-standardized AMS in this, the Polis Rift region, differs from the other areas (Fig. 2-5a). From the faulted margins they exhibit an S>L fabric as shown by the elongate confidence cones for k_{MAX} and k_{INT} , and a small k_{MIN} confidence cone (Fig. 2-5a, sub-area I). The AMS axes are symmetrically compatible with stress directions of the last 5 Ma verified from fault orientations and from seismic data (Payne & Robertson, 2000; Borradaile & Hamilton, 2004).

In the basin, non-standardized data permit straightforward fabric interpretations (Fig. 2-5a, sub-area II). These younger strata have S>L depositional fabric as shown by the elongate confidence cones for k_{MAX} and k_{INT} in the foliation and a tight, near-vertical k_{MIN} confidence cone. The magnetic foliation is parallel to the bedding. k_{MAX} and k_{INT} lie

within the bedding plane and k_{MAX} is possibly a flow-alignment, since it is parallel to the rift axis (*cf.* Sagnotti et al., 1994). Raw, non-standardized AMS data demonstrates the effects of higher susceptibility specimens in which depositional-controlled AMS fabrics dominate.

In the Galataria region, non-standardized specimens exhibit an $L \approx S$ fabric, which appears nearly isotropic from its large, overlapping confidence cones (Fig. 2-5a, sub-area III). Nevertheless, the mean-tensor axes are similar to the other two preceding localities in this region.

How are these low- κ samples affected by relatively high- κ specimens? Standardizing the specimen AMS to κ , reveals similar susceptibility directions overall but demonstrate different confidence cone shapes (Fig. 2-5b, sub-areas I-III). All show $L \gg S$ ODs. The progressive increase in size of the confidence cones from west to east may be due to the smaller sample sizes ($n = 152$ to $n = 25$). The NE-trending k_{MAX} $L \gg S$ fabric agrees with the crustal tension-axis required for the paired normal faults defining the Polis Graben and the normal fault zone defining the Pegia fault system (Payne & Robertson, 2000). The $L \gg S$ fabric of the AMS data is also symmetrically compatible with the current tectonic stress regime deduced from earthquake data (Borradaile & Hamilton, 2004; their fig. 2).

2.10 - Localized sampling: Southern slopes of Troodos (subareas IV, V, VI)

The three eastern-most detailed sub-areas show little difference between standardized and non-standardized samples (Fig. 2-5, sub-areas IV-VI). The Omodhos-Pakhna subarea (IV) displays an $L \approx S$ OD fabric with a shallow northward dipping

'foliation'. The Lefkara and Lymbia (sub-areas V and VI) localities display an S>L OD fabric as shown by the elongate confidence cones k_{MAX} and k_{INT} and a tight k_{MIN} confidence cone with a shallow NNE dipping foliation. These OD fabrics in the eastern localities represent a dominant sedimentary fabric with some secondary tectonic control. However, all are compatible with a south-directed movement (southerly *vergence*) within the limestone cover.

2.11 - Regional scale AMS

Non-standardized AMS data of the five regional scale domains (Fig. 2-6a, sub-areas I-V) exhibit similar OD's for all areas. All five groups exhibit an S>>L fabric as shown by the elongate confidence cones for k_{MAX} and k_{INT} and a tight k_{MIN} confidence cone near vertical (Borradaile, 2001). This OD is similar to the results exhibited in the *density-contoured* data in Lagroix and Borradaile (2000). The S-component of the fabric is bedding-controlled and k_{MAX} is kinematically compatible with N-S extension, parallel to the aligned phyllosilicates caused by the stretching of the sedimentary cover (Lagroix & Borradaile, 2000).

But how are these low susceptibility samples affected by relatively high susceptibility samples that may be considered as statistical outliers? Standardizing the specimen ellipsoids to κ , AMS data of the five regional scale groups (Fig. 2-6b) reveals similar overall AMS axes but different confidence-cone shapes and, thus, different fabric ODs in the L-S range. These differences change progressively from L \approx S in the east to L>S in the west. This corresponds to the increasing tectonic strain from east to west, inferred from earthquake data (Borradaile & Hamilton, 2004; Arvidsson et al., 1998; Ben-

Avraham, et al.,1988; Papazachos & Papaioannou, 1999) and overall structural trends (Robertson, 2000; Borradaile & Hamilton, 2004). In contrast, raw data (non-standardized) are weighted by higher susceptibility depositional subfabrics, rather than the weak tectonic ones compatible with supra-subduction SW-directed shortening (Lagroix & Borradaile, 2000).

2.12 - Regional scale AARM

Only standardized data are presented for AARM to avoid the spurious effects due to the large variance in remanence intensity. Domains I, II & V (Fig. 2-6c) show similar overall AARM axes to standardized AMS (Fig.2-6b). This verifies the important contribution of magnetite to some AMS fabrics. They show an $L \approx S$ OD similar to the eastern-most standardized AMS, perhaps due to a near-uniaxial shape of magnetite, which when arranged in a weak planar fabric has a strong A_{MIN} zone-axis girdle. Thus, the N-S extensional trend (seen in the AMS) is less effectively expressed but the fabric axes are kinematically compatible with movement directed toward the SW (or subduction to the NE). AARM fabrics for the other two sub-areas (Fig. 2-6c, sub-areas III & IV) exhibit $S \gg L$ fabrics; AARM axes indicate a more southerly directed movement. The AARM fabric may be a composite of the stylolitic cleavage incompletely overprinting the bedding fabric (Lagroix & Borradaile, 2000).

Chapter 3 – Magnetic Mineralogy

3.1 - Introduction

As seen in previous chapters, understanding the magnetic mineralogy can be an important fact when interpreting magnetic fabrics. Therefore at least a brief introduction into some of the theories and background is necessary. Definitions of some of the more relevant terminology can be found Appendix 1, and a more in depth discussion of magnetic theory is provided in O'Reilly (1984).

Most magnetic measurements and techniques are based on the Néel equation:

which is $\tau = 1/C \exp. [Kv]/[KT]$ (for magnetite).

Relaxation time (remanence to decay) is related proportionally to coercivity, volume and inversely to temperature. Therefore by measuring remanence or coercivity one can investigate magnetic volume (grain size and concentration).

From the Néel equation and other magnetic theory equations one can determine which magnetic properties/measurements or combinations of measurements are dependent on concentration and which are dependent on composition (Table 3-1).

Table 3-1. Different Magnetic Techniques and their dependence on concentration, composition, and microstructure. Modified from (O'Reilly, 1984).

	Intensive (independent of concentration)	Extensive (dependent on concentration)
Intrinsic (Dependent on composition)	Curie Temperature (T_C)	Magnetic Saturation (M_S) High-field Susceptibility (κ_{HF})
Extrinsic (Dependent on composition and Microstructure)	Coercivity (B_C) Coercivity of remanence (B_{CR}) M_{RS}/M_S Verweij Transition Temperature (T_V) Königsberger ratio (Q) Unblocking Temperature (T_{UB})	Saturation Remanence (M_{RS}) -and other remanence measurements (κ_{ARM} , p_{ARM}) Low-field Susceptibility (κ)

From Table 3-1 it can be seen that due to their intrinsic nature, Curie Temperature is an excellent property to assess magnetic composition whereas Magnetic Saturation is useful for determining concentration. The measurements in the extrinsic section of Table 3-1 can also be useful but usually involve either a combination of measurements or set assumptions about the rock in question. These magnetic assessments may be more complicated because of the added dependency of Microstructure, which may include grain size, shape, internal stress and interactions, but added variables also mean added information in the process.

Magnetic granulometry determines either the actual or effective magnetic grain size of a mineral. Effective magnetic grain size refers to magnetic domain state or behaviour of a magnetic particle, regardless of the actual grain size dimensions of the particle. Domain states change from superparamagnetic (SP), to single domain (SD), to pseudo-single domain (PSD), and to multidomain (MD) with increasing grain size. Magnetite has been the most extensively studied magnetic mineral due to its dominance in both volume and magnetic contribution. Hence, most conventional magnetic granulometric studies focus only on converting domain states to effective magnetite grain sizes, although there are exceptions (Hunt et al, 1995, their table 2 for references).

- Multi-domain (MD) - Containing several magnetic domains, each with a domain wall that can usually move when a weak magnetic field is applied ($>2 \mu\text{m}$)
- Pseudo-single domain (PSD) - A magnetic domain that behaves as a single-domain particle (usually between 2 to $0.1 \mu\text{m}$)
- Single domain (SD) - A grain containing only one magnetic domain (usually between $0.1 \mu\text{m}$ & $0.02\mu\text{m}$)

- Superparamagnetic (SP) - A ferromagnetic grain that has strong paramagnetic properties, but loses any remanence over a few minutes (usually $< 0.02\mu\text{m}$; Borradaile & Jackson, 2004)

For titanomagnetites, it may not be possible to define universal magnetic domain sizes because of microstructural variations from grain to grain and rock to rock. However, the boundaries for PSD probably lie between 0.5 and a few μm (O'Reilly, 1984)

There are basically two types of magnetic measurements that can be used for magnetic granulometry. The first method is the use of magnetic hysteresis loops, and the second involves the analysis of different types of remanent magnetization (Banerjee et al., 1981).

In the most simplistic terms, magnetic hysteresis measures a sample's standardized coercivity and remanence properties at a constant temperature to deduce information about the samples magnetic mineralogy and magnetic volume or grain size.

Remanent magnetization studies also compare remanence measurements with different components of the Néel equation to deduce a sample's magnetic volume.

3.2 - Purpose

Studies of the magnetic mineralogy of marine sediments tend to fall into a number of categories; commonly related to continuous sequences, hence "magnetostratigraphy".

1. Investigations to determine different mineralogical contributions to AMS and ARM (Borradaile, 2001; Rochette et al., 1992; and succinctly reviewed by Jackson, 1991).

2. Investigations of biogenic (mainly bacterial) contributions of magnetic material to marine sediments (e.g., Kirschvink & Chang, 1984; Chang & Kirschvink, 1989; Vali & Kirschvink, 1989; McNeill, 1990).
3. Investigations to determine core correlation and as an indicator of variations of terrigenous sedimentation (e.g., Mead et al., 1986; Hall et al., 1989).
4. Investigations studying diagenesis, authigenesis, or oxidation of magnetic minerals (e.g., Karlin & Levi, 1985; Karlin, 1990a,b; Wang & Van der Voo, 2004).
5. Investigations examining the origin of the sediment NRM, in order to assess the reliability of NRM data for the determination of the geomagnetic paleopolarity and relative paleointensity (e.g., Kent & Lowrie, 1974; Lowrie & Heller, 1982; Tauxe & Wu, 1990).

The present study examines:

1. Hysteresis to determine grain sizes and some magnetic mineralogy (Borradaile & Hamilton, 2003; Dunlop, 2002a,b; Wang & Van de Voo, 2004)
2. κ and κ_{ARM} to determine concentration and mineralogy
3. SIRM and thermal demagnetism in various ways to determine composition and concentration
4. κ_{ARM}/κ (grain size and volume)(King et al., 1982; Banerjee et al, 1981)
5. $\kappa_{ARM}/SIRM$ and $SIRM/\kappa$ to determine relative grain size (Vigliotti et al., 1999).

3.3 - Hysteresis

A rock's remanence-bearing properties are characterized by saturation isothermal remanence (SIRM = M_{RS}) after exposure to a large field or magnetic saturation (M_S) *in the presence* of a large field. Similarly, the tenacity of remanence is important, measured by coercivity (B_C , in the presence of a field), coercivity of remanence (B_{CR} , required to remove M_{RS}) or the ease of demagnetation in an alternating field (AF) (Fig. 3-1). Wasilewski (1973) plots B_C against B_{CR} to infer magnetite grain size; and similarly, Day et al. (1977) plots M_{RS}/M_S against B_{CR}/B_C . The "Day plot" has been most popular, until recently, when plotting hysteresis data.

The success of the Day plot lies in its reasonable success in separating behaviour according to the presence of single-domain (SD), pseudo-single domain (PSD) or multidomain (MD) magnetite, especially where the specimens contain magnetite in just one of these categories. However, SP magnetite is difficult plot due to its highly variable magnetic properties, which overlap other domains in some instances. These categories are traditionally shown as rectangular fields with the data from sample sets plotting clusters in one or more of the domain sizes (Fig. 3-2). Unfortunately, although these plots are highly functional and user-friendly, they fail to discriminate the reality of mixed grain-size distributions that encompass more than one grain size, or more than one magnetic mineral or those that include SP magnetite. Dunlop (2002a,b) addressed these issues with the addition of domain-state mixing lines to the Day plot and studies of theoretical and actual mixing lines of magnetite with titanomagnetite (Fig. 3-2).

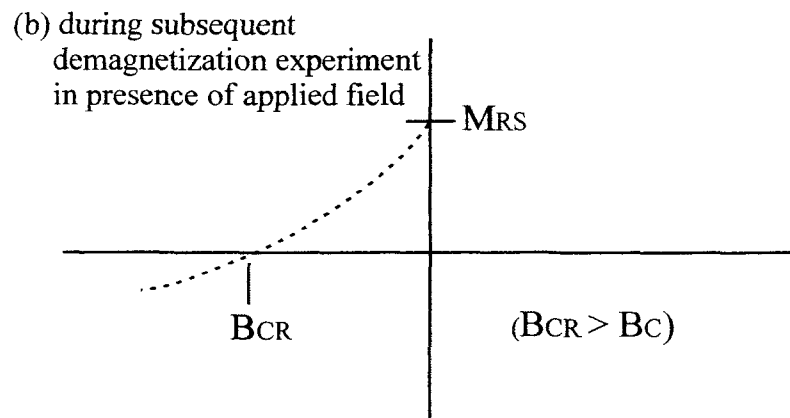
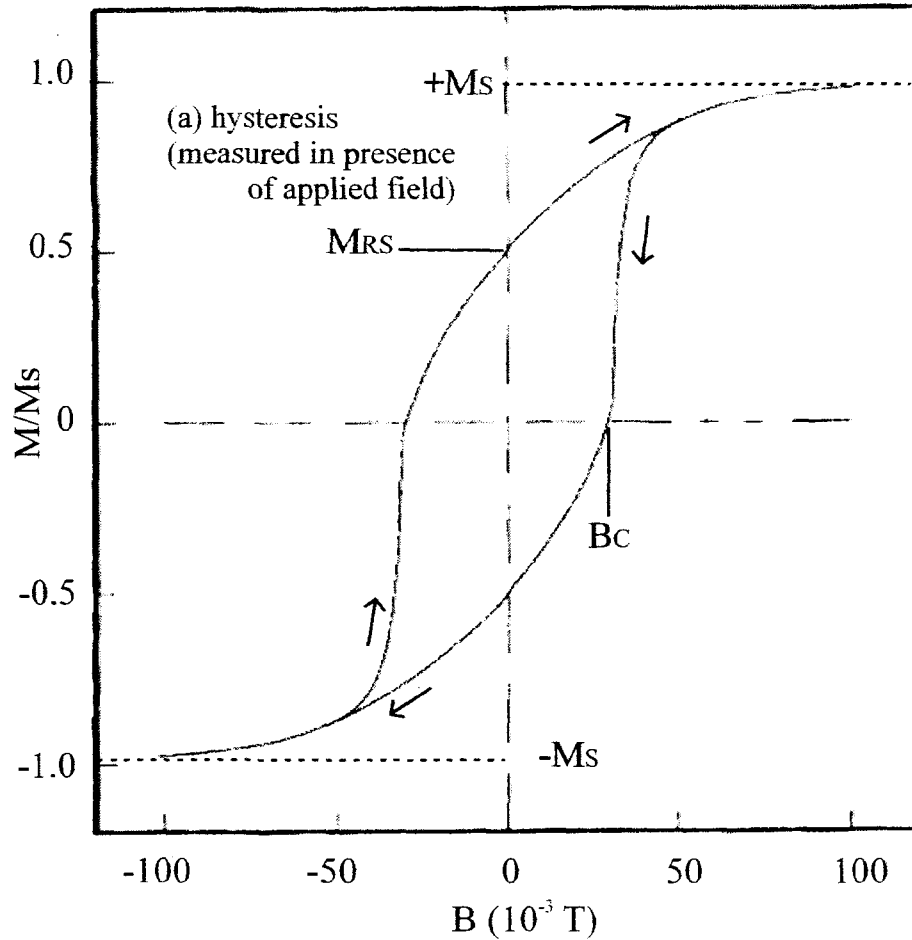


Figure 3-1. (a) An example of a hysteresis loop and the magnetic properties used in a Day Plot (1977); M_s = saturation magnetization, BC = coercivity, MRS = remanent saturation at zero applied field. (b) in a separate demagnetization experiment, BCR = coercivity of remanence.

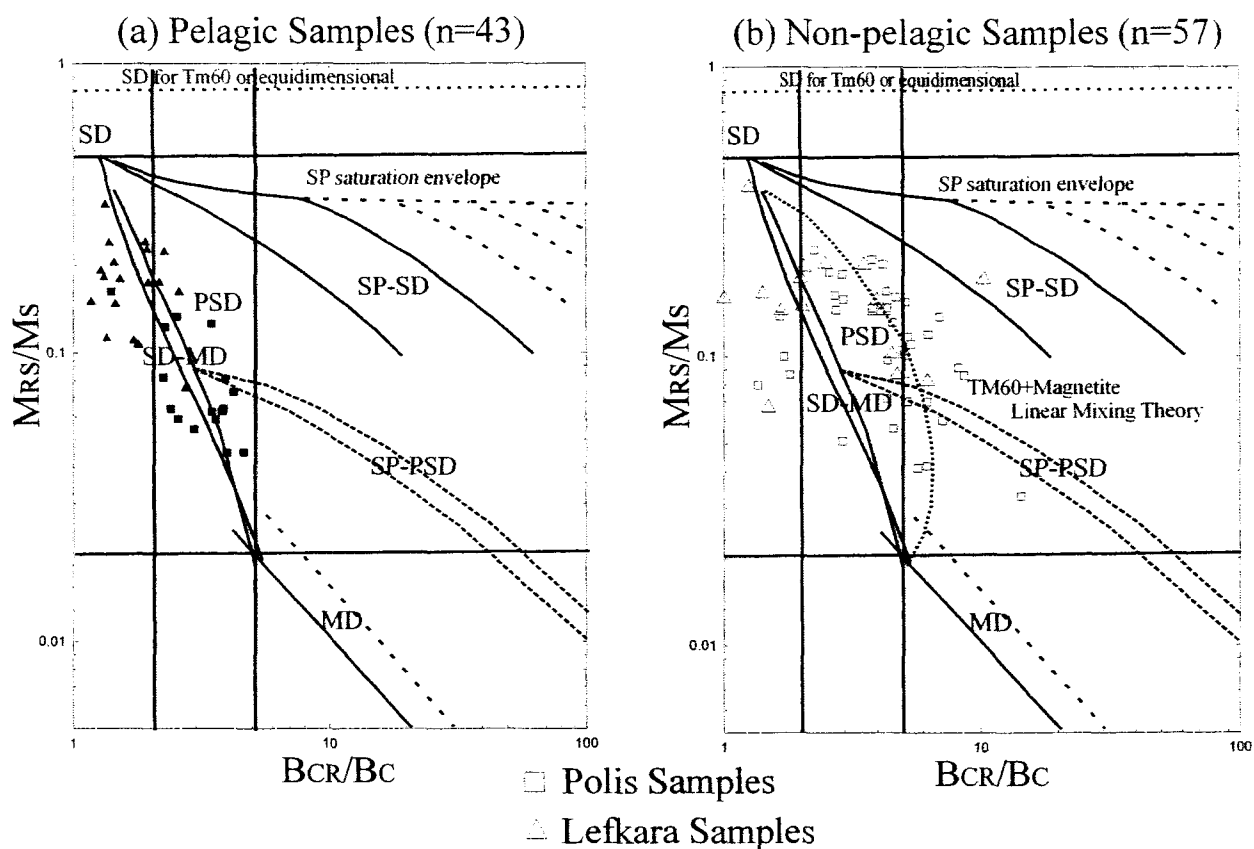


Figure. 3-2. Day Plots (Day et al. 1977) with the effective grain sizes (magnetic domains) and some relevant mixing lines of these domains (Dunlop, 2002a). (a) Pelagic limestone samples (n=43) plotting along SD-MD mixing lines (Dunlop, 2002a) in PSD domain of Day et al. (1977). (b) Non-pelagic limestone samples (n=57) mostly plotting along TM60 + magnetite linear mixing theory line (Dunlop, 2002a) in the PSD domain (Day et al., 1977).

Recently, Wang & Van der Voo (2004) have modified the Day plot by eliminating the variable B_{CR} and plotting only M_{RS}/M_S (or hysteresis squareness) against B_C to investigate differences in magnetic mineralogy of Mid-ocean ridge basalts (MORB) whose main magnetic minerals include titanomagnetite $Fe_{3-x}Ti_xO_4$ with $x = 0.6$ (TM₆₀), titanomaghemite (TM₆₀ low-temperature alteration product), and magnetite. They demonstrate that the theoretical linear relationship between these variables essentially

show M_S differences and since magnetite has a M_S about 3.8 times greater than TM_{60} , differences in MORB magnetic mineralogy can be and have been assessed experimentally (Fig.3-3). Furthermore, Wang & Van der Voo (their fig. 6, 2004) demonstrate that samples with titanomaghemite plot at different point between the TM_{60} and magnetite trend-lines, confirming progressive oxidation of TM_{60} over time perpendicular to the ridge axis.

Other progressive hysteresis plots examine M_{RS}/M_S versus B_C versus B_{CR} in three-dimensional projections and use either regression surfaces (Borradaile & Lagroix, 2000) or confidence regions in two-dimensional planes (Borradaile & Hamilton, 2003) to assess differences in sample sets. Spectral methods using the entire hysteresis curve instead of just four points, have also been employed successfully and have given insight into the magnetic behaviour of bimodal mixtures (Jackson et al. 1990; Carter-Stiglitz et al., 2001). Unfortunately, these techniques are unfeasible in the present study due to their rather involved statistics and procedures.

An alternating gradient force magnetometer (MicroMag) was used to determine the parameters of the hysteresis loop. The instrument was developed commercially by Princeton Measurements Corporation (Princeton, NJ, USA). The specimen required has dimensions of no more than 2mm x 2mm x 1mm and its mass cannot exceed much more than ~100 mg. Thus it is difficult to make representative measurements for rocks that are heterogeneous, at that scale.

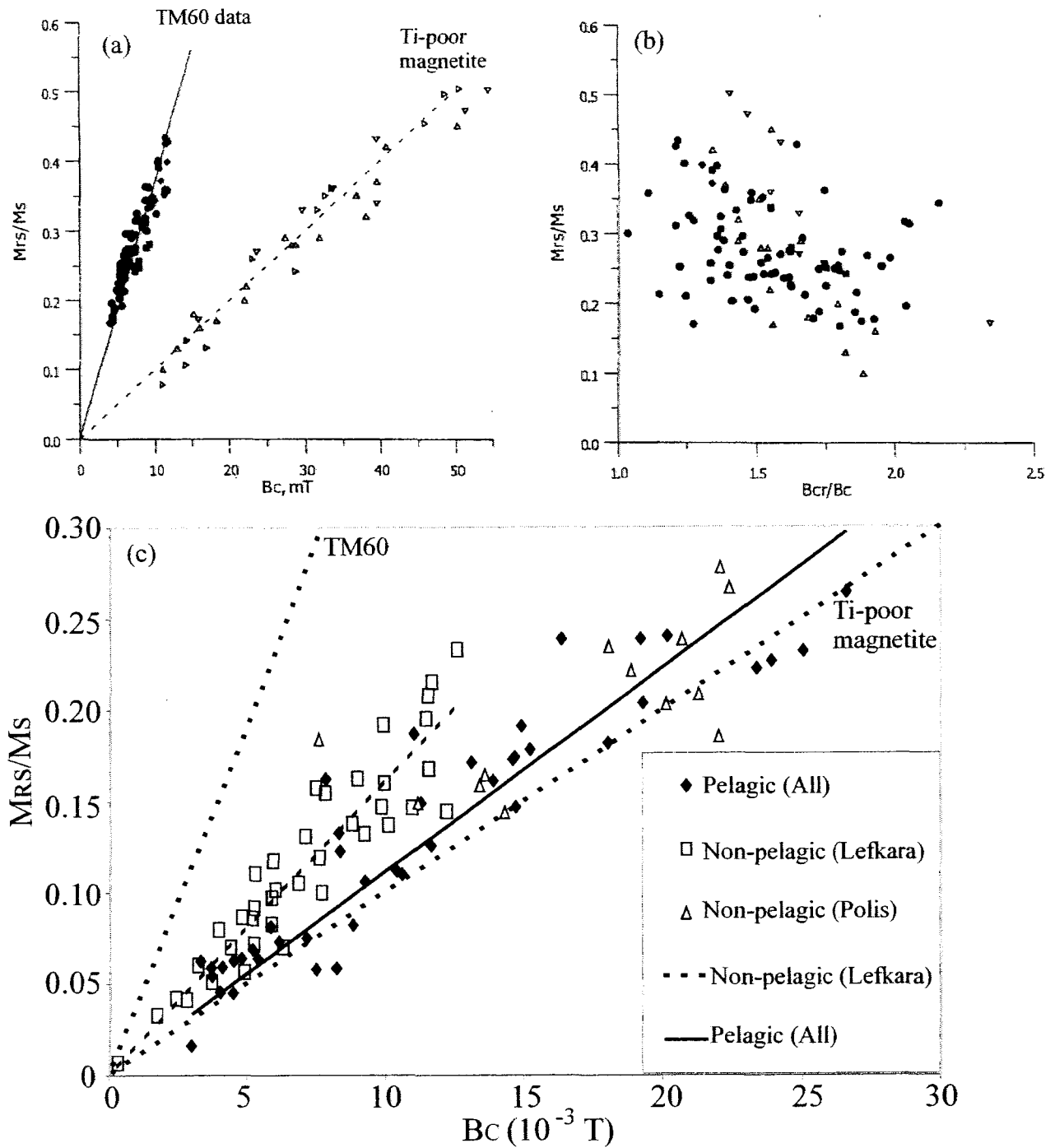


Figure 3-3. (a) Squareness (M_{RS}/M_S) versus coercive force (B_c) for young unoxidized MORB (closed symbols) and low-Ti or Ti-free magnetite with different grain sizes (open triangular symbols). (b) Day-plot of same samples showing no diagnostic differences between TM60 and low-Ti magnetite (data and graphs reproduced from Wang & Van de Voo, 2004). (c) Squareness (M_{RS}/M_S) versus coercive force (B_c) for Cyprus limestones with ti-poor magnetite (slope=0.01) and TM60 (slope=0.38) trend-lines (Wang & Van de Voo, 2004). Pelagic ($n=43$, slope=0.0112, $R^2=0.8473$), Lefkara non-pelagic ($n=39$, slope=0.162, $R^2=0.863$), and Polis non-pelagic ($n=13$).

The main limitation of this method is the size of the standard rock-magnetic core specimen being tested. The average mass of the limestone cores for this study is ~23 g (10.55 cm³), therefore, at the most the Micromag hysteresis specimen represents ~0.04% of the core from which it was taken (Borradaile & Lagroix, 2000). If any heterogeneity is present within the core then the hysteresis data from the small sample may not represent the core sample's magnetic properties accurately. Fortunately, the limestones of this study are relatively fine-grained and nearly homogeneous at that scale, so the hysteresis data of the smaller specimens is representative as replicate measurements show. That being said, hysteresis was only used as a somewhat preliminary magnetic study to look at the samples as a whole to assess overall grain sizes and possible magnetic compositional variations. Hysteresis was not examined in a stratigraphic context because intra-sample variation may obscure the inter-site variation in the stratigraphy.

A selection of specimens from early sample sets (before stratigraphic sampling was performed) was chosen randomly to examine some of their magnetic characteristics by use of hysteresis plots. These samples were grouped based on locations and basic lithology/facies (i.e., pelagic and non-pelagic) (Appendix 6). Pelagic limestones (chalks) (n = 43) were characterized by aphyric grain size and visible skeletal and non-skeletal debris and other visible detritus characterized non-pelagic limestones (n = 57). Although this classification scheme is not as detailed as others (Borradaile et al, 1993), it is appropriate for the purpose of this study. The hysteresis data was plotted on Day Plots with the addition of selected mixing lines to assess both grain-sizes and possible compositional differences (Fig. 3-2.) also as Mrs/Ms (or hysteresis squareness) versus Bc to investigate possible differences in magnetic mineralogy (Fig. 3-3c.).

In Figure 3-2a all samples plot on or near the magnetite SD-MD mixing line in the PSD range with the Polis samples cluttering closer to the SD range than the Lefkara cluster of samples. The tight clustering of samples seen in the Polis and Lefkara pelagic samples attest to the homogeneous nature and similar depositional environment of these fine-grained samples. The non-pelagic samples (Fig. 3-2b.) exhibit a much wider distribution on the Day plot due to either the more heterogeneous nature of these coarser grained samples or differences in depositional environments. These samples mostly plot to the right of the SD-MD mixing line near the right boundary of the PSD range. Unfortunately the constitution of these samples is more difficult to interpret due to the many mixing possibilities that could cause the samples to plot in this area and the fact that coercivity parameters do not behave linearly as a function of mixing ratios (Carter-Stiglitz et al., 2001). For this reason, theoretical mixing curves of data with bimodal mixtures usually fail to completely explain data from natural mixtures (Dunlop, 2002a). When comparing our samples to experimentally derived mixing lines (Dunlop, 2002a), the majority of non-pelagic samples of Cyprus tend to plot between the SD-MD mixing line for magnetite and the SD-MD mixing line for TM_{60} . Therefore, these samples *could* represent mixtures of magnetite and TM_{60} but this is inconclusive due to other possibilities that could have similar effects, such as the presence of other minerals like titanomaghemite, minor hematite or SP grains of magnetite.

By plotting M_{RS}/M_S (or squareness) versus B_C (Fig. 3-3c.) it is hoped that more insight into differences in magnetic mineralogy will be evident. On examination of the pelagic samples it is noted that they have a well-defined trend-line near that of magnetite. In contrast, the non-pelagic Lefkara samples form a well-defined trend line between the

magnetite trend-line and TM_{60} trend-line, whereas the non-pelagic Polis samples do not form a well-defined trend-line due to their small sample set ($n = 13$), but do tend to plot near the magnetite trend line. There are two main possibilities for the well-defined trend line of the non-pelagic Lefkara samples. First, these samples magnetic mineralogy may be dominated by titanomaghemite of some intermediate oxidation state, such as that found in oxidized pillow basalts (Wang & Van der Voo, 2004). Second, these samples may have a relatively uniform bimodal mixture of magnetite and TM_{60} . The non-pelagic Polis samples probably represent non-uniform mixtures of different magnetic minerals within a small size range, but the small sample set ($n = 13$) and the wide age range (55-0 Ma) that the Polis rocks cover, interpretations are somewhat uncertain.

3.4 - Sedimentary sequence and Sampling Strategy

Omodhos-Pakhna, Lefkara, and Lymbia (subareas IV-VI from AMS section, Fig. 2-5, $N = 55$) were sampled with special attention to stratigraphic sequence for examination of stratigraphic changes in magnetic mineralogy (Appendix 2 & 7). These three subareas cover a relatively continuous sequence of samples from lower Lefkara formation (54 Ma) to upper Pakhna Formation (6Ma) (Figs. 3-4 & 3-5). Although their biostratigraphy is unknown, numerous previous studies have been conducted on the sections (Mantis, 1970; Eaton and Robertson, 1993; Eaton, 1987; Kahler, 1994; Kahler and Stow, 1998; Lord et al., 2000). Unfortunately, the distribution and development of different lithological units within the Lefkara Formation is not uniform due to tectonic events, paleotopography, and redeposition of sediment (Lord et al., 2000). Therefore, the ages for the sections in this study are most precise at the identifiable stratigraphic

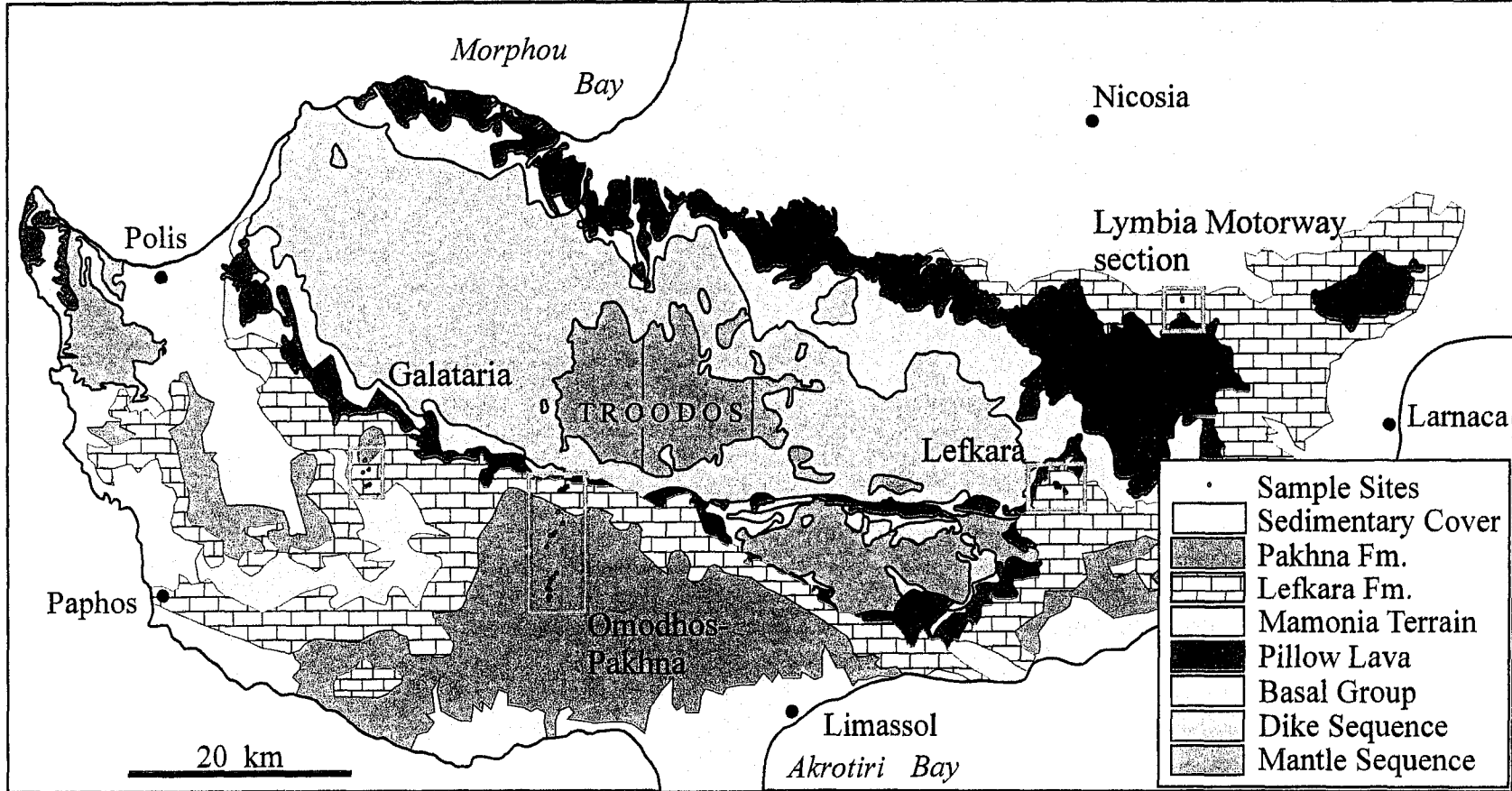


Figure 3-4. Geological map of South and West Cyprus showing locations of stratigraphic sampling.

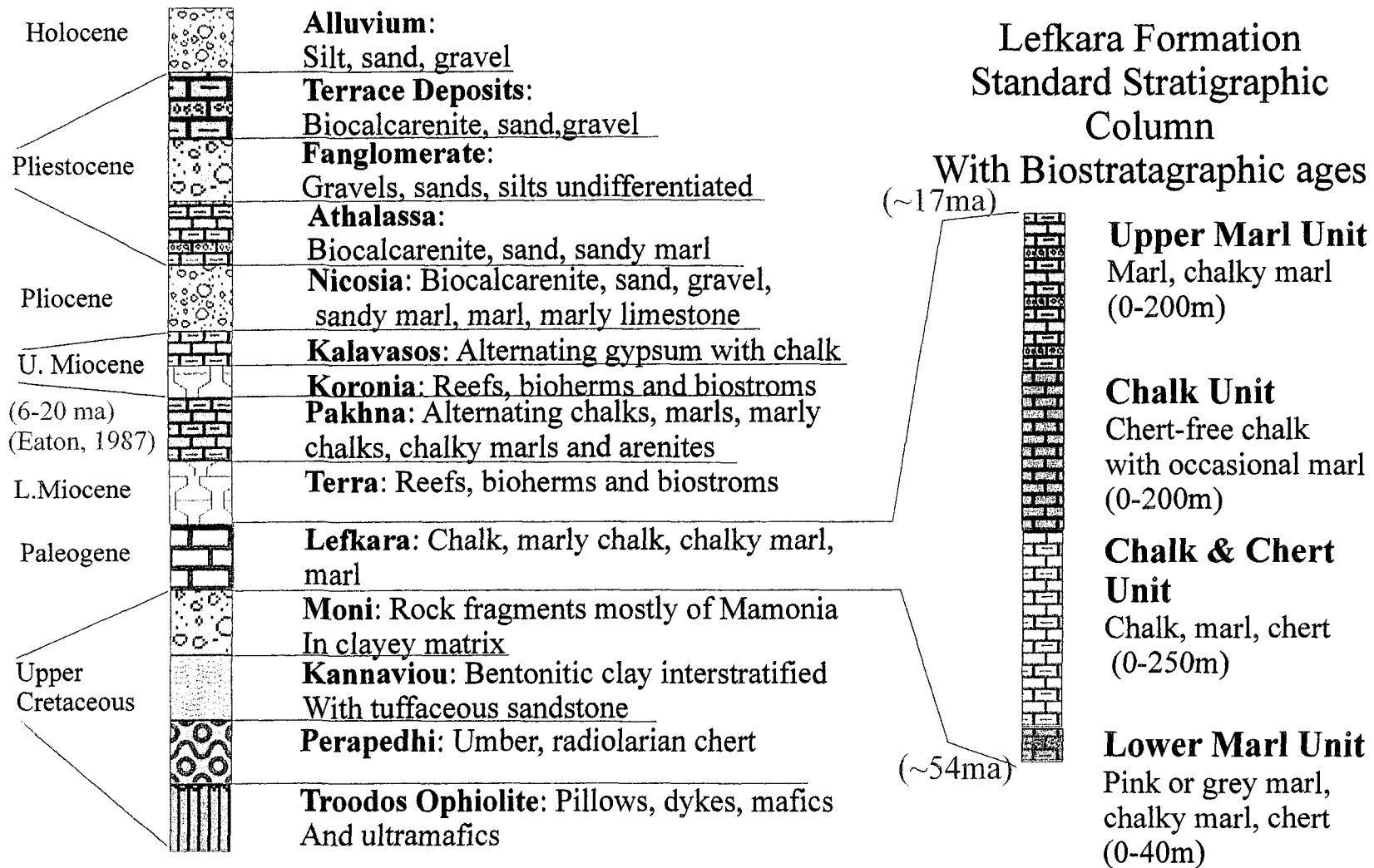


Figure 3-5. Circum Troodos Sedimentary Succession and ultramafic basement (Geological survey department of Cyprus 1979) with biostratigraphic ages for relevant limestone units.

boundaries from the from the most proximal and accepted biostratigraphic study. Samples not taken near stratigraphic boundaries have their ages estimated by stratigraphic order and estimated sedimentation rate. Samples that have overlapping age determinations or are less than 0.5 Ma apart in age are averaged. The continuous nature of our sample set is punctuated by an approximately 15 million year hiatus between 35 Ma to 20 Ma. This hiatus corresponds to the start of major glaciations in the Southern Hemisphere (Haq et al., 1987) and is thought to be caused by subsequently enhanced bottom current erosion (Vali et al., 1980; Miller et al., 1987). Therefore, this Cyprus hiatus does not reflect the effects of tectonic uplift as proposed by Robertson et al. (1991) but represent more global sedimentological effects (Kahler and Stow, 1998)

3.5 – Methods for Magnetic Mineralogy

As shown in the chapter on AMS, the specimen's bulk susceptibilities $[\kappa = \sqrt[3]{(k_{MAX} k_{INT} k_{MIN})}]$ can be a first guide to the magnetic mineralogy.

By examining κ in relation to a sample's stratigraphic sequence it is possible to see changes in mineralogy through time and in different formations (Fig. 3-6). κ_{ARM} can also be examined in the same way as κ (Fig. 3-6), but since it measures remanence, variation between samples are completely due to ferromagnetic minerals and are not affected by a sample's diamagnetic or paramagnetic minerals. Therefore, κ_{ARM} is a better indicator of stratigraphic variation of magnetite than κ .

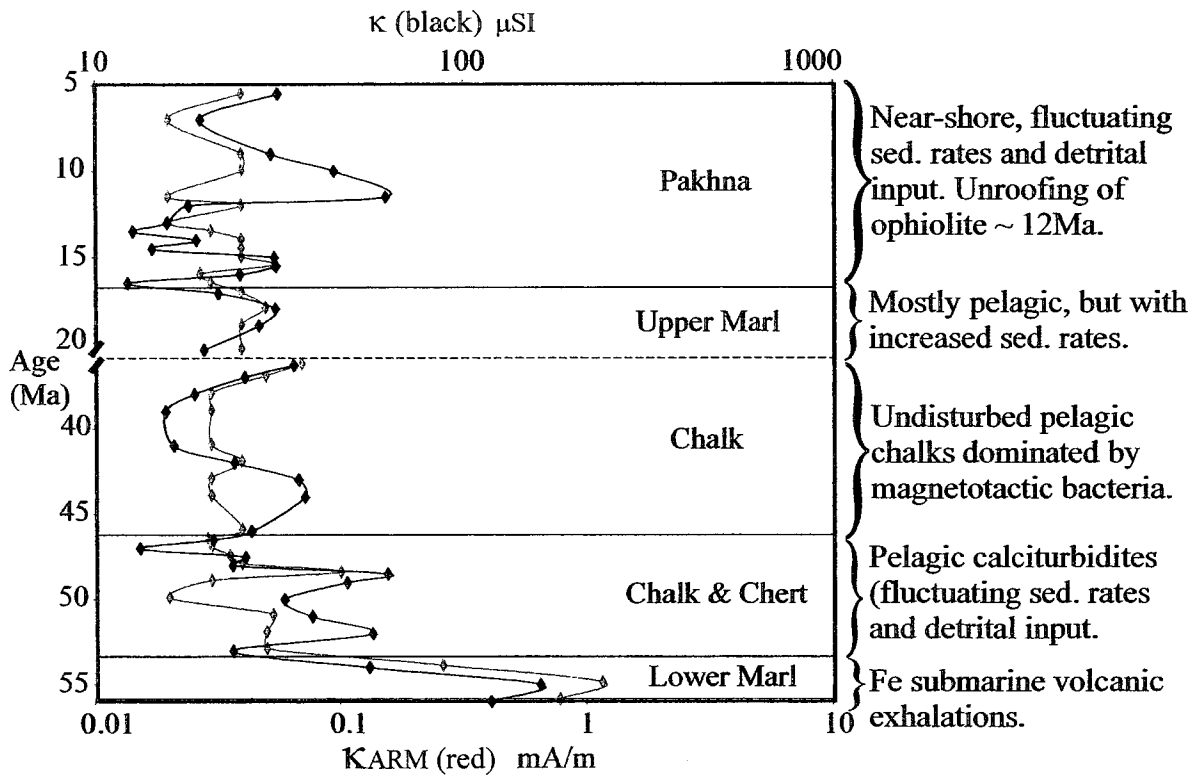


Figure 3-6. KARM and κ versus stratigraphic sequence, demonstrating differences in magnetic mineralogy through time.

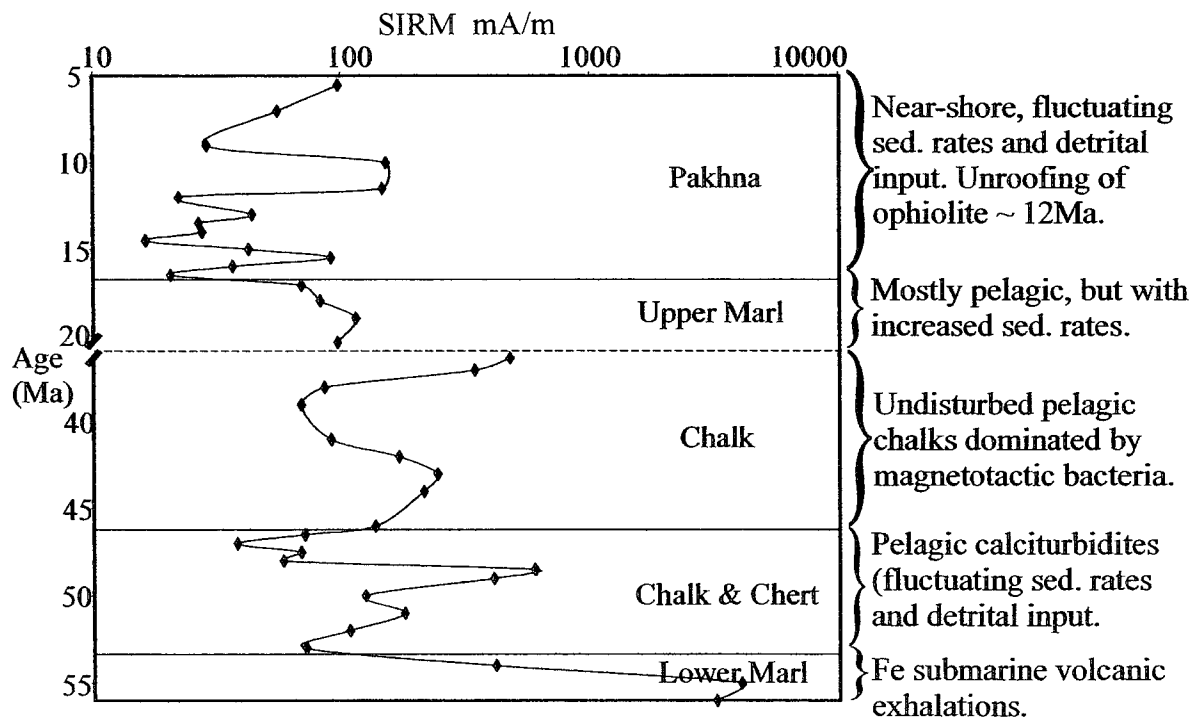


Figure 3-7. SIRM versus stratigraphic sequence, demonstrating differences in magnetic mineralogy through time.

The examination of SIRM results should reveal magnetic contribution better than κ ARM and κ because it is not affected by a sample's diamagnetic or paramagnetic minerals (like κ) and, compared to κ ARM values, grain size has very little affect (for the size range present in these samples) (Peters & Dekkers, 2003). Therefore SIRM is primarily a function of ferromagnetic mineralogy and concentration (Fig. 3-7). The SIRM data demonstrates a slight overall decrease in remenance with fluctuating values in the Pakhna formation and the Chalk & Chert section of the Lefkara formation similar to the κ ARM data.

As seen in the previous chart of magnetic properties (Table 3-1), Curie temperature (T_C) is the only intrinsic property, which is dependent only on ferromagnetic mineral composition. Therefore by comparing Curie Temperature data with SIRM data one can infer the different magnetic contribution of minerals. By thermally demagnetizing a specimen to 200°C, one essentially randomizes the SIRM intensity caused by the TM_{60} fraction of the specimen. Therefore by subtracting the SIRM intensities after thermal demagnetization of 200°C from the original SIRM, the SIRM caused by the TM_{60} fraction can be isolated ($SIRM_{TD200}$). Furthermore, to minimise the effects of differing sedimentation rates one can normalize it to the original SIRM by the following equation:

$$SIRM_{TD200}/SIRM \times 100 = \% \text{ of SIRM intensity after TD200} = \% \text{ of SIRM } \textit{not} \text{ caused by } TM_{60}.$$

The $SIRM_{TD200}/SIRM$ data (Fig. 3-8) exhibits a general trend to increasing TM_{60} contribution with the exception of the Chalk Unit. The low TM_{60} contribution of SIRM but overall high SIRM intensity of the Chalk unit may represent a lack of clastic input with the major magnetic contribution due to fossil magnetotactic bacteria.

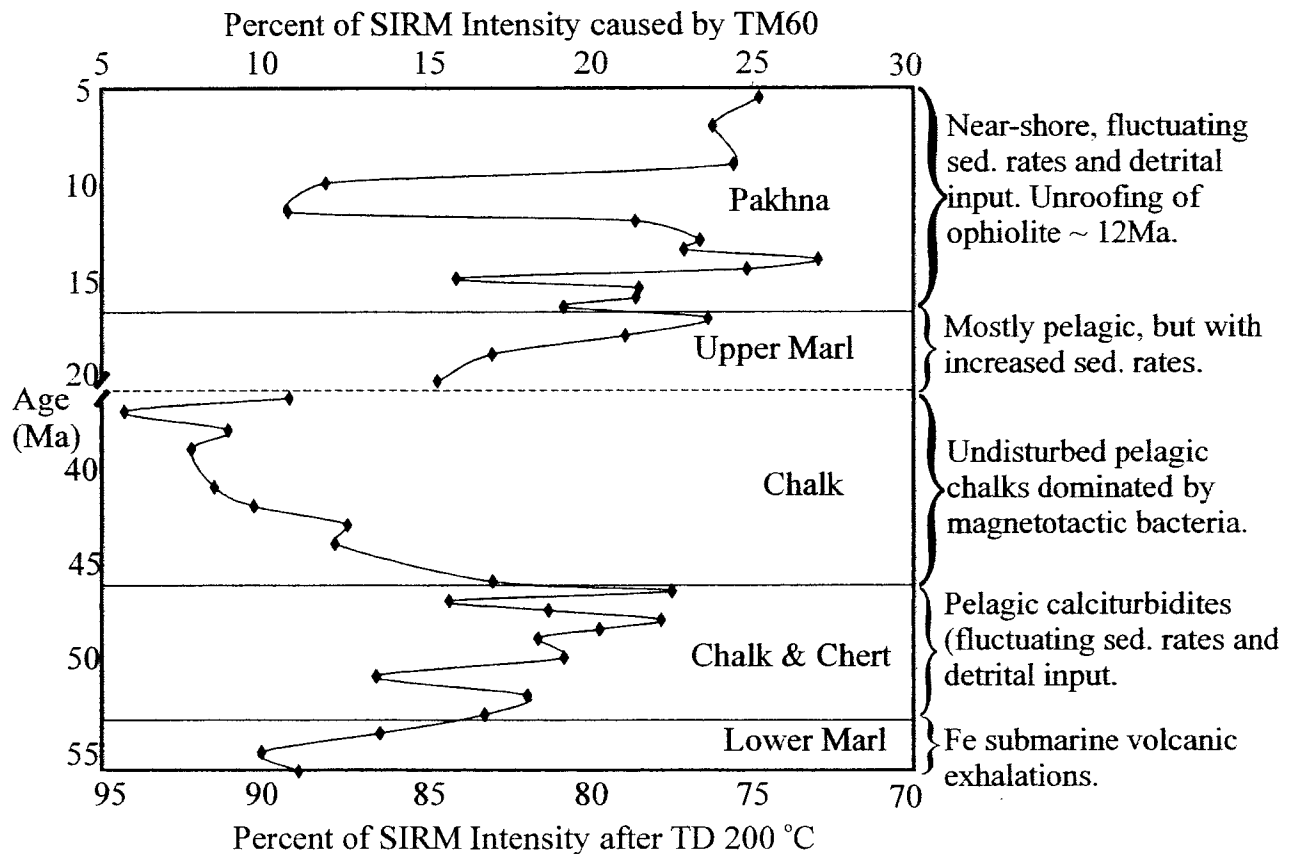


Figure 3-8. SIRM_{200°C}/SIRM versus stratigraphic sequence. SIRM values after thermal demagnetization to 200°C/SIRM values before thermal demagnetization versus stratigraphic sequence demonstrating differences TM60 contributions through time.

Many factors may complicate the combination of SIRM data with Curie temperatures. First, the use of $SIRM_{TD200}/SIRM$ ratio to analyze TM_{60} contribution assumes that no other high remanence/low T_C minerals are present (such as goethite). This possibility can be assessed quite easily by examination of the hysteresis data. Second, oxidation of TM_{60} increases T_C , $SIRM_{TD200}/SIRM$ only isolates TM_{60} with low oxidation coefficients. This in turn, means that fluctuations in $SIRM_{TD200}/SIRM$ ratios may represent fluctuations of TM_{60} contribution *or* fluctuation rates in the oxidation of TM_{60} (or both). This complication could possibly be assessed by performing thermal demagnetization on the same samples at 300°C and examining $SIRM_{TD300}/SIRM$ ratio versus the $SIRM_{TD200}/SIRM$ ratio. The difference in ratios should be equivalent to TM_{60} with an oxidation coefficient of 0.2 (Ozdemir and O'Reilly, 1982a). Higher oxidation TM_{60} components of these specimens would not be possible to assess in a similar fashion due to the titanomaghemite inversion temperature at 350°C , which would change the mineralogy.

3.6 – Methods for Magnetic Granulometry

Both κ and κ_{ARM} , dependent variably on magnetic domain size; κ values increase through the SD PSD-MD range whereas κ_{ARM} exhibits the reverse trend through the same range. Therefore, ratios of κ_{ARM}/κ can show grain size differences with higher ratios of κ_{ARM}/κ indicative of finer magnetite sizes (Banerjee et al, 1981). Experimental verification of this relationship between κ_{ARM} and κ lead to a simple phenomenological model, which can be used to detect changes in either the relative grain-size or amount of magnetite in natural materials (Fig. 3-9)(King et al., 1982).

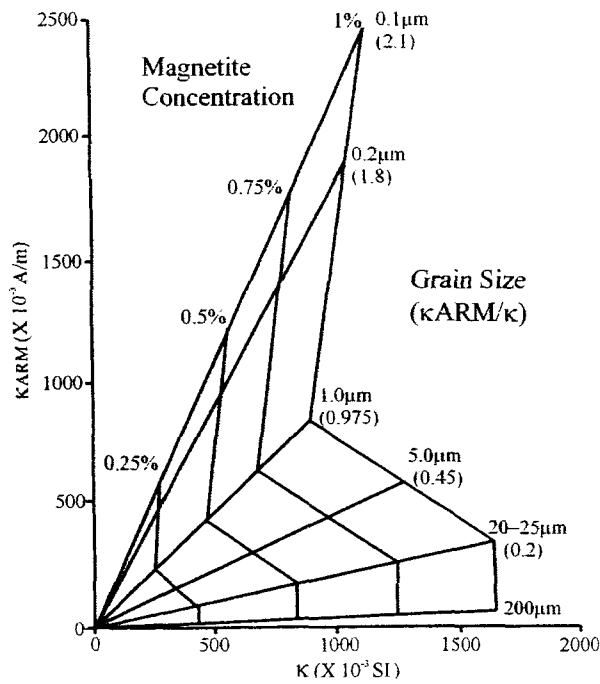


Figure 3-9. King et al. (1982) Plot. K_{ARM} versus K , and relative grain-size or amount of magnetite in natural materials using experimental models.

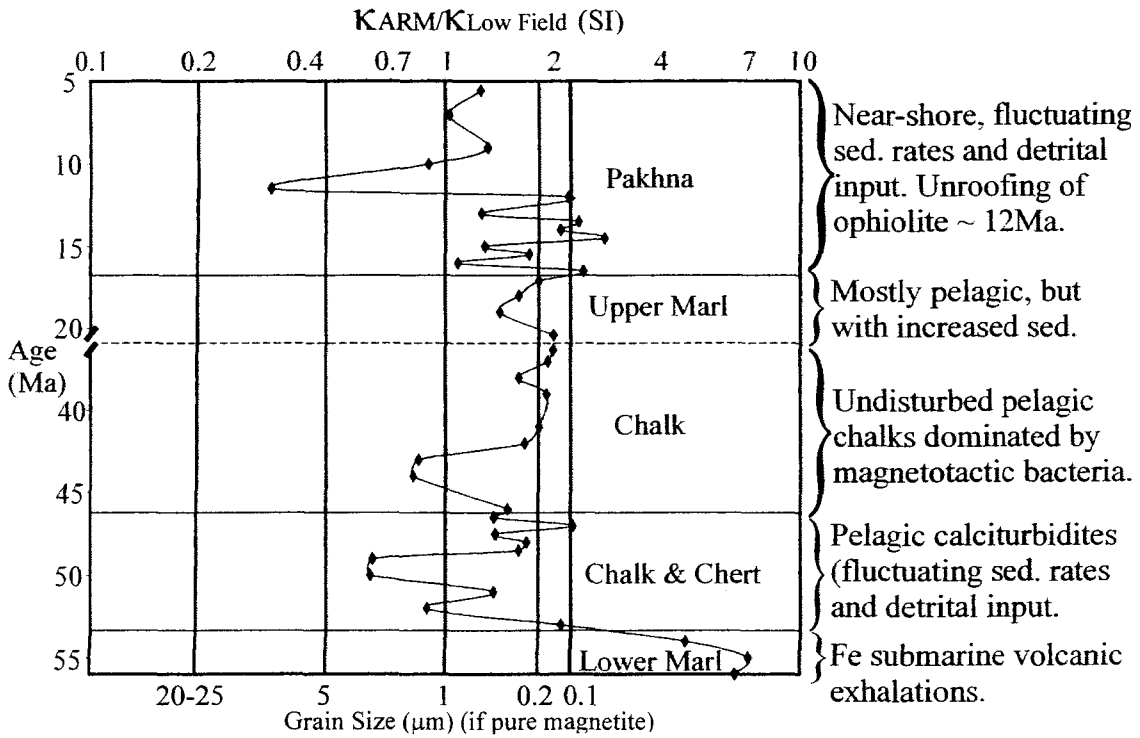


Figure 3-10. $K_{ARM}/K_{Low Field}$ versus stratigraphic sequence demonstrating ferromagnetite grain size changes through time. Grain size from King et al. (1982) assuming pure magnetite in low concentrations.

It must be stressed that several complications have to be considered when using the King et al., (1982) model quantitatively. First, the presence of SP magnetite would only affect the κ value and not the κ_{ARM} value of a sample, making the sample appear to have coarser magnetite than actually present. Hysteresis data from the present study shows that SP magnetite is probably not a contributing factor in these samples. Second, the effect of magnetic interactions with varying concentrations of magnetite may affect κ_{ARM}/κ differently. Again this is not a problem for this study due to the extremely low concentrations of ferromagnetic minerals in these samples as seen from the bulk κ values mentioned above. Third, an increase in the shape anisotropy of magnetite from 1 to 1:1.5 (axial ratio) may increase the κ_{ARM}/κ value slightly. Fourth, complications arise due to the shifting of the abscissa by the κ of the non-magnetic matrix. This final complication may be the most likely to affect the effectiveness of the King model for the samples in this study since minor amounts of clay may switch a limestone sample from diamagnetic to paramagnetic. The abscissa is shifted to larger values by a paramagnetic matrix and to lower values by a diamagnetic matrix.

Due to the extremely low κ_{ARM}/κ values found in the limestone samples (and therefore low magnetic mineral concentration values), the standard King model cannot be used. Instead, the κ_{ARM}/κ ratios and their corresponding grain-size are plotted on a stratigraphic column with the corresponding specimen's κ_{ARM}/κ value (Fig. 3-10). From this data, it can be seen that the majority of the specimens (with the exception of the Lower Marl) have magnetite in the PSD size range (PSD $\sim 0.1\mu\text{m}$ to $20\mu\text{m}$), which corresponds acceptably with the hysteresis data. In fact, most of the upper chalk unit plot in the $0.2\mu\text{m}$ to $0.1\mu\text{m}$ range, which corresponds with the size of magnetotactic bacteria

(Kirschvick, 1983) showing that these rocks have had little or no contamination from clastic or exhalative processes.

In addition to κ ARM/ κ ratios, relative grain size may also be examined using SIRM/ κ ratios (Fig. 3-11) and κ ARM/ SIRM ratios (Fig. 3-12) (Vigliotti et al., 1999). Similar to κ ARM/ κ , lower values of SIRM/ κ ratios and κ ARM/ SIRM ratios *should* correspond to larger magnetite grain sizes, but κ ARM /SIRM contradicts this. The simple reason for these discrepancies is that these ratios are dependent on composition as well as grain size. Since different minerals have different κ ARM, κ , and SIRM values their ratios will differ accordingly.

3.7 - Stratigraphic Interpretation of Magnetic Mineralogy and Granulometry

Lower Marl (56 to 53.5 Ma)

The lower marl represents the oldest unit of the Lefkara Formation overlying pillows at the section sampled (Lymbia) and umbers at some other locations (Fig. 3-5). These samples consist of pink marl, chalky marl and chert (Fig. 3-13). The samples of this formation are characterized by relatively high κ ARM/ κ representing very fine grain sizes, relatively high SIRM representing above average magnetic concentrations, and relatively low SIRM/SIRM_{TD200} ratios representing low TM₆₀ content (Fig. 3-14).

These magnetic properties and the pinkish hue of the samples indicate that the main magnetic carriers in these rocks are probably accumulations of very fine-grained Fe from hydrothermal exhalations of a nearby active vent system.

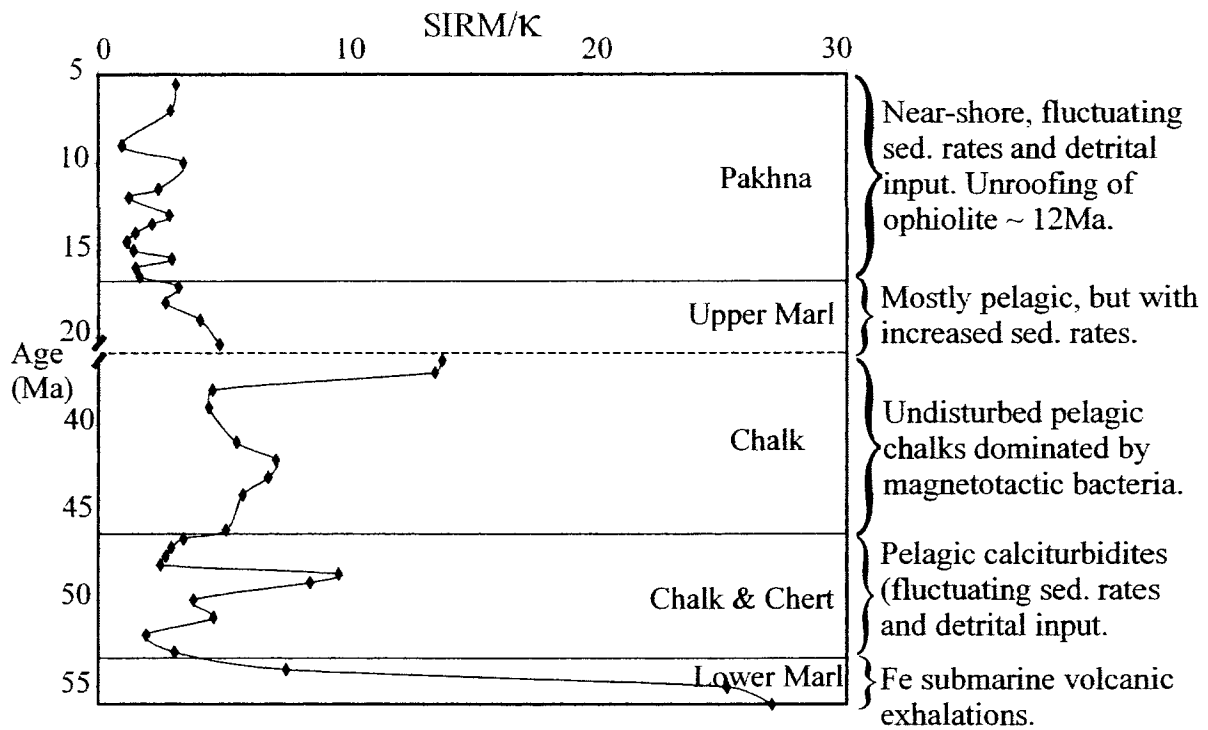


Figure 3-11. SIRM/K versus stratigraphic sequence.

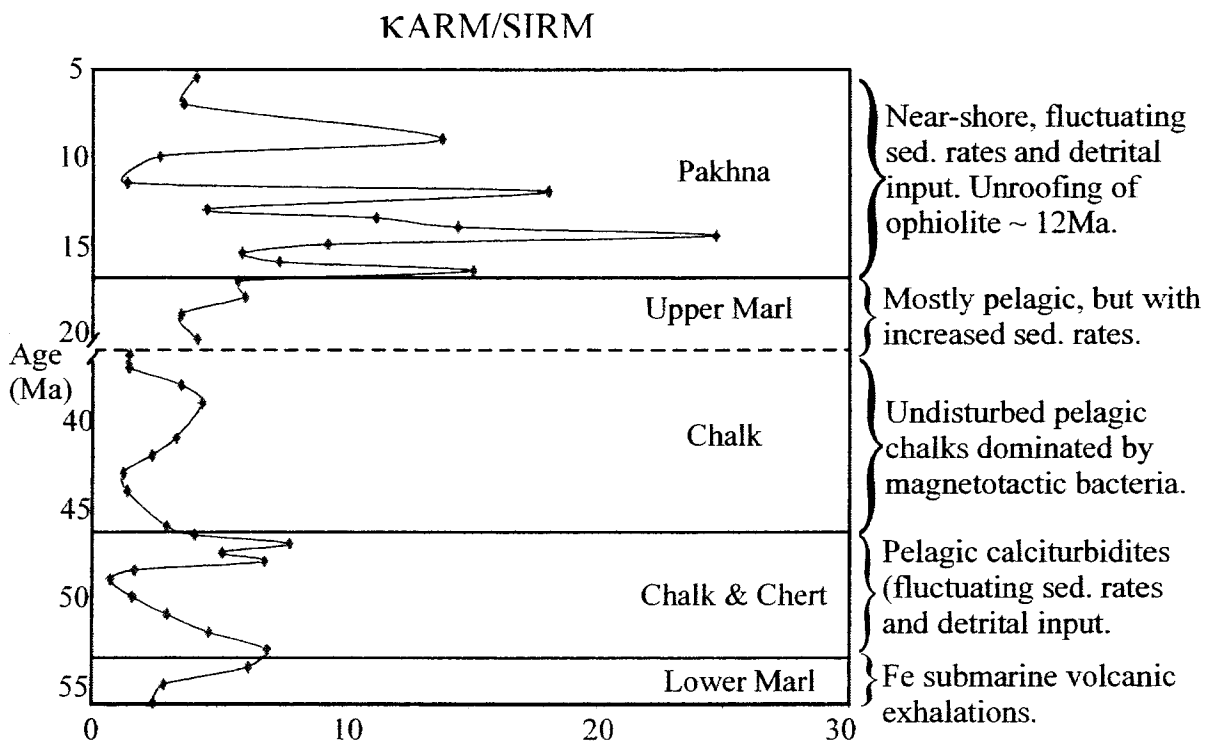


Figure 3-12. KARM/SIRM versus stratigraphic sequence.



Figure 3-13. Lefkara Lower Marl Unit. Lymbia highway section demonstrating the characteristic pink hue of the Lefkara Lower Marl unit.

Chalk and Chert (53.5 to 46.2 Ma)

The Chalk and Chert unit of the Lefkara formation is comprised of chalk marl, and chert and directly overlies the lower marl unit (Fig. 3-15). The samples of this section are characterized by fluctuating low K_{ARM}/K , fluctuating SIRM, and fluctuating high SIRM/SIRM_{TD200} ratios (Fig. 3-14).

These large fluctuations in magnetic properties can be attributed to the presence of abundant pelagic calciturbidites (Robertson, 2000), which would rework and redeposit differing amounts of coarser pelagic sediments with finer pelagic sediments of different mineralogies. These sediments were later partially replaced by chert.

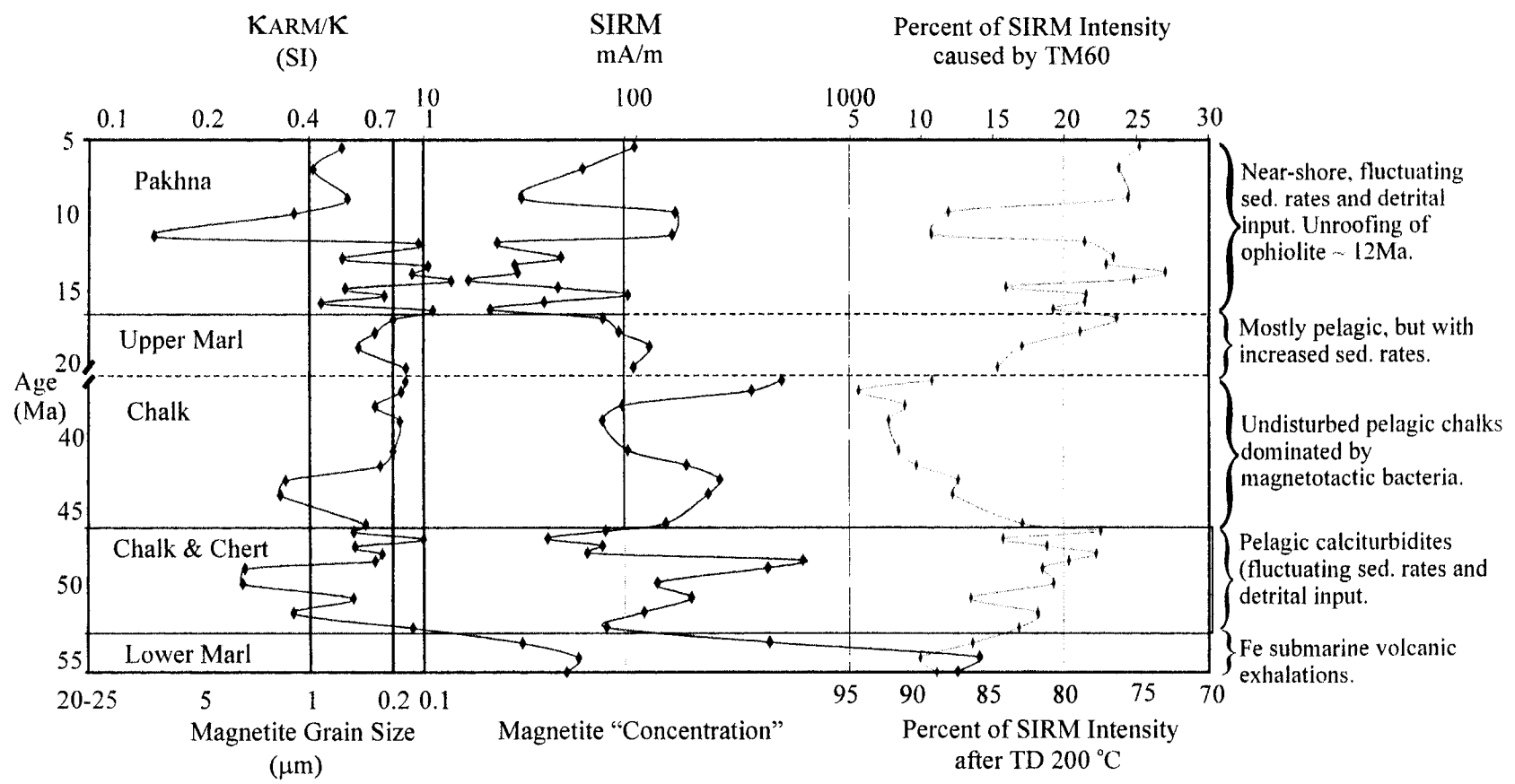


Figure 3-14. Amalgamation of Figures 3-10, 3-7, and 3-8 for ease of comparison.

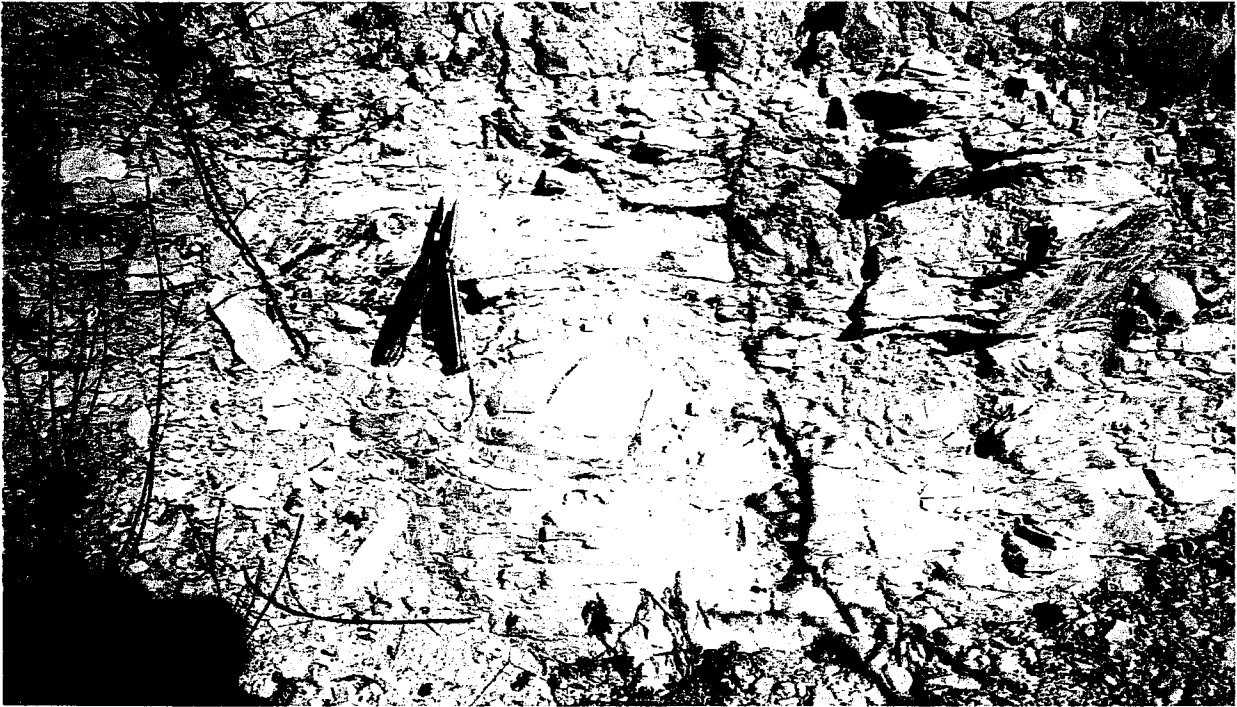


Figure 3-15. Chalk and Chert Unit. Close-up of chert nodule in typical Chalk and Chert Unit from Lefkara formation.



Figure 3-16. Chalk Unit. Example of Chalk Unit from Lefkara type location near Upper Lefkara Village.

Chalk (46.2 to 36.3 Ma)

The Chalk unit of the Lefkara Formation is comprised of chert-free chalk with occasional marl and directly overlies the Chalk and Chert unit (Fig. 3-16). These samples are characterized by high κ_{ARM}/κ ratios representing small grain sizes (mostly in the 0.1–0.2 μm size range), large smooth changes in SIRM representing gradational changes in concentration, and decreasing $\text{SIRM}/\text{SIRM}_{\text{TD200}}$ ratios from intermediate (bottom of unit) to very low (top of unit) representing increasing contributions of magnetite (Fig. 3-14).

The smooth changes of this unit represent gradational changes in sedimentation rates best seen in the SIRM data, which represents magnetic concentration. The decreasing $\text{SIRM}/\text{SIRM}_{\text{TD200}}$ ratios and high κ_{ARM}/κ ratios attest to the increasing contribution of magnetite from magnetotactic bacteria. The decrease in $\text{SIRM}/\text{SIRM}_{\text{TD200}}$ ratios and increase in SIRM values in the upper part of the unit can either be attributed to a decreasing sedimentation rate of calcareous material or an increasing productivity of fossil magnetotactic bacteria.

Upper Marl (20.4 to 15.4 Ma)

The Upper Marl unit of the Lefkara Formation is comprised of marl and marly chinks and overlies the Chalk unit unconformity. These samples are characterized by high κ_{ARM}/κ ratios representing small grain sizes, decreasing SIRM values, and increasing $\text{SIRM}/\text{SIRM}_{\text{TD200}}$ ratios (Fig. 3-14).

Although the κ_{ARM}/κ ratios still show a pelagic grain-size distribution, the decreasing SIRM and increasing $\text{SIRM}/\text{SIRM}_{\text{TD200}}$ ratios attest to decreasing input of magnetotactic bacteria to the magnetic contribution of the unit. This decrease in

magnetotactic bacteria can be attributed to a gradual increase in sedimentation rates from the pelagic chalk units below to the more detrital nature of the Pakhna Formation above.

Pakhna (15.4 to 5.5 Ma)

The Pakhna Formation is comprised of alternating chalks, marls, marly chalks, chalky marls, and arenites forming a gradational contact with the underlying upper marl unit of the Lefkara Formation (Fig 3-17). These samples are characterized by fluctuating/decreasing κ_{ARM}/κ ratios, fluctuating SIRM values, and fluctuating high SIRM/SIRM_{TD200} ratios (Fig. 3-14).



Figure 3-17. Pakhna Formation. Ideal sampling section North of Pakhna type section.

The fluctuating high SIRM/SIRM_{TD200} ratios and fluctuating/decreasing κ_{ARM}/κ ratios can be attributed to fluctuation input of detrital TM₆₀ in these samples. The fluctuating SIRM values show a copasetic relationship to the SIRM/SIRM_{TD200} ratios, which means SIRM is not a useful indication of magnetic concentration in this section since SIRM is also dependent on magnetic mineralogy.

Polis Basin (<5 Ma)

Although the stratigraphic samples end in the upper Pakhna unit, the present study also has a substantial amount of susceptibility data (κ) from the Polis basin sub-area (local sub-area II, Fig. 3-5), which is comprised of limestones that were deposited subsequent to the deposition of the Pakhna (Fig. 3-4). The Polis basin samples exhibit a mean κ of 141 μ SI (Fig. 2-2a), which is over three times greater than the mean κ of total samples of the study. This is thought to represent an even greater contribution of detrital material from the Troodos ophiolite than all previous formations.

4 – Conclusions

1. Low- κ rocks such as limestone may show unstable AMS axes due to sub-equal competition from subfabrics of diamagnetic calcite and paramagnetic clays, with traces of magnetite. They may also show specimens of either positive or negative bulk susceptibility and this requires some care in plotting either orientations or shapes (Borradaile & Jackson, 2004). In the limestone cover to the Troodos ophiolite of Cyprus, such low- κ subfabrics commonly arise from a weak tectonic overprint on depositional fabrics.
2. Standardizing AMS principal values of specimens to their κ equalizes the contributions of subfabrics/specimens with different κ in the overall sample mean-tensor. Thus, one subfabric may be emphasized or neutralized. This may have a similar effect to determining a PSD (pseudo-single domain, see magnetic mineralogy section) magnetite subfabric with AARM (Lagroix & Borradaile, 2000), although it is not a satisfactory substitute for AARM.
3. Applying the above techniques to the limestone cover of Cyprus isolates depositional fabrics from neotectonic fabrics associated with NNE subduction; neotectonic fabrics associated with rifting; and composite fabrics from feeble stylolitic foliation imprints on bedding.
4. Standardizing AMS data for petrofabrically homogenous subareas or domains reveals fabrics compatible with neotectonic stress trajectories in post-Paleogene strata. This is well shown in the Polis basin (<5Ma) and the Galataria sub-area (43Ma to 62Ma) (Figure 2-5b, sub-areas II and III respectively), which show

nearly identical fabrics in rocks with 40 million years age difference, but similar tectonic setting.

5. Examination of AMS tensors for sub-areas, and also for larger regions reveals tectonically significant axes, related to stress rather than finite strain. The orientation distribution of the mean tensor has an ellipsoid shape that may reveal the relative magnitudes of the principal stresses.
6. The examination of SIRM magnitudes at different demagnetization temperatures appears to be an innovative method of determining differences in magnetic mineralogy and concentration. This new method has proven particularly useful in cases of a bimodal magnetic mineralogy where the minerals in question have vastly different Curie temperatures (ie. Magnetite~ 585°C and TM⁶⁰~ 180°C).
7. From the plotting of κ_{ARM}/κ versus stratigraphic sequence, approximate stratigraphic control on magnetite grain sizes can be determined. In more complicated systems with more ferromagnetic minerals than just magnetite, relative grain size may also still be determined.
8. The combination and comparison of multiple magnetic techniques against stratigraphic sequence can illustrate changes in sedimentary and tectonic environments that may not be easily recognizable otherwise.

5 –Discussion: Paleomagnetism and Tectonic Implications for Cyprus

Plate Scale Tectonics

By studying paleomagnetism and the paleopoles of Cyprus ophiolites and other previously published paleomagnetic data, an APWP for Cyprus has been proposed by Borradaile and Lucas (2003). The APWP demonstrates that the Troodos microplate was located in equatorial latitudes between 88 and ~50 Ma and possessed a vertical intra-plate axis upon which its 60° anticlockwise rotation was based. Subsequently, during the time of limestone formation on Cyprus, the microplate drifted northwards to 34°N with minor anticlockwise rotation about a vertical axis located to the west of Cyprus (Table 2-1) (fig. 12, of Borradaile & Lucas, 2003).

Regional Scale Tectonics

The magnetic fabrics determined by AMS from 1090 specimens from 419 sites over Southern Cyprus (~2000 km²), demonstrate that much can be ascertained about the regional tectonics of Cyprus during the past 54 million years.

Non-standardized AMS for the five regional domains of this study (Fig. 2-6a) all show similar S>>L ODs (characteristic of bedding controlled depositional magnetic fabrics) with a k_{MAX} direction kinematically compatible with N-S extension, parallel to the alignment of the phyllosilicates caused by the stretching of the sedimentary cover over the Troodos ophiolite (Lagroix & Borradaile, 2000).

Examination of standardized AMS fabrics (Fig. 2-6b) reveal similar AMS axes, but show an east to west progression from L≈S to L>S ODs. This progression corresponds to the increasing tectonic strain from east to west, as inferred from

earthquake data and structural trends (Borradaile & Hamilton, 2004; Arvidsson et al., 1998; Ben-Avraham, et al., 1988; Papazachos & Papaioannou, 1999; and Robertson, 2000).

AARM data for these samples (Fig. 2-6c) demonstrate similar magnetic fabric axes as standardized AMS but different (weaker) ODs possibly due to the near-uniaxial shape of magnetite. Other deviations from the standardized AMS ODs are probably due to composite fabrics of stylolitic cleavage incompletely overprinting the original bedding fabric (Lagroix & Borradaile, 2000).

Local Scale Tectonics

By examining the AMS data of different stratigraphic units and at a more local scale one can further define the tectonic regimes and justify the regional scale interpretations.

Local sub-areas adjacent to the Polis rift (I, II, III) demonstrate a wide variety of non-standardized AMS fabrics (Fig. 2-5a) including a neo-tectonic fabric (I), a depositional bedding fabric (II), and a possible composite fabric (III). Upon standardization of AMS (Fig. 2-5b), these three sub-areas appear to homogenize demonstrating a strong tectonic fabric corresponding to strain trajectories compatible to the formation of the Polis rift valley (Payne & Robertson, 2000) and the current tectonic stress regime deduced from earthquake data (Borradaile & Hamilton, 2004).

The three easternmost local sub-areas exhibit little difference between non-standardized (Fig. 2-5c) and standardized samples (Fig. 2-5d). Elongate confidence cones k_{MAX} and k_{INT} and a tight k_{MIN} confidence cone characterize all of these fabrics with a shallow NNE dipping foliation. These OD fabrics represent a primary sedimentary fabric

with some secondary tectonic control, similar to that seen in the corresponding regional sub-areas.

Magnetostratigraphy and Tectonic Implications

It was hoped that the present study would help resolve the timing of the uplift and subsequent erosion of the Troodos ophiolite. The use of the $SIRM/SIRM_{TD200}$ ratio as an indicator of TM_{60} contribution is expected to demonstrate presence of a sharp transition from low $SIRM/SIRM_{TD200}$ ratio values to higher values at the time of uplift. The data shows the presence of significant TM_{60} through out the entire Pakhna, Upper Marl Unit, and the older Chalk and Chert unit (Fig. 3-14). The presence of TM_{60} in the Chalk and Chert unit could be due to contributions from submarine volcanism similar to that found in the Lower Marl unit just below it. The Pakhna unit and Upper Marl Unit, in contrast, was deposited in a relatively shallow environment (<1 km depth) (Robertson, 2000), therefore submarine volcanism is not expected to contribute any significant part to these rocks. Therefore, it is believed that the gradual increase in the $SIRM/SIRM_{TD200}$ ratio in the Upper Marl Unit represents the first signs of uplift and erosion of the Troodos ophiolite, which may slightly predate 20 Ma. Unfortunately, due to the large hiatus in the sedimentary record, more precise chronometry is not possible.

Also of significant interest is the presence of a temporary sharp decrease in the $SIRM/SIRM_{TD200}$ ratio and $KARM/K$ ratio at about 12 Ma (Fig. 3-14). This corresponds with the first record of coarse ultra-mafic material in the Cyprus limestone cover sequence documented by Orszag-Sperber et al.(1989) and probably represents a time of very rapid uplift and unroofing of the pillow and dike sequences (fig. 8, Robertson, 2000).

References

- Arvidsson, R, Ben-Avraham, Z., Ekström, G., & Wdowinski, S., 1998. Plate tectonic framework for the October 9, 1996 Cyprus earthquake. *Geophysical Research Letters*, **25**, 2241-2244
- Banerjee, S.K., King, J., & Marvin, J., 1981. A rapid method for magnetic granulometry with applications to environmental studies. *Geophysical Research Letters*, **8**, 333-336.
- Ben-Avraham, Z., Kempler, D., & Ginzburg, A., 1988. Plate convergence in the Cyprean Arc. *Tectonophysics*, **146**, 231-240.
- Blatt, H., Middleton, G.V., & Murray, R.C., 1980. *Origin of Sedimentary Rocks*, Prentice Hall, New Jersey. 766.
- Blow, W.H., 1969, Late Middle Eocene to Recent planktonic foraminiferal biostratigraphy, IN *Proceedings of the First International Conference on Planktonic Microfossils*: Geneva, Brill, Leiden, p199-421.
- Borradaile, G.J., 1988. Magnetic susceptibility, petrofabrics and strain. *Tectonophysics*, **156**, 1-20.
- Borradaile, G.J., 2001. Magnetic fabrics and petrofabrics: their orientation-distributions and anisotropies. *Journal of Structural Geology*, **23**, 1581-1596.
- Borradaile, G.J., 2003. Spherical Orientation Data :Tensors. In *Statistics of earth science data : their distribution in space, time, and orientation*, Springer-Verlag, New York.293-326.
- Borradaile, G.J., Chow, N., & Werner, T., 1993. Magnetic hysteresis of limestones: Facies control?. *Physics of the Earth and Planetary Interiors*, **141**, 213-226.
- Borradaile, G.J., & Hamilton, T.D., 2004. Magnetic fabrics may proxy as neotectonic stress trajectories, Polis Rift, Cyprus. *Tectonics*, **23**, TC1001, doi:10.1029/2002TC001434
- Borradaile, G. J. & Hamilton, T. 2003. Limestones distinguished by magnetic hysteresis in three-dimensional projections, *Geophysical Research Letters*., **30**, No. 18, 1973, 10.1029/2003GL017892.
- Borradaile, G.J.,& Henry, B., 1997. Tectonic applications of magnetic susceptibility and its anisotropy. *Earth Science Reviews*, **42**, 49-93.

- Borradaile, G.J., & Jackson, M., 2004. Anisotropy of magnetic susceptibility (AMS): magnetic petrofabrics of deformed rocks. IN Martin-Hernandez, F., Luneburg, C.M., Aubourg, C. & Jackson, M.(eds). *Magnetic Fabric: Methods and Applications*. Geological Society, London, Special Publications, **238**, 299-360.
- Borradaile, G.J., & Kehlenbeck, M. M., 1996. Possible cryptic tectono-magnetic fabrics in "post-tectonic" granitoid plutons of the Canadian Shield, *Earth and Planetary Science Letters*, **137**, 119-127.
- Borradaile, G. J. & Mothersill, J. S. 1984. Coaxial deformed and magnetic fabrics without simply correlated magnitudes of principal values. *Physics of the Earth and Planetary Interiors*, **56**, 254-265.
- Borradaile, G.J. & Lacroix, F., 2000. Magnetic characterization of limestones using a new hysteresis projection. *Geophysics Journal International*, **141**, 213 - 226.
- Borradaile, G.J., & Lacroix, F., 2001. Magnetic fabrics reveal Upper Mantle flow fabrics in the Troodos Ophiolite Complex, Cyprus. *Journal of Structural Geology*, **23**, 1299-1317.
- Borradaile, G.J., & Stupavsky, M., 1995. Anisotropy of magnetic susceptibility: measurement schemes. *Geophysical Research. Letters*, **15**, 1957-1960.
- Borradaile, G.J., & Tella, S., & McArthur, J., 1989. Magnetic fabric as a kinematic indicator of faults: a test case. *Annals de Tectonicae*, **3**, 3-11.
- Carter-Stiglitz, B., Moskowitz, B., & Jackson, M., 2001. Unmixing magnetic assemblages and the magnetic behavior of bimodal mixtures. *Journal of Geophysical Research*, **106**, 26397-26411.
- Chang, S.-B.R., & Kirschvink, J.L., 1989. Possible biogenic magnetite fossils from the Miocene marine clay of Crete, IN (eds.) Kirschvink, J.L, Jones, D.S., & MacFadden. *Magnetite Biomineralization and Magnetoreception in Organisms*, Plenum, New York, 647-669.
- Cifelli, F., Rossetti, F., Mattei, M., Hirt, A.M., Funicello, R., & Tortorici, L., 2004. An AMS, structural and paleomagnetic study of quaternary deformation in eastern Sicily. *Journal of Structural Geology*, **26**, 29-46.
- Collinson, D. W. 1983. *Methods in Rock Magnetism and Palaeomagnetism: Techniques and Instrumentation*. Chapman and Hall, New York, 503 pages.
- Day, R., Fuller, M. & Schmidt, V.A., 1977. Hysteresis properties of titanomagnetites: Grain size and composition dependence, *Physics of the Earth and Planetary Interiors*, **13**, 260-267.

De Wall, H., Bestmann, M. & Ullemeyer, K., 2000. Anisotropy of susceptibility in Thassos marble: a comparison between measured and modelled data. *Journal of Structural Geology*, 22, 1761-1771.

Dunlop, D.J., 2002a. Theory and application of the Day plot (M_{rs}/M_s versus H_{cr}/H_c) 1. Theoretical curves and tests using titanomagnetite data. *Journal of Geophysical Research*. **107**, NO. B3, 10.1029/2001JB000486,2002

Dunlop, D.J., 2002b. Theory and application of the Day plot (M_{rs}/M_s versus H_{cr}/H_c) 2. Application to data for rocks, sediments and soils. *Journal of Geophysical Research*. **107**, NO. B3, 10.1029/2001JB000487,2002

Dunlop, D. J. & Özdemir, Ö. 1997. *Rock Magnetism: Fundamentals and Frontiers*. Cambridge University Press, Cambridge , 573 pages.

Eaton, S., 1987. The Sedimentology of Mid to Late Miocene Carbonates and Evaporites in Southern Cyprus. PhD thesis, University of Edinburgh, 240. (unpublished).

Eaton, S., & Robertson, AHF., 1993. The Miocene Pakhna Formation, southern Cyprus and its relationship to the Neogene tectonic evolution of the Eastern Mediterranean. *Sedimentary Geology*, **86**, 273-296.

Flinn, D., 1965. On the Symmetry Principle and the Deformation Ellipsoid. *Geology Magazine*. **102**, 36-45.

Girdler, R. W., 1961. The measurement and computation of anisotropy of magnetic susceptibility in rocks. *Geophysical Journal of the Royal Astronomical Society*, **5**, 34-44.

Hall, F. R., Bloemendal, J., Arthur, M.A., and Aksu, A.E, 1989. Middle to Late Quaternary sediment fluxes in the Labrador Sea, ODP Leg 105, Site 646: A synthesis of rock magnetic, oxygen isotopic, carbonate, and planktonic foraminiferal data, *Proceedings of Ocean Drilling Program*, **105**, 653-665.

Hamilton, T.D., Borradaile, G.J., & Lagroix, F., Sub-fabric identification by standardization of AMS: an example of inferred neotectonic structures from Cyprus. IN Martin-Hernandez, F., Luneburg, C.M., Aubourg, C. & Jackson, M.(eds). *Magnetic Fabric: Methods and Applications*. Geological Society, London, Special Publications, **238**, 527-540.

Haq, B.U., Hardenbol, J., and Vail, P.R., 1987, Chronology of fluctuating sea levels since the Triassic. *Science*, **235**, 1156-1167.

Henry, B., 1983, Interprétation quantitative de l'anisotropie de susceptibilité magnétique: *Tectonophysics*, **91**, 165-177.

- Henry, B., 1989, Magnetic fabric and orientation tensor of minerals in rocks: *Tectonophysics*, **165**, 21–28.
- Henry, B., 1990. Magnetic fabric implications for the relationships between deformation mode and grain growth in slates from the Borrowdale Volcanic Group in the English Lake District. *Tectonophysics*, **178**: 225-230.
- Henry, B., 1992. Modelling the relationship between magnetic fabric and strain in polymineralic rocks. *Physics of the Earth and Planetary Interiors.*, **70**, 214-218.
- Hellwege, K.H. & Hellwege, M., 1967. Magnetic properties, II. In: H.von Borchers, H. Hausen, K.H. Hellwege, K. Schafer & E. Schmidt (Editors), *Landolt-Bornstein: Zahlenwerte und Funktionen aus Physik. Chemie, Astronomie, Geophysik und Technik*, II/10, Springer, Berlin.
- Hunt, C. P., Moskowitz, B. M. & Banerjee, S. K. 1995. Magnetic properties of rocks and minerals. In: *A Handbook of Physical Constants, vol. 3* (edited by Ahrens, T. J.). American Geophysical Union, Washington, DC, 189–204.
- Ihmlé, P.F., Hirt, A.M., Lowrie, W. & Dietrich, D., 1989. Inverse fabric in deformed limestones of the Morcles Nappe, Switzerland. *Geophysical Research Letters*, **16**: 1383-1386.
- Jackson, M.J., Worm, H.U., & Banerjee, S.K., 1990. Fourier analysis of digital hysteresis data: rock magnetic applications. *Physics of the Earth and Planetary Interiors*, **65**, 78-87.
- Jackson, M. J. 1991. Anisotropy of magnetic remanence: a brief review of mineralogical sources, physical origins, and geological applications, and comparison with susceptibility anisotropy. *Pure and Applied Geophysics* **136**, 1–28.
- Jackson, M.J., Craddock, J.P., Ballard, M., Van der Voo, R., & McCabe, C., 1989. Anhyseretic remanent magnetic anisotropy and calcite strains in Devonian carbonates from the Appalachian Plateau, New York. *Tectonophysics*, **161**, 43-53.
- Jelinek, V., 1978. Statistical processing of anisotropy of magnetic susceptibility measured on groups of specimens. *Studia Geophysica et Geodetica*, **22**, 50-62.
- Jelinek, V., 1981. Characterization of the magnetic fabric of rocks. *Tectonophysics*, **79**, 63-67.
- Kahler, G., 1994. Stratigraphy and Sedimentology of the Paleogene Lefkara Formation, Cyprus. PhD thesis, University of Southampton. (unpublished).
- Kahler, G., & Stow, D., 1998. Turbidites and contourites of the Palaeogene Lefkara Formation, southern Cyprus. *Sedimentary Geology*, **115**, 215-231.

- Karlin, R., 1990a. Magnetic diagenesis in marine sediments from the Oregon Continental Margin, *Journal of Geophysical Research*, **95**, 4405-4420.
- Karlin, R., 1990b. Magnetic mineral diagenesis in suboxic sediments at Bettis Site W-N, NE Pacific Ocean, *Journal of Geophysical Research*, **95**, 4421-4436.
- Karlin, R., & Levi, S., 1983. Geochemical and sedimentological control on the magnetic properties of hemipelagic sediments, *Journal of Geophysical Research*, **90**, 10373-10392
- Kent, D.V., & Lowrie, W., 1974. Origin of Magnetic instability in sediment cores from the central North Pacific, *Journal of Geophysical Research*, **79**, 2987-3000.
- King, J., Banerjee, S. K., Marvin, J. & Ozdemir, O. 1982. A comparison of different magnetic methods for determining the relative grain size of magnetite in natural materials:some results from lake sediments. *Earth and Planetary Science Letters*. **59**, 404-419.
- Kirschvick, J.L., 1983. Biogenic ferrimagnetism: a new biomagnetism. IN *Biomagnetism: An Interdisciplinary Approach*, (ed.) Williamson, S., Plenum, New York, 472-492.
- Kirschvink, J.L., & Chang, S.-B.R. 1984. Ultrafine-grained magnetite in deep-sea sediments: Possible bacterial magnetofossils. *Geology*. **12**, 559-562.
- Kissel, C., Barrier, E., Laj, C., & Lee, T.Q., 1986. Magnetic fabric in “undeformed” marine clays from compressional zones. *Tectonics*. **5**, 769-781.
- Krishnan, K.S., Guha, B.C. & Banerjee, S.K., 1933. Investigation on magneto-crystalline action, Part I. Diamagnetics. *Philos. Trans. Royal Society London, Serial A*. **231**, 235-262.
- Lagroix, F. & Borradaile, G. J., 2000. Tectonics of the Circum-Troodos Sedimentary Cover of Cyprus, from Rock Magnetic and Structural Observations. *Journal of Structural Geology*, **22**, 453-469.
- Lord, A.R., Panayides, I., Urquhart, E., & Xenophontos, C. 2000. A biochronostratigraphical framework for the Late Cretaceous-Recent circum-Troodos sedimentary sequence, Cyprus. In: Panayides, I., Xenophontos, C. & Malpas, J., (eds) *Proceedings of the Third International Conference on the Geology of the Eastern Mediterranean*. Cyprus Geological Survey Department, Nicosia, Cyprus, 289-297.
- Lowrie, W. & Heller, F. 1982. Magnetic Properties of Marine Limestones. *Reviews of Geophysics and Space Physics*, **20-2**, 171-192.
- Mantis, M., 1970, Upper Cretaceous-Tertiary foraminiferal zones in Cyprus: *Epithris*, **3**, 227-241.

- Mattei, M., Speranza, F., Argentieri, A., Rosetti, F., Sagnotti, L. & Funicello, R. 1999. Extensional tectonics in the Amantea Basin (Calabria, Italy): a comparison between structural and magnetic anisotropy data. *Tectonophysics*, **307**, 33-49.
- McNeill, D.F., 1990. Biogenic magnetite from surface Holocene carbonate sediments, Grand Bahama Bank. *Journal of Geophysical Research*, **95-B4**, 4363-4371.
- Mead, G.A., Tauxe, L., & LaBrecque, J.L., 1986. Oligocene paleoceanography of the South Atlantic: paleoclimatic implications of sediment accumulation rates and magnetic susceptibility measurements, *Paleoceanography*, **1**, 273-284.
- Miller, K.G., Fairbanks, R.G., Mountain, G.S., 1987. Tertiary oxygen isotope synthesis, sea level history and continental margin erosion. *Paleoceanography*, **2-1**, 1-19.
- Nakamura, N. & Borradaile, G.J., 2001. Strain, anisotropy of anhysteretic remanence, and anisotropy of magnetic susceptibility in a slaty tuff *Physics of the Earth and Planetary Interiors*, **125**: 85-93.
- O'Reilly, W. 1984. *Rock and Mineral Magnetism*. Blackie, Glasgow , 220 pages.
- Orszag-Sperber, F., Rouchy, J.M., & Elion, P., 1989, The sedimentary expression of regional tectonic events during the Miocene-Pliocene transition in Southern Cyprus basins. *Geological Magazine*, **126**, 291-299.
- Owens, W.H. & Rutter, E.H., 1978. The development of magnetic susceptibility anisotropy through crystallographic preferred orientation in a calcite rock. *Physics of the Earth and Planetary Interiors*, **16**: 215-222.
- Owens, W.H., & Bamford, D., 1976. Magnetic, seismic, and other anisotropic properties of rock fabrics. *Phil. Trans. Royal Society London.*, **A283**: 55-68.
- Ozdemir, O., & O'Reilly, W., 1982. High temperature hysteresis and other magnetic properties of synthetic monodomain titanomagnetites, *Physics of the Earth and Planetary Interiors*, **25**, 406-418.
- Papazachos, B.C. & Papaioannou, Ch. A., 1999. *Lithospheric boundaries and plate motions in the Cyprus area*. *Tectonophysics*, **308**: 193-204.
- Payne, A.S., & Robertson, A.H.F. 2000. Structural evolution and regional significance of the Polis graben system, western Cyprus. In: Panayides, I., Xenophontos, C. & Malpas, J., (eds) *Proceedings of the Third International Conference on the Geology of the Eastern Mediterranean*. Cyprus Geological Survey Department, Nicosia, Cyprus, 45-59.

Peters, C., & Dekkers, M.J., 2003. Selected room temperature magnetic parameters as a function of mineralogy, concentration and grain size. *Physics and Chemistry of the Earth*, **28**, 659-667.

Ramsay, J.G. 1967. *Folding and Fracturing of Rocks*. McGraw-Hill, New York.

Reilinger, R.E., McClusky, S.C., Oral, M.B., King, R.W., Toksoz, M.N., Barka, A.A., Kinik, I., Lenk, O., & Sanli, I., 1997. Global position system measurements of present-day crustal movements in the Arabia-Africa-Eurasia plate collision zone. *Journal of Geophysical Research*, **102**, 9983-9999.

Robertson, A.H.F., 2000. Tectonic evolution of Cyprus in its Easternmost Mediterranean setting, In: Panayides, I., Xenophontos, C., & Malpas, (Eds.), *Proceedings of the Third International Conference on the Geology of the Eastern Mediterranean*. 11-44.

Robertson, A.H.F., 1990. Tectonic evolution of Cyprus, In: Malpas, J., Moores, E., Panayiotou, A., & Xenophontos, C. (Eds.), *Ophiolites: Oceanic Crustal Analogues, Proceedings of the Symposium "Troodos 1987"*. Cyprus Geological Survey Department, 235-250.

Robertson, A.H.F., Eaton, S., Follows, E.J., & McCallum, J.E., 1991. The role of local tectonics versus global sea-level changes in the Neogene evolution of the Cyprus active margin. *International Association of Sedimentology, Special Publication*, **12**, 331-369.

Robertson, A.H.F., Kidd, R.B., Ivanov, M.K., Limonov, A.F., Woodside, J.M., Galindo-Zaldicar, J., & Nieto, L., 1995. Eratosthenes seamount: collisional processes in the easternmost Mediterranean in relation to the Plio-Quaternary uplift of southern Cyprus. *Terra Nova*, **7**, 254-264.

Rochette, P., 1988. Inverse magnetic fabric in carbonate-bearing rocks, *Earth & Planetary Science Letters*, **90**, 229-237.

Rochette, P., Jackson, M. J., & Aubourg, C., 1992. Rock magnetism and the interpretation of anisotropy of magnetic susceptibility. *Reviews of Geophysics*, **30**, 209-226.

Sagnotti, L., Faccenna, C., Funiciello, R., & Mattei, M., 1994. Magnetic fabric and structural setting of Plio-Pleistocene clayey units in an extensional regime: the Tyrrhenian margin of central Italy. *Journal of Structural Geology*, **16**, 1243-1257

Sagnotti, L., Speranza, F., Winkler, W., Mattei, M., & Funiciello, R., 1998. Magnetic fabric of clay sediments from the external northern Apennines (Italy). *Physics of the Earth and Planetary Interiors*, **105**, 73-93.

Stacey, F. D. & Banerjee, S. K. 1974. *The Physical Principles of Rock Magnetism*. Elsevier, Amsterdam, 195.

Tarling, D.H., & Hrouda, F., 1993. *The magnetic anisotropy of rocks*. Chapman and Hall, London, 217.

Tauxe, L. 1998. *Paleomagnetic principles and practice*. Kluwer, Dordrecht, 299.

Tauxe, L., & Wu, G., 1990. Normalized remanence in sediments of the western Equatorial Pacific: Relative paleointensity of the geomagnetic field?, *Nature*, **56**, 12337-12350.

Vali, P.R., Mitchum, R.M., Shipley, T.H., & Buffler, R.T., 1980. Unconformities of the North Atlantic. *Philosophical Transactions Research Society of London*. **294**, 137-155.

Vali, H., & Kirschvink, J.L., 1989. Magnetofossil dissolution in a paleomagnetically unstable deep-sea sediment. *Nature*, **339**, 203-206.

Vigliotti, L., Capondi, L., & Torii, M., 1999. Magnetic properties of sediments deposited in suboxic-anoxic environments: relationships with biological and geochemical proxies. *Geological Society Special Publication*, **151**, 71-83.

Voight, W., & Kinoshita, S., 1907. Bestimmung absoluter Werte von Magnetisierungszahlen, insbesondere für Kristalle. *Annals of Physics*. **24**, 492-514.

Wang, D., & Van der Voo, R., 2004. The hysteresis properties of multidomain magnetite and titanomagnetite/titanomaghemite in mid-ocean ridge basalts. *Earth and Planetary Science Letters*. **220**, 175-184.

Wasilewski, P.J., 1973. Magnetic hysteresis in natural materials. *Earth and Planetary Science Letters*, **20**, 67-72.

Werner, T. & Borradaile, G. J., 1996. Paleoremanence dispersal across a transpressed Archean Terrain: Deflection by anisotropy or by late compression? *Journal of Geophysical Research*, **10**, 5531-5554.

**Appendix 1. Glossary of Magnetic and Tectonic Fabric Terminology
from Borradaile and Jackson (2004)**

We generally follow the usage of Collinson (1983) and Hunt et al (1995); symbols differ to varying degrees in standard references (Stacey & Banerjee 1974, O'Reilly 1984, Dunlop & Özdemir 1997, Tauxe 1998).

Magnetism & anisotropy terminology

<i>p</i>	magnetic dipole moment [Am^2]; a measure of the strength of a magnet.
<i>M</i>	volumetric magnetization intensity [A/m]; dipole moment per unit volume.
<i>J</i>	mass-specific magnetization intensity [Am^2/kg]; dipole moment per unit mass.
<i>H</i>	magnetic field [A/m]. In the absence of free currents, the tangential component of <i>H</i> is continuous across a material boundary.
<i>B</i>	magnetic induction [T] = [Wb/m^2] = [$\text{J}/(\text{Am}^2)$]. $B = \mu_0(H + M)$, where μ_0 , the permeability of free space, is a fundamental physical constant ($\mu_0 = 4\pi \times 10^{-7} \text{ H/m}$). The normal component of <i>B</i> is continuous across a material boundary.
κ	magnetic susceptibility [dimensionless]; the ratio of induced magnetization to magnetizing field $\kappa = M / H$, measured in a low direct field (e.g., SQUID magnetometer) or alternating field (e.g., induction coil). To preserve linear magnetization-field response ($M = \kappa H$), the field must not affect the remanence of any permanently magnetizable content, i.e., usually $\leq 10 \text{ mT}$. Induction coil methods use low frequencies ($\leq 20 \text{ KHz}$) to suppress conductivity responses. κ is frequency dependent for conductive materials and for viscous superparamagnetic grains.
<i>AMS</i>	anisotropy of magnetic susceptibility with principal values $\kappa_{MAX} \geq \kappa_{INT} \geq \kappa_{MIN}$, described as a second-rank tensor. Where the principal values have the same sign, this may be visualized as magnitude ellipsoid.
<i>AMS ellipsoid</i>	The AMS tensor possesses a representation surface, a quadric of radii <i>r</i> . Only where the principal susceptibilities have the same sign and where none are zero can we define a magnitude ellipsoid (<i>the AMS ellipsoid</i>) with radii $1/\sqrt{r}$.
$\bar{\kappa}$	Bulk susceptibility; commonly given as arithmetic mean of the principal susceptibilities, $(\kappa_{MAX} + \kappa_{INT} + \kappa_{MIN})/3$, if all principal values have same sign. The geometric mean is preferred, especially if the anisotropy is large, as in AARM or finite strain; requires non-zero, same-sign principal susceptibilities.
<i>Standardized</i>	Principal values (κ_{MAX} , etc.) may be standardized simply by dividing by $\bar{\kappa}$. For the finite strain tensor, principal axes must be standardized using their <i>geometric</i> mean since anisotropies may be large.
<i>P</i>	Anisotropy degree, $P = \kappa_{MAX} / \kappa_{MIN}$
<i>L</i>	Magnetic lineation $L = \kappa_{MAX} / \kappa_{INT}$ cf. Flinn's <i>a</i>
<i>F</i>	Magnetic foliation $F = \kappa_{INT} / \kappa_{MIN}$ cf. Flinn's <i>b</i>
<i>P_j or P'</i>	Jelinek's (1981) "corrected" anisotropy degree, reflecting eccentricity of the magnitude ellipsoid for a second rank tensor where all principal values have the same sign. Ranges from 1.0 (sphere, isotropy) upward, original definition involved normalization with arithmetic mean of susceptibility but for higher anisotropies, e.g. AARM or strain the geometric mean may be preferable.
<i>T</i>	Jelinek's (1981) shape parameter for the magnitude ellipsoid, measuring the range from prolate ($T=+1$) through neutral ($T=0$) to oblate ($T=-1$) ellipsoids, independent of eccentricity; identical to Lode's parameter (1926), <i>v</i> of structural geology.

χ	mass-specific susceptibility [$\text{m}^3 \text{kg}^{-1}$]; $\chi = J/H = \kappa / \text{density}$.
DC	direct current used to apply a steady field, for IRM or as a bias field to generate an ARM.
AF	Alternating field; laboratory applied sine wave field damped so that its amplitude decays progressively and usually linearly with time.
Remanence	magnetization that persists in the absence of an applied magnetic field. In contrast induced magnetization, measured during the study of AMS, disappears when the applied field is removed.
κ_i	intrinsic magnetic susceptibility [dimensionless]; not directly measured for high-susceptibility materials, where it is “screened” by self-demagnetization.
μ	(relative) magnetic permeability. In linear materials and/or in weak applied fields, $\mu = 1 + \kappa_i$, and absolute permeability $\mu_{abs} = \mu\mu_0$ relates magnetic induction B and (internal) magnetic field H $B = \mu_0(H + M) = \mu_0(H + \kappa_i H_i) = \mu_0 H(1 + \kappa_i) = \mu_0 \mu H = \mu_{abs} H$
ARM	anhysteretic remanent magnetization; laboratory remanence due to small DC field biasing the moments scattered during the decay of a simultaneously decaying large alternating field.
AARM	anisotropy of anhysteretic remanent magnetization
κ_{ARM} or A	anhysteretic susceptibility, M_{ARM}/H_{dc} [dimensionless]. Mean value is $\bar{A} = \overline{\kappa_{ARM}} = (\kappa_{ARM,MAX} \kappa_{ARM,INT} \kappa_{ARM,MIN})^{1/3}$, where $\kappa_{ARM,MAX} \geq \kappa_{ARM,INT} \geq \kappa_{ARM,MIN}$ (Geometric mean is wisest, since anisotropies are large and ARM's are always positive values.)
pARM	Partial anhysteretic remanent magnetization (that due to grains in a selected range of coercivities).
pAARM	Anisotropy of pARM.
MD	multidomain (remanence-bearing) grain: for <i>magnetite</i> usually >5 domains and >2 μm diameter but shape-dependent
SD	Remanence-bearing grain with a unique direction of spontaneous magnetization (in one domain); for <i>magnetite</i> 20-100 nm but shape-dependent
SP	Superparamagnetic grains are SD but thermally unstable; for <i>magnetite</i> <20nm but shape-dependent
PSD	Pseudo-single domain; remanence-bearing grain that has some remanence properties like SD and therefore desirable in routine paleomagnetism (for magnetite 2-5 domains, ~0.1-2 μm in diameter, depending on shape.
Polydomain	umbrella term for MD & PSD characteristics.
TM	Titanomagnetite series $\text{Fe}_{3-x}\text{Ti}_x\text{O}_4$ e.g., TM60 = $\text{Fe}_{2.4}\text{Ti}_{0.6}\text{O}_4$
IRM	Isothermal remanent magnetization; remanence acquired in a large DC field
SIRM	Saturation isothermal magnetization; saturation remanence acquired in a large DC field
AIRM	Anisotropy of isothermal remanent magnetization
Inverse AMS fabric	Due to (a) SD magnetite grain in which κ_{MIN} must be parallel to the long-axis OR (b) the presence of some mineral (e.g., calcite, tourmaline) in which κ_{MIN} is parallel (or ~parallel) to the crystallographic axis associated with the long habit

<i>Blended AMS fabric</i>	Rock AMS fabric that combines magnetic subfabrics <i>without</i> a simple one-to-one mapping or parallelism of their principal magnitudes, e.g., κ_{MIN} for one sub-fabric is inclined to κ_{MIN} for another subfabric. The subfabrics may be due to some combination of minerals with inverse and normal AMS, OR to some combination of competing petrofabrics.
<i>Diamagnetism</i>	Universal negative susceptibility response, usually $\dot{A} -14\mu\text{SI}$. Loosely refers to some minerals, which if pure, would only show a diamagnetic response, e.g., quartz, calcite. However, natural examples commonly have overwhelming positive responses from inclusions. Rocks such as quartzite and limestone are rarely diamagnetic. Diamagnetism is not temperature-dependent.
<i>Paramagnetism</i>	Positive response to an applied field with $0 < \kappa < 2000 \mu\text{SI}$ for most pure rock-forming minerals. (Unfortunately, matrix minerals are rarely pure and κ may be much higher due to high- κ microscopic-submicroscopic inclusions or exsolutions (e.g., iron-oxide; see “ferro”magnetic). Paramagnetic susceptibility decreases inversely with temperature.
<i>“Ferro”-magnet</i>	Umbrella term for magnetically-ordered phase, more specifically and more accurately described as, e.g., ferrimagnetic (magnetite) or antiferromagnetic (hematite). Sometimes stoichiometrically controlled, e.g., pyrrhotite (Fe_{1-x}S) is ferrimagnetic for $x \geq 0.125$, otherwise antiferromagnetic. Ferromagnetism mostly decreases non-linearly with increasing temperature and disappears above Curie temperature (ferrimagnets) or Néel temperature (antiferromagnets).

Structural & petrofabric terminology

<i>Strain</i>	Change of shape; homogeneously, keeping parallel lines parallel and straight lines straight; or heterogeneously. Homogeneous finite strain, a second rank tensor, may always be represented by a magnitude ellipsoid since principal magnitudes are always positive. Strain history (accumulation of incremental strains) may not be deduced from a single state of homogeneous finite strain.
$X \geq Y \geq Z$	Principal stretches or finite strains, axes of the finite strain ellipsoid (Ramsay, 1967). [Note that Flinn’s original work (1961) used the convention, $Z \geq Y \geq X$, which was never widely adopted]. Stretch = $(\text{new length})/(\text{old length})$.
<i>Flinn’s a, b</i>	$a = X/Y$, $b = Y/Z$ describes the magnitude ellipsoid of the finite strain tensor and the orientations-distribution tensor; (x, y) coordinates of the Flinn and Woodcock plots. Comparable older terms in AMS are L and F .
<i>Flinn’s k</i>	$k = (a-1)/(b-1)$; a measure strain ellipsoid shape from oblate ($k = 0$) through plane strain ($k = 1$) to prolate $k = \infty$.
<i>Ramsay’s K</i>	$K = \ln(a)/\ln(b)$: \log_{10} scaling of the Flinn plot disperses low anisotropy data points for greater clarity; points separated by similar distances on the log-plot have similar strain-differences.
<i>L-S scheme</i>	Flinn’s (1965) qualitative scheme; associates shape or mineral fabrics for a homogenous sample of specimens with the appropriate finite-strain or orientation-distribution ellipsoid. L = prolate, $L=S$ neutral; S =oblate, general cases, e.g. $L>S$ or $L<S$. Importantly recognizes the smooth spectrum of possibilities <i>vis-à-vis</i> historically incorrect notion of discrete symmetry classes.
<i>OD</i>	Orientation Distribution: frequency distribution of axes or directions in three-dimensions, illustrated on a stereogram or by an orientation tensor that is visualized by its magnitude ellipsoid.

<i>Orthorhombic</i>	Mirror symmetry across three mutually orthogonal planes: no axial-symmetric rotation the planes' intersections; e.g. a magnitude ellipsoid representing for finite strain or AMS. End-member prolate and oblate ellipsoids possess higher, rotational symmetry about one axis. AMS ellipsoids never have less than orthorhombic symmetry whereas most rock-forming minerals have lower crystal symmetry.
<i>Material line/plane</i>	Physically characterized line, usually in a continuum, that may be tracked through a strain history, e.g., bedding.
<i>Non-material line</i>	A finite strain axis (<i>X, Y, or Z</i>) or some other distinct linear property (e.g., line of no finite strain) defined by the state of strain at any point in a strain history. While their orientation may be determined they are rarely tied to any material line (one exception would be <i>incremental</i> strain axes during simple shear strain history).
<i>Deformation</i>	Changes in location of parts of a material with respect to an external reference frame. May comprise any combination of: (i) translation (ii) rigid body rotation (iii) strain (iv) volume change.
<i>Deform. Mechanism</i>	Material processes by which internal relative displacements are achieved; including crystal-plasticity, diffusion, pressure solution, particulate flow, etc.
<i>Co-axial</i>	A strain-history or fabric-evolution in which the orthogonal principal axes remain parallel to the same material lines as events progress; including pure shear or compaction ($X=Y>I>Z$) or general coaxial flattening $X>Y>I>Z$; cf. <i>non-coaxial</i> . Older terms irrotational/ rotational may be confused with the internal rotation of material lines during coaxial strain history or even with external rigid-body rotation.
<i>Vorticity</i>	The rate and sense of finite strain axis rotation (in some complex three-dimensional manner), usually with respect to the rate of accumulation of strain increments. Usually very difficult to relate to the orientation of material lines.
<i>PDO</i>	Preferred dimensional orientation, for example of strained objects such as pebbles, grains or any other clasts, fossils, lapilli (<i>L-S</i> scheme).
<i>PCO</i>	Preferred crystallographic orientation, for example an alignment of minerals by growth, rotation or solid-state plastic deformation into a linear-planar fabric (<i>L-S</i> scheme).

Appendix 2- Sub-Areas Sample Location, Age, and Formation Data

Sample	Location	Easting	Northing	Bed dip dir.	Bed Dip	Age(Ma)	Biostrat	Formation
TH01	Lymbia	538565	3872933	257	30	54.0	Kahler	Lower Marl
TH02	Lymbia	538608	3872942	257	30	55.0	Kahler	Lower Marl
TH03	Lymbia	538609	3872942	257	30	56.0	Kahler	Lower Marl
TH04	Lymbia	538657	3874592	330	5	48.0-62.0		Lower Marl
TH05	Lymbia	538595	3874584	330	5	48.0-62.0		Lower Marl
TH06	Lymbia	538702	3874601	330	5	48.0-62.0		Lower Marl
TH07	Omodhos/Pakhna	483117	3858097	190	20	47.4	Kahler	Chalk & Chert
TH08	Omodhos/Pakhna	483117	3858097	190	10	47.2	Kahler	Chalk & Chert
TH09	Omodhos/Pakhna	483117	3858097	190	10	47.0	Kahler	Chalk & Chert
TH10	Omodhos/Pakhna	483105	3858125	190	10	47.5	Kahler	Chalk & Chert
TH11	Omodhos/Pakhna	482954	3857920	165	16	46.8	Kahler	Chalk & Chert
TH12	Omodhos/Pakhna	482890	3857897	140	12	46.6	Kahler	Chalk & Chert
TH13	Omodhos/Pakhna	482768	3857827	90	25	46.4	Kahler	Chalk & Chert
TH14	Omodhos/Pakhna	482677	3857772	180	26	46.0	Kahler	Chalk
TH15	Omodhos/Pakhna	482630	3857730	135	18	44.0	Kahler	Chalk
TH16	Omodhos/Pakhna	482630	3857730	140	14	43.0	Kahler	Chalk
TH17	Omodhos/Pakhna	482608	3857728	170	5	42.0	Kahler	Chalk
TH18	Omodhos/Pakhna	482581	3857686	225	26	41.0	Kahler	Chalk
TH19	Omodhos/Pakhna	482541	3857655	280	17	39.0	Kahler	Chalk
TH20	Omodhos/Pakhna	482541	3857655	280	17	38.0	Kahler	Chalk
TH21	Omodhos/Pakhna	482485	3857615	72	22	37.0	Kahler	Chalk
TH22	Omodhos/Pakhna	482485	3857615	124	18	36.3	Kahler	Chalk
TH23	Omodhos/Pakhna	482260	3855916	0	0	16.7	Eaton	Pakhna
TH24	Omodhos/Pakhna	482702	3854857	232	18	16.4	Eaton	Pakhna
TH25	Omodhos/Pakhna	481968	3854090	250	10	16.0	Eaton	Pakhna
TH26	Omodhos/Pakhna	481799	3853866	195	15	15.9	Eaton	Pakhna
TH27	Omodhos/Pakhna	481800	3853871	220	10	15.9	Eaton	Pakhna
TH28	Omodhos/Pakhna	481795	3853870	210	14	15.8	Eaton	Pakhna
TH29	Omodhos/Pakhna	481721	3853872	250	12	15.8	Eaton	Pakhna
TH30	Omodhos/Pakhna	481644	3853878	238	8	15.7	Eaton	Pakhna
TH31	Omodhos/Pakhna	481365	3852838	180	14	15.6	Eaton	Pakhna
TH32	Omodhos/Pakhna	481369	3852839	204	12	15.5	Eaton	Pakhna
TH33	Omodhos/Pakhna	482152	3850455	130	6	15.4	Eaton	Pakhna
TH34	Omodhos/Pakhna	481815	3850150	150	8	15.0	Eaton	Pakhna
TH35	Omodhos/Pakhna	481641	3849934	190	6	14.5	Eaton	Pakhna
TH36	Omodhos/Pakhna	481618	3849757	0	0	14.0	Eaton	Pakhna
TH37	Omodhos/Pakhna	481411	3849429	200	14	13.5	Eaton	Pakhna
TH38	Omodhos/Pakhna	481306	3849116	180	6	13.0	Eaton	Pakhna
TH39	Omodhos/Pakhna	481306	3849116	190	8	12.0	Eaton	Pakhna
TH40	Omodhos/Pakhna	481520	3848443	150	14	11.5	Eaton	Pakhna
TH41	Omodhos/Pakhna	481469	3848371	200	10	10.0	Eaton	Pakhna
TH42	Omodhos/Pakhna	481416	3848302	192	4	7.0	Eaton	Pakhna
TH43	Omodhos/Pakhna	481549	3848911	190	5	9.0	Eaton	Pakhna
TH44	Omodhos/Pakhna	481469	3848075	185	5	5.5	Eaton	Pakhna
TH45	Galataria	465074	3858155	195	16	48.0-62.0		Chalk & Chert
TH46	Galataria	465261	3858254	200	6	48.0-62.0		Chalk & Chert
TH47	Galataria	464796	3859414	15	38	48.0-62.0		Chalk & Chert

Appendix 2- Sub-Areas Location, Age, and Formation Data

Sample	Location	Easting	Northing	Bed dip dir.	Bed Dip	Age(Ma)	Biostrat	Formation
TH48	Galataria	464970	3860581	25	18	48.0-62.0		Chalk & Chert
TH49	Galataria	465306	3859634	0	6	48.0-62.0		Chalk & Chert
TH50	Lefkara	526308	3858718	300	18	51.5	Kahler	Chalk & Chert
TH51	Lefkara	526406	3858800	110	24	50.5	Kahler	Chalk & Chert
TH52	Lefkara	528093	3857690	140	4	52.0	Kahler	Chalk & Chert
TH53	Lefkara	528315	3857433	145	8	53.0	Kahler	Chalk & Chert
TH54	Lefkara	527279	3858301	100	4	51.0	Kahler	Chalk & Chert
TH55	Lefkara	527361	3858247	130	6	50.0	Kahler	Chalk & Chert
TH56	Lefkara	527430	3858164	0	0	49.0	Kahler	Chalk & Chert
TH57	Lefkara	527494	3858072	0	4	48.5	Kahler	Chalk & Chert
TH58	Lefkara	527592	3857999	50	8	48.0	Kahler	Chalk & Chert
TH59	Lefkara	527547	3858094	0	0	20.4	Kahler	Upper Marl
TH60	Lefkara	527547	3858094	0	0	19.0	Kahler	Upper Marl
TH61	Lefkara	527648	3857986	326	18	18.0	Kahler	Upper Marl
TH62	Lefkara	527676	3857932	0	0	17.1	Kahler	Upper Marl
GBPOL01	Polis Rift	441868	3876978					
GBPOL02	Polis Rift	441868	3876978					
GBPOL03	Polis Rift	441532	3876016					
GBPOL04	Polis Rift	441266	3876012					
GBPOL05	Polis Rift	439874	3876114					
GBPOL06	Polis Rift	440987	3876061					
GBPOL07	Polis Rift	441171	3875674					
GBPOL08	Polis Rift	440681	3874880					
GBPOL09	Polis Rift	441100	3875061					
GBPOL10	Polis Rift	441822	3874616					
GBPOL11	Polis Rift	442151	3874276					
GBPOL12	Polis Rift	442258	3874179					
GBPOL13	Polis Rift	442493	3873918					
GBPOL14	Polis Rift	442495	3874895					
GBPOL15	Polis Valley	445073	3875632			<5.0		
GBPOL16	Polis Valley	445062	3875477			<5.0		
GBPOL17	Polis Rift	444856	3874862					
GBPOL18	Polis Rift	444348	3873809					
GBPOL19	Polis Rift	444348	3873809					
GBPOL20	Polis Valley	442801	3877925			<5.0		
GBPOL21	Polis Rift	442694	3877173					
GBPOL22	Polis Rift	442605	3877100					
GBPOL23	Polis Rift	442402	3877051					
GBPOL24	Polis Valley	446177	3875736			<5.0		
GBPOL25	Polis Rift	444143	3873158					
GBPOL26	Polis Rift	443735	3872960					
GBPOL27	Polis Rift	443925	3873366					
GBPOL28	Polis Rift	445295	3869120					
GBPOL29	Polis Rift	445225	3867153					
GBPOL30	Polis Rift	445458	3866842					
GBPOL31	Polis Rift	447340	3865758					
GBPOL32	Polis Rift	447627	3865733					

Appendix 2- Sub-Areas Location, Age, and Formation Data

Sample	Location	Easting	Northing	Bed dip dir.	Bed Dip	Age(Ma)	Biostrat	Formation
GBPOL33	Polis Rift	447407	3865516					
GBPOL34	Polis Rift	448175	3865606					
GBPOL35	Polis Valley	448595	3865773			<5.0		
GBPOL36	Polis Rift	446206	3867798					
GBPOL37	Polis Rift	446309	3868351					
GBPOL38	Polis Rift	446526	3868256					
GBPOL39	Polis Rift	445816	3868164					
GBPOL40	Polis Valley	447522	3868164			<5.0		
GBPOL41	Polis Valley	447826	3868116			<5.0		
GBPOL42	Polis Valley	449115	3869115			<5.0		
GBPOL43	Polis Valley	449968	3870034			<5.0		
GBPOL44	Polis Valley	449791	3870090			<5.0		
GBPOL45	Polis Valley	449805	3869818			<5.0		
GBPOL46	Polis Valley	450222	3869057			<5.0		
GBPOL47	Polis Valley	448426	3871457			<5.0		
GBPOL48	Polis Valley	448820	3871588			<5.0		
GBPOL49	Polis Valley	448937	3872088			<5.0		
GBPOL50	Polis Valley	452707	3871759			<5.0		
GBPOL51	Polis Rift	453290	3871780					
GBPOL52	Polis Rift	454124	3871811					
GBPOL53	Polis Rift	455012	3872117					
GBPOL54	Polis Rift	438716	3876167					
GBPOL55	Polis Rift	441934	3875067					
GBPOL56	Polis Rift	441827	3874627					
GBPOL57	Polis Rift	442318	3875105					
GBPOL58	Polis Rift	442993	3875005					
GBPOL59	Polis Rift	443120	3875233					
GBPOL60	Polis Rift	443348	3875695					
GBPOL61	Polis Rift	443677	3876077					
GBPOL62	Polis Valley	444337	3876452			<5.0		

Appendix 3 - Sub-Areas Magnetic Fabric Data

Samples	μSI	μSI	μSI	μSI	Pj	T	0=para
	Kmax	Kint	Kmin	Kmean			1=diamag
1 GBPOL15A	1.031	0.988	0.980	166	1.056	-0.668	0
2 GBPOL15B	1.009	1.002	0.988	154	1.021	0.317	0
3 GBPOL16A	1.038	1.010	0.953	49	1.090	0.352	0
4 GBPOL16B	1.036	1.002	0.962	50	1.077	0.099	0
5 GBPOL16C	1.017	1.004	0.978	50	1.040	0.308	0
6 GBPOL16D	1.044	0.988	0.968	55	1.080	-0.462	0
7 GBPOL20A	1.024	1.009	0.966	133	1.062	0.498	0
8 GBPOL20B	1.028	1.012	0.959	143	1.075	0.547	0
9 GBPOL20C	1.021	1.018	0.961	142	1.070	0.908	0
10 GBPOL24A	1.007	1.001	0.990	52	1.017	0.337	0
11 GBPOL24B	1.003	0.999	0.997	51	1.005	-0.332	0
12 GBPOL24B	1.014	0.999	0.985	51	1.029	-0.060	0
13 GBPOL24C	1.014	1.010	0.976	49	1.042	0.793	0
14 GBPOL35A	1.117	1.014	0.882	10	1.267	0.177	1
15 GBPOL35B	1.070	0.991	0.941	10	1.137	-0.201	1
16 GBPOL35C	1.072	1.001	0.930	9	1.152	0.035	1
17 GBPOL35D	1.063	0.986	0.952	11	1.118	-0.361	1
18 GBPOL40A	1.566	0.963	0.662	1	2.401	-0.129	0
19 GBPOL40B	1.216	1.013	0.810	2	1.503	0.100	0
20 GBPOL40C	1.097	0.993	0.917	10	1.196	-0.114	1
21 GBPOL40D	1.187	0.971	0.867	11	1.376	-0.281	1
22 GBPOL41A	1.085	1.032	0.891	17	1.226	0.492	0
23 GBPOL41B	1.085	1.032	0.891	17	1.226	0.492	0
24 GBPOL41C	1.031	1.004	0.965	15	1.068	0.215	0
25 GBPOL42A	1.007	1.000	0.991	257	1.016	0.146	0
26 GBPOL42B	1.006	1.003	0.990	426	1.017	0.602	0
27 GBPOL42C	1.011	1.002	0.985	191	1.026	0.325	0
28 GBPOL42D	1.006	1.002	0.990	510	1.017	0.497	0
29 GBPOL43A	1.003	0.999	0.997	95	1.006	-0.332	0
30 GBPOL43B	1.013	0.999	0.987	79	1.026	-0.042	0
31 GBPOL44A	2.790	1.001	-0.358	1	1.026	-0.042	0
32 GBPOL44B	1.823	1.002	-0.547	1	1.026	-0.042	0
33 GBPOL45A	1.127	1.014	0.873	3	1.292	0.173	1
34 GBPOL45B	1.218	1.035	0.792	3	1.547	0.245	1
35 GBPOL45C	1.111	0.995	0.903	4	1.231	-0.060	1
36 GBPOL45D	3.262	1.565	0.195	2	24.052	0.478	1
37 GBPOL46A	1.009	1.004	0.986	319	1.024	0.592	0
38 GBPOL46B	1.025	0.988	0.986	157	1.045	-0.902	0
39 GBPOL46B	1.005	0.997	0.996	155	1.009	-0.714	0
40 GBPOL46C	1.004	1.003	0.992	204	1.013	0.983	0
41 GBPOL47A	1.072	1.014	0.918	10	1.170	0.285	1
42 GBPOL47B	1.055	1.027	0.922	10	1.153	0.593	1
43 GBPOL47C	1.116	0.976	0.917	10	1.222	-0.358	1
44 GBPOL48A	1.010	1.005	0.984	504	1.027	0.601	0
45 GBPOL48B	1.013	1.007	0.979	462	1.036	0.679	0
46 GBPOL49A	1.009	1.000	0.990	136	1.018	0.044	0
47 GBPOL49B	1.019	0.997	0.983	123	1.037	-0.192	0
48 GBPOL49C	1.020	0.994	0.984	127	1.037	-0.472	0
49 GBPOL50A	1.008	1.002	0.989	334	1.019	0.347	0

Appendix 3 - Sub-Areas Magnetic Fabric Data

Samples	μ SI	μ SI	μ SI	μ SI	Pj	T	0=para
	Kmax	Kint	Kmin	Kmean			1=diamag
50 GBPOL50B	1.007	0.998	0.993	548	1.014	-0.340	0
51 GBPOL50C	1.008	0.998	0.993	431	1.015	-0.289	0
52 GBPOL62A	1.090	1.002	0.914	11	1.192	0.043	0
53 GBPOL62B	1.035	0.990	0.975	13	1.064	-0.489	0
1 GBPOL01A	1.020	0.998	0.980	95	1.040	-0.096	0
2 GBPOL01B	1.017	0.996	0.986	184	1.031	-0.387	0
3 GBPOL01C	1.009	0.998	0.992	94	1.017	-0.246	0
4 GBPOL02A	1.100	0.990	0.917	29	1.199	-0.164	0
5 GBPOL02B	1.021	1.000	0.978	42	1.043	0.010	0
6 GBPOL02C	1.050	1.034	0.920	38	1.155	0.773	0
7 GBPOL02D	1.034	1.000	0.966	38	1.070	0.016	0
8 GBPOL03A	1.084	1.023	0.901	24	1.208	0.373	1
9 GBPOL03B	1.028	0.989	0.982	25	1.051	-0.661	1
10 GBPOL03C	1.042	0.998	0.961	27	1.084	-0.071	1
11 GBPOL04A	1.725	1.137	0.509	2	3.568	0.316	1
12 GBPOL04B	1.371	0.968	0.753	3	1.834	-0.162	1
13 GBPOL04C	1.073	1.009	0.923	4	1.163	0.179	1
14 GBPOL04D	1.209	1.033	0.799	5	1.520	0.241	1
15 GBPOL04E	1.289	0.892	0.868	4	1.558	-0.858	1
16 GBPOL04F	1.300	1.111	0.692	4	1.938	0.502	1
17 GBPOL05A	1.257	0.933	0.852	2	1.505	-0.533	1
18 GBPOL05B	1.032	0.995	0.972	30	1.062	-0.208	1
19 GBPOL05C	1.056	0.997	0.949	28	1.113	-0.071	1
20 GBPOL05D	1.056	1.023	0.924	29	1.149	0.512	1
21 GBPOL06A	1.181	1.062	0.796	7	1.505	0.459	1
22 GBPOL06B	1.106	0.998	0.904	7	1.224	-0.017	1
23 GBPOL06C	1.082	0.990	0.932	8	1.161	-0.196	1
24 GBPOL07A	1.049	0.990	0.961	34	1.092	-0.314	0
25 GBPOL07B	1.017	1.001	0.981	38	1.037	0.151	0
26 GBPOL07C	1.067	0.990	0.945	24	1.130	-0.239	0
27 GBPOL07D	1.015	1.004	0.979	28	1.037	0.407	0
28 GBPOL07E	1.073	0.999	0.931	29	1.152	-0.013	0
29 GBPOL07F	1.073	1.013	0.919	28	1.169	0.263	0
30 GBPOL08A	1.075	1.019	0.911	23	1.184	0.352	1
31 GBPOL08B	1.054	0.979	0.967	25	1.097	-0.717	1
32 GBPOL08C	1.092	0.992	0.922	26	1.184	-0.141	1
33 GBPOL08D	1.068	1.021	0.916	27	1.171	0.413	1
34 GBPOL09A	1.190	0.978	0.858	10	1.391	-0.201	0
35 GBPOL09B	1.312	0.888	0.857	9	1.606	-0.834	0
36 GBPOL10A	1.109	1.037	0.868	4	1.288	0.449	1
37 GBPOL10B	1.468	1.129	0.602	2	2.533	0.411	1
38 GBPOL11A	1.015	1.002	0.982	30	1.034	0.207	1
39 GBPOL11B	1.013	1.000	0.986	30	1.026	0.006	1
40 GBPOL11C	1.023	1.001	0.975	27	1.048	0.088	1
41 GBPOL12A	1.029	0.994	0.977	28	1.054	-0.322	1
42 GBPOL12B	1.021	1.003	0.975	28	1.047	0.241	1
43 GBPOL12C	1.035	1.005	0.960	26	1.078	0.217	1
44 GBPOL13A	1.038	1.000	0.962	23	1.078	0.018	1
45 GBPOL13B	1.044	0.982	0.974	24	1.079	-0.758	1

Appendix 3 - Sub-Areas Magnetic Fabric Data

Samples	μ SI	μ SI	μ SI	μ SI	Pj	T	0=para
	Kmax	Kint	Kmin	Kmean			1=diamag
46 GBPOL13C	1.014	0.998	0.986	24	1.028	-0.136	1
47 GBPOL13D	1.013	0.997	0.989	25	1.024	-0.329	1
48 GBPOL14A	1.031	0.993	0.975	28	1.058	-0.363	1
49 GBPOL14B	1.014	1.003	0.982	28	1.033	0.340	1
50 GBPOL14C	1.060	1.023	0.920	27	1.158	0.500	1
51 GBPOL17A	1.025	0.990	0.983	43	1.045	-0.661	0
52 GBPOL17B	1.037	1.033	0.932	44	1.129	0.919	0
53 GBPOL17C	1.038	0.990	0.972	45	1.070	-0.454	0
54 GBPOL17D	1.028	1.003	0.968	47	1.063	0.187	0
55 GBPOL17E	1.029	0.997	0.973	46	1.057	-0.141	0
56 GBPOL18A	1.064	1.004	0.935	11	1.139	0.098	1
57 GBPOL18B	1.274	0.958	0.818	10	1.569	-0.289	1
58 GBPOL18C	1.054	1.007	0.941	16	1.121	0.185	1
59 GBPOL19A	1.017	0.995	0.987	27	1.031	-0.495	1
60 GBPOL19B	1.045	0.999	0.957	26	1.092	-0.022	1
61 GBPOL19C	1.093	0.986	0.926	27	1.182	-0.251	1
62 GBPOL19D	1.036	0.991	0.972	26	1.067	-0.399	1
63 GBPOL21A	1.014	1.003	0.981	45	1.034	0.340	0
64 GBPOL21B	1.075	0.974	0.954	34	1.136	-0.650	0
65 GBPOL21C	1.029	0.988	0.982	35	1.052	-0.760	0
66 GBPOL22A	1.076	1.001	0.927	39	1.160	0.037	0
67 GBPOL22B	1.301	1.271	0.604	31	2.420	0.939	0
68 GBPOL22B	1.036	1.004	0.960	34	1.079	0.172	0
69 GBPOL23A	1.029	0.994	0.976	64	1.055	-0.342	0
70 GBPOL23B	1.013	0.998	0.987	62	1.025	-0.119	0
71 GBPOL23C	1.004	1.000	0.995	62	1.009	0.002	0
72 GBPOL23D	1.011	0.997	0.991	63	1.021	-0.381	0
73 GBPOL23E	1.008	0.999	0.991	64	1.017	-0.087	0
74 GBPOL25A	1.056	1.016	0.931	29	1.138	0.378	1
75 GBPOL25B	1.027	1.000	0.972	29	1.056	0.013	1
76 GBPOL25C	1.010	1.000	0.989	28	1.021	0.005	1
77 GBPOL25D	1.026	1.006	0.967	28	1.062	0.307	1
78 GBPOL26A	1.033	0.997	0.970	30	1.064	-0.143	1
79 GBPOL26B	1.055	1.019	0.929	30	1.140	0.446	1
80 GBPOL26C	1.094	1.018	0.897	29	1.222	0.274	1
81 GBPOL27A	1.015	1.001	0.983	28	1.032	0.119	1
82 GBPOL27B	1.020	1.003	0.976	29	1.045	0.241	1
83 GBPOL27C	1.041	0.990	0.969	27	1.076	-0.385	1
84 GBPOL28A	1.048	0.985	0.968	17	1.087	-0.558	1
85 GBPOL29A	1.036	1.015	0.949	24	1.096	0.539	1
86 GBPOL29B	1.016	1.007	0.976	22	1.042	0.562	1
87 GBPOL30A	1.025	1.005	0.970	20	1.057	0.285	1
88 GBPOL30B	1.104	1.013	0.893	20	1.238	0.187	1
89 GBPOL30C	1.079	1.013	0.913	21	1.183	0.239	1
90 GBPOL30D	1.031	0.992	0.977	20	1.056	-0.444	1
91 GBPOL31A	1.076	1.032	0.899	20	1.206	0.532	1
92 GBPOL31B	1.140	0.956	0.917	20	1.260	-0.620	1
93 GBPOL31C	1.025	1.010	0.965	20	1.064	0.511	1
94 GBPOL31D	1.113	1.029	0.872	19	1.284	0.358	1

Appendix 3 - Sub-Areas Magnetic Fabric Data

Samples	μ SI	μ SI	μ SI	μ SI	Pj	T	0=para
	Kmax	Kint	Kmin	Kmean			1=diamag
95 GBPOL32A	1.178	1.021	0.831	15	1.421	0.179	1
96 GBPOL32B	1.113	1.015	0.884	15	1.261	0.198	1
97 GBPOL32C	1.087	0.984	0.933	15	1.168	-0.299	1
98 GBPOL32D	1.092	1.008	0.907	16	1.204	0.142	1
99 GBPOL33A	1.051	0.983	0.967	25	1.091	-0.607	1
100 GBPOL33B	1.099	1.003	0.906	23	1.213	0.048	1
101 GBPOL33C	1.047	1.000	0.953	25	1.098	0.023	1
102 GBPOL33D	1.131	1.022	0.864	22	1.313	0.250	1
103 GBPOL33E	1.030	0.998	0.971	25	1.060	-0.052	1
104 GBPOL33F	1.026	0.998	0.975	21	1.051	-0.079	1
105 GBPOL34A	1.027	1.000	0.972	10	1.056	0.013	1
106 GBPOL34B	1.103	1.024	0.884	10	1.252	0.322	1
107 GBPOL34C	1.090	0.969	0.945	12	1.163	-0.647	1
108 GBPOL34D	1.061	0.998	0.943	12	1.126	-0.038	1
109 GBPOL36A	1.031	1.013	0.956	22	1.082	0.542	1
110 GBPOL36B	1.042	1.000	0.958	23	1.088	0.021	1
111 GBPOL37A	1.051	1.031	0.922	20	1.152	0.719	1
112 GBPOL37B	1.066	1.006	0.931	21	1.144	0.136	1
113 GBPOL38A	1.019	0.997	0.983	27	1.037	-0.192	1
114 GBPOL38A	1.033	1.004	0.963	27	1.072	0.174	1
115 GBPOL38B	1.042	0.996	0.962	26	1.082	-0.124	1
116 GBPOL38C	1.031	1.008	0.962	26	1.073	0.348	1
117 GBPOL39A	1.056	0.989	0.956	21	1.106	-0.312	1
118 GBPOL39B	1.065	0.985	0.952	21	1.122	-0.394	1
119 GBPOL51A	1.041	0.989	0.970	26	1.076	-0.460	1
120 GBPOL51B	1.064	1.041	0.901	25	1.197	0.727	1
121 GBPOL51C	1.074	1.008	0.923	25	1.164	0.165	1
122 GBPOL52A	1.089	0.976	0.939	5	1.166	-0.472	1
123 GBPOL52B	1.118	0.952	0.938	7	1.214	-0.834	1
124 GBPOL52C	1.796	0.967	0.575	4	3.219	-0.089	1
125 GBPOL52D	1.097	1.019	0.893	6	1.231	0.278	1
126 GBPOL53A	1.029	1.016	0.955	72	1.082	0.670	0
127 GBPOL53B	1.027	1.020	0.953	133	1.086	0.804	0
128 GBPOL53C	1.026	1.009	0.964	167	1.066	0.468	0
129 GBPOL53D	1.035	1.001	0.964	138	1.073	0.078	0
130 GBPOL53E	1.015	1.012	0.972	170	1.049	0.841	0
131 GBPOL54A	1.024	1.003	0.972	23	1.053	0.179	1
132 GBPOL54B	1.250	1.048	0.762	18	1.654	0.287	1
133 GBPOL54C	1.055	0.990	0.956	20	1.105	-0.278	1
134 GBPOL55A	1.100	1.014	0.895	15	1.230	0.210	1
135 GBPOL55B	1.170	1.078	0.791	17	1.512	0.582	1
136 GBPOL55C	1.045	1.006	0.950	17	1.101	0.199	1
137 GBPOL56A	1.201	0.991	0.839	10	1.433	-0.070	0
138 GBPOL56B	1.203	0.984	0.843	6	1.428	-0.132	0
139 GBPOL56C	1.217	0.997	0.823	8	1.480	-0.021	0
140 GBPOL57A	1.038	0.988	0.974	28	1.069	-0.545	1
141 GBPOL57B	1.047	0.999	0.955	27	1.096	-0.017	1
142 GBPOL58A	1.042	1.010	0.949	28	1.098	0.328	1
143 GBPOL58B	1.073	1.020	0.912	9	1.180	0.368	1

Appendix 3 - Sub-Areas Magnetic Fabric Data

Samples	μ SI	μ SI	μ SI	μ SI	Pj	T	0=para
	Kmax	Kint	Kmin	Kmean			1=diamag
147 GBPOL60A	1.120	1.034	0.862	2	1.309	0.389	1
148 GBPOL60B	1.144	0.968	0.902	4	1.276	-0.406	1
149 GBPOL60C	1.213	0.970	0.849	3	1.435	-0.252	1
150 GBPOL61A	1.122	0.988	0.901	10	1.246	-0.165	1
151 GBPOL61B	1.048	1.010	0.943	10	1.112	0.296	1
152 GBPOL61C	1.077	1.001	0.926	10	1.163	0.037	1
1 TH45A	1.023	1.012	0.964	25	1.065	0.609	0
2 TH45B	1.087	0.967	0.950	11	1.157	-0.735	0
3 TH45C	1.053	0.996	0.953	14	1.104	-0.119	0
4 TH45D	1.030	1.017	0.953	15	1.087	0.677	0
5 TH45E	1.016	1.007	0.976	22	1.042	0.562	0
6 TH46A	1.179	1.015	0.835	6	1.414	0.132	0
7 TH46B	1.193	0.957	0.874	7	1.378	-0.416	0
8 TH46C	1.080	1.028	0.900	7	1.207	0.464	0
9 TH46D	1.253	1.130	0.705	8	1.854	0.640	0
10 TH46E	1.150	1.012	0.858	6	1.340	0.124	0
11 TH47A	1.125	1.028	0.863	27	1.310	0.320	0
12 TH47B	1.121	1.003	0.888	27	1.261	0.042	0
13 TH47C	1.398	1.221	0.585	25	2.589	0.689	0
14 TH47D	1.044	1.003	0.954	26	1.094	0.105	0
15 TH47E	1.020	1.011	0.968	34	1.057	0.673	0
16 TH48A	1.067	0.987	0.947	14	1.128	-0.307	0
17 TH48B	1.087	0.992	0.926	13	1.175	-0.143	0
18 TH48C	1.118	1.028	0.869	13	1.293	0.329	0
19 TH48D	1.071	0.969	0.962	13	1.126	-0.860	0
20 TH48E	1.019	1.005	0.975	27	1.046	0.343	0
21 TH49A	1.043	1.026	0.933	22	1.127	0.694	0
22 TH49B	1.029	1.005	0.966	20	1.065	0.245	0
23 TH49C	1.044	0.980	0.976	22	1.078	-0.863	0
24 TH49D	1.024	1.008	0.968	24	1.059	0.440	0
25 TH49E	1.025	1.014	0.961	18	1.071	0.675	0
26 TH50A	1.033	1.019	0.950	22	1.093	0.678	0
27 TH50B	1.022	1.005	0.974	23	1.050	0.284	0
28 TH50C	1.023	1.007	0.970	24	1.056	0.396	0
29 TH51A	1.021	1.000	0.980	34	1.042	0.010	0
30 TH51B	1.020	0.997	0.983	43	1.038	-0.241	0
31 TH51C	1.015	1.006	0.980	43	1.037	0.473	0
32 TH52A	1.016	0.999	0.985	57	1.032	-0.103	0
33 TH52B	1.016	1.000	0.985	58	1.032	0.008	0
34 TH52C	1.013	1.000	0.987	54	1.026	0.007	0
35 TH53A	1.023	1.014	0.964	24	1.067	0.722	0
36 TH53B	1.036	1.006	0.959	23	1.081	0.240	0
37 TH53C	1.010	1.001	0.989	24	1.021	0.205	0
38 TH54A	1.019	1.008	0.974	62	1.048	0.508	0
39 TH54B	1.013	1.006	0.981	70	1.034	0.551	0
40 TH54C	1.019	1.008	0.974	56	1.048	0.528	0
41 TH55A	1.027	1.004	0.970	26	1.059	0.214	0
42 TH55B	1.042	0.998	0.962	36	1.084	-0.083	0
43 TH55C	1.011	1.009	0.980	35	1.035	0.821	0

Appendix 3 - Sub-Areas Magnetic Fabric Data

Samples	μ SI	μ SI	μ SI	μ SI	Pj	T	0=para
	Kmax	Kint	Kmin	Kmean			1=diamag
47 TH57A	1.024	1.011	0.966	63	1.062	0.565	0
48 TH57B	1.018	1.016	0.967	57	1.060	0.933	0
49 TH57C	1.023	1.011	0.967	66	1.061	0.577	0
50 TH58A	1.016	0.997	0.988	21	1.029	-0.327	0
51 TH58B	1.020	1.016	0.964	25	1.065	0.861	0
52 TH58C	1.018	1.010	0.973	24	1.050	0.643	0
53 TH59A	1.026	1.016	0.959	19	1.076	0.701	0
54 TH59B	1.094	0.976	0.936	20	1.175	-0.470	0
55 TH59C	1.054	1.013	0.937	20	1.127	0.331	0
56 TH60A	1.047	0.987	0.968	27	1.085	-0.509	0
57 TH60B	1.025	1.005	0.971	29	1.057	0.263	0
58 TH60C	1.037	1.005	0.959	28	1.082	0.201	0
59 TH61A	1.024	1.001	0.976	31	1.049	0.079	0
60 TH61B	1.059	0.983	0.961	32	1.107	-0.531	0
61 TH61C	1.027	1.010	0.964	30	1.068	0.486	0
62 TH62A	1.031	1.005	0.965	23	1.068	0.216	0
63 TH62B	1.038	0.995	0.969	23	1.072	-0.234	0
64 TH62C	1.050	0.997	0.955	19	1.099	-0.088	0
65 TH01F	1.025	1.016	0.960	68	1.074	0.735	0
66 TH01G	1.033	1.008	0.960	42	1.077	0.307	0
67 TH02F	1.018	1.014	0.969	177	1.056	0.841	0
68 TH02G	1.020	1.012	0.969	119	1.057	0.679	0
69 TH02H	1.019	1.012	0.969	185	1.056	0.745	0
70 TH04A	1.017	1.005	0.979	51	1.039	0.376	0
71 TH04B	1.013	1.001	0.986	53	1.027	0.149	0
72 TH04C	1.014	1.003	0.983	52	1.032	0.257	0
73 TH04D	1.013	1.002	0.985	52	1.029	0.207	0
74 TH04E	1.016	1.002	0.982	50	1.034	0.185	0
75 TH04F	1.013	1.004	0.983	53	1.031	0.381	0
76 TH05A	1.019	1.009	0.973	60	1.049	0.563	0
77 TH05B	1.017	1.007	0.977	51	1.042	0.507	0
78 TH05C	1.014	1.008	0.979	55	1.038	0.689	0
79 TH05D	1.019	1.011	0.970	51	1.054	0.686	0
80 TH05E	1.022	0.997	0.981	48	1.043	-0.190	0
81 TH06A	1.028	1.007	0.966	24	1.066	0.347	0
82 TH06B	1.020	1.000	0.980	25	1.041	0.010	0
83 TH06C	1.026	1.012	0.963	22	1.069	0.582	0
84 TH06D	1.013	1.004	0.983	24	1.031	0.435	0
85 TH06E	1.037	0.993	0.971	23	1.068	-0.319	0
86 TH06F	1.022	1.003	0.976	22	1.048	0.211	0
87 TH06G	1.040	0.999	0.962	22	1.081	-0.039	0
88 TH08F	1.029	1.022	0.951	15	1.091	0.839	0
89 TH09F	1.053	1.006	0.944	13	1.115	0.169	0
90 TH09G	1.059	0.991	0.953	13	1.112	-0.261	0
91 TH10F	1.021	1.010	0.971	36	1.054	0.564	0
92 TH10G	1.009	1.006	0.985	37	1.027	0.780	0
93 TH11F	1.043	0.983	0.976	13	1.075	-0.771	0
94 TH12F	1.019	1.007	0.975	31	1.047	0.438	0
95 TH12G	1.032	1.000	0.968	31	1.066	0.016	0

Appendix 3 - Sub-Areas Magnetic Fabric Data

Samples	μ SI	μ SI	μ SI	μ SI	Pj	T	0=para
	Kmax	Kint	Kmin	Kmean			1=diamag
99 TH14G	1.020	1.000	0.981	25	1.040	0.010	0
100 TH16F	1.015	1.007	0.979	36	1.039	0.545	0
101 TH17F	1.019	1.006	0.975	23	1.046	0.409	0
102 TH17G	1.023	0.999	0.979	25	1.045	-0.080	0
103 TH18F	1.025	1.013	0.964	16	1.068	0.610	0
104 TH19A	1.020	1.013	0.968	15	1.058	0.756	0
105 TH19B	1.037	0.985	0.979	16	1.065	-0.772	0
106 TH20A	1.030	1.019	0.953	18	1.089	0.724	0
107 TH20B	1.026	1.006	0.969	19	1.060	0.286	0
108 TH21A	1.053	1.004	0.946	21	1.113	0.117	0
109 TH21B	1.070	0.985	0.949	31	1.131	-0.380	0
110 TH22B	1.021	1.007	0.972	35	1.052	0.422	0
111 TH22C	1.028	0.988	0.985	34	1.050	-0.864	0
112 TH23A	1.070	0.982	0.952	17	1.128	-0.478	0
113 TH23B	1.037	1.000	0.964	16	1.076	0.018	0
114 TH24A	1.136	0.978	0.900	9	1.267	-0.280	0
115 TH24B	1.077	0.998	0.930	9	1.159	-0.040	0
116 TH25A	1.025	0.999	0.976	35	1.050	-0.047	0
117 TH25B	1.012	1.001	0.987	36	1.025	0.117	0
118 TH26A	1.035	0.999	0.967	22	1.071	-0.050	0
119 TH26B	1.020	1.009	0.972	29	1.052	0.579	0
120 TH27A	1.084	0.973	0.948	23	1.153	-0.604	0
121 TH27B	1.046	0.999	0.957	19	1.093	-0.037	0
122 TH28A	1.023	1.014	0.964	20	1.066	0.675	0
123 TH28B	1.041	1.015	0.946	19	1.104	0.463	0
124 TH29A	1.022	0.999	0.979	39	1.044	-0.048	0
125 TH29B	1.014	1.004	0.983	42	1.032	0.391	0
126 TH30A	1.029	1.005	0.967	21	1.064	0.245	0
127 TH30B	1.034	1.009	0.959	20	1.079	0.350	0
128 TH31A	1.015	0.998	0.987	82	1.029	-0.211	0
129 TH31B	1.022	0.993	0.985	75	1.039	-0.549	0
130 TH32A	1.013	1.005	0.982	85	1.033	0.488	0
131 TH32C	1.017	1.001	0.982	86	1.035	0.075	0
132 TH33A	1.019	1.004	0.978	19	1.043	0.260	0
133 TH33B	1.030	0.995	0.976	20	1.056	-0.260	0
134 TH34A	1.020	0.997	0.984	30	1.037	-0.264	0
135 TH34B	1.026	0.994	0.981	31	1.047	-0.419	0
136 TH35A	1.036	0.998	0.967	13	1.071	-0.094	0
137 TH35B	1.040	1.007	0.955	15	1.091	0.251	0
138 TH36A	1.022	0.989	0.989	19	1.038	-1.000	0
139 TH36B	1.037	1.000	0.964	19	1.077	0.018	0
140 TH37A	1.038	1.006	0.958	12	1.085	0.219	0
141 TH37B	1.042	1.003	0.956	13	1.090	0.112	0
142 TH38A	1.056	1.001	0.946	15	1.116	0.027	0
143 TH38B	1.024	1.006	0.970	17	1.057	0.345	0
144 TH39A	1.026	0.996	0.978	17	1.049	-0.239	0
145 TH39B	1.030	1.014	0.957	19	1.080	0.584	0
146 TH40A	1.013	1.000	0.987	62	1.026	0.006	0
147 TH40B	1.007	1.002	0.992	61	1.015	0.337	0

Appendix 3 - Sub-Areas Magnetic Fabric Data

Samples	μSI	μSI	μSI	μSI	Pj	T	0=para
	Kmax	Kint	Kmin	Kmean			1=diamag
151 TH42B	1.014	1.008	0.978	31	1.039	0.642	0
152 TH43A	1.033	1.002	0.966	19	1.069	0.094	0
153 TH43B	1.030	1.009	0.962	19	1.072	0.399	0
154 TH44A	1.023	1.003	0.974	31	1.051	0.212	0
155 TH44B	1.026	0.998	0.977	32	1.051	-0.113	0

Appendix 4 -Regional Area Sample Location and Formation

Sample	Northing	Easting	Formation	Sample	Northing	Easting	Formation
CY9701	3844700	500540	?	FL98212	3851037	481200	Pakhna
CY9702	3844950	499550	?	FL98213A	3851618	480922	Pakhna
CY9703	3847180	495020	?	FL98214	3852065	481041	Pakhna
CY9704	3846875	492570	?	FL98215A	3850217	481762	Pakhna
CY9705	3850500	492425	?	FL98216	3849676	481533	Pakhna
CY9706	3851450	492500	?	FL98217A	3849172	481383	Pakhna
CY9707	3855025	492150	?	FL98218	3848433	481477	Pakhna
CY9708	3856300	492320	?	FL98219A	3847673	481254	Pakhna
CY9709	3856590	487900	?	FL98220	3846092	480339	Pakhna
CY9710	3856590	487900	?	FL98222	3842511	479742	Pakhna
CY9711	3854020	488020	?	FL98223A	3841925	479638	Pakhna
CY9712	3854550	486580	?	FL98225A	3839085	478406	Pakhna
CY9713	3854550	486580	?	FL98226	3840536	494153	Pakhna
CY9714	3853200	484775	?	FL98228	3842115	493364	Pakhna
CY9715	3851075	484150	?	FL98229A	3842271	492773	Pakhna
CY9721	3837700	491800	?	FL98230	3842922	492235	Pakhna
CY9722	3840000	485850	?	FL98231A	3843861	492351	Pakhna
CY9723	3836525	466600	?	FL98232	3844565	492617	Pakhna
CY9724	3836800	466100	?	FL98233A	3844565	492617	Pakhna
CY9725	3840525	460850	?	FL98234	3846550	491806	Pakhna
CY9726	3840525	460850	?	FL98237A	3847019	492281	Pakhna
CY9727A	3840525	460850	?	FL98238	3847275	491572	Pakhna
CY9727B	3853520	450600	?	FL98239A	3848215	491436	Pakhna
CY9728	3855825	451600	?	FL98240	3848712	490936	Pakhna
CY9729	3857450	452620	?	FL98241A	3849639	490008	Pakhna
CY9730	3859400	452810	?	FL98242	3850396	489979	Pakhna
CY9731	3859400	452810	?	FL98243A	3852950	487920	Pakhna
CY9732	3864700	447175	?	FL98244	3852838	487811	Pakhna
CY9748	3879650	508975	?	FL98245A	3852613	486880	Pakhna
CY9749	3878700	510000	?	FL98246	3851892	486643	Pakhna
CY9750	3878700	510000	?	FL98248	3851204	486149	Pakhna
CY9751	3878200	517900	?	FL98249A	3850751	485832	Pakhna
CY9752	3843100	499050	?	FL98250	3850271	485229	Pakhna
CY9766	3845650	507600	?	FL98253A	3849181	484552	Pakhna
FL98004	3846302	507713	Lefkara	FL98254	3841947	459400	Pakhna
FL98005	3846302	507713	Lefkara	FL98255	3842926	460941	Pakhna
FL98006	3846241	507764	Lefkara	FL98256	3843319	461842	Pakhna
FL98015	3845847	508559	Lefkara	FL98257A	3843535	463075	Pakhna
FL98016	3845741	508435	Lefkara	FL98259A	3852590	474566	Lefkara
FL98024	3844559	508056	Lefkara	FL98260	3853136	474579	Lefkara
FL98027	3843069	511336	Pakhna	FL98261A	3853136	474579	Lefkara
FL98031A	3843239	511721	Lefkara	FL98272	3853891	478898	Lefkara
FL98036	3849151	502799	Lefkara	FL98273	3854789	479207	Lefkara
FL98054	3850910	499887	Lefkara	FL98275	3855879	478561	Lefkara
FL98060	3852513	528236	Lefkara	FL98279A	3857177	475178	Lefkara
FL98061A	3852442	527241	Lefkara	FL98280	3857404	475118	Lefkara
FL98067A	3853393	532861	Lefkara	FL98281	3857670	473832	Pakhna
FL98070	3854132	532583	Lefkara	FL98282	3854594	471199	Lefkara
FL98074	3854931	531541	Lefkara	FL98283A	3854027	471365	Lefkara

Appendix 4 -Regional Area Sample Location and Formation

Sample	Northing	Easting	Formation	Sample	Northing	Easting	Formation
FL98083A	3856493	528292	Lefkara	FL98287	3850032	466538	Lefkara
FL98084	3856525	528556	Lefkara	FL98288	3849534	465813	Lefkara
FL98085A	3856420	528855	Lefkara	FL98289A	3846154	463102	Lefkara
FL98086	3856880	528627	Lefkara	FL98290	3842359	459795	Pakhna
FL98087A	3851003	496704	Pakhna	FL98291A	3842534	458685	Pakhna
FL98088	3850846	496397	Pakhna	FL98296	3848945	460364	Lefkara
FL98089A	3850611	496535	Pakhna	FL98297	3849302	460542	Lefkara
FL98090	3850163	496865	Pakhna	FL98298	3849879	460670	Lefkara
FL98091A	3849509	496962	Pakhna	FL98299	3850384	460417	Lefkara
FL98093A	3847540	496983	Pakhna	FL98300	3851422	459916	Lefkara
FL98094	3846575	497269	Pakhna	FL98301A	3850822	458888	Kalavassos
FL98095	3844816	497936	Pakhna	FL98302	3850071	458666	Lefkara
FL98096	3844673	498575	Pakhna	FL98304	3849544	458688	Lefkara
FL98097A	3844006	498581	Pakhna	FL98305A	3854529	462776	Pakhna
FL98098	3843645	498885	Pakhna	FL98306	3855032	463100	Lefkara
FL98099A	3842967	498901	Pakhna	FL98307A	3855442	463667	Lefkara
FL98100	3842513	498861	Pakhna	FL98308	3859432	465364	Lefkara
FL98101A	3851978	490941	Pakhna	FL98309A	3860760	464810	Pakhna
FL98102	3854813	489940	Lefkara	FL98310	3861184	464853	Pakhna
FL98103	3855783	489580	Lefkara	FL98311A	3861789	465004	Pakhna
FL98104B	3855927	489549	Lefkara	FL98312	3863086	465187	Lefkara
FL98105A	3856094	489345	Lefkara	FL98313A	3864318	466279	Lefkara
FL98106	3855848	489824	Lefkara	FL98315A	3860682	464565	Pakhna
FL98107A	3856106	490038	Lefkara	FL98316	3859396	464787	Pakhna
FL98108	3856215	489753	Lefkara	FL98317A	3859555	461353	Pakhna
FL98109A	3856769	489552	Lefkara	FL98318	3859642	460704	Pakhna
FL98110	3857419	486310	Lefkara	FL98319A	3859323	460223	Pakhna
FL98113A	3846318	507645	Lefkara	FL98320	3856679	457034	Pakhna
FL98114	3846047	507758	Pakhna	FL98321A	3853559	450343	Lefkara
FL98115A	3845872	507670	Pakhna	FL98322	3854003	451239	Pakhna
FL98116	3845840	507665	Pakhna	FL98323A	3854807	451438	Pakhna
FL98117A	3845734	507812	Pakhna	FL98324	3855423	451497	Pakhna
FL98118	3845598	507825	Pakhna	FL98325A	3853893	453613	Pakhna
FL98119A	3845037	507577	Pakhna	FL98326	3853421	453726	Pakhna
FL98121A	3844716	507692	Pakhna	FL98327A	3853005	454292	Pakhna
FL98122	3844767	507586	Pakhna	FL98328	3856273	451685	Pakhna
FL98126	3842814	507713	Pakhna	FL98329A	3856634	452423	Pakhna
FL98128	3845484	497096	Pakhna	FL98330	3857463	452473	Pakhna
FL98136	3846179	495940	Pakhna	FL98331A	3858266	452740	Pakhna
FL98137A	3846347	495675	Pakhna	FL98332	3859494	452649	Pakhna
FL98138	3846734	495446	Pakhna	FL98333A	3861226	451767	Kalavassos
FL98139A	3846734	495446	Pakhna	FL98334	3861940	449963	Nicosia
FL98140	3846879	495347	Pakhna	FL98335A	3862528	449102	Pakhna
FL98141A	3846879	495347	Pakhna	FL98336	3863331	448247	Pakhna
FL98142	3847364	494989	Pakhna	FL98337A	3863250	447145	Pakhna
FL98146	3847158	494021	Pakhna	FL98338	3862728	446160	Pakhna
FL98147A	3846643	493428	Pakhna	FL98339A	3862437	445396	Pakhna
FL98148	3846641	492921	Pakhna	FL98340	3861900	444029	Pakhna
FL98149A	3838655	494008	Pakhna	FL98341A	3861814	442806	Pakhna

Appendix 4 -Regional Area Sample Location and Formation

Sample	Northing	Easting	Formation	Sample	Northing	Easting	Formation
FL98153A	3839813	485703	Pakhna	FL98346	3848853	492265	Pakhna
FL98154	3839336	484642	Pakhna	FL98347A	3854248	492445	Lefkara
FL98156	3839336	484642	Pakhna	FL98348	3854538	491855	Lefkara
FL98157A	3837415	481937	Pakhna	FL98349A	3855115	491610	Lefkara
FL98158	3837939	479151	Pakhna	FL98350	3840800	505200	Kalivasos
FL98159A	3837939	479151	Pakhna	FL98352	3841591	508681	Pakhna
FL98160A	3837860	475223	Nicosia	FL98353A	3841297	511693	Pakhna
FL98161A	3837860	475223	Nicosia	FL98354	3842260	512394	Pakhna
FL98162A	3837771	473189	Nicosia	FL98355	3840913	512703	Pakhna
FL98166	3836443	469359	Lefkara	FL98356	3865568	448443	Pakhna
FL98167A	3835262	467671	Lefkara	FL98357A	3864907	448676	Pakhna
FL98168	3835262	467671	Lefkara	FL98358	3865239	448957	Pakhna
FL98169A	3835479	467088	Lefkara	FL98359A	3866560	449166	Pakhna
FL98170	3836222	466468	Lefkara	FL98360B	3867889	449674	Nicosia
FL98171	3836044	489657	Reef	FL98361A	3869361	450218	Nicosia
FL98172	3836363	489372	Pakhna	FL98363A	3875068	446218	Nicosia
FL98173A	3837089	486410	Pakhna	FL98364C	3872516	445626	Nicosia
FL98174	3836740	484068	Pakhna	FL98365	3871152	445731	Pakhna
FL98175A	3837126	483453	Pakhna	FL98366	3866855	445433	Pakhna
FL98176	3837957	484309	Pakhna	FL98367A	3865355	446835	Pakhna
FL98177A	3836978	483111	Nicosia	FL98368	3837963	471439	Pakhna
FL98179	3835796	468256	Pakhna	FL98369A	3841124	471423	Nicosia
FL98180	3835796	468256	Pakhna	FL98370	3841679	474531	Pakhna
FL98181A	3837178	463819	Pakhna	FL98371A	3841679	474531	Pakhna
FL98182	3837178	463819	Pakhna	FL98372	3842015	517144	Pakhna
FL98183A	3842253	463594	Pakhna	FL98373A	3842015	517144	Lefkara
FL98184	3842440	463883	Pakhna	FL98374	3842015	517144	Lefkara
FL98185A	3842698	464633	Pakhna	FL98379A	3840672	524593	Lefkara
FL98186	3843092	465260	Pakhna	FL98383	3846981	527531	Pakhna
FL98187A	3843248	466811	Pakhna	FL98388	3847894	525957	Lefkara
FL98188A	3844612	468071	Reef	FL98389A	3847663	525144	Lefkara
FL98190	3845359	470448	Lefkara	FL98390	3847867	524444	Lefkara
FL98191A	3845622	471439	Pakhna	GBFL001A	3861640	546700	Lefkara
FL98192	3847322	473074	Pakhna	GBFL002	3861750	545850	Lefkara
FL98193A	3847853	474235	Pakhna	GBFL003A	3863000	544100	Lefkara
FL98194	3848564	475170	Pakhna	GBFL004	3862300	543640	Lefkara
FL98195	3849525	476037	Pakhna	GBFL005	3863050	542420	Lefkara
FL98196	3850851	476326	Pakhna	GBFL006	3866340	545600	Lefkara
FL98198	3851837	478564	Pakhna	GBFL007A	3865500	548380	Lefkara
FL98199A	3852445	479452	Pakhna	GBFL008	3864980	549900	Lefkara
FL98200	3839371	491026	Pakhna	GBFL010	3864259	550621	Pakhna
FL98201	3840419	490113	Pakhna				
FL98202	3841340	490098	Pakhna				
FL98203A	3842847	489860	Pakhna				
FL98204	3844476	488807	Pakhna				
FL98205A	3846374	486221	Pakhna				
FL98206	3846714	485654	Pakhna				
FL98207	3847502	484850	Pakhna				
FL98208	3848709	484592	Pakhna				

Appendix 5 - Regional Magnetic Fabric Data

Sample	Declination	Minimum			Intermediate			Maximum	
		Inclination	Intensity	Dec.	Inc.	Intensity	Dec.	Inc.	Intensity
FL1 (I)									
FL98342A	350.8	43.4	-26.6	248.8	12.5	-26.3	146.5	43.9	-25.6
FL98342B	226.2	19.9	-25.4	14.6	67.0	-24.7	132.1	11.1	-24.4
FL98342C	53.8	25.9	-26.4	265.8	60.2	-25.9	150.6	13.7	-25.6
FL98341B	233.7	60.6	-12.9	360.0	18.4	-12.3	97.7	22.0	-12.3
FL98343B	189.0	85.2	72.6	295.7	1.4	75.2	25.8	4.6	76.4
FL98340A	94.0	61.9	5.8	282.0	29.5	6.5	190.2	3.3	6.9
FL98340B	84.8	54.7	6.6	180.4	4.0	7.6	273.2	35.1	7.7
FL98340C	256.2	82.3	3.8	43.8	7.3	4.3	134.3	5.7	4.6
FL98340D	180.0	45.0	5.5	38.9	37.9	5.6	292.0	20.5	5.9
FL98339B	259.4	72.1	9.8	134.8	10.4	10.5	42.1	14.4	10.9
FL98339C	239.3	52.8	14.6	89.5	33.3	15.1	349.5	14.7	15.5
FL98339D	277.8	48.9	10.5	18.0	8.8	11.1	115.4	39.8	11.2
FL98367B	310.7	27.8	-24.8	56.7	27.6	-23.9	183.5	48.9	-22.5
FL98365B	130.9	1.3	-33.4	222.8	55.3	-29.0	40.0	34.6	-25.0
FL98366A	278.6	42.6	2.8	166.6	22.1	5.1	57.3	39.2	7.5
FL98366B	46.2	46.3	7.9	297.0	17.4	11.2	192.6	38.5	12.4
FL98366C	101.5	72.5	11.0	260.6	16.4	11.1	352.4	5.9	11.4
FL98338B	124.8	57.2	-3.4	269.0	27.6	-2.8	7.8	16.3	-2.3
FL98338C	33.6	65.9	-4.0	278.6	10.7	-3.7	184.3	21.4	-3.3
FL98363B	126.2	77.5	38.1	286.0	11.8	39.1	16.9	4.2	39.5
FL98364A	225.3	53.5	32.9	91.8	27.0	33.8	349.6	22.6	34.2
FL98364B	66.2	82.2	27.4	283.5	6.2	28.2	193.0	4.7	29.1
FL98364C	11.2	76.1	38.0	246.5	8.0	39.3	154.9	11.3	40.1
FL98368A	331.6	26.3	-22.6	218.0	39.0	-21.9	85.8	39.7	-20.9
FL98368B	176.9	23.9	-23.6	287.9	39.0	-19.9	63.7	41.5	-19.8
FL98368C	152.9	81.2	-40.8	5.8	7.4	-17.0	275.1	4.7	-8.2
FL98337B	15.8	11.6	-20.3	262.0	63.0	-19.9	111.1	24.0	-19.6
CY9732A	276.7	63.4	-10.7	77.0	25.3	-10.5	170.7	7.9	-10.0
CY9732B	300.5	46.2	-11.0	80.9	36.4	-10.8	187.2	20.8	-10.5
CY9732C	246.0	74.4	-10.1	83.6	14.9	-9.7	352.4	4.5	-9.2
CY9732D	90.0	90.0	-10.9	90.0	90.0	-10.7	270.0	90.0	-9.9
CY9732D	97.8	7.8	-10.8	195.4	44.0	-10.5	360.0	45.0	-10.4
CY9732E	55.0	65.3	-7.9	301.8	10.3	-7.6	207.5	22.2	-7.5
FL98336A	79.8	8.1	6.0	175.6	35.2	6.5	338.7	53.6	6.8
FL98336B	163.9	60.4	2.6	350.1	29.4	3.2	258.6	2.7	3.4
FL98356B	289.2	61.9	2.2	43.2	12.2	3.1	138.9	24.9	3.5
FL98356C	262.5	62.3	3.0	43.4	22.2	3.7	140.0	15.8	4.1
FL98357B	104.2	68.2	21.5	257.2	19.7	22.2	350.5	9.2	23.5
FL98357C	227.7	77.0	16.8	67.5	12.2	17.8	336.5	4.3	17.9
FL98358A	90.9	40.7	28.9	249.8	47.3	30.2	351.5	10.7	31.6
FL98358B	295.4	86.3	32.3	96.9	3.5	33.0	187.0	1.2	33.9
FL98358C	267.2	54.1	28.8	75.0	35.3	30.0	169.2	5.8	30.3
FL98335B	233.9	54.3	3.2	82.3	32.3	3.4	343.5	13.5	4.0
FL98335C	225.8	70.0	10.4	110.8	8.8	10.9	17.9	17.9	11.7
FL98359B	276.9	47.9	3.7	100.0	42.0	4.5	8.6	1.6	5.0
FL98359D	299.6	78.3	4.0	102.9	11.2	4.7	193.5	3.3	5.5
FL98360A	209.5	72.7	10.3	76.4	12.0	10.8	343.7	12.2	11.5

Appendix 5 - Regional Magnetic Fabric Data

Sample	Declination	Minimum			Intermediate			Maximum	
		Inclination	Intensity	Dec.	Inc.	Intensity	Dec.	Inc.	Intensity
FL98360B	248.3	61.9	3.4	139.9	9.5	4.1	45.2	26.2	4.7
FL98334A	242.6	47.6	31.1	66.7	42.3	31.9	334.9	2.1	32.2
FL98334B	211.8	81.4	28.0	104.5	2.6	28.8	14.2	8.2	29.2
FL98334C	258.3	46.1	30.8	137.6	26.2	32.1	29.4	32.3	33.6
FL98361B	338.7	88.4	187.5	139.1	1.5	191.8	229.1	0.5	192.4
FL98361C	203.8	80.6	266.2	305.6	1.9	270.3	35.9	9.2	271.5
FL98321B	335.9	79.0	-14.1	113.9	8.2	-13.4	205.0	7.2	-12.4
FL98321C	263.1	25.8	-10.2	111.4	61.2	-9.9	358.9	11.9	-9.4
CY9727B	210.5	74.2	13.2	54.8	14.5	13.6	323.2	6.2	14.4
CY9727B1	238.2	74.4	7.3	78.2	14.7	7.9	346.8	5.1	8.3
CY9727B3	165.7	58.4	15.4	331.7	30.9	15.7	65.5	6.3	16.0
CY9727B4	194.8	69.2	18.6	89.5	5.7	19.1	357.4	19.9	19.7
CY9727B5	197.0	64.8	19.3	56.9	19.9	19.9	321.4	14.9	20.3
FL98322A	212.2	0.6	-11.4	122.0	12.1	-11.2	305.2	77.8	-9.6
FL98322B	103.8	58.7	-18.8	266.7	30.1	-18.4	1.2	7.6	-17.8
FL98322C	244.3	75.3	-19.2	74.6	14.5	-18.8	343.9	2.5	-18.0
FL98322D	232.9	2.9	-12.1	336.5	78.0	-12.0	142.3	11.7	-11.7
FL98323B	72.8	36.6	-29.5	228.0	50.7	-29.4	333.5	12.3	-28.5
FL98324A	267.0	47.1	11.6	97.9	42.4	11.7	2.9	5.4	13.3
FL98324B	3.5	37.6	12.2	249.1	28.2	12.6	132.9	39.5	14.2
FL98324C	226.1	11.4	11.7	14.0	76.6	12.0	134.7	6.9	12.8
CY9728A	300.9	77.0	26.0	100.1	12.2	26.6	191.0	4.5	27.2
CY9728B	360.0	84.3	35.7	180.0	0.0	37.2	180.0	5.7	37.2
CY9728B	39.6	71.9	35.9	130.4	0.3	36.6	220.5	18.1	38.1
CY9728C	279.8	66.1	47.1	74.7	21.9	47.5	168.5	9.2	48.6
CY9728C	180.0	5.7	46.1	0.0	84.3	47.6	360.0	85.7	48.1
CY9728D	292.4	65.3	33.4	53.8	13.5	34.2	148.8	20.3	34.5
CY9728E	64.5	77.2	27.6	246.0	12.8	28.3	155.9	0.3	28.9
FL98328A	214.7	80.0	15.7	109.3	2.7	16.2	18.9	9.6	16.7
FL98328B	268.7	81.0	16.7	62.6	8.1	17.3	153.2	3.9	17.9
FL98328C	245.0	66.5	12.6	92.6	21.0	13.8	358.8	9.9	14.1
FL98328D	290.1	59.4	16.5	107.3	30.6	17.2	198.0	1.2	17.9
FL98333B	263.2	24.4	-34.1	105.4	63.9	-33.8	357.2	8.7	-33.6
FL98329B	275.7	2.7	15.1	160.3	83.7	15.8	5.9	5.7	16.2
FL98329C	282.9	58.4	19.2	116.0	31.0	19.7	22.5	5.8	20.0
FL98329D	260.9	82.0	21.3	88.3	7.9	22.1	358.2	1.0	23.2
FL98330A	222.1	64.9	9.8	99.7	14.1	10.4	4.3	20.3	11.1
FL98330B	239.3	52.0	8.2	123.0	19.1	8.8	20.8	31.4	9.0
FL98330C	153.4	65.9	10.6	280.7	15.2	11.0	15.8	18.3	11.9
CY9729A	57.6	81.1	13.4	260.9	8.2	14.0	170.4	3.5	14.4
CY9729A	270.0	90.0	13.5	90.0	90.0	14.2	90.0	90.0	14.5
CY9729B	40.6	75.7	13.2	261.2	10.9	13.7	169.5	9.1	14.1
CY9729C	326.9	56.5	12.9	123.3	31.3	13.2	220.0	10.9	13.3
CY9729D	315.0	70.7	11.0	135.0	0.0	11.9	135.0	19.3	12.0
FL98332A	180.0	75.3	-17.0	0.0	0.0	-16.1	0.0	14.7	-16.0
FL98332A	132.8	30.5	-16.7	330.5	58.2	-16.2	227.5	8.0	-15.9
FL98332B	57.1	42.1	-17.8	169.2	22.7	-17.5	279.3	39.4	-17.0
FL98332C	270.2	57.0	-17.6	62.7	29.9	-16.8	160.1	12.6	-16.0

Appendix 5 - Regional Magnetic Fabric Data

Sample	Declination	Minimum			Intermediate			Maximum	
		Inclination	Intensity	Dec.	Inc.	Intensity	Dec.	Inc.	Intensity
FL98331B	91.2	80.9	-10.2	220.8	5.9	-9.8	311.5	7.0	-8.9
FL98331C	97.0	68.5	-8.8	205.7	7.2	-8.4	298.4	20.1	-8.2
CY9730A	83.7	64.9	-15.4	266.3	25.1	-15.1	175.8	1.0	-13.7
CY9730B	287.5	39.2	-15.2	127.3	49.0	-14.9	25.7	10.0	-14.6
CY9730C	305.6	53.9	-14.3	53.8	12.8	-14.0	152.3	33.1	-13.8
CY9731A	140.9	34.7	-16.5	276.5	45.9	-15.5	33.3	23.7	-15.0
CY9731B	95.6	20.1	-14.6	331.6	56.8	-13.6	195.5	25.2	-13.0
CY9731C	282.5	73.5	-15.4	114.1	16.2	-14.7	23.2	3.2	-14.6
CY9731C	282.5	73.5	-15.4	114.1	16.2	-14.7	23.2	3.2	-14.6
CY9731D	322.1	18.1	-14.3	147.8	71.8	-14.1	52.7	1.7	-13.8
FL98325B	97.6	66.8	15.7	294.3	21.6	16.5	201.8	5.8	16.9
FL98326B	90.0	90.0	-4.1	90.0	90.0	-4.0	90.0	90.0	-3.6
FL98326B	115.1	38.3	-4.7	293.1	51.7	-3.7	24.3	1.0	-3.0
FL98327C	103.4	51.9	-4.1	281.9	38.0	-3.9	12.5	0.8	-3.1
FL98320A	338.3	69.8	19.5	128.4	17.7	20.4	221.4	9.4	21.0
FL98320B	36.5	85.8	15.4	169.1	2.9	16.0	259.3	3.1	16.2
FL98302A	136.6	34.5	-14.7	270.0	45.0	-14.7	27.9	25.1	-14.3
FL98302B	79.4	29.2	-16.7	220.2	54.2	-16.5	338.4	18.9	-15.3
FL98302C	306.0	78.5	-14.3	48.1	2.4	-14.0	138.6	11.2	-13.2
FL98302D	189.7	66.2	-13.9	309.0	12.2	-13.1	43.6	20.1	-12.8
FL98291B	302.6	75.2	31.6	95.3	13.2	33.1	186.9	6.5	33.3
FL98291C	102.7	78.4	30.7	261.3	10.8	31.5	352.1	4.1	32.1
FL98304A	281.3	26.2	-11.8	160.4	46.3	-11.7	29.3	32.1	-11.4
FL98304B	325.1	63.0	-10.8	218.2	8.4	-10.6	124.2	25.5	-10.3
FL98301B	350.4	68.0	-31.3	174.4	21.9	-30.8	83.8	1.4	-30.5
FL98301C	225.0	56.2	-27.4	225.0	35.3	-27.0	45.0	33.8	-26.4
FL98301C	134.5	8.3	-27.3	26.2	65.0	-26.6	228.1	23.4	-26.5
FL98301D	255.6	53.4	-31.7	95.0	35.1	-31.6	358.4	9.4	-30.5
FL98254C	309.6	38.2	-13.9	171.2	43.6	-13.4	58.4	22.2	-13.0
FL98290A	74.5	76.9	19.3	269.3	12.6	20.2	178.6	3.2	21.3
FL98290B	341.6	81.6	19.3	161.6	8.4	20.2	151.4	46.1	20.3
FL98290C	221.2	3.3	20.2	131.0	2.7	21.1	2.2	85.8	23.1
FL98300A	39.7	74.5	37.8	237.1	14.8	39.0	145.9	4.4	39.4
FL98300B	270.5	73.4	37.7	74.7	16.0	38.7	166.0	4.3	39.1
FL2 (II)									
FL98319B	102.2	73.5	5.7	249.1	13.9	6.6	341.3	8.6	7.1
FL98296A	263.7	71.6	-3.5	166.6	2.4	-2.9	75.8	18.3	-2.6
FL98296C	185.9	80.7	2.5	73.6	3.6	3.2	343.1	8.6	3.5
FL98299B	232.1	58.5	5.1	83.1	27.7	5.7	345.7	13.8	6.4
FL98299C	294.7	74.5	6.4	122.0	15.4	6.9	31.5	1.9	7.3
FL98297B	270.0	90.0	-9.6	270.0	90.0	-9.2	270.0	90.0	-8.8
FL98297B	171.0	74.1	-9.8	70.1	3.1	-9.6	339.2	15.5	-8.8
FL98297C	160.5	26.0	-5.8	335.8	64.0	-5.6	69.6	1.8	-4.8
FL98298A	78.6	51.3	-10.4	217.3	31.0	-10.1	320.4	20.7	-9.5
FL98298C	40.4	62.8	-11.6	270.0	18.4	-11.0	173.3	19.3	-10.9
FL98318A	315.7	66.5	3.0	124.4	23.1	4.1	216.2	4.1	4.8
FL98318B	90.0	90.0	-4.8	90.0	90.0	-4.7	270.0	90.0	-3.9
FL98318B	174.0	3.9	-6.1	83.4	8.3	-4.5	288.9	80.8	-3.6

Appendix 5 - Regional Magnetic Fabric Data

Sample	Declination	Minimum			Intermediate			Maximum	
		Inclination	Intensity	Dec.	Inc.	Intensity	Dec.	Inc.	Intensity
CY9725A	97.0	31.1	-20.4	305.1	55.6	-19.9	195.1	13.2	-19.5
CY9725B	95.6	38.1	-21.1	247.6	48.4	-20.4	354.2	14.2	-19.9
CY9725C	93.4	17.8	-22.5	310.6	68.1	-22.0	187.5	12.4	-21.6
CY9725D	133.3	5.1	-22.0	233.4	62.9	-21.7	40.8	26.6	-21.0
CY9725E	82.8	62.3	-22.7	272.3	27.4	-22.5	180.3	3.9	-21.6
CY9726A	90.0	23.2	-12.0	197.9	35.7	-11.6	334.4	45.2	-11.1
CY9726B	94.5	29.5	-11.4	250.9	58.3	-11.1	358.4	10.5	-10.3
CY9726B	180.0	79.4	-11.3	180.0	74.5	-11.0	360.0	15.5	-10.4
CY9726C	284.2	44.1	-13.3	90.0	45.0	-13.2	187.2	7.1	-12.7
CY9726D	90.0	45.0	-13.6	278.6	44.7	-13.2	184.3	4.3	-12.2
CY9726E	255.0	32.7	-6.9	126.5	44.1	-6.2	5.2	28.2	-5.1
CY9726F	92.8	19.2	-14.2	234.6	66.1	-13.7	358.0	13.7	-13.1
CY9727A1	260.3	41.6	11.5	67.3	47.6	11.8	164.5	6.5	12.4
CY9727A2	296.7	41.8	12.2	90.0	45.0	12.6	194.1	13.7	13.4
CY9727A2	270.0	90.0	10.7	90.0	90.0	12.7	90.0	90.0	14.7
CY9727A3	108.3	59.1	10.0	250.0	25.2	10.2	348.1	16.8	10.5
CY9727A4	96.0	9.9	13.9	188.4	13.3	15.2	330.2	73.3	15.6
CY9727A5	278.0	21.7	12.2	149.9	57.2	12.5	17.9	23.4	13.1
FL98255A	3.8	79.7	8.3	247.2	4.7	9.4	156.5	9.2	9.6
FL98255B	307.0	39.1	14.5	152.3	48.8	14.9	47.5	11.1	15.8
FL98317B	159.9	77.3	11.1	22.9	9.3	11.9	291.5	8.5	12.3
FL98317C	81.7	62.9	9.9	319.5	15.2	11.9	223.3	21.9	12.0
FL98317D	307.6	77.0	9.7	117.0	12.8	10.2	207.5	2.3	10.5
FL98256A	71.2	73.5	21.8	267.0	15.9	23.0	175.8	4.3	23.6
FL98256B	184.0	9.9	17.1	86.3	37.4	24.5	286.3	50.9	34.2
FL98256B	192.7	5.2	22.0	92.2	63.4	24.2	285.2	26.0	26.7
FL98256C	351.5	45.4	20.6	168.6	44.5	22.2	260.0	1.4	24.2
FL98256C	60.5	1.0	20.2	328.7	60.5	21.4	151.0	29.5	22.6
FL98305B	219.3	58.6	34.6	2.7	26.1	35.5	100.9	16.2	35.7
FL98305C	350.5	82.1	39.1	184.1	7.7	39.9	93.9	1.8	40.5
FL98257C	162.6	0.9	-3.3	71.3	54.6	-2.4	253.3	35.4	-1.7
FL98306A	266.3	65.1	-10.2	100.7	24.2	-9.4	8.3	5.5	-8.8
FL98306B	137.3	40.3	-8.5	29.1	20.2	-8.1	279.2	42.8	-7.4
FL98306C	80.4	10.5	-10.7	190.0	61.2	-9.7	345.1	26.5	-9.5
FL98289B	352.3	85.9	-21.8	105.2	1.6	-19.7	195.3	3.8	-18.5
FL98183B	39.2	69.9	404.7	266.0	14.1	416.9	172.4	14.0	418.2
FL98183C	83.8	74.0	383.1	339.7	4.0	390.4	248.6	15.5	393.0
FL98183D	89.4	85.2	343.7	302.2	4.1	353.8	212.0	2.6	354.5
FL98307B	248.1	33.4	-10.4	27.5	49.0	-9.7	143.5	20.9	-9.2
FL98307C	88.1	63.5	-11.7	255.2	25.9	-11.1	347.7	5.1	-10.6
FL98181B	114.0	63.4	4.1	19.1	2.4	5.4	287.9	26.5	6.1
FL98182A	141.6	41.5	8.2	290.9	44.2	9.3	36.9	15.9	9.9
FL98184A	258.3	29.1	7.3	164.2	7.5	7.7	61.2	59.7	8.3
FL98184B	258.5	41.3	-5.2	113.9	42.9	-5.1	5.7	18.6	-4.1
FL98184C	277.3	52.5	81.8	168.2	14.1	83.9	68.4	33.9	86.2
FL98315B	295.1	69.4	4.6	198.8	2.4	6.4	107.9	20.5	6.8
FL98185B	49.8	60.8	67.4	256.6	26.5	68.8	160.9	11.4	69.4
FL98185C	8.8	84.1	63.5	171.8	5.7	65.3	262.0	1.7	65.6

Appendix 5 - Regional Magnetic Fabric Data

Sample	Declination	Minimum			Intermediate			Maximum		
		Inclination	Intensity	Dec.	Inc.	Intensity	Dec.	Inc.	Intensity	
FL98316A	252.9	55.8	3.8	97.1	31.7	5.0	0.0	11.3	5.1	
FL98316B	219.2	39.6	2.4	319.0	11.6	3.4	62.3	48.0	3.7	
FL98309B	36.0	64.4	-12.7	250.6	21.5	-11.9	155.3	13.2	-11.4	
FL98310A	308.0	73.7	19.5	89.7	12.9	19.9	181.9	9.7	21.8	
FL98310B	220.8	67.9	11.3	128.2	1.1	11.7	37.8	22.1	12.7	
FL98311B	130.5	56.9	4.4	296.9	32.3	5.1	30.8	6.2	5.9	
FL98312A	316.1	81.2	83.6	121.1	8.5	84.6	211.5	2.2	85.9	
FL98312B	16.8	82.2	85.3	274.1	1.7	86.9	183.9	7.6	88.2	
FL98186A	152.6	6.5	48.5	57.4	38.9	49.1	250.6	50.3	52.1	
FL98186B	170.5	64.1	47.2	23.1	22.2	48.3	287.9	12.6	48.7	
FL98186C	29.4	71.1	46.5	282.2	5.8	48.2	190.3	17.9	50.6	
FL98308A	237.4	63.3	-14.7	108.4	17.5	-14.3	12.0	19.4	-13.5	
FL98308B	291.8	6.3	-9.6	198.6	26.7	-9.5	34.0	62.5	-8.6	
FL98308C	65.1	26.8	-14.2	317.5	31.0	-13.7	187.6	46.8	-13.3	
FL98308D	222.0	12.6	-9.1	315.0	13.3	-8.4	90.0	71.6	-8.1	
FL98288A	184.0	40.3	-6.4	279.0	5.8	-5.5	15.7	49.1	-5.2	
FL98288B	266.4	10.8	-4.7	107.5	78.5	-4.5	357.2	4.0	-4.0	
FL98288C	283.0	54.5	-6.4	93.7	35.2	-5.9	186.8	4.4	-3.7	
FL98288D	29.2	26.0	-6.3	270.0	45.0	-5.5	138.2	33.7	-5.0	
FL98288D	207.0	50.8	-5.7	312.5	12.3	-5.3	51.7	36.5	-5.3	
CY9724A	42.2	80.3	16.9	287.3	4.1	18.0	196.7	8.7	18.6	
CY9724B	335.2	81.8	20.0	107.0	5.5	21.0	197.5	6.1	21.6	
CY9724B	270.0	86.4	19.7	90.0	3.6	20.9	90.0	86.1	22.0	
CY9724C	121.7	87.5	20.0	266.3	2.0	21.0	356.4	1.4	21.6	
CY9724D	299.5	80.1	15.3	115.2	9.9	16.6	205.3	0.7	17.1	
CY9724E	90.0	78.4	20.6	270.0	11.6	22.1	270.0	59.0	22.5	
CY9724E	188.2	85.2	20.4	291.2	1.1	22.1	21.3	4.7	22.7	
CY9724F	292.0	75.1	19.7	97.3	14.5	20.7	188.3	3.6	21.6	
CY9724G	180.0	87.7	21.6	180.0	79.4	23.1	0.0	2.3	23.5	
CY9724G	42.9	82.4	21.7	291.1	2.8	22.9	200.8	7.0	23.9	
FL98313B	128.7	46.3	-13.3	225.8	6.7	-12.9	322.1	42.9	-12.5	
FL98170A	0.5	61.8	9.5	212.9	24.4	10.3	116.7	13.3	10.7	
FL98170D	234.0	38.4	13.7	73.5	49.9	14.2	331.8	9.7	14.8	
FL98287B	108.8	43.4	-10.2	270.0	45.0	-10.1	9.7	9.5	-9.0	
CY9723A	88.5	18.3	7.5	246.2	70.3	8.1	356.2	7.0	8.5	
CY9723B	92.2	10.1	11.5	308.2	77.6	13.0	183.4	7.1	14.0	
CY9723C	81.2	16.7	14.7	294.6	70.2	15.2	174.4	10.3	16.0	
CY9723D	322.9	61.9	11.5	94.6	19.6	11.6	191.8	19.4	12.6	
CY9723E	103.2	61.8	12.8	284.5	28.2	13.2	194.2	0.5	13.9	
CY9723F	246.8	75.0	8.4	66.8	15.0	9.5	25.2	62.2	10.2	
CY9723G	103.0	25.3	11.7	322.9	57.5	12.2	202.2	18.0	12.4	
CY9723G	90.0	90.0	12.1	270.0	90.0	12.1	270.0	90.0	13.1	
CY9723H	73.8	23.6	12.7	224.1	63.5	13.6	338.1	13.4	14.2	
CY9723I	12.3	78.2	8.0	113.3	2.3	8.2	203.8	11.6	8.6	
FL98187A	130.8	0.2	12.3	40.7	9.5	13.0	222.1	80.5	13.3	
FL98187B	333.8	53.6	8.0	65.5	1.3	13.0	156.5	36.4	15.0	
FL98187C	203.5	32.0	10.9	84.5	37.8	11.8	320.4	35.8	13.8	
FL98169B	248.2	86.8	17.4	92.3	2.9	18.1	2.2	1.3	19.1	

Appendix 5 - Regional Magnetic Fabric Data

Sample	Declination	Minimum			Intermediate			Maximum	
		Inclination	Intensity	Dec.	Inc.	Intensity	Dec.	Inc.	Intensity
FL98169C	142.9	68.4	19.1	277.0	15.4	20.1	11.1	14.8	21.4
FL98167B	322.7	55.8	22.1	92.2	23.4	23.7	193.1	23.4	25.6
FL98167C	204.7	74.2	22.9	62.7	12.6	24.3	330.6	9.4	24.8
FL98168A	39.8	77.0	24.5	192.0	11.6	26.2	283.2	5.9	27.2
FL98168B	30.3	68.3	27.1	174.6	17.9	29.3	268.5	11.9	29.8
FL98168C	329.4	76.3	25.7	215.6	5.6	27.1	124.4	12.4	27.9
FL98188A	112.8	4.1	16.4	21.0	23.9	18.3	212.0	65.8	19.2
FL98188B	295.2	69.1	11.3	159.6	15.2	13.1	65.7	13.9	14.1
FL98179B	96.3	23.8	-13.6	290.3	65.5	-13.4	188.7	5.3	-12.5
FL98180A	195.0	31.4	-12.8	61.5	48.4	-12.5	300.9	24.3	-11.5
FL98180B	256.8	57.3	-14.7	156.9	6.3	-14.0	63.0	31.9	-13.6
FL98166A	3.3	74.8	37.3	243.6	7.6	39.3	151.8	13.0	39.9
FL98166B	23.3	40.4	38.4	143.4	30.5	39.8	257.4	34.6	40.8
FL98166C	180.0	83.5	32.7	180.0	63.4	33.7	0.0	6.5	34.0
FL98166C	184.1	88.0	32.0	54.5	1.3	34.0	324.4	1.5	34.3
FL98285B	31.9	32.8	-8.0	261.8	45.0	-7.5	141.0	27.0	-6.1
FL98285C	50.6	82.0	-5.1	273.1	5.9	-4.8	182.6	5.4	-3.9
FL98286A	321.1	66.8	-11.6	61.7	4.5	-10.7	153.6	22.7	-10.1
FL98286B	134.0	78.7	-7.2	262.1	7.0	-5.4	353.2	8.8	-4.7
FL98286C	77.5	68.7	-7.1	277.3	20.1	-6.4	184.8	6.6	-6.2
FL98190A	194.3	32.9	13.9	70.1	41.0	14.5	307.7	31.6	15.4
FL98190B	149.8	72.0	6.6	311.5	17.1	7.4	43.1	5.3	7.9
FL98282C	188.5	85.5	10.8	21.2	4.4	11.8	291.1	1.0	12.4
FL98283B	97.7	71.5	-4.6	268.5	18.3	-3.8	359.4	2.8	-2.9
FL98283D	226.0	64.6	-3.9	70.9	23.3	-3.0	336.8	9.5	-2.3
FL98284A	167.3	68.5	-6.2	52.1	9.5	-5.7	318.8	19.1	-5.2
FL98284B	141.0	75.0	-4.8	256.4	6.6	-4.5	347.9	13.4	-3.7
FL98370A	143.0	42.4	13.6	253.3	20.8	14.4	2.2	40.4	15.1
FL98370B	176.9	23.9	18.2	22.3	63.8	19.5	271.4	10.0	20.5
FL98191B	199.3	63.2	32.9	340.7	21.5	34.3	76.9	15.1	36.9
FL98369B	3.3	36.4	-14.4	121.3	32.4	-14.0	239.7	36.9	-13.7
FL98369C	150.7	81.0	-15.7	306.1	8.2	-15.0	36.6	3.7	-14.6
FL98192A	113.4	35.0	-3.6	250.0	46.0	-2.7	6.1	23.0	-1.3
FL98162A	270.0	78.9	-10.2	90.0	0.0	-9.1	90.0	11.1	-9.0
FL98162A	227.3	50.5	-9.7	16.0	35.2	-9.5	117.4	15.7	-9.3
FL98281C	259.1	61.2	22.8	80.7	28.8	23.7	350.3	0.7	24.0
FL98193B	277.3	7.9	5.8	165.0	69.8	6.1	9.9	18.5	6.9
FL98371B	354.8	68.0	46.8	198.3	20.3	47.5	105.3	8.0	48.5
FL98371C	2.4	49.4	48.8	233.8	28.1	49.8	128.2	26.7	50.3
FL98372A	153.4	29.6	11.8	153.4	0.0	12.0	333.4	60.4	12.6
FL98372B	38.3	72.3	14.6	216.5	17.7	14.8	306.7	0.5	15.4
FL98372C	292.8	69.4	14.0	175.9	9.8	14.4	82.7	18.5	15.5
FL98259C	307.1	81.9	3.5	98.5	7.1	5.3	189.0	3.8	5.9
FL98260B	114.2	71.9	-3.9	227.9	7.5	-3.4	320.1	16.4	-3.0
FL98261B	249.7	72.0	-2.6	68.2	18.0	-2.2	158.3	0.4	-1.7
FL98280C	18.0	55.1	21.9	232.2	29.9	23.7	132.6	16.2	24.1
FL98194A	47.3	35.1	1.2	199.7	51.6	5.9	307.5	13.6	6.9
FL98194A	179.0	65.9	4.5	21.7	22.4	5.1	288.2	8.4	5.6

Appendix 5 - Regional Magnetic Fabric Data

Sample	Declination	Minimum			Intermediate			Maximum	
		Inclination	Intensity	Dec.	Inc.	Intensity	Dec.	Inc.	Intensity
FL98279B	348.3	75.8	2.4	79.5	0.3	3.0	169.5	14.2	3.2
FL98160A	90.0	90.0	25.0	270.0	90.0	26.0	270.0	90.0	26.5
FL98160A	94.2	76.4	25.0	245.4	11.9	26.0	336.7	6.4	26.9
FL98160B	230.8	78.9	24.7	90.2	8.6	25.9	359.1	6.9	26.8
FL98161B	237.9	32.4	25.4	5.1	43.6	27.2	127.2	29.2	28.4
FL98195B	109.4	20.8	14.6	233.3	55.7	14.9	8.8	25.9	15.4
FL98195C	266.4	74.9	13.0	121.5	12.5	13.4	29.6	8.4	14.0
FL98196B	208.9	68.9	6.4	306.5	2.9	7.4	37.6	20.9	7.7
FL98196C	335.9	83.7	4.9	101.3	21.4	6.9	167.9	82.5	8.9
FL98225B	145.7	81.7	54.3	299.7	7.5	55.8	30.2	3.6	56.0
FL98275C	286.5	61.6	-2.7	74.5	24.6	-2.3	170.7	13.2	-2.2
FL98198A	57.5	80.6	23.3	165.3	2.9	24.0	255.8	8.9	24.4
FL98198B	82.2	51.0	18.4	330.2	16.9	26.6	228.4	33.9	35.4
FL98272B	118.9	20.0	16.7	3.9	49.2	17.2	223.0	33.8	18.0
FL98158A	93.6	84.6	37.7	280.4	5.4	38.5	190.4	0.7	38.9
FL98158B	132.7	84.4	38.4	297.2	5.4	39.5	27.3	1.5	39.6
FL98159B	91.6	87.4	34.2	288.8	2.4	39.1	198.8	0.9	39.6
FL98273B	90.0	90.0	-17.9	90.0	90.0	-17.7	270.0	90.0	-17.1
FL98273B	121.2	29.7	-17.8	270.0	56.3	-17.7	22.8	14.5	-17.1
FL98273B	74.1	39.4	-17.8	289.4	44.8	-17.3	180.0	18.4	-17.0
FL98273C	265.5	55.8	-15.8	110.7	31.6	-15.5	13.3	11.8	-14.8
FL98273D	271.0	51.4	-17.7	78.1	37.9	-17.2	173.0	6.3	-16.6
FL98199B	344.7	18.8	22.8	93.4	43.3	26.0	237.6	40.7	28.1
FL98199C	145.2	10.0	27.1	288.3	77.5	27.5	53.9	7.3	28.7
FL98223B	53.2	82.9	28.6	257.8	6.4	29.4	167.5	2.9	29.7
FL98223C	311.1	84.9	36.6	51.1	0.9	37.3	141.1	5.1	37.8
FL98222B	292.3	77.4	40.2	199.5	0.6	41.8	109.3	12.5	42.1
FL98222C	249.5	76.0	40.7	49.7	13.2	42.2	140.7	4.6	42.4
FL3 (III)									
FL98220A	133.3	84.0	35.3	265.6	4.0	36.2	355.9	4.4	37.4
FL98220B	285.2	74.9	40.3	57.5	10.3	41.2	149.5	10.9	41.6
FL98220C	58.9	86.1	39.1	166.4	1.2	41.0	256.5	3.7	41.7
FL98213B	60.2	65.8	-8.6	299.5	12.9	-7.9	204.7	20.1	-7.3
FL98214A	158.3	66.6	-12.3	292.8	16.9	-11.2	27.7	15.7	-10.6
FL98214B	314.6	4.6	-10.3	51.9	57.5	-10.0	221.7	32.1	-8.8
FL98214C	235.4	63.2	-4.5	92.7	21.9	-3.7	356.6	14.7	-2.3
FL98212A	41.0	50.4	8.0	231.5	39.1	8.6	137.3	5.1	8.9
FL98212B	260.5	19.4	8.1	132.5	60.3	8.8	358.5	21.7	9.7
FL98219B	61.5	83.2	58.6	270.8	6.0	59.3	180.4	3.3	59.9
FL98217B	63.3	70.4	7.0	276.1	16.7	7.8	183.1	10.0	8.5
FL98217C	90.0	71.6	9.0	258.9	18.1	9.9	349.9	3.3	10.6
FL98218A	323.7	72.4	40.5	105.8	14.0	41.9	198.4	10.4	42.8
FL98218B	13.3	81.2	53.7	261.6	3.3	54.3	171.1	8.1	55.3
FL98218C	93.9	47.5	58.7	283.4	42.1	59.6	189.1	4.8	60.9
FL98216A	139.9	78.6	-5.6	282.6	9.1	-5.2	13.7	6.8	-4.7
FL98216B	286.2	51.6	-7.4	93.2	37.7	-6.6	188.1	6.3	-5.8
FL98216C	135.0	82.8	-7.8	135.0	76.7	-7.4	315.0	7.2	-7.0
FL98216C	90.2	57.0	-8.3	251.8	31.6	-7.4	347.0	8.4	-6.3

Appendix 5 - Regional Magnetic Fabric Data

Sample	Declination	Minimum			Intermediate			Maximum	
		Inclination	Intensity	Dec.	Inc.	Intensity	Dec.	Inc.	Intensity
FL98215B	244.7	35.7	14.0	117.4	40.1	14.1	358.8	29.6	14.8
FL98157B	108.4	43.5	23.4	347.9	28.2	23.5	237.1	33.4	24.0
FL98211B	11.9	57.9	11.8	275.8	3.8	12.4	183.5	31.8	13.1
FL98211C	126.2	52.4	11.7	287.8	36.1	12.7	24.4	8.9	12.8
FL98177B	259.6	67.1	4.4	51.8	20.5	5.7	145.5	9.8	6.0
FL98210A	306.2	83.5	48.5	73.3	3.9	50.0	163.6	5.2	50.6
FL98210B	30.9	77.7	44.3	259.4	8.2	45.9	168.1	9.1	46.5
FL98175B	272.3	40.1	-16.7	17.8	17.6	-15.5	126.1	44.7	-13.7
FL98175C	318.9	3.9	-16.6	54.4	54.5	-16.3	226.1	35.2	-14.1
FL98209B	28.2	72.2	14.3	271.6	8.2	15.1	179.3	15.7	15.6
FL98209C	49.4	19.2	14.3	161.8	47.6	14.8	304.7	36.1	16.8
FL98174A	162.1	86.9	14.3	32.2	2.0	14.6	302.1	2.3	15.5
FL98174B	275.5	49.7	12.7	56.5	33.4	13.3	160.3	19.9	14.1
CY9715A	23.4	74.6	23.4	273.3	5.4	24.1	181.9	14.4	24.7
CY9715B	112.5	54.0	21.8	284.3	35.7	22.2	17.1	3.9	22.7
CY9715C	270.0	45.0	25.1	40.0	32.7	25.4	149.2	27.1	26.4
CY9715D	287.7	41.5	24.4	100.3	48.3	24.7	194.4	3.7	25.1
CY9715E	104.0	28.2	22.5	224.5	43.5	22.9	353.3	33.5	24.0
FL98176A	135.0	81.3	26.5	315.0	8.7	26.9	315.0	84.2	27.4
FL98176A	16.9	64.8	26.4	225.5	22.5	26.6	130.9	10.9	27.8
FL98176B	68.1	81.3	16.9	302.3	5.1	17.9	211.6	7.0	18.1
FL98176C	42.2	62.7	33.1	182.6	21.7	33.5	279.0	15.7	34.3
FL98176D	342.6	54.7	16.1	200.4	29.2	16.5	99.9	18.0	16.9
FL98253B	233.3	79.3	4.1	107.6	6.3	4.3	16.7	8.6	5.2
FL98208A	292.5	63.7	11.5	38.1	7.6	11.8	131.7	25.0	12.2
FL98208B	323.5	66.1	13.2	112.1	20.8	14.1	206.5	11.4	14.7
FL98208C	248.2	76.4	14.4	88.5	12.7	15.3	357.5	4.5	15.8
FL98154A	201.8	76.7	15.6	64.6	9.8	16.2	333.1	8.8	17.0
FL98154B	232.2	77.1	28.6	31.3	12.1	29.8	122.3	4.4	30.1
FL98154C	222.8	35.6	7.3	64.4	52.4	17.0	320.4	10.5	17.5
FL98154C	264.9	63.4	14.2	135.3	17.7	15.1	38.9	19.2	15.8
FL98154D	235.1	66.7	27.8	125.3	8.3	28.8	32.0	21.6	31.0
FL98156A	137.8	71.5	13.5	33.1	4.8	14.5	301.6	17.8	14.7
FL98156B	328.8	70.9	15.6	186.5	15.3	16.5	93.4	11.1	16.7
FL98156C	355.4	66.6	13.2	96.1	4.6	14.1	188.0	22.8	14.6
FL98156D	301.1	67.9	15.8	50.4	7.7	16.5	143.3	20.6	16.7
CY9714A	292.3	73.6	18.0	102.6	16.2	18.7	193.4	2.6	19.5
CY9714B	327.4	73.4	16.0	69.2	3.5	16.4	160.2	16.2	16.7
CY9714B	45.0	80.6	16.1	225.0	9.4	16.7	225.0	54.7	16.9
CY9714B	315.0	84.4	16.0	315.0	54.7	16.5	135.0	5.6	16.6
CY9714C	45.0	85.5	16.8	225.0	4.5	17.5	225.0	54.7	17.6
CY9714C	112.7	85.2	16.6	244.0	3.2	17.0	334.2	3.6	17.4
CY9714D	89.1	30.1	20.5	257.3	59.4	21.1	356.1	5.2	21.5
FL98207C	94.4	82.5	9.1	268.6	7.5	10.5	358.7	0.7	12.3
FL98250A	295.6	56.2	13.4	93.3	31.8	14.3	189.8	10.3	14.6
FL98250C	215.5	66.8	24.7	108.3	7.2	25.8	15.4	21.9	26.1
FL98206A	140.9	43.8	69.2	286.7	40.8	70.7	32.9	17.9	71.3
FL98206B	161.2	71.0	60.2	276.5	8.4	61.0	9.1	16.9	62.2

Appendix 5 - Regional Magnetic Fabric Data

Sample	Declination	Minimum			Intermediate			Maximum		
		Inclination	Intensity	Dec.	Inc.	Intensity	Dec.	Inc.	Intensity	
FL98153B	163.5	82.8	2.7	49.4	3.0	3.6	319.0	6.6	3.6	
FL98153C	272.6	6.0	5.4	22.7	73.1	5.8	180.9	15.7	7.1	
FL98153D	306.9	71.0	2.8	75.6	12.2	3.3	168.7	14.4	3.9	
FL98249C	6.2	84.1	110.2	147.4	4.6	115.3	237.7	3.7	115.6	
CY9722A	307.8	61.7	3.0	103.5	26.1	3.4	198.5	10.1	3.9	
CY9722B	270.0	90.0	5.3	90.0	90.0	5.5	90.0	90.0	6.1	
CY9722B	225.0	75.3	5.4	45.0	14.7	5.6	45.0	76.7	5.8	
CY9722B	45.0	71.2	4.9	225.0	18.8	5.7	225.0	40.3	5.9	
CY9722B	235.8	79.0	5.2	66.5	10.8	5.5	336.1	2.0	5.8	
CY9722C	95.8	25.3	4.7	341.6	40.8	5.7	208.0	38.6	6.0	
CY9722D	149.6	77.4	4.9	250.0	2.3	5.4	340.5	12.3	5.7	
FL98248A	72.5	78.6	20.4	221.8	9.8	21.6	312.8	5.7	22.1	
FL98205B	80.7	73.5	43.4	271.7	16.2	44.2	180.8	3.0	44.9	
FL98205C	225.1	10.2	50.7	125.8	41.8	52.3	325.9	46.4	52.8	
FL98110A	46.4	30.8	-12.0	297.4	28.6	-11.1	173.7	45.5	-10.1	
FL98110B	91.0	53.3	-12.0	231.5	29.9	-10.0	333.0	19.3	-9.6	
FL98173B	285.7	57.4	11.7	76.9	29.3	12.2	174.4	13.1	12.6	
FL98173C	217.2	73.2	7.7	64.6	15.0	8.5	332.6	7.4	8.7	
FL98173D	200.9	44.0	8.8	80.1	27.9	8.9	329.9	33.1	9.4	
CY9712A	90.0	45.0	-19.0	297.8	41.5	-18.7	194.8	14.3	-17.9	
CY9712B	83.1	30.3	-19.5	275.1	59.1	-18.9	176.2	5.3	-18.0	
CY9712C	99.7	37.5	-19.2	267.7	51.9	-18.8	5.2	5.9	-18.0	
CY9712D	36.7	84.5	-19.4	146.6	1.9	-19.1	236.8	5.1	-18.9	
CY9713A	270.0	6.0	-8.1	90.0	81.5	-7.6	90.0	84.0	-7.4	
CY9713A	93.9	9.5	-8.1	357.3	34.6	-7.5	197.1	53.8	-7.1	
CY9713B	349.4	40.3	-8.7	134.3	43.9	-8.5	243.0	18.4	-8.2	
CY9713C	84.9	10.1	-8.9	180.0	26.6	-8.0	335.8	61.2	-8.0	
CY9713C	270.0	90.0	-8.6	90.0	90.0	-8.2	270.0	90.0	-7.9	
CY9713C	270.0	90.0	-8.6	90.0	90.0	-8.3	270.0	90.0	-8.2	
CY9713D	228.2	42.3	-9.7	84.0	41.7	-9.1	336.3	18.8	-8.5	
CY9713E	279.9	39.9	-9.5	69.3	45.8	-8.8	176.2	15.8	-7.6	
FL98246A	229.1	80.4	20.2	75.3	8.6	21.5	344.7	4.2	21.7	
FL98246B	90.0	83.0	19.6	270.0	7.0	20.2	270.0	85.2	21.1	
FL98246B	37.3	77.1	19.7	245.2	11.4	20.4	154.0	5.9	20.8	
FL98245B	90.0	90.0	9.5	90.0	90.0	9.9	90.0	90.0	10.3	
FL98245B	276.3	48.5	9.4	65.5	37.2	9.6	167.9	15.7	10.4	
FL98152A	11.2	76.7	38.9	246.4	7.7	40.2	154.9	10.8	40.5	
FL98152B	195.6	86.7	31.8	71.7	1.9	32.5	341.7	2.8	33.3	
FL98244A	139.9	78.6	23.9	282.6	9.1	24.3	13.7	6.8	24.7	
FL98244B	69.5	75.7	22.8	265.9	13.7	24.2	174.9	3.9	24.7	
FL98244C	264.5	75.5	22.4	106.0	13.5	23.3	14.8	5.1	24.0	
CY9709A	340.5	63.2	-12.3	100.0	14.0	-11.7	195.9	22.4	-11.5	
CY9709B	263.8	13.5	-12.3	30.6	68.1	-11.8	169.6	16.9	-11.2	
CY9709C	237.6	81.1	-12.9	80.9	8.2	-12.6	350.4	3.5	-12.4	
CY9709D	319.6	62.4	-12.6	213.3	8.4	-11.9	119.1	26.1	-11.8	
CY9709E	22.2	38.4	-12.1	218.9	50.4	-11.7	118.8	8.3	-11.4	
CY9709F	239.7	49.0	-12.2	134.3	13.0	-11.8	33.9	38.0	-11.3	
CY9710A	69.4	60.3	-9.3	286.6	24.4	-8.9	189.3	15.8	-8.4	

Appendix 5 - Regional Magnetic Fabric Data

Sample	Declination	Minimum			Intermediate			Maximum		
		Inclination	Intensity	Dec.	Inc.	Intensity	Dec.	Inc.	Intensity	
CY9710B	352.7	78.1	-11.5	228.3	6.8	-11.1	137.1	9.7	-10.9	
CY9710C	0.0	73.6	-10.2	0.0	60.6	-9.8	180.0	16.4	-9.4	
CY9710C	275.2	14.1	-10.3	72.6	74.8	-10.0	183.8	5.6	-9.3	
CY9710D	82.6	14.3	-10.4	296.8	72.8	-10.0	175.0	9.2	-9.6	
FL98243B	78.7	77.3	57.4	273.3	12.3	60.1	182.6	3.1	61.5	
FL98243C	148.1	59.7	52.4	24.8	17.8	54.7	286.7	23.7	56.1	
FL98243D	220.1	74.4	38.8	56.6	15.0	40.6	325.4	4.2	41.5	
CY9711A	125.7	30.3	-3.0	0.0	45.0	-2.5	235.2	29.7	-2.3	
FL98204A	118.4	57.5	9.4	236.4	16.7	10.4	335.2	27.0	11.3	
FL98204B	265.6	71.6	6.7	110.9	16.8	7.6	18.7	7.4	7.7	
FL98204C	61.2	41.2	10.7	270.0	45.0	11.1	164.7	14.8	11.8	
FL98204C	112.6	67.2	10.7	272.2	21.5	11.4	5.1	7.2	11.8	
FL98204D	59.7	78.3	7.5	272.6	9.8	7.9	181.5	6.2	8.2	
FL98151B	70.8	75.1	8.3	297.1	10.4	10.0	205.2	10.6	10.5	
FL98151C	310.3	79.2	11.5	119.9	10.7	12.4	210.3	1.9	12.8	
FL98105B	48.0	23.7	-15.4	241.2	65.7	-14.7	140.2	4.9	-13.9	
FL98172A	246.9	26.3	-23.6	5.2	43.9	-23.3	136.9	34.7	-5.5	
FL98104A	131.3	4.2	-9.3	41.0	4.1	-8.5	267.2	84.1	-7.8	
FL98104C	267.2	59.2	-8.3	118.0	27.1	-7.9	21.0	13.5	-7.8	
FL98104D	297.5	22.1	-9.3	139.1	66.4	-9.0	30.7	7.8	-8.0	
FL98109B	276.3	33.5	-14.5	124.3	53.1	-14.0	15.6	13.6	-13.7	
FL98103A	168.6	26.9	6.1	49.8	43.5	6.4	279.0	34.6	6.8	
FL98106A	80.7	72.7	-8.9	259.5	17.3	-8.0	349.6	0.3	-7.0	
FL98106B	144.8	54.1	-9.3	335.5	35.4	-8.3	241.9	5.1	-7.9	
FL98171B	95.6	41.0	-18.0	293.3	47.7	-17.8	193.4	8.9	-17.0	
FL98171C	90.0	90.0	-20.4	270.0	90.0	-19.6	270.0	90.0	-19.2	
FL98171C	268.9	29.0	-20.0	134.9	51.4	-19.9	12.6	23.1	-19.5	
FL98108A	214.6	56.8	24.9	116.2	5.4	25.8	22.7	32.6	26.6	
FL98108B	343.7	85.4	40.4	242.2	0.9	42.8	152.2	4.6	43.4	
FL98203B	328.6	81.2	11.2	186.0	7.0	12.0	95.3	5.3	12.5	
FL98203C	223.9	65.2	17.3	95.5	16.0	18.6	0.0	18.4	19.0	
FL98102A	302.2	20.9	-19.7	188.6	46.3	-18.6	48.5	36.3	-17.4	
FL98102B	128.9	31.9	-18.9	14.7	33.3	-18.1	250.8	40.3	-17.8	
FL98102C	269.4	69.4	-19.3	73.7	19.9	-18.5	165.6	5.1	-18.0	
FL98242A	284.3	37.0	12.5	104.4	53.0	13.1	14.3	0.1	14.0	
FL98242B	275.0	13.2	12.7	139.1	71.9	13.5	7.9	12.1	14.7	
FL98241B	279.0	58.4	8.0	145.5	22.9	8.9	46.4	20.5	9.5	
FL98107B	175.3	76.7	-5.6	318.1	10.6	-5.2	49.6	7.9	-4.0	
FL98202A	235.3	60.5	24.2	129.5	8.8	24.5	34.8	28.0	25.5	
FL98202B	238.9	47.3	21.5	42.3	41.5	21.7	139.8	8.4	22.6	
FL98202C	160.4	79.0	17.2	293.1	7.5	17.9	24.2	8.0	18.7	
FL98201B	257.2	17.3	-14.4	138.6	56.9	-14.1	356.4	27.2	-13.7	
FL98240A	20.6	19.4	84.2	282.2	22.7	84.8	147.2	59.4	85.1	
FL98240B	97.2	10.1	48.6	305.9	78.5	48.8	188.1	5.4	50.0	
FL98101B	250.4	53.9	-13.7	103.9	31.3	-13.3	3.8	16.1	-12.4	
FL98200A	136.6	87.1	-17.2	121.0	45.8	-15.2	313.7	86.8	-13.2	
FL98200B	269.3	50.9	-18.4	99.5	38.7	-17.4	5.5	5.0	-16.2	
FL98200C	100.7	49.1	-16.1	272.5	40.6	-14.9	6.0	4.0	-14.4	

Appendix 5 - Regional Magnetic Fabric Data

Sample	Declination	Minimum			Intermediate			Maximum		
		Inclination	Intensity	Dec.	Inc.	Intensity	Dec.	Inc.	Intensity	
CY9706C	298.1	81.7	-11.4	87.8	7.2	-5.4	178.3	4.2	-3.7	
CY9706D	241.1	25.8	-8.2	360.0	45.0	-7.7	132.1	33.9	-7.3	
CY9706E	270.0	90.0	-7.8	90.0	90.0	-7.7	90.0	90.0	-7.3	
CY9706E	8.6	67.6	-8.2	118.2	7.9	-7.5	211.2	20.8	-7.3	
CY9704A	306.3	15.3	-4.7	213.9	8.8	-2.3	95.1	72.3	-1.6	
CY9704C	234.5	55.8	-2.7	110.8	20.7	-2.3	10.2	25.9	-2.0	
CY9704C	315.0	84.4	-2.6	315.0	54.7	-2.1	135.0	5.6	-2.0	
FL98232C	311.1	69.2	-8.4	110.3	19.5	-8.0	202.7	6.8	-7.4	
FL98229B	225.0	87.4	-2.9	225.0	82.0	-2.1	45.0	2.6	-1.7	
FL98148A	316.1	38.9	12.4	105.5	46.9	12.7	213.0	15.7	13.5	
FL98148B	102.3	38.6	15.5	342.8	31.6	16.1	226.9	35.4	17.0	
FL98148C	243.0	76.2	14.7	61.6	13.8	16.1	151.6	0.3	16.6	
FL98148D	331.2	81.2	13.9	138.6	8.6	14.6	228.9	1.9	15.3	
FL98228D	273.2	4.1	-28.1	12.4	65.6	-27.5	181.4	24.0	-27.2	
FL98147B	184.7	66.9	17.8	289.8	6.3	18.4	22.4	22.2	18.6	
FL98147C	270.0	71.6	14.6	56.3	15.5	15.2	149.0	9.7	15.7	
FL98147D	212.7	74.7	17.8	48.8	14.8	18.2	317.7	4.1	19.4	
FL98149B	303.7	84.6	22.1	42.1	0.8	27.2	132.2	5.4	29.5	
FL98149C	331.8	83.9	32.7	94.4	3.3	33.5	184.7	5.1	33.9	
FL98149D	335.1	68.8	28.3	187.8	18.1	29.7	94.3	10.7	30.1	
FL98146B	259.0	19.7	-4.0	17.6	53.3	-3.7	157.2	29.6	-2.5	
FL98226A	70.3	52.1	-11.9	330.0	7.9	-11.8	234.0	36.7	-10.6	
FL98226B	178.2	64.0	-11.3	341.5	25.0	-10.5	74.6	6.6	-9.0	
FL98226C	154.1	35.3	-14.9	264.7	26.5	-14.0	22.5	43.1	-13.7	
FL98142A	33.6	75.8	23.5	257.1	10.4	24.3	165.4	9.6	25.2	
FL98142A	33.6	75.8	23.5	257.1	10.4	24.3	165.4	9.6	25.2	
FL98142B	93.2	74.7	30.3	208.9	6.8	31.1	300.5	13.7	31.6	
CY9703A	18.4	82.1	8.9	320.7	59.4	9.4	198.4	7.9	9.7	
CY9703B	73.3	14.4	7.4	295.6	70.9	7.8	166.5	12.3	8.0	
CY9703C	241.5	12.8	8.6	355.5	60.9	8.8	145.2	25.6	9.5	
CY9703D	12.9	69.8	7.3	244.8	12.8	7.5	151.2	15.4	8.0	
CY9703D	270.0	77.9	6.9	270.0	41.6	7.8	90.0	12.1	8.0	
CY9703D	90.0	90.0	7.3	270.0	90.0	7.3	90.0	90.0	8.2	
FL98140A	260.4	65.8	7.8	142.1	12.0	8.1	47.5	20.7	8.5	
FL98140B	301.9	55.2	5.4	110.2	34.2	5.7	204.0	5.5	6.1	
FL98141B	16.8	80.9	-3.3	265.0	3.4	-2.4	174.5	8.5	-2.1	
FL98141C	48.7	73.9	3.0	251.7	14.8	3.5	160.1	6.0	4.2	
FL98138A	83.1	76.8	10.0	273.9	12.9	10.6	183.3	2.4	12.0	
FL98138B	70.7	44.7	7.2	228.7	43.1	7.4	329.4	11.2	8.3	
FL98138C	0.0	81.7	9.4	360.0	63.4	10.1	180.0	8.3	10.4	
FL98138C	90.0	83.0	9.1	270.0	7.0	9.8	270.0	85.2	10.6	
FL98138C	301.2	70.9	9.0	83.5	15.3	9.9	176.6	11.1	10.1	
FL98139B	254.0	75.7	7.0	107.2	12.0	8.0	15.5	7.6	9.9	
FL98137A	180.0	69.4	9.3	180.0	65.8	9.4	360.0	24.2	10.0	
FL98137A	331.6	63.6	8.5	70.4	4.3	9.2	162.5	26.0	9.6	
FL98137B	82.5	72.9	9.0	288.1	15.5	9.2	196.1	7.0	9.8	
FL98136A	113.2	76.4	13.1	287.7	13.5	13.9	18.0	1.2	14.3	
FL98136B	10.4	82.7	15.0	252.5	3.4	15.4	162.2	6.4	15.6	

Appendix 5 - Regional Magnetic Fabric Data

Sample	Declination	Minimum			Intermediate			Maximum		
		Inclination	Intensity	Dec.	Inc.	Intensity	Dec.	Inc.	Intensity	
FL98088A	92.7	51.4	-16.8	275.9	38.5	-16.0	184.7	1.6	-13.8	
FL98088B	66.5	40.8	-13.8	303.4	32.3	-13.4	189.8	32.4	-12.8	
FL98089B	141.3	54.2	-11.8	355.9	30.7	-11.3	255.7	16.6	-11.0	
FL98087B	39.9	63.8	-17.9	230.4	25.8	-16.9	138.4	4.2	-16.7	
FL98090A	78.9	76.3	3.3	286.6	12.1	4.0	195.3	6.2	4.8	
FL98090C	270.0	71.6	11.7	94.2	18.4	11.8	3.8	1.3	13.5	
FL98090D	172.5	39.4	11.0	329.4	48.2	11.5	72.8	11.7	13.4	
FL98091B	238.1	57.3	9.8	94.3	27.4	10.1	355.5	16.5	11.1	
FL98091C	274.6	66.3	8.6	82.6	23.3	9.5	174.5	4.4	11.6	
FL98093B	234.2	60.4	13.6	121.0	12.6	14.8	24.7	26.3	15.0	
FL98093C	45.8	65.9	14.9	272.2	17.1	15.5	177.0	16.4	16.1	
FL98093D	250.7	71.9	12.2	49.2	17.1	12.8	141.1	7.0	13.5	
FL98128A	70.5	45.4	8.1	317.2	21.4	8.7	210.1	36.9	8.9	
FL98128B	281.4	20.0	9.0	66.3	66.0	9.8	186.7	12.7	10.6	
FL98094A	107.7	55.5	2.3	242.3	25.8	3.0	343.1	21.3	3.9	
FL98094B	130.2	43.4	2.8	235.1	15.2	4.0	339.6	42.6	4.2	
FL98094C	316.2	83.0	5.5	106.0	6.1	6.1	196.4	3.5	7.1	
FL98095B	355.1	10.0	6.9	238.9	68.3	9.2	88.6	19.1	10.8	
FL98095C	174.2	71.5	10.4	267.8	1.2	11.2	358.3	18.4	12.8	
FL98095C	174.2	71.5	10.4	267.8	1.2	11.2	358.3	18.4	12.8	
FL98096A	107.4	22.5	9.5	326.5	62.0	9.7	204.2	15.9	10.6	
FL98096B	327.2	36.0	8.6	141.3	53.9	8.7	235.1	2.8	10.6	
FL98097B	115.9	57.3	19.2	321.7	30.0	19.7	224.8	11.7	21.4	
FL98097C	102.8	61.6	21.9	248.7	24.1	22.5	345.1	14.1	22.6	
FL98097D	224.2	60.0	17.8	26.9	28.9	18.1	121.0	7.5	18.9	
FL98100A	315.0	86.4	47.0	315.0	54.7	47.8	135.0	3.6	47.9	
FL98100A	106.9	70.7	46.8	272.0	18.7	47.9	3.5	4.6	48.6	
FL98100B	254.0	29.3	34.9	102.1	57.6	35.3	351.3	12.7	35.8	
FL98098A	282.4	54.0	37.6	126.6	33.6	39.4	28.8	11.6	40.7	
FL98098B	169.7	47.7	56.4	356.3	42.1	57.2	263.3	3.3	58.6	
FL98099B	135.1	10.3	2.8	22.6	64.5	3.4	229.6	23.1	4.9	
CY9752A	54.4	76.3	24.1	286.0	8.7	25.1	194.4	10.6	25.6	
CY9752B	92.6	66.4	24.2	276.6	23.2	25.2	186.0	1.5	25.9	
CY9752C	87.0	14.0	26.9	338.5	51.7	28.3	187.0	34.8	28.6	
CY9752D	216.8	61.5	23.1	77.1	22.5	23.3	340.1	16.6	24.8	
CY9702A	29.4	33.1	9.4	151.2	38.9	9.7	273.7	33.7	10.2	
CY9702B	91.3	57.0	5.4	252.4	31.6	6.1	347.8	8.6	6.3	
CY9702C	313.5	52.0	6.0	84.4	27.1	6.4	187.9	24.5	6.8	
FL98054A	222.4	5.7	43.3	321.1	56.7	44.2	128.7	32.7	45.7	
FL98054B	222.1	57.1	25.1	97.1	20.3	25.9	357.3	24.7	26.7	
FL4 (IV)										
CY9701A	82.4	47.0	6.0	316.1	28.9	6.4	208.5	28.7	6.9	
CY9701A	90.0	90.0	6.0	270.0	90.0	6.3	90.0	90.0	6.4	
CY9701B	282.4	71.5	6.5	16.7	1.4	7.2	107.2	18.4	7.5	
CY9701C	312.4	80.6	6.9	128.5	9.4	7.6	218.6	0.6	8.0	
CY9701D	342.6	16.7	10.9	237.9	40.3	11.3	90.0	45.0	11.5	
CY9701E	344.6	72.8	9.5	129.4	14.2	9.9	221.8	9.5	10.2	
FL98350A	308.5	39.0	-24.9	59.4	23.8	-24.5	172.5	41.6	-24.2	

Appendix 5 - Regional Magnetic Fabric Data

Sample	Declination	Minimum			Intermediate			Maximum		
		Inclination	Intensity	Dec.	Inc.	Intensity	Dec.	Inc.	Intensity	
FL98350B	245.3	71.3	-31.0	68.1	18.7	-30.4	337.8	0.9	-30.1	
FL98119B	280.7	67.2	16.6	39.7	11.5	17.6	133.7	19.4	18.7	
FL98119C	264.8	53.1	13.6	87.8	36.9	14.3	356.7	1.5	14.6	
FL98122A	90.4	41.3	-24.9	331.7	28.7	-23.9	218.8	35.3	-20.1	
CY9766A	102.1	22.9	7.4	335.8	54.5	7.8	203.8	25.5	8.3	
CY9766B	92.5	20.1	5.2	297.3	68.0	6.0	185.7	8.5	6.8	
CY9766C	101.2	46.5	3.4	260.9	41.7	3.8	0.2	10.2	4.7	
FL98113B	120.2	68.2	-8.5	313.8	21.2	-7.7	222.0	4.7	-7.3	
FL98116A	177.0	36.5	6.9	50.3	38.9	9.4	292.4	30.1	10.0	
FL98116B	232.5	59.8	6.2	19.9	26.1	6.8	116.9	14.1	7.6	
FL98116C	9.3	79.9	3.4	188.1	10.1	6.1	278.2	0.2	6.5	
FL98115B	66.8	57.6	4.3	225.8	30.6	4.8	321.5	9.5	5.3	
FL98115D	246.6	80.5	4.0	77.1	9.4	4.6	346.8	1.7	5.9	
FL98121C	88.9	32.8	-18.4	257.5	56.7	-17.9	355.5	5.2	-17.1	
FL98121D	259.4	35.1	-18.0	78.3	55.7	-17.8	169.1	0.9	-16.3	
FL98004A	234.7	67.9	3.8	139.9	1.9	4.6	49.1	22.0	4.9	
FL98005B	45.1	67.3	45.2	179.0	16.2	46.2	273.6	15.5	46.8	
FL98126A	159.2	1.4	21.8	61.8	79.1	22.0	249.5	10.8	22.6	
FL98126B	299.8	7.0	37.8	46.4	66.8	38.8	207.0	22.0	39.2	
FL98114A	143.5	84.8	14.5	244.7	1.0	17.8	334.8	5.1	18.1	
FL98114B	288.5	78.8	16.0	43.6	4.8	16.6	134.4	10.1	17.6	
FL98006A	215.5	70.0	4.1	73.3	16.0	4.6	339.9	11.6	4.8	
FL98006A	215.5	70.0	4.1	73.3	16.0	4.6	339.9	11.6	4.8	
FL98117B	41.3	55.3	5.6	132.4	0.8	6.1	222.9	34.7	8.5	
FL98118A	275.2	9.1	19.2	120.4	80.0	19.6	5.8	4.2	20.7	
FL98118B	233.5	80.8	20.1	23.5	8.0	22.5	114.2	4.5	24.6	
FL98118C	265.7	48.2	16.2	39.9	32.0	16.9	146.0	24.0	18.2	
FL98024B	60.3	42.6	25.4	265.7	44.5	27.2	162.6	13.0	27.6	
FL98016A	41.0	25.8	15.9	185.3	59.2	16.2	303.2	15.6	17.4	
FL98016B	99.0	79.4	17.8	271.4	10.5	18.0	1.6	1.4	19.3	
FL98015B	82.2	46.2	10.5	321.1	26.4	11.0	213.0	32.1	11.3	
FL98352A	117.4	45.7	20.2	319.1	42.7	20.7	218.6	11.2	21.4	
FL98352B	106.6	51.5	35.7	0.4	12.6	36.6	261.1	35.7	37.2	
FL98352C	154.9	73.0	20.9	25.9	10.9	21.9	293.3	12.9	22.5	
FL98352D	141.0	58.8	40.7	260.4	16.5	41.6	358.6	25.6	42.0	
CY9748A	31.4	43.7	3.1	125.1	3.9	3.3	219.1	46.0	3.9	
CY9748E	27.3	35.3	4.5	267.3	35.3	4.8	147.3	35.3	5.2	
CY9749A	19.7	76.4	95.7	137.8	6.5	102.4	229.2	11.9	103.9	
CY9749B	38.9	71.2	88.7	295.0	4.7	93.1	203.5	18.2	94.2	
CY9749C	15.8	74.6	64.7	141.5	9.1	69.2	233.5	12.3	70.0	
CY9749D	13.2	68.5	84.9	169.9	19.9	89.5	262.8	7.8	91.9	
CY9750A	117.4	58.1	62.5	8.2	11.6	66.3	271.6	29.3	67.1	
CY9750B	128.1	48.5	62.9	338.9	37.2	71.7	236.6	15.7	73.4	
CY9750C	118.6	60.2	55.4	318.8	28.3	59.0	224.1	8.7	59.6	
CY9750D	106.6	65.0	76.9	303.2	24.1	82.0	210.4	6.3	82.3	
CY9750E	108.7	65.3	72.4	260.3	22.1	77.5	354.7	10.6	77.6	
FL98036A	332.6	12.1	9.7	75.8	46.7	10.1	232.0	40.7	10.6	
FL98027B	293.7	41.5	16.4	27.6	4.5	17.0	122.6	48.1	17.4	

Appendix 5 - Regional Magnetic Fabric Data

Sample	Declination	Minimum			Intermediate			Maximum		
		Inclination	Intensity	Dec.	Inc.	Intensity	Dec.	Inc.	Intensity	
FL98027C	240.2	42.3	13.6	119.3	29.4	14.1	7.3	33.6	14.5	
FL98027D	276.4	25.8	12.4	95.3	64.2	13.1	186.2	0.4	14.3	
FL98353B	61.9	76.8	43.1	220.8	12.4	44.3	311.8	4.6	44.7	
FL98031B	87.2	41.2	1.9	308.9	40.5	2.4	198.3	22.4	3.1	
FL98354A	254.0	16.5	-17.9	12.3	57.9	-17.3	155.5	26.6	-16.6	
FL98354B	275.8	57.5	-17.0	121.3	30.0	-15.8	24.5	11.5	-15.1	
FL98355A	343.8	25.7	-29.2	94.5	36.3	-28.7	227.3	42.8	-27.7	
FL98355B	70.9	16.9	-24.9	328.0	36.3	-24.2	181.2	48.7	-23.5	
FL98355C	162.7	82.0	-27.8	11.0	7.0	-27.3	280.5	3.8	-26.5	
FL98355D	112.6	24.6	-27.6	345.3	52.9	-27.3	215.4	25.9	-26.2	
FL98001B	33.0	75.3	48.3	251.1	11.7	50.0	159.3	8.8	50.9	
FL98373B	289.5	62.7	7.1	83.2	24.9	8.1	178.2	10.7	9.2	
FL98373C	171.4	76.4	7.9	22.9	11.6	9.3	291.5	6.9	9.9	
FL98374B	347.2	66.7	5.8	160.3	23.1	6.3	251.3	2.5	8.1	
CY9751A	261.9	52.6	153.3	84.1	37.4	158.8	353.3	1.0	161.2	
CY9751B	264.4	54.7	132.1	97.1	34.6	137.5	2.9	6.0	139.5	
CY9751C	255.4	46.0	143.0	74.5	44.0	147.6	164.9	0.5	149.2	
FL5 (V)										
FL98390A	223.0	84.8	39.7	318.1	0.5	41.2	48.1	5.2	42.1	
FL98379B	286.6	78.3	11.5	73.6	9.8	12.2	164.7	6.2	13.6	
FL98389B	322.9	36.1	12.8	70.6	22.6	17.1	185.4	45.3	17.5	
FL98388B	276.9	41.4	-6.3	100.8	44.5	-5.9	8.8	2.1	-5.0	
FL98061B	161.4	75.9	-9.5	14.3	11.9	-6.7	282.7	7.4	-6.3	
FL98383B	83.7	74.7	4.5	252.8	2.6	5.3	343.5	6.2	5.9	
FL98060B	306.0	60.0	13.8	136.0	29.6	14.6	43.5	4.3	15.3	
FL98083B	230.8	86.2	14.0	103.9	2.3	15.4	13.8	3.0	15.7	
FL98084A	55.7	79.6	32.9	283.3	7.1	33.9	192.3	7.6	34.3	
FL98084B	305.6	80.4	43.4	43.4	1.3	45.3	133.6	9.6	45.7	
FL98084C	7.3	80.3	33.2	105.5	1.4	34.6	195.7	9.6	34.8	
FL98086A	252.3	80.9	14.5	73.7	9.1	16.0	343.7	0.2	16.8	
FL98086B	235.0	76.0	19.8	32.2	12.9	20.5	123.4	5.2	20.8	
FL98085B	212.2	84.9	20.0	327.9	2.2	20.7	58.1	4.6	21.3	
FL98082A	166.1	72.0	22.2	313.6	15.3	23.9	46.2	9.2	25.3	
FL98082B	129.4	66.4	25.2	258.7	15.5	26.3	353.7	17.4	26.9	
FL98082C	303.7	81.6	20.2	123.7	0.0	22.0	123.7	8.4	22.0	
FL98080A	334.1	74.1	-23.0	242.3	0.5	-22.6	152.2	15.9	-22.4	
FL98080B	73.1	48.3	-21.6	273.9	39.8	-20.6	175.1	10.5	-18.4	
FL98075A	115.1	66.8	-2.9	290.4	23.1	-2.0	21.2	1.7	-1.7	
FL98074A	149.5	61.6	-7.8	318.5	28.0	-6.5	51.0	4.6	-6.2	
FL98070B	141.7	75.4	8.1	285.5	11.9	9.5	17.3	8.4	10.1	
FL98067B	126.4	15.7	5.6	19.5	45.9	6.0	229.9	39.8	7.2	
GBFL005B	32.4	82.2	14.2	168.8	5.7	16.2	259.4	5.4	16.3	
GBFL005C	92.7	72.7	12.6	284.0	16.7	13.9	193.0	3.1	14.2	
GBFL004A	30.2	78.3	7.2	287.1	2.7	7.9	196.5	11.4	8.7	
GBFL004B	147.8	62.3	8.6	270.3	15.7	9.4	6.9	22.2	10.1	
GBFL004C	100.2	82.1	6.2	265.0	7.6	7.0	355.3	2.0	7.5	
GBFL003C	288.4	65.1	24.3	48.9	13.2	25.2	144.0	20.7	27.3	
GBFL003D	283.7	74.7	20.2	95.7	15.2	21.1	186.3	2.0	21.7	

Appendix 5 - Regional Magnetic Fabric Data

Sample	Declination	Minimum			Intermediate			Maximum	
		Inclination	Intensity	Dec.	Inc.	Intensity	Dec.	Inc.	Intensity
GBFL006A	241.9	76.1	16.1	71.0	13.7	16.7	340.5	2.1	18.0
GBFL006B	307.6	74.8	13.6	114.2	14.8	14.6	205.1	3.4	15.2
GBFL002A	114.1	62.4	9.4	280.1	26.9	10.1	13.0	5.7	10.5
GBFL002B	176.5	81.6	6.3	300.9	4.8	8.6	31.5	6.9	9.0
GBFL002C	222.1	60.0	8.0	122.6	5.4	8.8	29.5	29.4	9.1
GBFL001B	90.0	90.0	-10.5	90.0	90.0	-10.4	90.0	90.0	-9.5
GBFL001B	278.8	16.7	-10.8	65.4	70.2	-10.2	185.6	10.3	-9.5
GBFL001C	282.2	31.2	-11.8	116.8	58.0	-11.6	16.2	6.6	-10.5
GBFL007B	126.6	80.1	18.9	274.2	8.4	19.7	4.9	5.3	20.0
GBFL008A	270.0	71.6	-6.1	36.2	11.1	-5.6	129.1	14.5	-5.4
GBFL008B	298.7	63.2	-4.6	81.7	21.9	-4.2	177.7	14.6	-3.3
GBFL008C	140.3	50.2	-4.6	293.0	36.5	-4.1	33.4	13.6	-3.8
GBFL010A	241.2	55.3	6.2	100.3	28.3	6.7	0.0	18.4	7.1
GBFL010B	37.0	80.4	11.7	257.0	7.4	12.2	166.2	6.1	12.7
GBFL010C	335.7	77.9	9.8	86.6	4.4	10.7	177.5	11.3	11.0

Appendix 6 - Hysteresis Data

Sample	Type	Hc (mT)	Hcr (mT)	Hcr/Hc	Mrs/Ms	Slope Correction (MAm ² /T*kg)
GBCY06B1	PELAGIC	8.33	18.93	2.27	0.12	7.35
GBCY06B2	PELAGIC	8.28	20.95	2.53	0.13	8.07
GBCY06C1	PELAGIC	7.84	11.04	1.41	0.16	7.68
GBCY06C2	PELAGIC	3.73	10.98	2.95	0.05	8.12
GBCY08A1	PELAGIC	4.10	10.47	2.56	0.06	6.04
GBCY08A2	PELAGIC	3.69	13.28	3.60	0.06	6.32
GBCY12A1	PELAGIC	4.51	17.23	3.82	0.06	3.23
GBCY12A2	PELAGIC	3.31	11.49	3.47	0.06	1.84
GBCY12B1	PELAGIC	8.22	4.27	0.52	0.06	1.32
GBCY12B2	PELAGIC	6.16	26.05	4.23	0.07	1.05
GBCY12C1	PELAGIC	5.20	2.60	0.50	0.07	1.64
GBCY12C2	PELAGIC	7.49	3.06	0.41	0.06	1.45
GBCY12D1	PELAGIC	5.38	12.92	2.40	0.06	2.99
GBCY12D2	PELAGIC	5.85	23.07	3.94	0.08	2.80
GBCY23B1	PELAGIC	2.99	2.17	0.73	0.02	3.12
GBCY23B2	PELAGIC	4.80	18.51	3.86	0.06	7.21
GBCY23C1	PELAGIC	4.02	18.55	4.62	0.05	5.11
GBCY23C2	PELAGIC	4.50	17.86	3.97	0.05	5.70
GBCY23D1	PELAGIC	8.83	19.79	2.24	0.08	4.84
GBCY23D2	PELAGIC	11.63	40.27	3.46	0.13	1.24
GBPOL03B	PELAGIC	7.14	19.50	2.73	0.08	6.20
GBPOL04F	PELAGIC	14.70	21.50	1.46	0.15	-5.74
GBPOL06B	PELAGIC	10.40	14.00	1.35	0.11	-0.98
GBPOL07B	PELAGIC	18.00	23.70	1.32	0.18	-28.70
GBPOL13C	PELAGIC	10.60	18.30	1.73	0.11	2.81
GBPOL18B	PELAGIC	23.90	46.20	1.93	0.23	1.21
GBPOL19C	PELAGIC	9.27	16.60	1.79	0.11	4.58
GBPOL23C	PELAGIC	26.63	14.01	0.53	0.26	-26.60
GBPOL25B	PELAGIC	19.21	10.28	0.54	0.24	2.39
GBPOL34C	PELAGIC	19.30	27.81	1.44	0.20	-3.79
GBPOL35B	PELAGIC	25.05	21.26	0.85	0.23	-1.28
GBPOL36B	PELAGIC	16.23	21.58	1.33	0.32	0.48
GBPOL37B	PELAGIC	14.92	18.96	1.27	0.19	1.71
GBPOL38C	PELAGIC	11.02	10.30	0.93	0.19	2.47
GBPOL39B	PELAGIC	13.88	35.84	2.58	0.16	2.46
GBPOL40B	PELAGIC	14.60	28.64	1.96	0.17	-6.28
GBPOL41B	PELAGIC	14.67	31.81	2.17	0.17	-7.98
GBPOL46B	PELAGIC	23.37	52.76	2.26	0.22	-25.71
GBPOL50C	PELAGIC	20.18	38.49	1.91	0.24	-33.73
GBPOL52B	PELAGIC	13.09	8.90	0.68	0.17	-0.85
GBPOL53E	PELAGIC	16.34	22.51	1.38	0.24	-9.09
GBPOL56C	PELAGIC	15.23	23.25	1.53	0.18	-7.51
GBPOL61B	PELAGIC	11.27	13.20	1.17	0.15	-1.09
GBCY03A	NON-PELAGIC	4.41	27.47	6.23	0.07	0.14
GBCY03B	NON-PELAGIC	5.25	22.97	4.38	0.07	-1.28
GBCY03C	NON-PELAGIC	3.73	10.98	2.95	0.05	-0.27
GBCY03D	NON-PELAGIC	6.85	34.40	5.02	0.11	-1.72
GBCY04A	NON-PELAGIC	2.81	16.18	5.76	0.04	-0.30
GBCY04C	NON-PELAGIC	1.71	24.70	14.43	0.03	-0.07

Appendix 6 - Hysteresis Data

Sample	Type	Hc (mT)	Hcr (mT)	Hcr/Hc	Mr/Ms	Slope Correction (MAM2/T*kg)
GBCY04D	NON-PELAGIC	0.31	42.13	135.90	0.01	-0.07
GBCY05A	NON-PELAGIC	3.22	23.01	7.14	0.06	1.25
GBCY09A	NON-PELAGIC	3.97	5.43	1.37	0.08	4.04
GBCY09B	NON-PELAGIC	5.89	25.77	4.37	0.10	4.63
GBCY09C	NON-PELAGIC	4.82	8.81	1.83	0.09	4.76
GBCY10C	NON-PELAGIC	7.47	22.24	2.98	0.16	0.17
GBCY13A	NON-PELAGIC	10.95	42.19	3.85	0.15	-9.02
GBCY13B	NON-PELAGIC	2.43	15.07	6.21	0.04	2.18
GBCY13D	NON-PELAGIC	9.85	43.17	4.38	0.15	-4.42
GBCY14A	NON-PELAGIC	4.90	22.65	4.62	0.06	-1.37
GBCY14B	NON-PELAGIC	11.54	48.40	4.19	0.21	-2.98
GBCY14C	NON-PELAGIC	6.30	33.24	5.27	0.07	-0.45
GBCY14D	NON-PELAGIC	5.89	30.48	5.18	0.08	-0.90
GBCY17B	NON-PELAGIC	9.93	29.34	2.95	0.19	-2.43
GBCY17C	NON-PELAGIC	7.81	40.20	5.15	0.15	-4.34
GBCY19A	NON-PELAGIC	5.30	28.62	5.40	0.11	-2.52
GBCY19B	NON-PELAGIC	5.19	45.07	8.68	0.09	-0.89
GBCY21C	NON-PELAGIC	7.09	32.58	4.60	0.13	1.77
GBCY21D	NON-PELAGIC	5.25	43.11	8.21	0.09	2.16
GBCY24A	NON-PELAGIC	6.03	30.78	5.11	0.10	2.27
GBCY24B	NON-PELAGIC	5.94	31.19	5.25	0.12	2.80
GBCY24C	NON-PELAGIC	12.57	28.64	2.28	0.23	4.35
GBCY24D	NON-PELAGIC	11.67	44.60	3.82	0.22	4.85
GBCY24E	NON-PELAGIC	9.95	47.19	4.74	0.16	5.50
GBCY24F	NON-PELAGIC	11.47	30.01	2.62	0.20	4.08
GBCY01B	NON-PELAGIC	9.23	6.38	0.69	0.13	2.87
GBCY10A	NON-PELAGIC	7.61	47.75	6.28	0.12	-0.89
GBCY13C	NON-PELAGIC	11.56	50.08	4.33	0.17	-4.31
GBCY15A	NON-PELAGIC	10.10	70.31	6.96	0.14	4.21
GBCY15B	NON-PELAGIC	7.70	13.32	1.73	0.10	4.51
GBCY20D	NON-PELAGIC	12.18	33.93	2.79	0.14	0.99
GBCY01A	NON-PELAGIC	8.99	24.82	2.76	0.16	3.24
GBCY05D	NON-PELAGIC	8.79	14.64	1.67	0.14	5.37
GBPOL08B	NON-PELAGIC	14.30	24.10	1.69	0.14	5.37
GBPOL12B	NON-PELAGIC	7.58	78.30	10.33	0.18	4.31
GBPOL17E	NON-PELAGIC	29.50	36.90	1.25	0.38	-15.10
GBPOL21C	NON-PELAGIC	30.75	14.74	0.48	0.28	-30.71
GBPOL26C	NON-PELAGIC	22.91	9.65	0.42	0.32	2.12
GBPOL27B	NON-PELAGIC	22.38	13.35	0.60	0.35	2.31
GBPOL29B	NON-PELAGIC	22.10	12.35	0.56	0.28	1.76
GBPOL30B	NON-PELAGIC	22.41	15.61	0.70	0.27	1.37
GBPOL31B	NON-PELAGIC	18.03	9.44	0.52	0.23	3.08
GBPOL32B	NON-PELAGIC	20.71	13.79	0.67	0.24	0.21
GBPOL33B	NON-PELAGIC	18.85	13.02	0.69	0.22	2.06
GBPOL43B	NON-PELAGIC	20.14	41.54	2.06	0.20	-24.36
GBPOL47C	NON-PELAGIC	13.57	19.39	1.43	0.16	0.85
GBPOL48B	NON-PELAGIC	21.31	53.58	2.51	0.21	-32.92
GBPOL49B	NON-PELAGIC	22.03	44.40	2.02	0.19	-46.50
GBPOL51B	NON-PELAGIC	13.37	13.45	1.01	0.16	1.23
GBPOL54C	NON-PELAGIC	11.15	22.82	2.05	0.15	-1.13

Appendix 7 - Magnetic Properties Data

Sample	Order	μ SI	mA/m	mA/m	mA/m	mA/m	mA/m	mA/m	%Mgt	%TM60
		Bulk K	Bulk A	SIRM	SIRM200	SIRM200/SIRM	"Magnetite"	TM60		
TH01B	56	55.10	0.26	418.37	319.62	0.76	319.62	98.75	76.40	23.60
TH02E	58	160.40	1.14	4036.95	3232.49	0.80	3232.49	804.46	80.07	19.93
TH03B	58	118.30	0.77	3193.20	2520.02	0.79	2520.02	673.18	78.92	21.08
TH07B	47	29.60	0.03	64.26	44.05	0.69	44.05	20.21	68.55	31.45
TH08C	46	15.50	0.03	37.95	28.25	0.74	28.25	9.70	74.44	25.56
TH09B	45	13.10	0.03	38.10	28.30	0.74	28.30	9.80	74.28	25.72
TH10B	48	36.60	0.05	104.25	74.76	0.72	74.76	29.49	71.71	28.29
TH11B	44	13.40	0.02	32.07	22.61	0.70	22.61	9.46	70.49	29.51
TH12B	43	31.50	0.04	93.53	64.09	0.69	64.09	29.44	68.52	31.48
TH13B	42	21.70	0.03	88.13	57.52	0.65	57.52	30.61	65.27	34.73
TH14B	39	26.60	0.04	136.66	99.65	0.73	99.65	37.00	72.92	27.08
TH15B	38	36.70	0.03	216.01	168.02	0.78	168.02	47.99	77.78	22.22
TH16B	37	35.70	0.03	244.40	189.15	0.77	189.15	55.25	77.39	22.61
TH17B	36	23.90	0.04	171.00	137.34	0.80	137.34	33.67	80.31	19.69
TH18B	35	16.30	0.03	90.81	74.06	0.82	74.06	16.75	81.55	18.45
TH19E	34	15.50	0.03	68.98	56.74	0.82	56.74	12.25	82.25	17.75
TH20B	33	18.60	0.03	85.50	69.36	0.81	69.36	16.15	81.12	18.88
TH21E	32	25.60	0.05	345.02	291.00	0.84	291.00	54.02	84.34	15.66
TH22C	31	34.70	0.07	478.56	379.08	0.79	379.08	99.48	79.21	20.79
TH23B	22	16.70	0.03	25.51	16.22	0.64	16.22	9.29	63.58	36.42
TH24E	21	8.90	0.03	15.50	12.22	0.79	12.22	3.29	78.79	21.21
TH25B	20	35.70	0.02	36.23	25.66	0.71	25.66	10.57	70.83	29.17
TH26B	19	25.60	0.03	46.01	35.70	0.78	35.70	10.30	77.61	22.39
TH27C	18	21.30	0.03	33.63	25.63	0.76	25.63	7.99	76.23	23.77
TH28A	17	19.60	0.03	31.46	16.61	0.53	16.61	14.86	52.78	47.22
TH29E	16	10.70	0.03	49.71	30.20	0.61	30.20	19.51	60.76	39.24
TH30A	15	20.60	0.03	34.82	24.73	0.71	24.73	10.09	71.02	28.98
TH31D	14	78.20	0.14	407.59	293.31	0.72	293.31	114.29	71.96	28.04
TH32C	13	85.90	0.12	426.51	311.01	0.73	311.01	115.50	72.92	27.08
TH33B	12	19.80	0.03	20.60	13.70	0.67	13.70	6.90	66.51	33.49
TH34B	11	30.80	0.04	42.75	31.66	0.74	31.66	11.09	74.06	25.94
TH35B	10	14.20	0.04	16.20	10.56	0.65	10.56	5.64	65.18	34.82
TH36B	9	18.90	0.04	27.63	17.40	0.63	17.40	10.23	62.98	37.02
TH37B	8	12.60	0.03	26.75	17.95	0.67	17.95	8.80	67.11	32.89
TH38E	7	15.70	0.02	44.15	29.41	0.67	29.41	14.75	66.60	33.40
TH39A	6	18.00	0.04	22.17	15.21	0.69	15.21	6.96	68.59	31.41
TH40B	5	61.60	0.02	147.03	116.54	0.79	116.54	30.48	79.27	20.73
TH41B	4	44.60	0.04	152.04	118.71	0.78	118.71	33.33	78.08	21.92
TH42B	3	30.20	0.04	55.91	37.02	0.66	37.02	18.89	66.21	33.79
TH43B	2	19.40	0.02	28.90	18.95	0.66	18.95	9.95	65.58	34.42
TH44B	1	31.50	0.04	97.58	63.23	0.65	63.23	34.35	64.80	35.20
TH50B	50	23.10	0.03	27.80	19.46	0.70	19.46	8.33	70.02	29.98
TH51C	49	40.10	0.05	151.03	103.93	0.69	103.93	47.10	68.82	31.18
TH52C	54	56.40	0.05	107.73	77.41	0.72	77.41	30.31	71.86	28.14
TH53C	55	23.60	0.05	71.85	52.57	0.73	52.57	19.28	73.17	26.83
TH54C	53	62.60	0.10	361.19	289.79	0.80	289.79	71.40	80.23	19.77
TH55C	52	32.60	0.02	124.56	88.14	0.71	88.14	36.43	70.75	29.25
TH56C	51	48.10	0.03	411.04	294.08	0.72	294.08	116.96	71.55	28.45
TH57C	40	62.10	0.10	600.62	418.53	0.70	418.53	182.09	69.68	30.32

Appendix 7 - Magnetic Properties Data

Sample	Order	μ SI	mA/m	mA/m	mA/m	mA/m	mA/m	%Mgt	%TM60	
		Bulk K	Bulk A	SIRM	SIRM200	SIRM200/SIRM	MTG	TM60		
TH58A	32	23.60	0.04	58.38	39.59	0.68	39.59	18.80	67.81	32.19
TH59E	28	19.80	0.04	96.66	72.15	0.75	72.15	24.51	74.64	25.36
TH60C	27	28.00	0.04	114.75	83.71	0.73	83.71	31.04	72.95	27.05
TH61C	26	31.00	0.05	82.49	56.84	0.69	56.84	25.65	68.90	31.10
TH62C	25	21.70	0.04	69.47	46.10	0.66	46.10	23.37	66.36	33.64

Limestones distinguished by magnetic hysteresis in three-dimensional projections

G. J. Borradaile and Tom Hamilton

Geology and Physics Department, Lakehead University, Thunder Bay, Canada

Received 4 June 2003; revised 15 August 2003; accepted 20 August 2003; published 30 September 2003.

[1] Magnetic hysteresis data determine the suitability of rocks for paleomagnetic work, provide clues to paleo-environment and paleo-climate and they may characterize depositional environments for limestones. However, the variables chosen for conventional two-dimensional hysteresis plots, such as that of *Day et al.* [1977], are not always suitable to discriminate between samples. Distinguishing samples by their regression surfaces in 3D hysteresis space may be more successful in some cases [Borradaile and Lagroix, 2000] but a 2D projection with a less arbitrary viewing axis is preferable for routine reporting. We show that limestone samples are simply discriminated in a new 2D projection produced by projecting hysteresis data from three dimensions ($x, y, z = Mr/Ms, Bcr, Bc$) onto a plane containing the Mr/Ms axis. The orientation of the plane is controlled by its x -axis that is defined by a suitably selected Bcr/Bc ratio, most often in the magnetite PSD range, $2 < (Bcr/Bc) < 4$. **INDEX TERMS:** 1527 Geomagnetism and Paleomagnetism: Paleomagnetism applied to geologic processes; 1533 Geomagnetism and Paleomagnetism: Remagnetization; 1540 Geomagnetism and Paleomagnetism: Rock and mineral magnetism; 1594 Geomagnetism and Paleomagnetism: Instruments and techniques. **Citation:** Borradaile, G. J., and T. Hamilton, Limestones distinguished by magnetic hysteresis in three-dimensional projections, *Geophys. Res. Lett.*, 30(18), 1973, doi:10.1029/2003GL017892, 2003.

1. Introduction

[2] The magnetic properties of sediments are valuable and efficient indicators of grain size and environmental conditions [Banerjee *et al.*, 1981; King *et al.*, 1982; Thompson and Oldfield, 1986]. This is directly due to the predominance of magnetite, which forms approximately 2 wt% of the crust on a modal basis, and the predominant role of grain-size controlling its magnetic domain structure. However, other physical factors for magnetite and other minerals are easily considered where necessary [Dunlop and Özdemir, 1997]. Attention is focused on limestones due to sedimentological and biogenic constraints and on the grain-size and low-stress state of its magnetite [Freeman, 1986; Henshaw and Merrill, 1980; Lowrie and Heller, 1982], which permits limestones depositional facies to be characterized by their hysteresis response [Borradaile *et al.*, 1993]. Hysteresis properties may also diagnose hard-remagnetization in carbonates [Channell and McCabe, 1994; Jackson, 1990; Jackson *et*

al., 1992; McCabe *et al.*, 1984], a serious complication in paleomagnetic work.

2. Magnetic Characterization

[3] A rock's remanence-bearing properties are characterized by saturation isothermal remanence (SIRM = Mr) after exposure to a large field or Ms in the presence of a large field. Similarly, the tenacity of remanence is important, measured by coercivity (Bc), coercivity of remanence (Bcr) or the ease of demagnetization in alternating field (AF). Cisowski [1981] plots decaying remanence with AF against progressive acquisition of IRM, and determination of SIRM to infer magnetite grain-size and separation. Wasilewski [1973] plots Bc against Bcr ; and most popular, *Day et al.* [1977] plot Mr/Ms against Bcr/Bc . The latter has now become synonymous with "hysteresis plot".

[4] The success of the Day plot comes from its ability to separate behavior according to the presence of single-domain (SD), pseudo-single domain (PSD) or multidomain (MD) magnetite, especially where the specimens contain magnetite in just one of these categories. These are traditionally shown as rectangular fields (Figure 1a) but, as Dunlop [2002a, 2000b] shows the reality of mixed grain-size distributions that encompass more than one type of domain-behavior, including superparamagnetic (SP) makes its use less clear-cut. Moreover, clear SD domain behavior is unlikely to be isolated [Lanci and Kent, 2003]. Viewing the data set along a less arbitrary axis through hysteresis space provides an ad hoc solution to magnetic discrimination. Linear discrimination functional analysis does this formally but with so few variables, it suffices to re-examine the data-set using a changed coordinate system. Since hysteresis experiments determine Bcr and Bc separately, it is profitable to make a three-dimensional hysteresis plot of Mr/Ms against Bcr , and Bc (Figure 1b). This plot successfully separates some data-sets but the choice of view is limited by the data-distribution and effective visual discrimination is not always possible, although regression-surfaces were always distinct [Borradaile and Lagroix, 2000].

[5] Without recourse to regression surfaces or other statistics that impede visual appreciation, it is possible to retain the information from the three variables (Bcr, Bc and Mr/Ms) and yet avoid the data-superposition of the traditional Day plot (Figure 1a). The simple principle is to project the data from 3D-hysteresis space onto a pre-selected plane, which contains the Ms/Mr axis. For example, two such planes are shown in Figure 1b, designated as the $Bcr = 10Bc$ and the $Bcr = Bc$ planes. Experience with approximately 500 hysteresis x - y - z points obtained from limestones using the

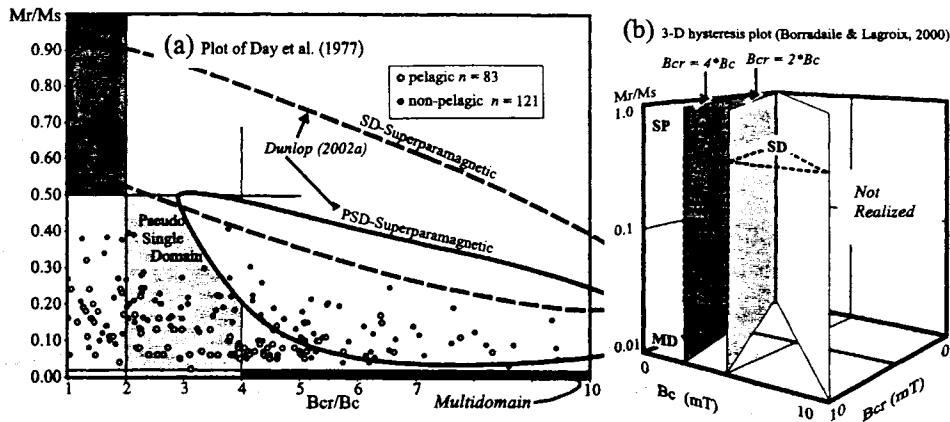


Figure 1. (a) The traditional two-dimensional hysteresis plot may fail to discriminate samples on the basis of hysteresis ratios. Here pelagic limestones are compared with shelf limestones, from sampling projects in UK and Israel. (b) A 3D plot of Bcr and Bc individually against Mr/Ms spaces may be more successful but data-points must be categorized by regression surfaces for recognition purposes. We will show that projecting the 3D data onto a vertical plane containing the Mr/Ms axis produces a 2D graph that successfully discriminates the data of (a). SD, PSD and MD refer to domain-size ranges for single, pseudo-single and multi-domain magnetite. SP = superparamagnetic behavior.

Princeton Measurements MicroMag 2900 shows us that suitably sensitive factors of Bc range from 1.5 to 5.0.

3. [4] The 2-D Projection Plane in 3D Hysteresis Space

[6] The approach is so simple that we were able to choose the optimum projection plane until the best visual discrimination was obtained. The calculations were simply performed in a spreadsheet in which we varied the orientation of the vertical projection plane. The choice was made less subjective by comparing the 95% confidence region for the bivariate distribution on the projection plane. For example, consider the small sample of shallow-water limestones (Figure 2); the bivariate data-set has $y = Mr/Ms$ and x defined by the coordinate of the hysteresis data projected onto the plane $Bcr = 1.8Bc$. Calculations were simplified by standardizing x and y according to traditional statistics, e.g.,

$$z_x = \frac{x - \bar{x}}{s_x} \text{ where } s_x = \text{standard deviation.}$$

With the data distributed about their centroid in equal units of standard deviations (Figure 2a), one may simply calculate the eigenvalues and eigenvectors of the distributions from

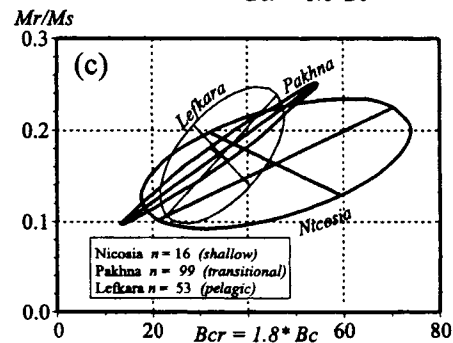
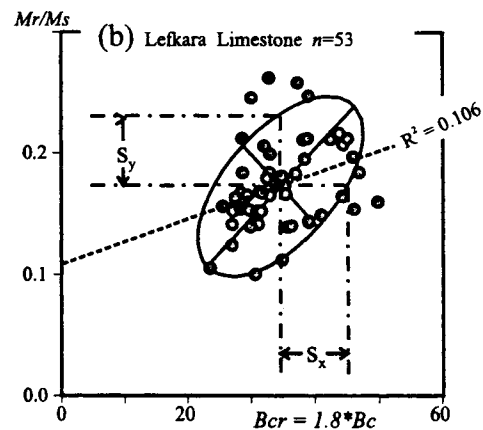
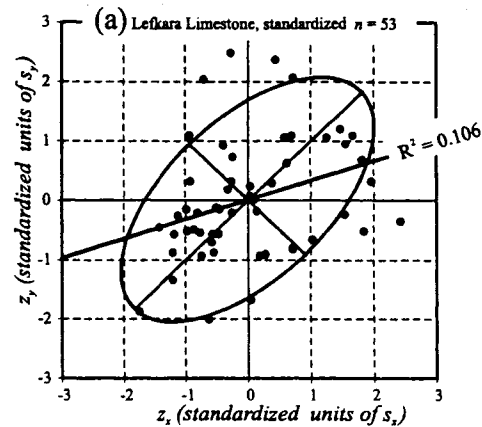


Figure 2. (opposite) (a) Further visual simplification for the bivariate distribution of the 3D data projected on to some particular projection plane is achieved by plotting 95% confidence regions. (a) Coordinates of the points on the projection plane are standardized in units of standard deviations, centered on the data-centroid; the eigenvalues and eigenvectors calculated from the variance-covariance matrix determine the elliptical confidence region. (b) Standardized values are back-transformed to show confidence regions on the hysteresis projection plane. (c) 95% confidence regions for three formations of the progressively shallowing post-Cretaceous limestone cover to the Troodos ophiolite of Cyprus on a 2D hysteresis-projection plane.

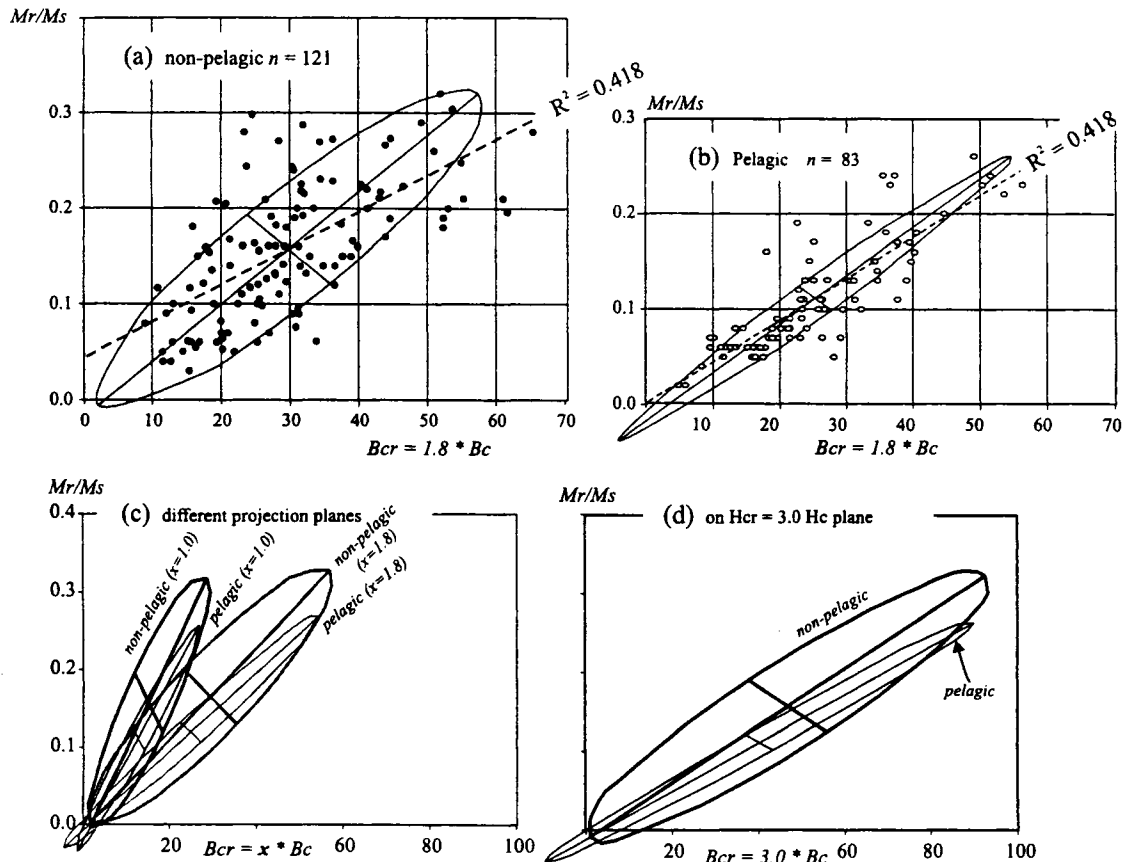


Figure 3. (a, b) The projection plane $Bcr = 1.8Bc$ in 3D hysteresis-space (Figure 1b, c) appears to discriminate the pelagic and non-pelagic limestones that were almost indistinguishable on the conventional Day Plot (Figure 1a). (c, d) different projection planes showing the overlap of 95% confidence regions for the pelagic and non-pelagic limestones of Figure 1a.

the variance-covariance matrix [e.g., Davis, 2002]. The coordinates of the confidence region may then be back-transformed to the original hysteresis scales (Figure 2b). For example, samples of three different and progressively shallower limestone formations, used by Borradaile and Lagroix [2000] in their 3D projection are shown in Figure 2c. The earlier 3D projection provided their precise inter-sample discrimination but only by viewing regression surfaces along an appropriate axis. The present 2D projection in hysteresis space has the advantage of simpler reporting as a plane-diagram (Figure 2c). Moreover, the plane's orientation is described by a Bcr/Bc ratio that itself may be characteristic of some magnetite domain-structure, since the upper and lower PSD limits are $2 < (Bcr/Bc) < 4$ [Dunlop, 2002a, 2000b].

[7] On the plot of Day *et al.* [1977], the initial example of limestone hysteresis data shows almost complete overlap of pelagic and non-pelagic data (Figure 1a) although it is reasonable to expect some differences in magnetic properties. These limestones, like most others, have quite simple constraints on their magnetic mineralogy. For example, fossil-bacterial magnetite may be expected to dominate pelagic limestones whereas clastic, aerial-volcanic and other organic sources may dominate shelf carbonates. Day-plot space shows a similar broad trend from PSD to SD due to broad grain-size distributions [Dunlop, 2002a]. However, projected onto an arbitrary "suitable" vertical plane through 3D hysteresis space (Figure 1b) the differ-

ence between the data clusters is maximized (Figure 3a and 3b). For these two samples this is achieved by a vertical projection plane close to the lower bound of PSD space (Figure 1b), e.g., $Bcr = 1.8Bc$. The confidence regions for differently chosen projection planes are presented in Figure 3c and 3d.

[8] Why should the use of a projection plane with $Bcr \sim 2Bc$ successfully separate the hysteresis data of pelagic versus non-pelagic samples (Figure 3)? Consideration of Figures 1a and 1b indicates this vertical plane lies close to the lower size-limit of PSD magnetite, and biogenic magnetite may show $Bcr/Bc < 1.8$ [Moskowitz *et al.*, 1993]. Evidently, such a plane separates the two samples with pelagic specimens (Figure 3b) lying low in the plane, projected from the SD field of 3D-space (Figure 1b) and non-pelagic specimens plotting higher, projected from the PSD 3-space. The broad swathe of superparamagnetic behavior [Dunlop, 2002a, 2000b] shown on Figure 1a acts most effectively at high Mr/Ms which helps to emphasize the definition of the non-pelagic sample higher in the 2D projection (Figure 3a). Organic magnetite may play different roles in pelagic and non-pelagic environments [Kirschvink and Chang, 1984; Moskowitz *et al.*, 1989] and the effects of mixing with magnetite of aerial-volcanic and detrital origin are difficult to model. However, the pelagic sample here seems to be dominated more by SD whereas the non-pelagic sample projects from the PSD field, higher on the Mr/Ms axis indicating some SP behavior.

[9] **Acknowledgments.** This research was supported financially by NSERC (Canada) to Graham Borradaile at the Lakehead University Rock Magnetism and Deformation Laboratory. For permission to sample and for generous logistical assistance, we thank the Geological Survey of Cyprus (Director Dr. George Petrides, Liaison Officer Dr. Ioannis Panayides) and the Geological Survey of Israel (Dr. Aryeh Shimron). Two anonymous reviewers and France Lagroix provided constructive reviews.

References

- Banerjee, S. K., J. W. King, and J. A. Marvin, A rapid method for magnetic granulometry with applications to environmental studies, *Geophys. Res. Lett.*, **8**, 333–336, 1981.
- Borradaile, G. J., N. Chow, and T. Werner, Magnetic hysteresis of limestones: Facies control?, *Phys. Earth Planet. Inter.*, **76**, 241–252, 1993.
- Borradaile, G. J., and F. Lagroix, Magnetic characterization of limestones using a new hysteresis projection, *Geophys. J. Internat.*, **141**, 213–226, 2000.
- Channell, J. E. T., and C. McCabe, Comparison of magnetic hysteresis parameters of unremagnetized and remagnetized limestones, *J. Geophys. Res.*, **99**, 4613–4623, 1994.
- Cisowski, S., Interacting versus non-interacting single-domain behaviour in natural and synthetic samples, *Phys. Earth Planetary Interiors*, **26**, 77–83, 1981.
- Davis, J. C., *Statistics and Data Analysis in Geology*, 3rd edn., J., Wiley, N.Y., 638 pp., 2002.
- Day, R., M. D. Fuller, and V. A. Schmidt, Hysteresis properties of titanomagnetites, grain size and compositional dependence, *Phys. Earth Planet. Inter.*, **13**, 260–267, 1977.
- Dunlop, D. J., Theory and application of the Day plot (Mrs/Ms versus Hcr/Hc) 1. Theoretical curves and tests using titanomagnetite data, *J. Geophys. Res.*, **107**(B3), 2056, doi:10.1029/2001JB000486, 2002a.
- Dunlop, D. J., Theory and application of the Day plot (Mrs/Ms versus Hcr/Hc) 2. Application to rocks, sediments and soils, *J. Geophys. Res.*, **107**(B3), 2057, doi:10.1029/2001JB000487, 2002b.
- Dunlop, D. J., and Ö. Özdemir, *Rock Magnetism, Fundamentals and Frontiers* (Cambridge Studies in Magnetism), Cambridge Univ. Press, New York, 573 pp., 1997.
- Freeman, R., Magnetic mineralogy of pelagic limestones, *Geophys. J. R. Astron. Soc.*, **85**, 433–452, 1986.
- Henshaw, P. C., and R. T. Merrill, Magnetic and chemical changes in marine sediments, *Rev. Geophys.*, **18**, 483–504, 1980.
- Jackson, M. J., W.-W. Sun, and J. P. Craddock, The rock magnetic fingerprint of chemical remagnetization in midcontinental Paleozoic carbonates, *Geophys. Res. Lett.*, **19**, 781–784, 1992.
- Jackson, M., Diagenetic sources of stable remanence in remagnetized Paleozoic cratonic carbonates, a rock magnetic study, *J. Geophys. Res.*, **95**, 2753–2761, 1990.
- King, J., S. K. Banerjee, J. Marvin, and Ö. Özdemir, A comparison of different magnetic methods for determining the relative grain size of magnetite in natural materials: Some results from lake sediments, *Earth Planet. Sci. Lett.*, **59**, 404–419, 1982.
- Kirschvink, J. L., and S.-B. R. Chang, Ultrafine-grained magnetite in deep-sea sediments, Possible bacterial magnetofossils, *Geology*, **12**, 559–562, 1984.
- Lanci, L., and D. V. Kent, Introduction of thermal activation in forward modeling of hysteresis loops for single-domain magnetic particles and implications for the interpretation of the day diagram, *J. Geophys. Res.*, **108**(B3), 2142, doi:10.1029/2001JB000944, 2003.
- Lowrie, W., and F. Heller, Magnetic properties of marine limestones, *Rev. Geophys.*, **20**, 171–192, 1982.
- McCabe, C., R. Van der Voo, and M. M. Ballard, Late Paleozoic remagnetization of the Trenton Limestone, *Geophys. Res. Lett.*, **11**, 979–982, 1984.
- Moskowitz, B. M., R. B. Frankel, D. A. Bazylinski, H. W. Jannasch, and D. R. Lovley, A comparison of magnetite particles produced anaerobically by magnetotactic and dissimilatory iron-reducing bacteria, *Geophys. Res. Lett.*, **16**, 665–668, 1989.
- Moskowitz, B. M., R. B. Frankel, and D. A. Bazylinski, Rock magnetic criteria for the detection of biogenic magnetite, *Earth Planet. Sci. Lett.*, **120**, 283–300, 1993.
- Thompson, R., and F. Oldfield, *Environmental Magnetism*, 227 pp., Allen and Unwin, London, 1986.
- Wasilewski, P. J., Magnetic hysteresis in natural materials, *Earth Planet. Sci. Lett.*, **20**, 67–72, 1973.

G. J. Borradaile and T. Hamilton, Geology and Physics Department, Lakehead University, Thunder Bay, ON P7B 5E1, Canada. (borradaile@lakeheadu.ca)

Magnetic fabrics may proxy as neotectonic stress trajectories, Polis rift, Cyprus

Graham J. Borradaile and Tom Hamilton

Geology Department, Lakehead University, Thunder Bay, Ontario, Canada

Received 2 July 2002; revised 26 September 2003; accepted 15 October 2003; published 6 January 2004.

[1] The Miocene Polis rift opened along a NNW axis, obviously in response to WSW relative extension and relative tension starting ~ 5 Myr ago. However, geologically young plate movements are believed to be closing the rift by sinistral transpression producing minor younger faults since 1 Ma. Modern earthquake solutions give E-W compression compatible with the younger faults. Magnetic fabrics using anisotropy of low field magnetic susceptibility (AMS) and anisotropy of anhysteretic remanent magnetization are kinematically compatible with stress axes required by the fault and rift geometry and thus were acquired in < 5 Ma. However, by different statistical treatments and selecting samples from different subareas it is possible to reveal sedimentary-depositional fabrics and perhaps also a composite AMS fabric related to young transpression (≤ 1 Ma). **INDEX TERMS:** 1518 Geomagnetism and Paleomagnetism: Magnetic fabrics and anisotropy; 8107 Tectonophysics: Continental neotectonics; 8123 Tectonophysics: Dynamics, seismotectonics; **KEYWORDS:** magnetic fabrics, stress trajectories, neotectonics. **Citation:** Borradaile, G. J., and T. Hamilton (2004), Magnetic fabrics may proxy as neotectonic stress trajectories, Polis rift, Cyprus, *Tectonics*, 23, TC1001, doi:10.1029/2002TC001434.

1. Introduction: Polis Rift, Cyprus, and its Tectonic History

[2] The Polis rift is a mid-Miocene fault valley, bounded by normal faults with throws of ≤ 100 m [Payne and Robertson, 1995; Robertson, 1990] (Figure 1). The NNW trending rift evidently formed above a northward dipping subduction zone, although it is argued that the northward component of motion is now stalled in favor of WSW subduction [Arvidsson *et al.*, 1998; Ben-Avraham *et al.*, 1988; Papazachos and Papaioannou, 1999; Robertson *et al.*, 1995] (Figure 2). The rift disrupts subhorizontal Miocene strata at the surface and its basin is filled with subhorizontal Pliocene sediments. Penetrative tectonic fabrics are not visible but the fracture orientations permit crude estimates of the orientations of paleostress trajectories according to traditional structural geology. A WSW-ENE minimum compressive stress trajectory is required for the

formation of the Polis rift, using accepted structural interpretation. However, fault solutions for the 1995 earthquakes indicate that the rift is instead being compressed EW to close the rift with sinistral transpression (Figure 1).

[3] Modern seismicity has been quite hazardous and is of concern to Cypriots. Historically, the region was devastated by earthquakes, causing abandonment of classical cities in the first few centuries before and after Christ. Present-day seismic events are monitored attentively. The modern seismic record, mainly from offshore events, shows a Benioff zone descending northward and northeastward from the south and southwest of Cyprus (Figure 2). The depths of the foci show that deeper subduction is now mostly to the WSW, compatible with the geodetically determined vectors of relative plate motion [Arvidsson *et al.*, 1998; Papazachos and Papaioannou, 1999]. Thus, recent seismicity and plate motion both indicate that the Polis rift is now undergoing transpressive closure with EW compression. Recently, however, the Polis region experienced onshore seismic events with body wave magnitudes of 5.8 and 5.3 respectively on 1995/02/23 and 1995/05/29, (Figure 1). The epicenters lay in the center and east of the rift but most injury and damage occurred on the western margin. Foci were shallow, at ~ 15 km. The centroid moment tensor (CMT; catalog available from <http://www.seismology.harvard.edu/>) for the two events yields almost indistinguishable fault plane solutions giving east plunging compression (trend and plunge $\sim 102/29$; see Harvard online seismology catalog, available at <http://www.seismology.harvard.edu/projects/CMT/2001>; see also online catalog from International Seismological Centre, Thatcham, UK, available at <http://www.isc.ac.uk/>) (Figures 1 and 6c). This is not compatible with the WSW extension required to create the WNW trending rift (~ 5 Ma) but more compatible with younger fault orientations (< 1 Ma). This switch in stress axis orientation may be due to changes in plate tectonic geometry.

2. May Magnetic Fabric Axes Proxy for Geologically Significant Paleostress Trajectories?

[4] Originally, paleomagnetism introduced measurements of anisotropy of induced magnetic susceptibility in low fields (AMS) in order to reject strongly anisotropic specimens [Fuller, 1963; Uyeda *et al.*, 1963]. Such materials would be unsuitable for paleomagnetism because the intrinsic anisotropy may have deflected the paleofield from its true orientation. Subsequently, AMS was found to be a

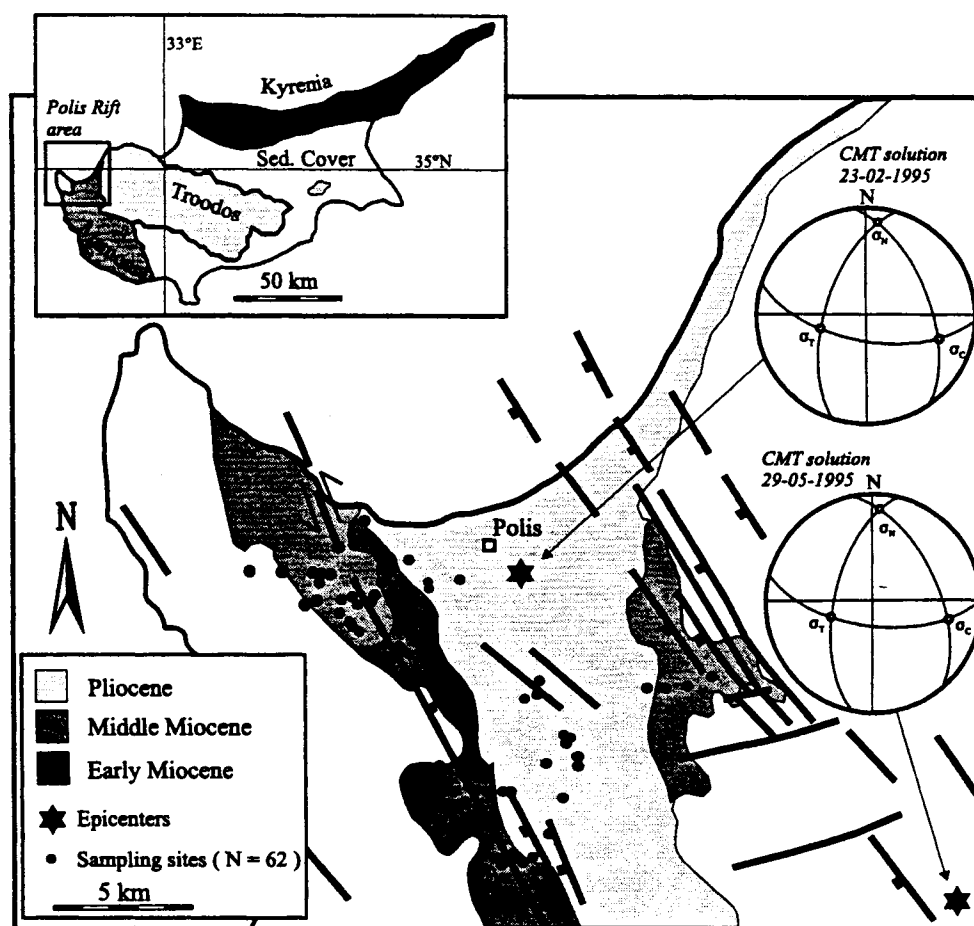


Figure 1. Location of the Polis rift in NW Cyprus. Pliocene sediments fill the valley between faulted Miocene and pre-Miocene rocks on the flanks. Although the bounding faults to the rift (~ 5 Ma) are Normal, recent seismic events give fault plane solutions with sinistral transpression across the rift. (Two events of 1995/02/23 mb = 5.8 event number 56311987; 1995/05/29 mb = 5.3 event number 052995A; see Harvard Seismology Bulletin, available from the online CMT catalog at <http://www.seismology.harvard.edu/projects/CMT/>; see also International Seismological Centre online bulletin, available at <http://www.isc.ac.uk/>); these are compatible with the orientations of younger faults (≤ 1 Ma).

sensitive indicator of the average preferred orientation of mineral grains and was applied to determine mineral alignment whether by tectonic, sedimentary or magmatic flow [Borradaile and Henry, 1997; Hrouda, 1982; Tarling and Hrouda, 1993]. The technique is sufficiently sensitive to detect the feeble strains and fabrics in neotectonic environments, although initially the literature may have overstated the simplicity of interpretation of magnetic fabrics. In fact, AMS blends contributions from different minerals, of different ages, with different orientation distributions and for which the physical response may also be either paramagnetic, diamagnetic or “ferro”-magnetic [Jackson and Tauxe, 1991; Rochette et al., 1992]. Moreover, the minerals’ AMS axes only map onto the orientation of crystallographic axes if the crystals are of high symmetry (e.g., orthorhombic, trigonal) due to fundamental symmetry relations [Nye, 1957] and, unfortunately, most paramagnetic rock forming minerals are monoclinic at best. Furthermore, ferromagnetic inclusions may disturb or completely mask the relationship

between crystallographic axes of the host grain and its AMS ellipsoid. Thus, at the single-crystal level, AMS axes and crystal axes rarely show a one-to-one correspondence [Borradaile, 1994; Borradaile and Werner, 1994; Lagroix and Borradaile, 2000a]. As if confounding of these different geological and magnetic factors was not troublesome enough, some minerals may even yield “inverse” fabrics in which AMS counter-intuitively represents their fabric orientation-distribution ellipsoids [Rochette, 1987, 1988; Rochette et al., 1992, 1999]. In this study, calcite is the main cause of inverse fabrics [Rochette, 1988] and its largest negative susceptibility corresponds with its crystallographic c axis, permitting a simple interpretation of calcite-dominated specimens that respond diamagnetically. However, single domain magnetite (SD) is the most often cited cause of inverse fabrics, or of mixed SD-MD “blended” fabrics (e.g., the “intermediate” fabrics of Rochette [1987]; Rochette et al. [1999]). The SD inverse contribution to a magnetic fabric arises because the spontaneous mag-

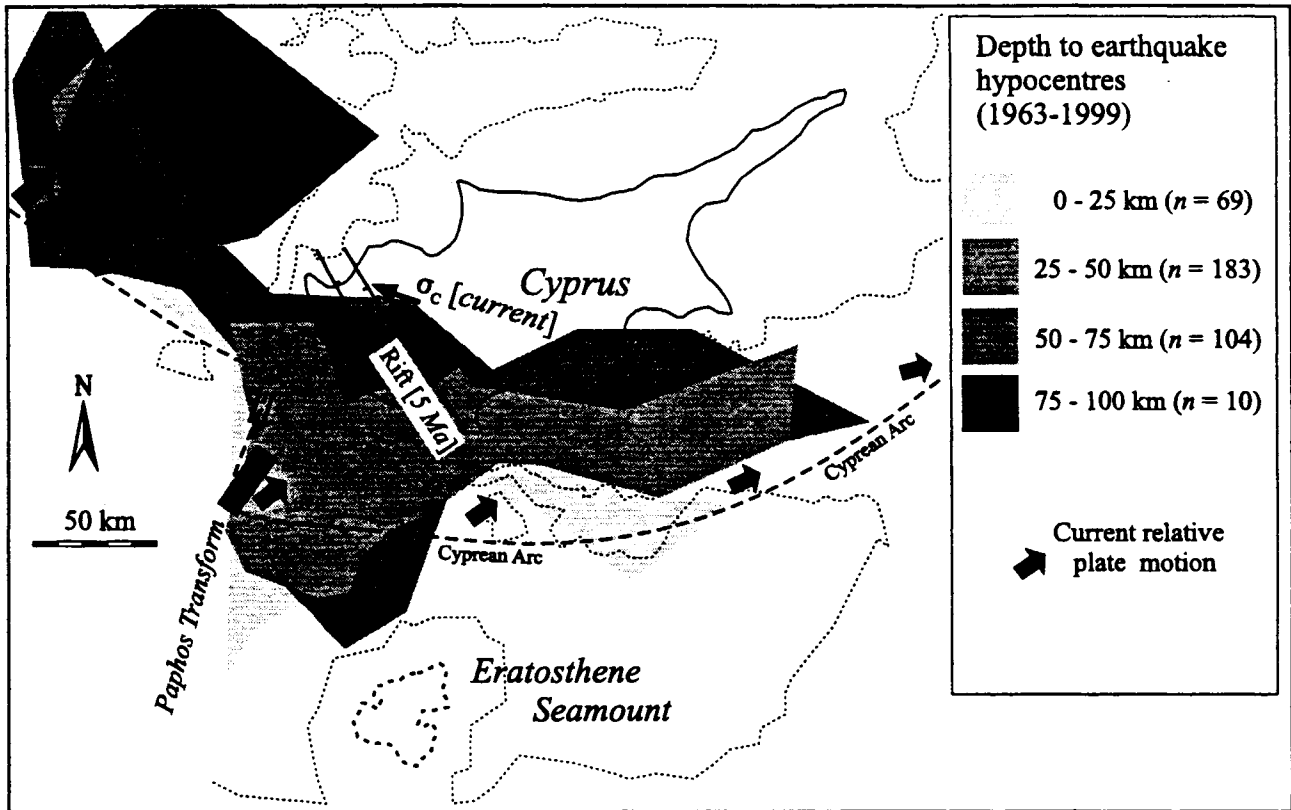


Figure 2. Depths to earthquake foci of seismic events (1963–1999) (see International Seismological Centre online bulletin, available at <http://www.isc.ac.uk/>), indicate a northward dipping Benioff zone. However, the deepest foci occur just to the west of Cyprus, which together with the geodetically determined plate vectors, confirms that current subduction is more toward the NE. It will be shown that this geological young compression and closure of the Polis rift is also detectable from cryptic magnetic fabrics. The pre-Pliocene, northward subduction is stalled by the obstruction of the Eratosthene seamount, giving rise to the present ESE-WNW compression [Arvidsson *et al.*, 1998; Papzachos and Papaioannu, 1999; Ben-Avraham *et al.*, 1988; Robertson *et al.*, 1995].

netization of a single domain must be parallel to its long axis, which cannot be enhanced during induced magnetization, when AMS is measured. In contrast, during the measurement of AMS, the induced magnetization may be increased perpendicular to the long axis. Thus the AMS magnitude-ellipsoid's long-axis will be perpendicular to the SD long-axis. Fortunately, anisotropy of remanent magnetization is congruent with shape, so that maximum remanence is parallel to grain long-axes. Therefore axes of anisotropy of anhysteretic remanent magnetization (AARM) correspond to the orientation-distribution for all magnetite grain sizes [Jackson, 1991; McCabe *et al.*, 1985; Stephenson *et al.*, 1986]. AARM is the most secure means by which to determine the true shape-fabric of magnetite, although data processing methods may help [Borradaile and Gauthier, 2001]. Our study found that complications due to the SD effect were negligible in these carbonate rocks. Thus the fabric contribution of magnetite is relatively straightforward, especially since its interpretation is simplified by the AARM technique.

[5] For the purposes of magnetic mineralogy, the limestones fall broadly into clay-bearing varieties that are

invariably paramagnetic, and more pure limestones that may be diamagnetic or have feeble paramagnetic susceptibilities. Both types have subordinate ferromagnetic responses due to ferrimagnetic magnetite and the distribution of their hysteresis parameters on a Day plot is similar (Figure 3a). The hysteresis response, determined using our Princeton Measurements MicroMag alternating gradient force magnetometer, is that of single domain (SD) or pseudo-single domain (PSD) magnetite with ferromagnetic susceptibilities and saturation remanences compatible with SD/PSD magnetite (Figures 3a and 3b) [Dunlop and Özdemir, 1997]. The lithologies and the fine grain size of the magnetite favor a fossil-bacterial origin for the magnetite, rather than clastic contamination [Borradaile and Lagroix, 2000; Lagroix and Borradaile, 2000b]. Furthermore, the frequency distribution of bulk susceptibility supports the partial control of magnetic anisotropy due to the magnetite traces. Any dilute concentration of high value, such as accessory, high susceptibility magnetite, tends to form a lognormal distribution (Figures 3c and 3d). Thus we see a competition between the diamagnetic matrix ($\sim -14 \times 10^{-6}$ SI), paramagnetic clay

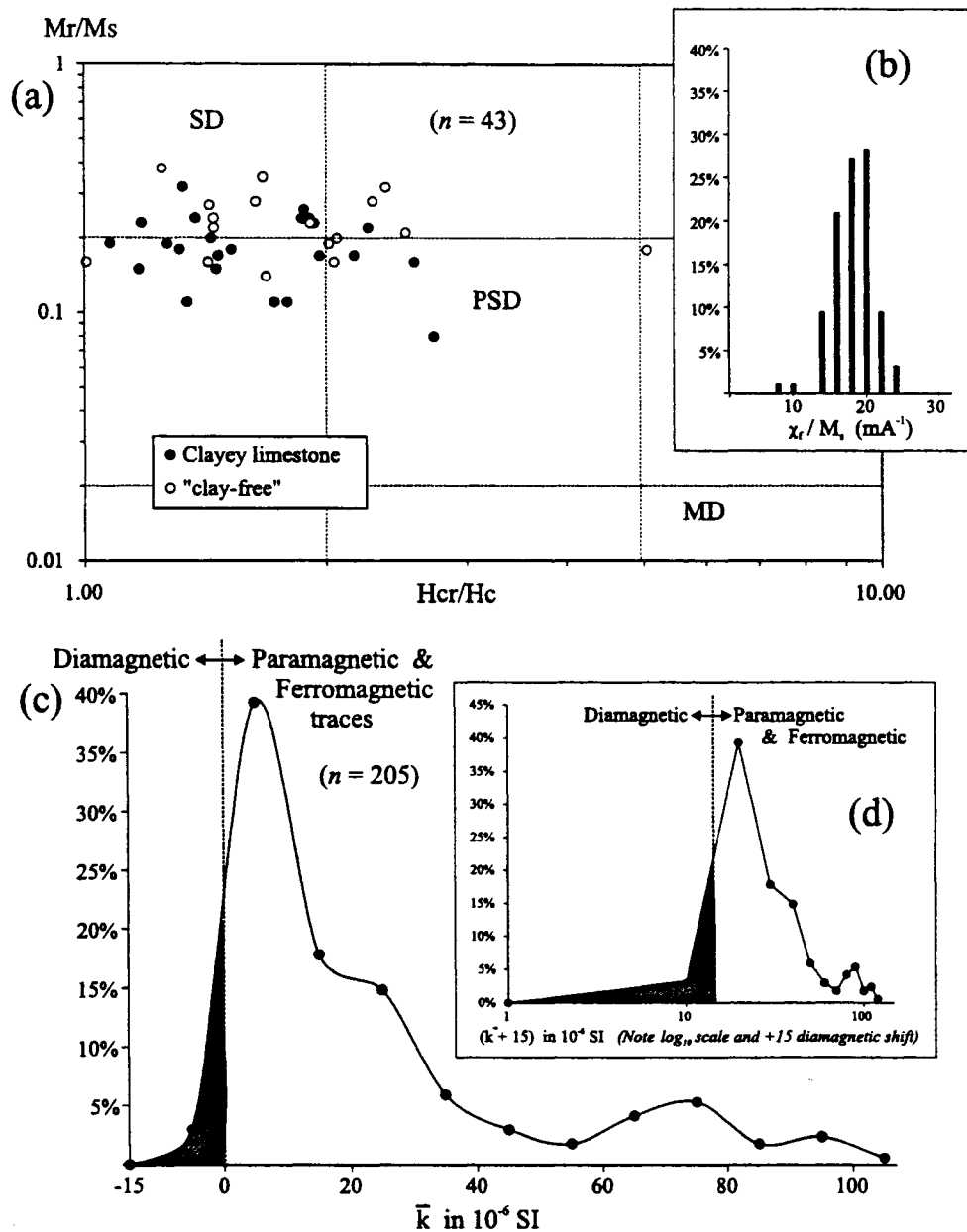


Figure 3. Rock magnetic experiments reveal that the limestones magnetic fabrics are due to a diamagnetic carbonate matrix, traces of paramagnetic clays and ferrimagnetic magnetite of single domain to pseudo-single-domain size. (a) Day *et al.* [1977] plot of hysteresis data showing the fine domain structure of the magnetite, perhaps due to fossil bacterial sources [Borradaile and Lagroix, 2000; Dunlop and Özdemir, 1997]. (M_s = saturation magnetization in applied field; M_r = zero-field remanence; H_{cr} = coercivity of remanence; H_c = coercivity). (b) Ferromagnetic susceptibility and saturation magnetization show ratios typical for fine-grained magnetite [Dunlop and Özdemir, 1997]. (c) Frequency distribution of bulk susceptibility combined with petrographic observations may attribute the susceptibility to the diamagnetic matrix (for calcite approx. $\sim -14 \times 10^{-6}$ SI), and traces of paramagnetic clay and fine-grained, single domain magnetite, probably of bacterial rather than clastic origin. Modal bulk susceptibility is $+16.1 \pm 7.1 \times 10^{-6}$ SI ($n = 205$). (d) The lognormal frequency distribution of bulk susceptibility is characteristic of a dilute concentration of a rare fraction with high values.

contamination in some specimens that gives susceptibilities up to $\sim +120 \times 10^{-6}$ SI, and the traces of magnetite that keep the net modal bulk susceptibility positive at $+16.1 \pm 7.1$ (s.e.) $\times 10^{-6}$ SI ($n = 205$).

[6] The AMS signal of PSD magnetite and clays provides a normal fabric contribution, the AMS magnitude-ellipsoid being congruent with the combined orientation-distribution ellipsoid of magnetite-grain-shapes and clay-mineral pre-

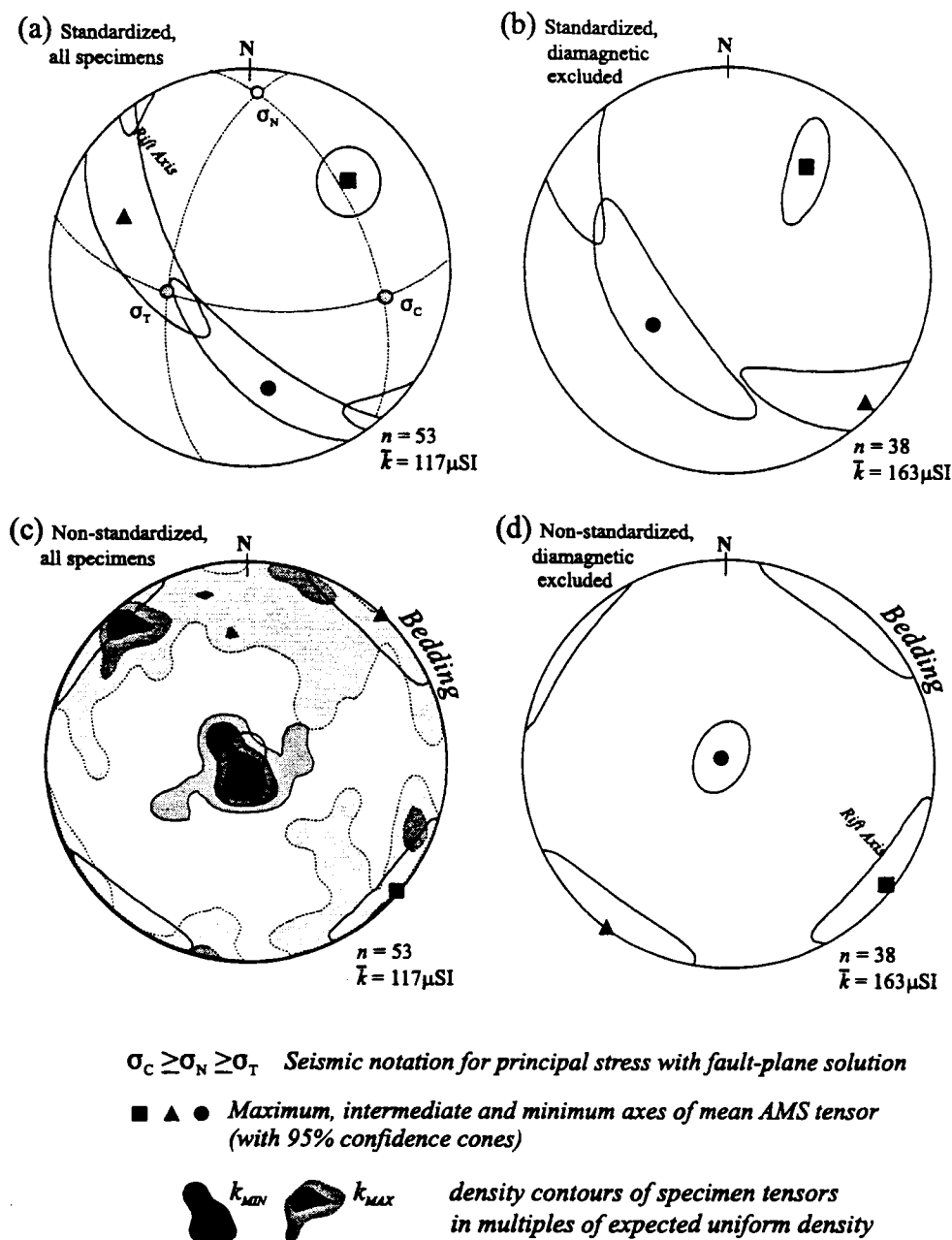


Figure 4. Pliocene sediment infill of the Polis rift; anisotropy of low field magnetic susceptibility (AMS) in (All stereograms in this paper are equal-area, lower hemisphere.) The mean tensor accounts for the magnitudes as well as the orientations of the individual specimen tensors. Thus different orientation distributions of the mean tensor result from standardizing or not standardizing the specimen tensors to a unit-bulk susceptibility [Jelinek, 1978; Borradaile, 2001]. The mean tensor, with 95% confidence limits on the orientations of its principal axes [Jelinek, 1978] is a powerful tool in interpreting magnetic petrofabrics, whereas traditional orientation distributions of AMS axes, shown by the density contours in Figure 4c may be more limited because they ignore the magnitudes of susceptibility axes.

ferred crystallographic orientation. Thus maximum susceptibility (k_{MAX}) defines the orientation of magnetite and clay mineral alignment whereas the minimum susceptibility (k_{MIN}) defines the mean normal to the planar fabric defined by the minerals. In specimens bearing SD magnetite, its

concentration is too low to form inverse fabrics because the clay fraction's paramagnetic normal fabric dominates.

[7] Despite the presence of trace amounts of fine-grained magnetite and of clay, the limestones' diamagnetic calcite matrix dominates the AMS signature in some specimens

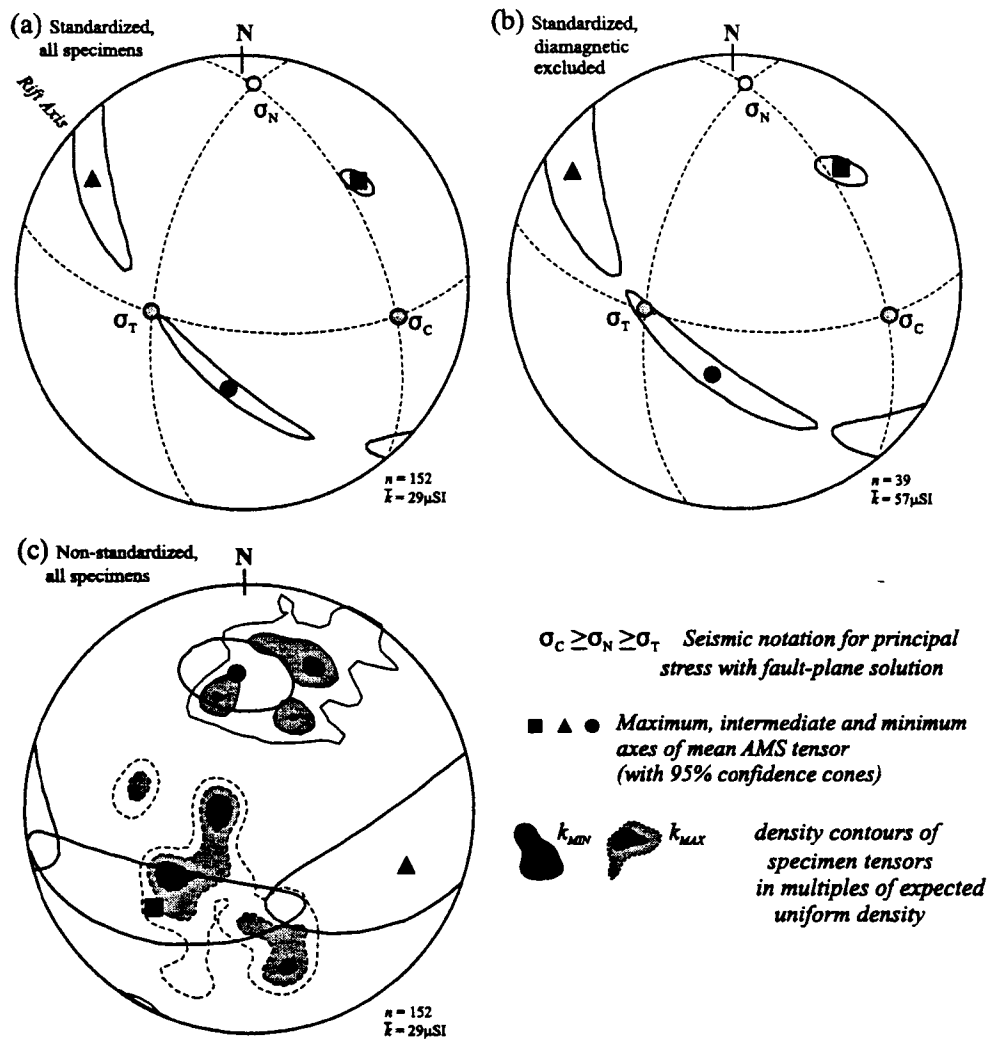


Figure 5. The faulted margins of the Polis rift; different data processing treatments of data for anisotropy of low field magnetic susceptibility (AMS).

(Figures 4c and 4d). Examples of net-paramagnetic specimens whose AMS axes are directly interpretable in terms of kinematics are shown in Figures 4b, 4d, and 5b. All samples are combined in Figures 4a, 4c, 5a, and 5c, including the majority of dominantly diamagnetic specimens whose maximum and minimum axes were switched. The orientation of susceptibility axes for individual specimens is shown in Figure 4c in the form of density contours. Of course, the traditional interpretation of the AMS orientations using individual specimens loses the information contained in the magnitudes of the susceptibility axes. Although the magnitudes and shapes of magnetic fabric ellipsoids rarely bears any direct relation to a causative process such as strain or flow [Borradaile and Henry, 1997; Hrouda, 1982; Tarling and Hrouda, 1993], the magnitudes do affect the interpretation of the orientation-distribution since the magnitudes may weight the significance of different specimens in different ways [Borradaile, 2001; Henry, 1989; Hrouda and Jelinek, 1999; Hrouda and Schulmann, 1990; Jelinek, 1978]. For this reason, the mean tensor of a sample of

specimens need not correspond closely to the traditional density-distribution of individual specimen axes, and any comparison is only valid with mean tensors for the sample, disregarding magnitudes (e.g., Figures 4c, 5c, and 6b).

[8] Magnetically determined orientation-distributions are interpreted in terms of finite strain or recrystallization fabrics in tectonically deformed or metamorphic rocks. In those cases, the magnetic anisotropy tensors correspond in orientation to the tensor-of-state that describes finite strain, in its broadest sense. In contrast, neotectonic environments lack penetrative deformation fabrics due to finite strain: they are affected by small strains which structural geologists would interpret due to incremental, almost infinitesimal strains [Ramsay, 1967; Ramsay and Huber, 1983]. Infinitesimal strain axes are traditionally associated with certain arrangements of fractures, calcite-twinning, and vein-mineral fibers. These strains are so small that the possibilities for changes in stress orientations are limited and the incremental strain axes are subparallel to the principal-stress trajectories. Thus the fracture pattern ties the incremental

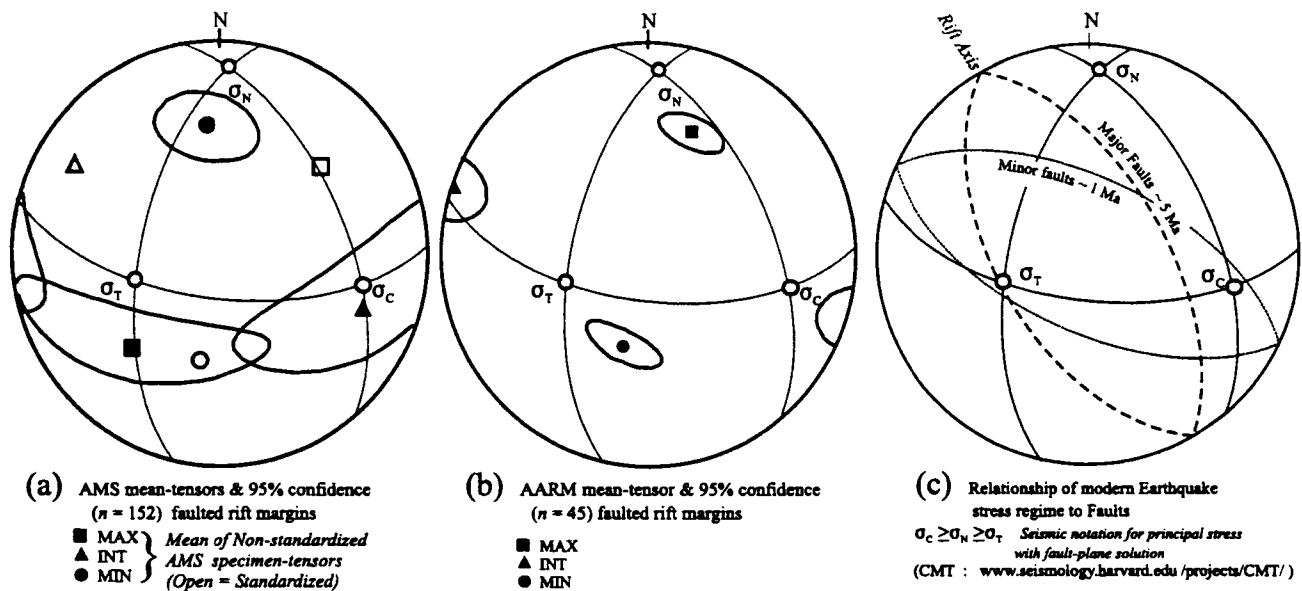


Figure 6. Polis rift faulted margins; (a) raw AMS compatible with rift closure; (b) AARM compatible with rift opening; (c) faults all compared with the centroid moment tensor solutions for the recent earthquakes. (1995/02/23 mb = 5.8; 1995/05/29 mb = 5.3; see Harvard Seismology Bulletin, available at <http://www.seismology.harvard.edu/projects/CMT/>).

strains and paleostress trajectories in a simple coaxial framework that is closely related to the fault plane solution of the 1995 earthquake, south of Polis (event number 052995A; see Harvard online seismology catalog, available from <http://www.seismology.harvard.edu/projects/CMT/>). Unfortunately, the structural geologist's traditional interpretation of mean stress trajectory orientations from fault orientations provides only a global and imprecise regional estimate. In contrast, magnetic fabrics may be obtained from almost any individual rock specimen, they sum the effects of thousands of events and, as we will see below from the literature and current observations, they help to strengthen the link between paleostress in any outcrop with the rift structure and with the 1995 earthquakes.

[9] Experimental work shows that magnetite's magnetic properties are sensitive to stresses of tectonic and sub-tectonic magnitude [Carmichael, 1968, 1969; Domen, 1962; Borradaile and Alford, 1987; Borradaile and Jackson, 1993; Jackson et al., 1993; Hamano et al., 1989; Kinoshita, 1968; Kalashkinov and Kapitsa, 1952; Kapicka, 1992; Nagata, 1966a, 1966b, 1970]. In particular, the maximum susceptibility of polydomain magnetite is deflected away from the maximum compressive stress axis, mostly due to nonreversible, domain wall rearrangements. However, bulk strains of $\leq 5\%$ may produce microscopic heterogeneous deformation in which grain-scale strain is capable of rigid-grain rotation. Much of the experimental work attempted to predict earthquakes from geomagnetic field variation due to susceptibility changes [e.g., Revol et al., 1977; Stacey, 1964]. Reports of experimental studies, involving a variety of deformation mechanisms, all show that maximum susceptibility (k_{MAX})

tends to align with minimum compressive stress direction under modest differential stress. Most studies concerned specimens in which the AMS was dominated by polydomain magnetite but under most circumstances the subtle realignment of paramagnetic grains also requires that k_{MAX} aligns with σ_{MIN} .

[10] It is understandable that very few field studies have the possibility to confirm a relationship between AMS and "stress," as opposed to "strain." They are mostly confined to Quaternary neotectonic environments where simple stratigraphy and single-event brittle tectonics permit a relatively unambiguous association between AMS fabrics and stress axes inferred from fracture patterns [Facenna et al., 1994; Mattei et al., 1997, 1999; Sagnotti and Speranza, 1993; Sagnotti et al., 1994; Winkler and Sagnotti, 1994]. Their advantage, as in the present study is that a young stratigraphy, devoid of penetrative deformation permits an association of magnetic fabrics with events that cannot endure more than a few Ma. In some neotectonic studies, stratigraphy constrains the acquisition of AMS fabrics to intervals of not more than several hundred thousand years. Even in more complicated geological environments, fortunate geological conditions may permit us to associate AMS axes with stress trajectories [Lagroix and Borradaile, 2000b; Borradaile and Kehlenbeck, 1996], rather than its much more common use as a finite strain marker [Tarling and Hrouda, 1993]. However, neotectonic environments have the advantage of fine biostratigraphic control, rock types with simple preexisting petrofabrics and close temporal relationships to contemporary ground stresses.

[11] In this study, AMS combines fabric contributions from diamagnetic calcite, paramagnetic clays and PSD magnetite in Miocene and Pliocene limestones. Isolating

the petrofabric contribution of the magnetite subfabric by determining the specimens' anisotropy to the acquisition of anhysteretic remanence (AARM) is a relatively recent development in magnetic fabrics [Jackson, 1991; McCabe *et al.*, 1985]. AARM responds only to the orientation-distribution of magnetite in our rocks, ignoring the fabrics of the paramagnetic clays and diamagnetic calcite. Of course, the matrix may dictate the orientation-distribution of magnetite, if it occurs as inclusions or mimetic overgrowths on the matrix grains. Regardless of magnetite grain size or domain structure, AARM gives a unique interpretation of magnetite preferred dimensional orientation (Figure 6), more simply interpreted kinematically than some AMS fabrics [Jackson, 1991; Jackson and Tauxe, 1991].

[12] Where all minerals produce normal fabrics, results of experimental and field studies indicate the following correspondence between AMS principal axes ($k > 0$), incremental extension (e), and compressive stress (σ): k_{MAX} parallel to e_{MAX} parallel to minimum compression, σ_{MIN} (σ_T); and k_{MIN} parallel to e_{MIN} parallel to maximum compression σ_{MAX} (σ_C). (By the convention of seismologists the principal stresses would be $\sigma_C \geq \sigma_N \geq \sigma_T$).

[13] Of course, the kinematic significance of the maximum and minimum susceptibility axes must be considered carefully for diamagnetic calcite crystals because their most "negative" susceptibility corresponds to the c axis, which aligns with the shortening or maximum compression direction.

3. Magnetic Fabrics: Methods

[14] We measured anisotropies of low field susceptibility (AMS) of 205 cores and anisotropy of anhysteretic remanent magnetization (AARM) for 45 cores, from 62 sites in the fault affected Miocene and younger strata of the Polis rift and from sediments unaffected by faulting in the rift basin (Figure 1). Cores were right cylinders 25 mm in diameter and 22 mm high prepared from oriented field specimens that were re oriented in a tilting-vice arrangement under a laboratory drill press. AMS was determined using a Sapphire Instruments SI2B device operating at 19,200 Hz and ~ 0.1 mT. The anisotropy measurement utilized the seven-orientation system [Nye, 1957; Borradaile and Stupavsky, 1995], which includes four body-diagonal measurements, improving precision over the traditional orientations confined to coordinate axes and their symmetry planes [e.g., Girdler, 1961]. Instrument control and real-time data processing were performed using the SI2B01 software package. A complete AMS determination and analysis requires less than 4 min per core. AARM was applied with a Sapphire Instruments three-axis, alternating field (AF) demagnetizer with supplementary DC coil to apply a bias field of 0.05 mT while the AF decayed from 60 mT down to zero. The initial or peak AF was 80 or 100 mT. Because of the use of the same seven-axis anisotropy scheme as in the AMS measurements, each ARM application was applied at 45° or 35.3° to the previous one. We have found that this effectively cleans out the ARM acquired in each preceding treatment for many rocks, although we verify this with full

three-axis demagnetization in new measurement campaigns. This tested technique speeds AARM measurement as the specimen does not always need to be completely three-axis cleaned between each ARM application, although it must be demagnetized before the first treatment [Werner and Borradaile, 1996]. The results of each ARM application were determined by measuring the remanence in a JR5a automatic spinner magnetometer (sensitivity 0.03 mA/m). Instrument control, measurement and simultaneous data reductions were performed using the SPIN01 software package. Complete AARM determination and analysis requires 18 min per core. Some specimens were rejected because of low ARM-intensities that yield poor precision for the tensor's determination, and occasionally some specimens are too anisotropic, deflecting remanence from the desired application direction. In these limestones, 30% of specimens were rejected when attempting to determine AARM [Lagroix and Borradaile, 2000b].

4. Magnetic Fabrics: Interpretation

[15] Magnetic fabrics, whether of AMS or AARM, are conveniently described by the magnitude ellipsoid of the second-rank anisotropy tensor. It is rarely possible to make a simple interpretation of the magnitudes of the ellipsoid axes as these usually blend contributions from diamagnetic, paramagnetic and ferromagnetic responses from different minerals that may even have different orientation distributions. Geologists now accept that interpretations of magnitudes in terms of a causative process are unduly optimistic, whether the mechanism is magmatic or depositional flow, finite strain, or stress-controlled metamorphic recrystallization [Borradaile and Henry, 1997; Hrouda, 1982; Tarling and Hrouda, 1993]. However, the orientations of the principal susceptibility directions usually do have some kinematic significance.

[16] For reconnaissance interpretations, orientations of the maximum, intermediate and minimum axes of individual specimens are usually presented on stereograms as points or density contours, just as with poles or axes in structural geology (e.g., Figures 4c and 5c). However, such plots may be of limited use. First, the peak concentrations of maximum, of intermediate and of minimum susceptibilities will not usually be orthogonal; the mean tensor of Jelinek [1978] is superior here. Second, if multiple subfabrics are present, the sample size may be insufficient to distinguish them and a blend of subfabric orientations may be illustrated. Third, the orientation-distribution represented by density contours ignores the relative importance of different mineral susceptibilities to the fabric, it is in fact a disguised "standardized tensor" distribution.

[17] Statistical characterization of an orientation-distribution of tensors is preferable to inspection of density contours but it is far more complex than for single-axis features such as used in structural geology [Scheidegger, 1965; Woodcock, 1977] because the orientations of the mean principal axes must be orthogonal, just as they are for individual specimens. This problem arises rarely with some traditional field-structural data [e.g., Lisle, 1989] but it is unavoidable

where the individual observations are of tensors, leading to some nontrivial considerations in the interpretation of orientation distributions of properties like AMS or AARM [Henry, 1989; Hrouda, 1982; Hrouda and Jelinek, 1999; Hrouda and Schulmann, 1990]. For this purpose, Jelinek [1978] devised a sophisticated statistical approach that permits mean orientations of a sample of specimen tensors to be meaningfully averaged and to determine their confidence cones, subject to some reasonable assumptions that are met here, as in most studies.

[18] Provided the underlying orientation distributions have unimodal concentrations of maximum, of intermediate and of minimum axes, the Jelinek mean tensor will usually provide a more meaningful characterization of the fabric. The 95% confidence cones around the mean axes indicate the symmetry of the orientation distribution, i.e., whether it is an L, L-S or S-tectonite in the terminology of structural geology [Flinn, 1965]. It is important to realize that this is unrelated to the shapes of the individual tensor ellipsoids; instead, they describe the shape of the orientation-distribution ellipsoid. Moreover, and perhaps appearing counterintuitive, the confidence cones need not show orthorhombic symmetry with respect to the mean axes and the "foliation" that contains the mean-maximum and mean-intermediate axes [Borradaile, 2001]. This may provide important clues to the presence of differently oriented subfabrics.

[19] Although it is now realized that the magnitudes and shapes of individual specimen tensors have little kinematic significance due to the complex merging of multiple mineralogical responses, specimen magnitudes do affect the calculation of the orientation of the mean tensor. The mean tensor's orientation may be strongly deflected toward the orientation of a few large-magnitude specimen tensors. However, high susceptibility specimens need not be considered as outliers in the pejorative statistical sense. They may provide useful information from a subfabric or second population of grains with a different orientation-distribution. That is the case in this study where specimens with larger concentrations of paramagnetic accessory clay minerals may strongly influence the orientation of the mean tensor for a subsample. We investigated the influence of such high susceptibility specimens and detected possible kinematically distinct subfabrics by two techniques [Borradaile, 2001]. One approach is to calculate the mean tensor for subsamples that exclude specimens of anomalous susceptibility. A less arbitrary approach is to recalculate the mean tensor using standardized specimen tensors. One may standardize specimen tensors by dividing each of their principal magnitudes (maximum, intermediate, and minimum) by the specimen mean susceptibility; this weights all specimens equally, regardless of their bulk susceptibility. Whereas this is the usual initial approach, it is not mandatory and nonstandardized mean tensors may yield useful information. If a subfabric of higher susceptibility and conflicting orientation is present, its contribution to the entire population of specimens is suppressed by standardization.

[20] Mean tensors are presented for nonstandardized and for the standardized specimen tensors for AMS of the rift basin (Figure 4) and for the faulted margins of the rift

(Figure 5), and for AARM (Figure 6). A further complication in the interpretation of the orientation-distribution of AMS arises where some specimens show a net paramagnetic AMS response whereas other specimens in the sample are more strongly influenced by the diamagnetic calcite matrix that produces an inverse fabric.

5. Rift Infill

[21] The sediments in the center of the rift valley were sampled as a control group, to avoid the proximity of fault influenced AMS fabrics. They show features compatible with undeformed horizontal sediments and some due to a feeble tectonic strain overprint. Taking the raw AMS specimen tensors, i.e., not standardizing them to unit susceptibility gives a sample weighted by the contribution of orientations of more highly susceptible specimens. Thus, in Figures 4c and 4d the magnetic foliation ($k_{\text{MAX}} - k_{\text{INT}}$) defines the bedding fabric. Moreover, k_{MAX} , corresponding to aligned clays, may define a current flow lineation since it is parallel to the rift axis (NW-SE).

[22] Standardizing the specimen tensors emphasizes the contribution from weakly susceptible specimens and thus emphasizes the role of the diamagnetic calcite matrix (Figure 4a); excluding purely diamagnetic specimens switches the roles of k_{INT} and k_{MIN} (Figure 4b), a feature commonly recognized from permutations of inverse fabrics and normal fabrics [Rochette *et al.*, 1992]. Clearly, the standardized, "diamagnetic-dominant" fabrics hint at the role of a weak calcite petrofabric that is a compromise between the AMS principal susceptibilities and the principal stress trajectories, superimposed on Figure 4a, which are due to recent seismicity with sinistral transpression along the rift axis. The k_{MAX} represents an alignment or extensional fabric NNE-SSW, which is compatible with rift genesis.

6. Faulted Margins of the Rift

[23] Outcrops along the faulted margins of the Polis rift are more fractured and whereas they show no penetrative petrofabrics their AMS fabrics are different from those of the sediments in the rift's center. This attests to at least a partial tectonic signature in the AMS fabrics. Standardized specimen tensors, whether they include or exclude the purely diamagnetic specimens (Figures 5a and 5b), reveal a shallow plunging NE extension fabric, compatible with rift opening. However, they show some association with the symmetry of the earthquake stress tensors. Nonstandardized specimen tensors emphasize the role of clays and associated fine magnetite, perhaps most sensitive indicators of incremental strains associated with Holocene and Pleistocene seismic activity. These show that the extension, defined by k_{MAX} is down to the SW (Figure 5c), similarly oriented to the earthquake tensional stresses (Figure 5a).

[24] The AARM technique isolates the contribution of a subfabric of remanence-bearing minerals and it is most successful with magnetite. These limestones are known to carry fine PSD magnetite of volcanoclastic or fossil origin

[Borradaile and Lagroix, 2000; Borradaile and Hamilton, 2003], but whereas all our specimens (152) yielded AMS fabrics, only 45 specimens carried sufficient remanence-bearing mineral grains to yield well-defined AARM subfabrics. A simple comparison of standardized AMS fabrics and of AARM fabrics (Figures 6a and 6b) indicates that both fabrics are similarly oriented near faults, with their maximum susceptibility NE-SW, in the extension direction expected during rifting with the intermediate axis parallel to the rift axis.

7. Conclusions

[25] By processing the AMS data differently and from different subareas, we have identified sedimentary depositional fabrics (Figure 4d) and rift opening fabrics with NE-SW extension (Figures 5a and 5b). AARM subfabrics corroborate the rift-opening event, with their NNE lineation (Figure 6b). Clearly, these petrofabrics developed in <5 Ma with grain alignments that would be much more difficult to discern by any other method. However, non-

standardized AMS fabrics may be modified by the effects of young sinistral transpression producing a blended fabric with magnetic lineation (k_{MAX}) oriented plunging SW, close to the extensional stresses associated with modern earthquakes (Figure 5c). This suggests that some magnetic fabrics are so sensitive that they may be reset in <1 Ma. The symmetry of all magnetic fabrics is generally compatible with the orientations of the actual faults (Figure 6c). Faults belong to two generations (~1 Ma and ~5 Ma); both the AMS and AARM fabrics are most compatible with the Pliocene major rift faults whereas the earthquake stress system is more compatible with the Pleistocene faults and sinistral transpression of the rift system due to E-W compression (Figure 6c).

[26] **Acknowledgments.** The Natural Sciences and Engineering Research Council of Canada (NSERC) funded Graham Borradaile for this work at the Lakehead University Rock Magnetism Laboratory. The authors were greatly assisted and encouraged by the Geological Survey Department of Cyprus, in particular through George Petrides (Director) and Ioannis Panayides. Philippe Robion, Charles Aubourg, John Geissman, and Bernard Henry provided constructive, insightful reviews.

References

- Arvidsson, R., Z. Ben-Avraham, G. Ekström, and S. Wdowinski (1998), Plate tectonic framework for the October 9, 1996 Cyprus earthquake, *Geophys. Res. Lett.*, *25*, 2241–2244.
- Ben-Avraham, Z., D. Kempler, and A. Ginzburg (1988), Plate convergence in the Cyprian Arc, *Tectonophysics*, *146*, 231–240.
- Borradaile, G. J. (1994), Paleomagnetism carried by crystal inclusions: The effect of preferred crystallographic orientations, *Earth Planet. Sci. Lett.*, *126*, 171–182.
- Borradaile, G. J. (2001), Magnetic fabrics and petrofabrics: Their orientation distributions and anisotropies, *J. Struct. Geol.*, *23*, 1581–1596.
- Borradaile, G. J., and C. Alford (1987), Relationship between magnetic susceptibility and strain in laboratory experiments, *Tectonophysics*, *133*, 121–135.
- Borradaile, G. J., and D. Gauthier (2001), AMS-detection of inverse fabrics without AARM, in ophiolite dikes, *Geophys. Res. Lett.*, *28*, 3517–3520.
- Borradaile, G. J., and T. Hamilton (2003), Limestones distinguished by magnetic hysteresis in three-dimensional projections, *Geophys. Res. Lett.*, *30*(18), 1973, doi:10.1029/2003GL017892.
- Borradaile, G. J., and B. Henry (1997), Tectonic applications of magnetic susceptibility and its anisotropy, *Earth Sci. Rev.*, *42*, 49–93.
- Borradaile, G. J., and M. Jackson (1993), Changes in magnetic remanence during simulated deep sedimentary burial, *Phys. Earth Planet. Inter.*, *77*, 315–327.
- Borradaile, G. J., and M. M. Kehlenbeck (1996), Possible crypto-tectonic magnetic fabrics in "Post-tectonic" granitoid plutons of the Canadian Shield, *Earth Planet. Sci. Lett.*, *137*, 119–127.
- Borradaile, G. J., and F. Lagroix (2000), Magnetic characterization of limestones using a new hysteresis projection, *Geophys. J. Int.*, *141*, 213–226.
- Borradaile, G. J., and M. Stupavsky (1995), Anisotropy of magnetic susceptibility: Measurement schemes, *Geophys. Res. Lett.*, *22*, 1957–1960.
- Borradaile, G. J., and T. Werner (1994), Magnetic anisotropy of some phyllosilicates, *Tectonophysics*, *235*, 233–248.
- Carmichael, R. S. (1968), Remanent and transitory effects of elastic deformation of magnetite crystals, *Philos. Mag.*, *17*, 911–927.
- Carmichael, R. S. (1969), Hydrostatic pressurization of magnetite, *Geophysics*, *5*, 775–779.
- Day, R., M. D. Fuller, and V. A. Schmidt (1977), Hysteresis properties of titanomagnetites, grain size and compositional dependence, *Phys. Earth Planet. Inter.*, *13*, 260–267.
- Domen, H. (1962), Piezo-remanent magnetism in rock and its field evidence, *J. Geomagn. Geoelectr.*, *13*, 66–72.
- Dunlop, D., and Ö. Özdemir (1997), *Rock Magnetism, Fundamentals and Frontiers*, 573 pp., Cambridge Univ. Press, New York.
- Facenna, C., R. Funiello, A. Bruni, M. Mattei, and L. Sagnotti (1994), Evolution of a transfer-related basin: The Ardea Basin (Latiou, central Italy), *Basin Res.*, *6*, 35–46.
- Flinn, D. (1965), On the symmetry principle and the deformation ellipsoid, *Geol. Mag.*, *102*, 36–45.
- Fuller, M. D. (1963), Magnetic anisotropy and paleomagnetism, *J. Geophys. Res.*, *68*, 293–309.
- Girdler, R. W. (1961), The measurement and computation of anisotropy of magnetic susceptibility in rocks, *Geophys. J. R. Astron. Soc.*, *5*, 34–44.
- Hamano, Y., R. Boyd, M. Fuller, and M. Lanham (1989), Induced susceptibility anisotropy of igneous rocks caused by uniaxial compression, *J. Geomagn. Geoelectr.*, *41*, 203–220.
- Henry, B. (1989), Magnetic fabric and orientation tensor of minerals in rocks, *Tectonophysics*, *165*, 21–27.
- Hrouda, F. (1982), Magnetic anisotropy of rocks and its application in geology and geophysics, *Geophys. Surv.*, *5*, 37–82.
- Hrouda, F., and J. Jelinek (1999), Theoretical models for the relationship between magnetic anisotropy and strain: Effect of triaxial magnetic grains, *Tectonophysics*, *301*, 183–190.
- Hrouda, F., and K. Schulmann (1990), Conversion of the magnetic susceptibility tensor into the orientation tensor in some rocks, *Phys. Earth Planet. Inter.*, *63*, 71–77.
- Jackson, M. (1991), Anisotropy of magnetic remanence: A brief review of mineralogical sources, physical origins, and geological applications and comparison with susceptibility anisotropy, *Pure Appl. Geophys.*, *136*, 1–28.
- Jackson, M. J., and L. Tauxe (1991), Anisotropy of magnetic susceptibility and remanence: Developments in the characterization of tectonic, sedimentary, and igneous fabric, *U.S. Natl. Rep. Int. Union Geod. Geophys. 1987–1990, Rev. Geophys.*, *29*, 371–376.
- Jackson, M., G. J. Borradaile, P. J. Hudleston, and S. K. Banerjee (1993), Experimental deformation of synthetic magnetite-bearing calcite sandstones: Effects on remanence, bulk magnetic properties and magnetic anisotropy, *J. Geophys. Res.*, *98*, 383–401.
- Jelinek, V. (1978), Statistical processing of anisotropy of magnetic susceptibility measured on groups of specimens, *Stud. Geoph. Geod.*, *22*, 50–62.
- Kalashnikov, A. G., and S. P. Kapitsa (1952), Magnetic susceptibility of rocks under elastic stresses, *Izv. Akad. Nauk SSSR, Ser. Fiz.*, *86*, 521–523.
- Kapicka, A. (1992), Magnetic susceptibility under hydrostatic pressure of synthetic magnetite samples, *Phys. Earth Planet. Inter.*, *70*, 248–252.
- Kinoshita, H. (1968), Studies on piezomagnetization III PRM and related phenomena, *J. Geomagn. Geoelectr.*, *20*, 155–167.
- Lagroix, F., and G. J. Borradaile (2000a), Magnetic fabric interpretation complicated by inclusions in mafic silicates, *Tectonophysics*, *325*, 207–225.
- Lagroix, F., and G. J. Borradaile (2000b), Tectonics of the Circum-Troodos Sedimentary Cover of Cyprus, from rock magnetic and structural observations, *J. Struct. Geol.*, *22*, 453–469.
- Lisle, R. J. (1989), The statistical analysis of orthogonal orientation data, *J. Geol.*, *97*, 360–364.
- Mattei, M., L. Sangotti, C. Facenna, and R. Funiello (1997), Magnetic fabric of weakly deformed clay-rich sediments in the Italian peninsula: Relationship with compressional and extensional tectonics, *Tectonophysics*, *271*, 107–122.
- Mattei, M., F. Speranza, A. Argenti, F. Rosetti, L. Sagnotti, and R. Funiello (1999), Extensional

- tectonics in the Amantea Basin (Calabria, Italy): A comparison between structural and magnetic anisotropy data, *Tectonophysics*, 307, 33–49.
- McCabe, C., M. J. Jackson, and B. B. Ellwood (1985), Magnetic anisotropy in the Trenton limestone: Results of a new technique, anisotropy of anhysteretic susceptibility, *Geophys. Res. Lett.*, 12, 333–336.
- Nagata, T. (1966a), Magnetic susceptibility of compressed rocks, *J. Geomagn. Geoelectr.*, 18, 73–80.
- Nagata, T. (1966b), Main characteristics of piezomagnetization and their qualitative interpretation, *J. Geomagn. Geoelectr.*, 18, 81–97.
- Nagata, T. (1970), Anisotropic magnetic susceptibility of rocks under mechanical stresses, *Pure Appl. Geophys.*, 78, 110–122.
- Nye, J. F. (1957), *The Physical Properties of Crystals*, 322 pp., Clarendon, Oxford, England.
- Papazachos, B. C., and C. A. Papaioannou (1999), Lithospheric boundaries and plate motions in the Cyprus area, *Tectonophysics*, 308, 193–204.
- Payne, A. S., and A. H. F. Robertson (1995), Neogene supra-subduction zone extension in the Polis graben system, west Cyprus, *J. Geol. Soc. London*, 152, 613–628.
- Ramsay, J. G. (1967), *Folding and Fracturing of Rocks*, 578 pp., McGraw-Hill, New York.
- Ramsay, J. G., and M. I. Huber (1983), *The Techniques of Modern Structural Geology*, vol. 1, *Strain Analysis*, 307 pp., Academic, San Diego, Calif.
- Revol, J., R. Day, and M. D. Fuller (1977), Magnetic behavior of magnetite and rocks stressed to failure—Relation to earthquake prediction, *Earth Planet. Sci. Lett.*, 37, 296–306.
- Robertson, A. H. F. (1990), Tectonic evolution of Cyprus, in *Ophiolites Oceanic Crustal Analogues: Proceedings of the Symposium "Troodos 1987,"* edited by J. Malpas et al., pp. 235–250, Geol. Surv. Dep., Nicosia, Cyprus.
- Robertson, A. H. F., R. B. Kidd, M. K. Ivanov, A. F. Limonov, J. M. Woodside, J. Galindo-Zaldicar, and L. Nieto (1995), Eratosthenes seamount: Collisional processes in the easternmost Mediterranean in relation to the Plio-Quaternary uplift of southern Cyprus, *Terra Nova*, 7, 254–264.
- Rochette, P. (1987), Magnetic susceptibility of the rock matrix related to magnetic fabric studies, *J. Struct. Geol.*, 9, 1015–1020.
- Rochette, P. (1988), Inverse magnetic fabric in carbonate-bearing rocks, *Earth Planet. Sci. Lett.*, 90, 229–237.
- Rochette, P., M. J. Jackson, and C. Aubourg (1992), Rock magnetism and the interpretation of anisotropy of magnetic susceptibility, *Rev. Geophys.*, 30, 209–226.
- Rochette, P., C. Aubourg, and M. Perrin (1999), Is this magnetic fabric normal? A review and case studies in volcanic formations, *Tectonophysics*, 307, 219–234.
- Sagnotti, L., and S. Speranza (1993), Magnetic fabrics analysis of the Plio-Pleistocene clay units of the Sant' Arcangelo basin, southern Italy, *Phys. Earth Planet. Inter.*, 77, 165–176.
- Sagnotti, L., C. Faccenna, R. Funicello, and M. Mattei (1994), Magnetic fabric and structural setting of Plio-Pleistocene clayey units in an extensional regime: The Tyrrhenian margin of central Italy, *J. Struct. Geol.*, 16, 1243–1257.
- Scheidegger, A. E. (1965), On the statistics of the orientation of bedding planes, grain axes, and similar sedimentological data, *U. S. Geol. Surv. Prof. Pap.*, 525-C, 164–167.
- Stacey, F. D. (1964), The seismo-magnetic effect, *Pure Appl. Geophys.*, 58, 5–22.
- Stephenson, A., S. Sadikun, and D. K. Potter (1986), A theoretical and experimental comparison of the anisotropies of magnetic susceptibility and remanence in rocks and minerals, *Geophys. J. R. Astron. Soc.*, 84, 185–200.
- Tarling, D. H., and F. Hrouda (1993), *The Magnetic Anisotropy of Rocks*, 217 pp., Chapman and Hall, New York.
- Uyeda, S., M. D. Fuller, J. C. Belshe, and R. W. Girdler (1963), Anisotropy of magnetic susceptibility of rocks and minerals, *J. Geophys. Res.*, 68, 279–291.
- Werner, T., and G. J. Borradaile (1996), Paleoremanence dispersal across a transpressed Archean terrain: Deflection by anisotropy or by late compression?, *J. Geophys. Res.*, 101, 5531–5545.
- Winkler, A., and L. Sagnotti (1994), Anisotropies of anhysteretic remanence and magnetic susceptibility of marly clays from central Italy, *Ann. Geofis.*, 27(5), 1027–1035.
- Woodcock, N. H. (1977), Specification of fabric shapes using an Eigenvalue method, *Geol. Soc. Am. Bull.*, 88, 1231–1236.

G. J. Borradaile and T. Hamilton, Geology Department, Lakehead University, Thunder Bay, Ontario, Canada P7B 5E1. (borradaile@lakeheadu.ca)

Sub-fabric identification by standardization of AMS: an example of inferred neotectonic structures from Cyprus

THOMAS D. HAMILTON,¹ GRAHAM J. BORRADAILE¹ &
FRANCE LAGROIX²

¹*Geology Department, Lakehead University, Thunder Bay, Ontario P7B 5E1, Canada
(e-mail: tdhamilton@canada.com, borradaile@lakeheadu.ca)*

²*Institute for Rock Magnetism, University of Minnesota, 100 Union Street S.E.,
Minneapolis, MN 55455-01, USA*

Abstract: Calcite petrofabrics are sensitive to weak strains, possibly being the most sensitive classical petrofabric indicator. Thus, calcareous sediments may reveal stress trajectories in neotectonic environments. Calcite aligns by crystal-plastic deformation and pressure solution produce corresponding alignments in accessory clay minerals and magnetite (possibly fossil-bacterial). Their alignments are rapidly and precisely detected by anisotropy of low field magnetic susceptibility (AMS) with net magnetic fabrics, which blend diamagnetic contributions from matrix calcite (diamagnetic bulk susceptibility $\kappa \sim -14 \mu\text{SI}$), accessory clay minerals ($\kappa = 100$ to $500 \mu\text{SI}$) and sometimes trace magnetite ($\kappa > 2 \text{SI}$). Their relative abundances and different anisotropies must be considered in interpreting AMS orientations, nevertheless our study reveals orientation distributions of AMS axes in sub-areas and regions that are sensibly interpreted as palaeostress trajectories in Neogene and Quaternary strata. The AMS axes may be correlated with the orientation of faults, plate-motion vectors and seismic solutions. Large samples (1090 specimens from 419 sites) are treated by different statistical approaches ('standardization') to emphasize or suppress the contribution of subfabrics with anomalous mean susceptibility. A sub-sample of 254 specimens from 219 sites, from different sub-areas was investigated by anisotropy of anhysteretic remanence (AARM), which isolates the orientation distributions of magnetite. Magnetic fabrics are mostly of the L-S kind with the magnetic lineations compatible with gravitational stretching of the sedimentary cover away from the Troodos massif and orthogonal to the principal faults and graben. The L-direction (k_{max}) shows a smooth variation in orientation, through the sub-areas, directed radially from the Troodos massif and the S-components of the magnetic fabrics are inclined gently to the bedding, compatible with vergence toward the Cyprean Arc to the S and SW of Cyprus.

Magnetic fabric analysis, most commonly using anisotropy of low-field magnetic susceptibility (AMS), is now well established as a non-destructive technique to isolate the mean orientation-distribution of crystals in an anisotropic rock. AMS blends contributions from different minerals that have different magnetic responses, i.e. paramagnetic, diamagnetic or 'ferromagnetic' (Rochette *et al.* 1992). In turn, the principal AMS axes may proxy for the principal axes of the orientation distribution ellipsoid of crystals (Henry 1989; Borradaile 2001) which, in turn, may reveal the finite strain axes in tectonically deformed rock (Tarling & Hrouda 1993; Borradaile & Henry 1997). In deformed calcite matrices, interpretation is somewhat complicated by an intrinsic counterintuitive arrangement of crystallographic and AMS axes, a so-called 'inverse fabric' (Rochette 1988), which nevertheless still permits sensible interpretations of their finite strain axes (Ihmlé *et al.* 1989; de Wall *et al.* 2000).

However, recent studies show that in neotectonic environments, with imperceptible penetrative strain, AMS axial orientations may be sensibly related to the orientations of joints or faults, for which stress axes are reliably inferred (Sagnotti *et al.* 1994, 1998; Mattei *et al.* 1999; Cifelli *et al.* 2004). In some instances, AMS axes may correlate with modern seismic solutions and plate movements (Kissel *et al.* 1986; Mattei *et al.* 1999; Borradaile & Hamilton 2004). Thus, AMS may proxy for stress trajectories under limited circumstances.

Our goal is to examine a large sample of AMS and AARM data from post-Palaeogene strata in Cyprus that correlate with the orientations of neotectonic structures or events (faults, rifts, Tertiary uplift). It will be shown that their orientations are consistent with stress trajectories inferred from those structures and recent plate motion trajectories. Sampling at two density levels verifies the homogeneity of the regional domains and the validity of the regional conclusions. Local

From: MARTÍN-HERNÁNDEZ, F., LÜNEBURG, C. M., AUBOURG, C. & JACKSON, M. (eds) 2004. *Magnetic Fabric: Methods and Applications*. Geological Society, London, Special Publications, **238**, 527–540. 0305-8719/04; \$15.00 © The Geological Society of London 2004.

sub-areas (I–VI) were structurally homogenous and sampled with as little lithological variation as possible over areas $\leq 30 \text{ km}^2$. The regional-scale domains (I–V) have an average area of $\sim 400 \text{ km}^2$.

Tectonic background

Our study concentrates on the limestone and marl sedimentary cover to the Cretaceous Troodos ophiolite. We exclude from this discussion the juxtaposed older allochthonous Mamonía and Kyrenia terranes, which include exotic formations as old as Triassic and perhaps even Carboniferous (Robertson 1990) (Fig. 1a). The Troodos terrane exposes an integral ophiolite sequence with mantle harzburgite and lherzolite at the base overlain by layered gabbros and dunite, sheeted dykes, a transitional sheeted-dyke to pillowed unit and a thick pillow basalt sequence (Malpas *et al.* 1990). Supra-Troodos sedimentation commenced in the Maastrichtian ($\sim 68 \text{ Ma}$) with a pelagic chalk blanket, to form a relatively continuous sequence to the present (Lord *et al.* 2000). Northwards subduction stalled in the Eocene, with southward thrusting of the Kyrenia Range. Subduction then retreated southwards to its present location off the south shore of Cyprus in the Miocene, initiating the present stress regime (Fig. 1b). Miocene extensional basins, most prominently the Polis graben, formed in response to changing stress trajectories during the retreat of the subduction zone's hinge away from the Troodos microplate. Subduction continued during the Pliocene, until the Eratosthenes Seamount reached the trench in the Pleistocene when serpentization-driven diapirism continued to uplift the Troodos dome (Robertson 2000). These events drastically changed the neotectonic regime in the last 5 Ma, which is evident from studies of structure (Robertson *et al.* 1995), earthquakes (Ben-Avraham *et al.* 1988; Arvidsson *et al.* 1998; Papazachos & Papaioannou 1999; Borradaile & Hamilton 2004) and global plate motion (Reilinger *et al.* 1997). The tectonic events, their principal plate-geometrical consequences and the reasonably inferred principal tensile or compressive stress trajectories are summarized in Figure 2.

Our previous studies indicated the potential for AMS (anisotropy of low field magnetic susceptibility) to indicate very weak strains and weak orientation distributions of minerals, like those accompanying calcite-crystal plastic mechanisms in neotectonic environments. AMS shows neotectonic potential in the limestone cover from the Palaeogene Lefkara Formation through the Neogene Paghna Formation to the

localized Pleistocene cover. Without regard to detailed stratigraphic level within the Troodos Cover sequence, Lagroix and Borradaile (2000) showed that the AMS principal axes correspond to kinematic patterns. k_{max} defines down-slope gravitational stretching away from the Troodos dome and locally into tectonic/depositional basins. In the Polis Rift Valley, AMS and AARM (anisotropy of anhysteretic remanent magnetization) axes correlate with principal stress trajectories inferred from Miocene and younger fault-orientations and by modern seismic fault-plane solutions (Borradaile & Hamilton 2004, Fig. 6).

Neotectonic interpretation potential of AMS?

The presence of consistently oriented AMS axes in young sedimentary rocks that are not related to depositional fabrics, itself argues for some subtle tectonic imprint (e.g. Sagnotti *et al.* 1994). In such environments, AMS axes may be oriented consistently and simply with respect to faults or joints. These structures have orientations uniquely associated with their cogent stress trajectories and thus by induction, the AMS axes may proxy as stress trajectories. Of course, AMS axes may proxy for stress trajectories in ancient rocks too, but their recognition requires fortunate circumstances (e.g. Borradaile & Kehlenbeck 1996). Usually, in ancient or severely deformed rocks, the association of AMS with finite strain axes with earlier tectonic events will mask any young and feeble AMS overprint associated with late stress increments. *Note that we use Flinn's L-S scheme (1965) equally to describe tensor magnitude ellipsoid shapes, whether they are for strain, AMS, stress or mineral ODs (petrofabrics).*

Calcite twinning and other crystal-plastic deformation have long been used in petrofabrics as sensitive indicators of incremental strain axes, which are essentially parallel to the causative palaeostress axes. Indeed, the association of calcite petrofabrics, their causative stress axial orientations and magnetic fabrics have been shown in some other studies (Owens & Bamford 1976; Owens & Rutter 1978; Jackson *et al.* 1989; Borradaile *et al.* 1989). The Neogene and Quaternary limestone and marl that covers the Troodos microplate shows evidence of weak to moderate strain, expressed by calcite twinning and, rarely, a feeble stylolitic cleavage. Calcite, accessory clay and magnetite traces are aligned and readily detectable in the AMS signal (Lagroix & Borradaile 2000). These minerals

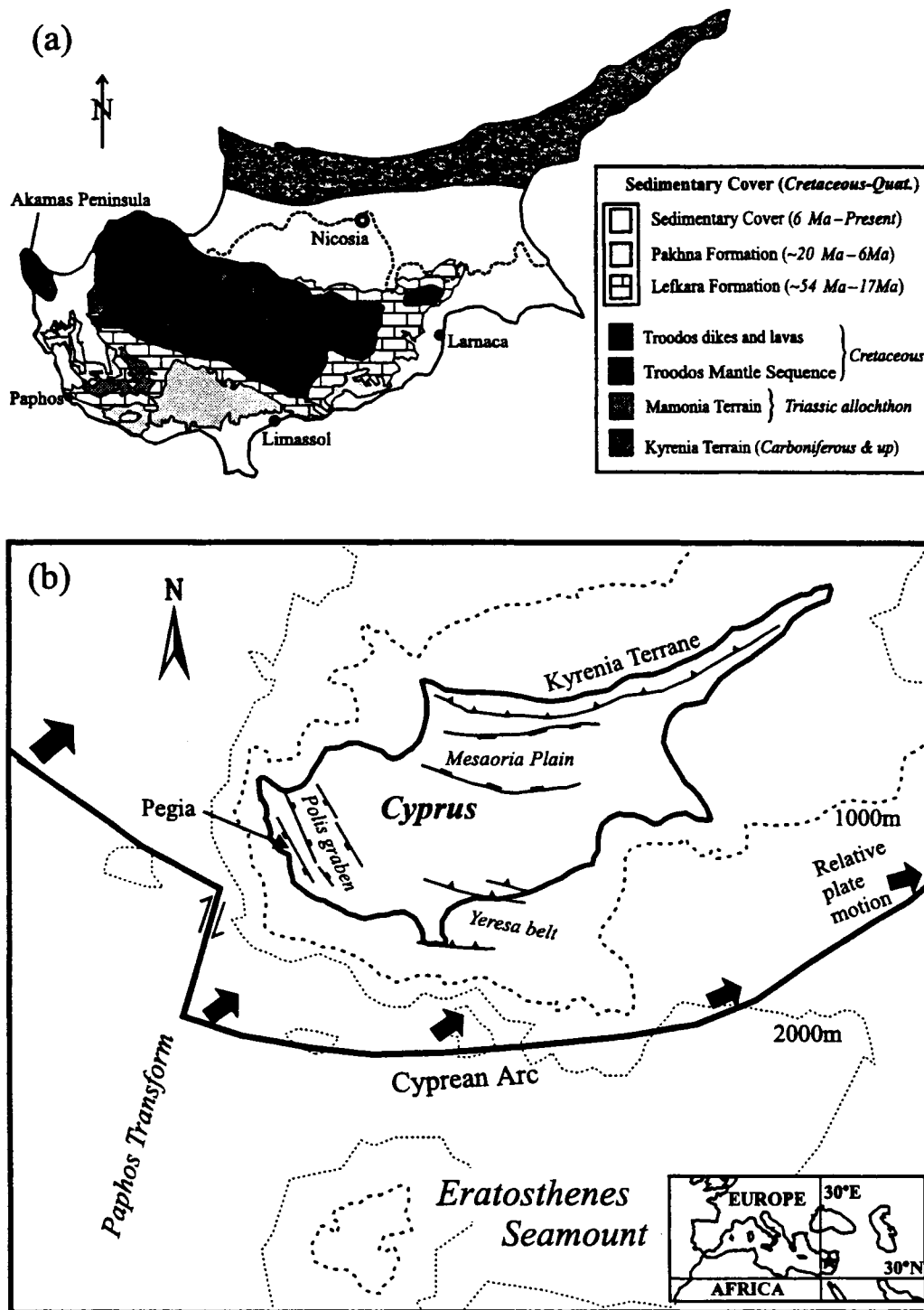


Fig. 1. Geology of Cyprus. (a) Major lithological units of Cyprus (Geological Survey Department, Cyprus, 1979). (b) Major Tectonic features of Cyprus (Robertson 1990; Arvidsson *et al.* 1998; Borradaile & Hamilton 2004).

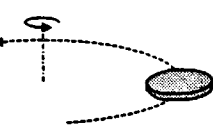
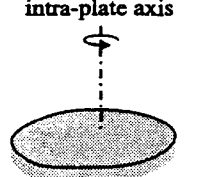
Age	Periods	Formations	Tectonic Events	
			Principal Stresses	Troodos Microplate Rotations
0.01	Holocene	Alluvium	Pegia and Polis	Final ~30° slow rotation (50 Ma - 10 Ma) distant rotation-axis 
	Pliocene	Terrace Deposits		
Fanglomerate				
2.0	Pliocene	Athalassa	Polis	
		Nicosia		
5.2	Messinian	Kalavassos	Mesaoria	
		Tortonian		
		Serravallian		
		Langhian		
		Burdigalian		
23.3	Oligocene	Terra	Yeresa	
35.4	Eocene	Lefkara	(Kyrenia)	~60° rotation intra-plate axis 
65.0	Maastrichtian	Moni		
		Campanian	Kannaviou	
			Perapedhi	
			Troodos Ophiolite	
88.0				

Fig. 2. Simplified stratigraphic and tectonic events for the Troodos terrane, and its sedimentary cover rocks.

contribute quite differently to AMS and to bulk susceptibility. Calcite is diamagnetic (usually quoted as $\kappa \sim -14 \mu\text{SI}$) but it has a large anisotropy and comprises >97% of the rocks' volumes. Its crystal-plastic deformation aligns the paramagnetic accessory clay minerals (100–500 μSI , $\leq 3\%$ by rock volume) and the scarce traces of magnetite. However, the latter may contribute significantly to AMS due to magnetite's high bulk susceptibility ($\sim 1.0\text{--}2.7 \text{ SI}$) (Hunt *et al.* 1995); and the grains may align either as overgrowths or inclusions associated with clay grains or as independent grains. Magnetite grains may be of clastic or bacterial origins; their hysteresis properties are compatible with the latter hypothesis (Borradaile & Lagroix 2000; Borradaile & Hamilton 2003).

The specimen's bulk susceptibilities ($\kappa = \sqrt{(k_{\text{max}}k_{\text{int}}k_{\text{min}})}$) are a first guide to the mineralogical controls on AMS. We present these for rather homogenous sub-areas (Fig. 3a), which justifies the subsequent interpretation of larger sampling schemes in regional domains (I–V) (Fig. 3b). The positive susceptibility sections of the histograms are scaled logarithmically and, to a first approximation, it appears that the weakly positive κ specimens have susceptibilities with a lognormal distribution, with most sub-areas and regional domains having modal κ in

the range $+15 \mu\text{SI} \leq \kappa \leq +35 \mu\text{SI}$. Only very low concentrations of accessory clay ($\leq 1000 \mu\text{SI}$) and trace magnetite ($\sim 2.0 \text{ SI}$) are required to raise the specimens' κ from the level of a pure calcite diamagnetic matrix (assumed to be $\sim -14 \mu\text{SI}$) to the levels of the positive κ specimens shown in Figure 3a, b. In the complete absence of magnetite, only 3% by volume of clay would be required to justify the positive κ values. Many specimens are truly diamagnetic and the linear scale for the diamagnetic part of the histogram clarifies the frequency distributions. For calcite κ is commonly quoted at $\sim -14 \mu\text{SI}$ (Voight & Kinoshita 1907) or -7.5 to $-39 \mu\text{SI}$ (Hunt *et al.* 1995). Whereas there are fairly modern high precision torque measurements for anisotropy (i.e. $k_{\text{max}} - k_{\text{min}}$; Hellwege & Hellwege 1967; Owens & Rutter 1978) there are apparently no recent high-precision measurements for the bulk value (κ), which hinders modelling and interpretation of AMS. Values for synthetic calcite would be preferable for modelling work (e.g. in Borradaile 1988) whereas measurements from natural calcite are contaminated by non-diamagnetic impurities. Our instrument has a low-drift environment ($< 0.05 \mu\text{SI}$) and is calibrated with MnO_2 ($\sim 1654 \mu\text{SI}$). Due to the small range of diamagnetic susceptibilities there may be some slight bin boundary bias in that part of the histogram.

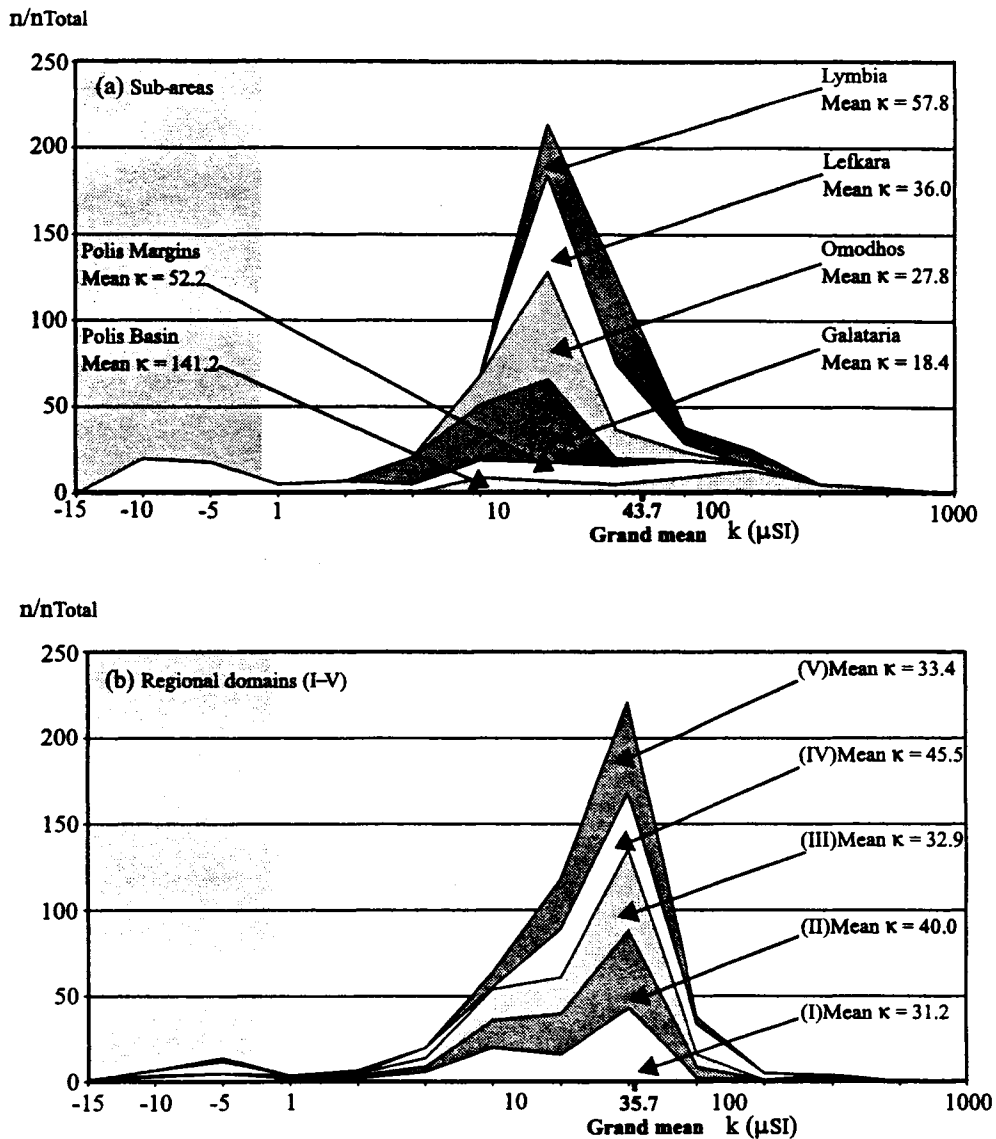


Fig. 3. Frequency distribution of bulk magnetic susceptibility (κ) for (a) sub-areas ($\sim 30 \text{ km}^2$) and (b) regional domains ($\sim 400 \text{ km}^2$). Data in the shaded box on the left represent diamagnetic specimens and their scale is linear. Data with $\kappa > 0$ represent paramagnetic specimens and are shown with a logarithmic scale.

The susceptibility frequency-distribution indicates that paramagnetic limestone is more common and it confirms that the rocks' susceptibilities, whether paramagnetic or diamagnetic are mostly bimineralic in origin. Interpreting AMS axes in such rocks necessitates the evaluation of the competition between weak paramagnetism and weak diamagnetism in the same specimens, and between weakly dia/paramagnetic specimens within a sample of several different specimens, for example from a sub-area.

A new plot of fabric anisotropy parameters, introduced by Borradaile & Jackson (this volume), simplifies the interpretation in this context. Jelinek's (1981) anisotropy parameters (P_j , T) are usually presented on Cartesian axes. Consequently, for weak degree of anisotropy (low-eccentricity ellipsoids with $P_j \sim 1.0$) the difference between T -values that describe ellipsoid shape is exaggerated. In the extreme case, the sphere (isotropic case, $P_j = 1.0$), which should plot at *one point* on the diagram actually

spread along the entire axis from $T = +1$ (prolate) to $T = -1$ (oblate). This biases the presentation and interpretation of all low- P_j anisotropies that are essentially near-isotropic, a matter of considerable relevance here where specimens straddle the diamagnetic-paramagnetic boundary. The new polar plot presents P_j radially and T along arcs; thus, all spheres plot

uniquely at the origin and the difference in shape between weak anisotropies is not exaggerated. Moreover, the plot facilitates the simultaneous presentation and comparison of positive and diamagnetic susceptibilities (Fig. 4). When working with anisotropies of diamagnetic rocks and weakly paramagnetic rocks it is also important not to overlook some non-trivial issues that

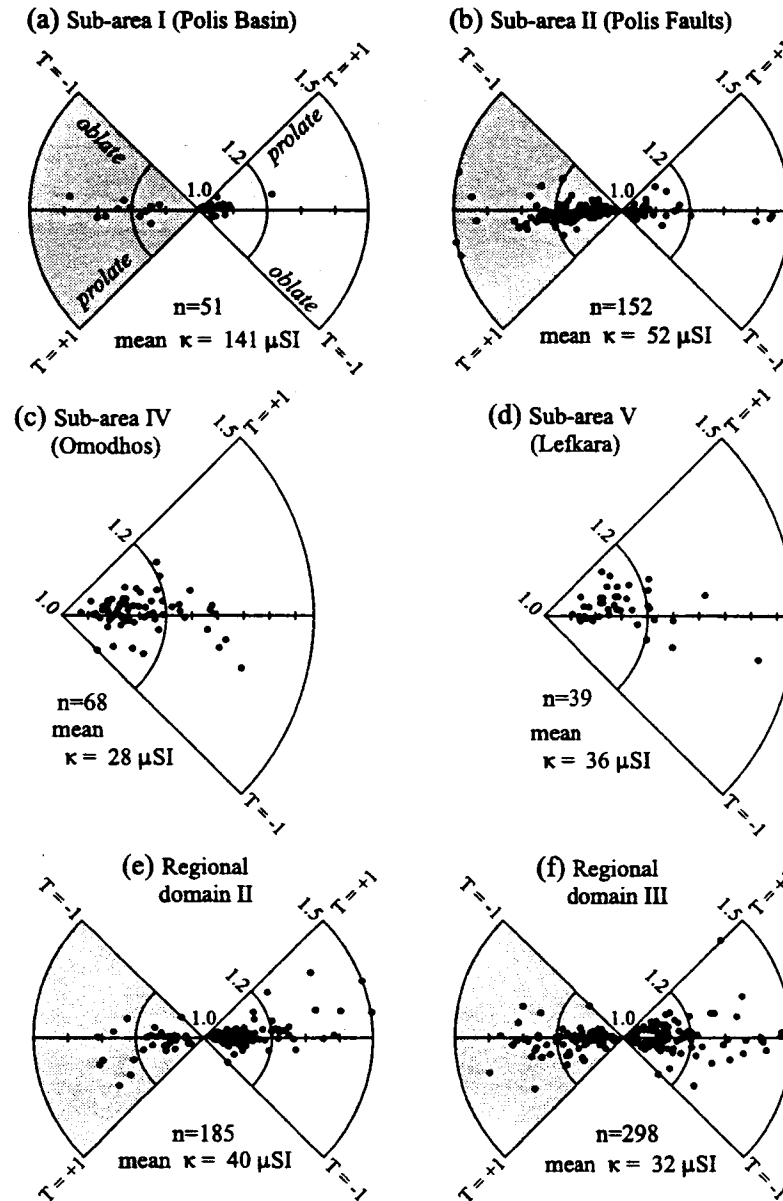


Fig. 4. Polar plots (see Borradaile & Jackson, this volume) of four select sub-areas (a)–(d) and two select regional domains (e, f). Shaded area represents diamagnetic specimens and white area represents paramagnetic specimens.

software must manage carefully:

- (1) Anisotropy is indeterminate for a specimen if some axes have positive susceptibility and others have negative susceptibility (Borradaile 2003). This occurs in some limestone specimens.
- (2) k_{\max} is obviously the largest absolute value for a paramagnetic material but for a diamagnetic material the most negative value represents the long axis of the magnitude ellipsoid.
- (3) Regardless of the convention for defining the ellipsoid in (2) above, the common diamagnetic minerals, quartz and calcite have the idiosyncrasy that under most metamorphic conditions their c axes tend to align parallel to the shortening axis (but see Borradaile & Jackson, this volume). Thus, c axes are parallel to the most negative susceptibility, which may be perpendicular to the rock's S -fabric. Calcite exhibits a strong prolate diamagnetic anisotropy with ($k_{\max} - k_{\min}$) estimated at $1.39 \mu\text{SI}$ (Krishnan *et al.* 1933; Hellwege & Hellwege 1967, p. 143) or $1.172 \pm 0.028 \mu\text{SI}$ (Owens & Rutter 1978). If we accept the much less certain but commonly quoted bulk susceptibility $\kappa \sim -14 \mu\text{SI}$, these precise anisotropy determinations indicate a large anisotropy of $\sim 10\%$.
- (4) Since most deformation mechanisms align calcite with its c axis (most negative susceptibility) parallel to shortening it produces an 'inverse fabric' (Rochette 1988; Ihmlé *et al.* 1989).

Examples of the anisotropies of both local-scale samples (Fig. 4a–d) and regional domains (Fig. 4e, f) indicate that the anisotropy degree (P_i) is similar for diamagnetic and paramagnetic limestones and that ellipsoid shape tends slightly toward the oblate case ($T > 0$) for both diamagnetic and paramagnetic specimens. Anisotropies are remarkably similar for the diamagnetic and paramagnetic fields and diamagnetic limestones are only absent in marl Formations in the Omodhos and Lefkara sub-areas (Fig. 4c, d).

Interpreting AMS

AMS orientations and magnitudes would reflect the orientation distribution of a monomineralic rock with a unique petrofabric. However, for rocks with multiple minerals with similar contributions to the net susceptibility or with multiple subfabrics some care is required in evaluating the influence of mineral abundances and subfabrics

(Borradaile 1988; Borradaile & Henry 1997). For rocks of high mean susceptibility (κ), AMS axes may be controlled by one or two or a few minerals (Henry 1983, 1990, 1992; Borradaile *et al.* 1986; Borradaile & Kehlenbeck 1996; Borradaile & Lagroix 2001; Nakamura & Borradaile 2001). In our limestones however, sub-equal competition from the diamagnetic matrix and paramagnetic clay complicate the issue. To illustrate the argument with hypothetical but not unrealistic values chosen for arithmetic simplicity, disperse a concentration of 5% clay (assume $\kappa = 266 \mu\text{SI}$) in a calcite matrix (assume $\kappa = -14 \mu\text{SI}$). The limestone's net susceptibility is approximately zero and the specimen may also be isotropic. It is for this reason that some AMS data from limestone must be examined carefully because the AMS directions are simply too unstable; their anisotropy is too low to define stable orientations of principal axes as itemized in the list above (Borradaile & Jackson, this volume). In worse cases, the principal susceptibilities may not all be of the same sign so that the AMS tensor may not be represented by any magnitude ellipsoid.

Although it is now realized that the magnitude ellipsoids of individual specimen tensors have little kinematic significance due to the complex blend of multiple mineralogical responses, specimen magnitudes do affect the calculation of the orientation of the mean tensor. The mean tensor's orientation may be strongly deflected toward the orientation of a few large-magnitude specimen tensors. However, high susceptibility specimens need not be considered as outliers in the disparaging statistical sense. They may provide useful information from a subfabric or second population of grains with a different orientation distribution. That is the case in this study where specimens with larger concentrations of paramagnetic accessory clay minerals may strongly influence the orientation of the mean tensor for a sub-sample. By recalculating the mean tensor using standardized specimen tensors, the influence of high susceptibility specimens and kinematically distinct subfabrics may be isolated, or emphasized (Borradaile 2001, 2003). Specimen tensors are standardized by dividing each of the principal magnitudes for a specimen (k_{\max} , k_{int} , k_{\min}) by κ ; this weights all specimens equally, regardless of their bulk susceptibility. Consequently the contribution high- κ subfabrics to the orientation distribution will be subdued in the net-AMS. On the other hand, the mean tensor for non-standardized specimens emphasizes the role of such subfabrics (Borradaile 2001, 2003).

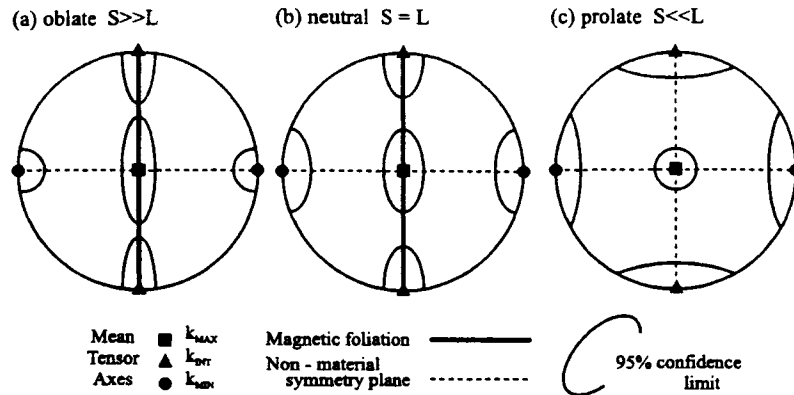


Fig. 5. Idealized symmetry of confidence cones about the mean orientations of the principal axes of the mean tensor for a petrofabrically homogeneous group of specimens. The shapes of confidence cones for tensor-mean principal axes may be used for other petrofabrically significant axes (as in orientation distributions of crystals), for finite strain axes and for principal stresses. The shape of the confidence cones may also be related to the relative magnitudes of the three principal mean axes: (a) elongate confidence ellipses in the maximum-intermediate plane define an ellipsoid with oblate symmetry ($S > L$) whereas (c) elongate confidence ellipses in the plane perpendicular to the maximum axis are associated with prolate symmetry ($L > S$). Flinn's (1965) L - S notation was initially introduced to describe finite strain ellipsoids or fabric ellipsoids but it is a useful shorthand for any anisotropy.

The following comparison of mean tensors for standardized versus non-standardized specimens in regional-scale and local-scale samples, display different AMS axes that reveal a rapidly changing tectonic regime, especially in the last 5 Ma. Sample mean tensors for standardized and non-standardized specimens are also compared profitably to previously determined AARM tensors.

Processing AMS data from low- κ specimens

The tectonic significance of AMS data in limestone having weak susceptibilities depends on a careful assessment of the mineralogical origins of AMS and the effects of specimen variation within the sample suite. Jelinek (1978) showed that the orientation distribution (OD) of a suite of tensors ('AMS ellipsoids') must be treated by a special statistical procedure so that the sample's mean tensor retains orthogonal axes, just like individual specimen tensors. Applying Jelinek statistics permits us to characterize a sample of AMS tensors much more effectively than with density contours, although the latter still have their use (Borradaile 2001, 2003). The shape and symmetry of the 95% confidence regions around the mean tensor's principal axes define the orientation distribution of specimen tensors in the L - S fabric scheme (Flinn 1965); thus regional suites of AMS ellipsoids define

the regional variation from S through L tectonites (Fig. 5).

Confidence cones for the mean tensor's principal axes reflect the shape of the orientation-distribution (OD) ellipsoid for the *sample*, not of individual tensors. For example, individual *prolate* ellipsoids scattered with their long axes in a plane define a sample with an orientation distribution described by an *oblate* ellipsoid (e.g. Borradaile 2003, pp. 286–287). Thus in AMS studies, if the mean $T_j > 0$ for *specimens*, it does not necessarily mean that their orientation distribution, described by the mean tensor, is also oblate (Borradaile 2001).

The sample's mean tensor and its confidence cones may be biased toward the orientation of specimens of anomalous κ . In this study, the anomalous specimen may be a diamagnetic one or a paramagnetic one in a contrasting matrix. The standardization technique described (dividing k_{\max} etc. by κ , etc.) suppresses this bias. Whereas it may change the orientation of the mean tensor, it may also change the shape of the confidence regions about the mean tensor's axes. Thus one may re-evaluate the OD of the mean tensor as an $L > S$ rather than $S > L$ fabric.

AMS measurements

AMS was determined using a Sapphire Instruments SI2B device operating at 19 200 Hz and

~0.1 mT. The anisotropy measurement utilized the seven-orientation system (Borradaile & Stupavsky 1995), which includes four body-diagonal measurements, improving precision over the more commonly used orientations confined to coordinate axes and their symmetry planes (e.g. Girdler 1961). Instrument control and real-time data processing were performed using the SI2B01 software package developed by G. J. Borradaile. A complete AMS determination and analysis requires less than four minutes per core. The low-field AMS was determined on 360 cores from 121 specimens of the local sampling campaign and 730 cores from 298 specimens of the regional sampling campaign of Lagroix and Borradaile (2000).

AARM: Anisotropy of anhysteretic remanent magnetization

AARM was determined using the same seven-axis anisotropy scheme as for AMS measurements. The specimen is fully demagnetized and then the seven differently oriented ARMs are applied and measured, in a sequence such that each ARM is inclined at 45° or 35.3° to the previous one. For many rock types, this effectively cleans the ARM acquired in each preceding treatment. This tested technique greatly reduces the measurement time because 3-axis AF cleaning between each ARM application is no longer necessary (Werner & Borradaile 1996). However, the success of this short-cut must be verified with each new measurement campaign and each new lithology. ARMs were imposed with a Sapphire Instruments three-axis Alternating Field (AF) demagnetizer outfitted with a supplementary d.c. coil applying a bias field of 0.05 mT. The AF decayed from a peak field of 80 or 100 mT to zero while the d.c. bias field was turned on from 60 mT to zero. The imposed ARM was measured in a JR5a automatic spinner magnetometer (sensitivity 0.03 mA/m). Instrument control, measurement and simultaneous data-reductions were performed using the SPIN01 software package developed by G. J. Borradaile. Complete AARM determination and analysis requires 18 minutes per core. We have only included AARM results from regional-scale sampling suite in this study. Of the original sample ($n = 1170$, Lagroix & Borradaile 2000), 201 cores were rejected for AARM determination. The criteria for accepting or rejecting the AARM results occur during measurement; results were rejected if intensities were <1 mA/m when measured in orientation 1 of the AARM scheme or if the AMS ellipsoid for the sample had a negative κ . In the present

study, for AARM we selected 254 cores from 229 specimens from the original suite published by Lagroix and Borradaile (2000).

Sampling strategy

The first level of sampling focused on structurally and lithologically homogenous sub-areas $\leq 30 \text{ km}^2$ that were densely sampled (Fig. 6). They include the Polis Rift Margins, Polis Basin, Galataria, Omodhos-Pakhna, Lefkara and Lymbia, designated sub-areas I–VI, respectively, yielding $n = 360$ cores from $N = 121$ sites. These areas include formations from the Lefkara up to the Athalassa Formation. The homogeneity of fabrics in these sub-areas justified the larger scale interpretation from the next level of sampling.

The second level of sampling was a diluted regional-scale campaign. The limestone specimens covered a wide age-range of the sedimentary cover, from the Lefkara Formation up to the Nicosia Formation (Lagroix & Borradaile 2000). Of the original sample suite (cores $n = 1170$, sites $N = 434$), a sub-sample ($n = 730$, $N = 298$) was analysed in five regional domains of similar tectonic style and trend (Fig. 7), each with an area of $\sim 400 \text{ km}^2$.

All hand specimens were oriented in the field and three to six cores (25 mm in diameter and 22 mm high) were drilled in the laboratory from each specimen, restored to geographic coordinates.

Localized sampling: Polis Rift Region (sub-areas I, II, III)

Non-standardized AMS in this, the Polis Rift region, differs from the other areas (Fig. 6a). From the faulted margins they exhibit an $S > L$ fabric as shown by the elongate confidence cones for k_{max} and k_{int} , and a small k_{min} confidence cone (Fig. 6a, sub-area I). The AMS axes are symmetrically compatible with stress directions of the last 5 Ma verified from fault orientations and from seismic data (Payne & Robertson 2000; Borradaile & Hamilton 2004).

In the basin, non-standardized data permit straightforward fabric interpretations (Fig. 6a, sub-area II). These younger strata have $S > L$ depositional fabric as shown by the elongate confidence cones for k_{max} and k_{int} in the foliation and a tight, near-vertical k_{min} confidence cone. The magnetic foliation is parallel to the bedding. k_{max} and k_{int} lie within the bedding plane and k_{max} is possibly a flow-alignment, since it is

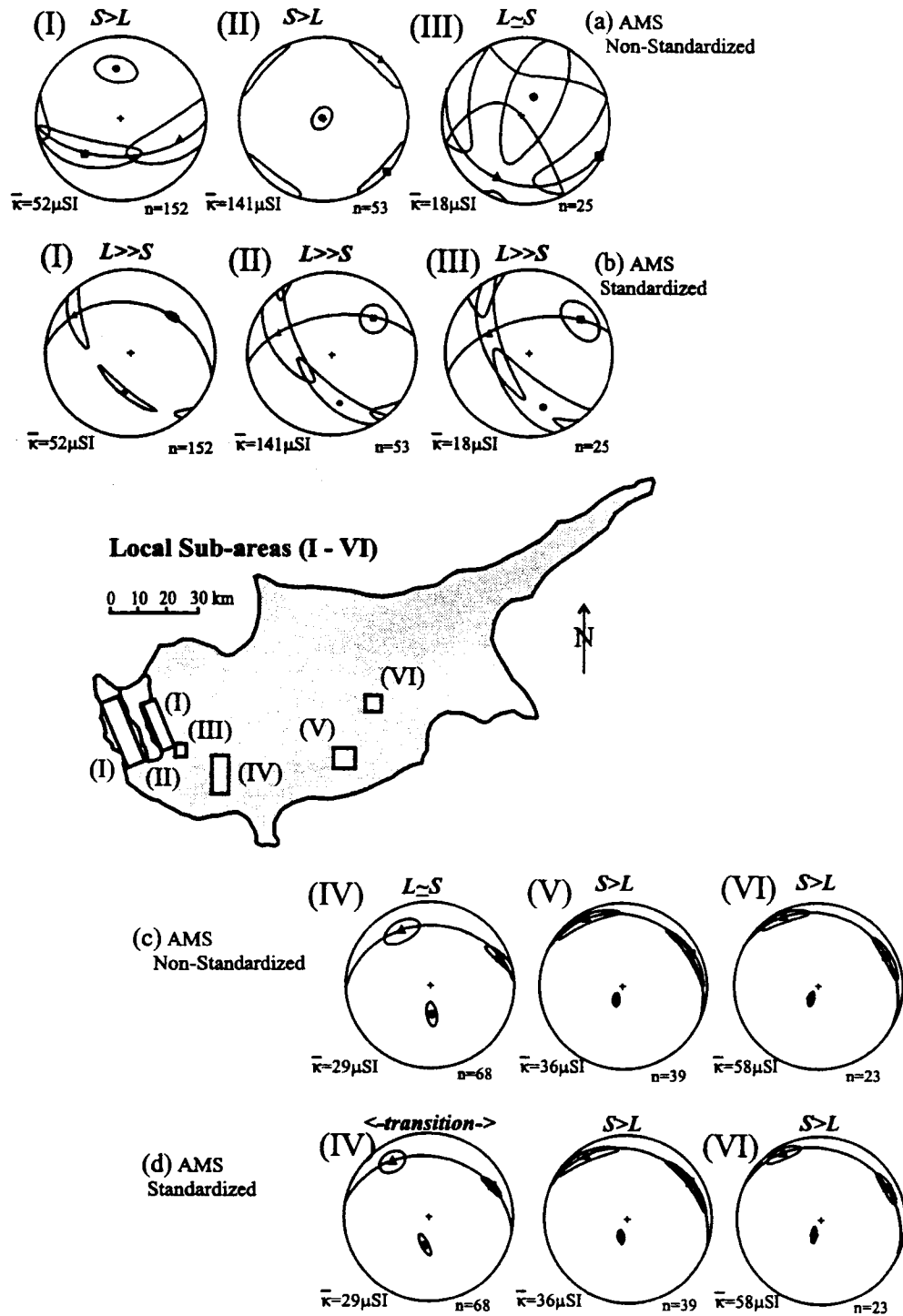


Fig. 6. Sub-areas of Cyprus (I–VI) and their magnetic fabrics as discriminated by standardization (specimen tensors standardized dividing by each specimen's κ). (a) Non-standardized AMS orientation distributions are biased by anomalously oriented subfabrics, especially with anomalously high- κ . (b) Standardized AMS fabrics usually suppress the contribution of specimens with anomalous orientations.

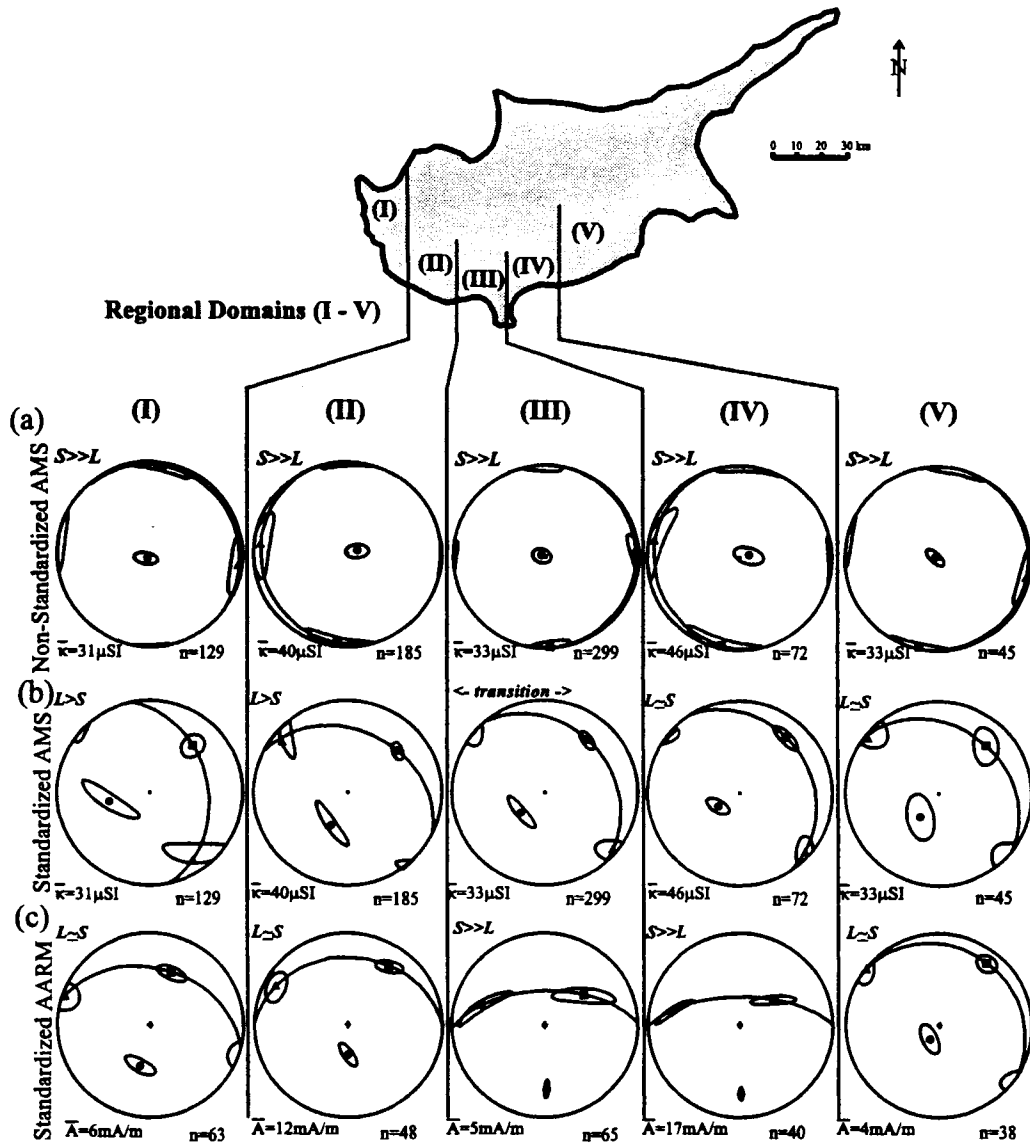


Fig. 7. Regional domains of Cyprus (I-V) and their magnetic fabrics. (a) Non-standardized AMS. (b) Standardized AMS. (c) Standardized AARM. AARM isolates the magnetite subfabric and when standardized, the contribution of anomalously oriented specimens is subdued.

parallel to the rift axis (*cf.* Sagnotti *et al.* 1994). Raw, non-standardized AMS data demonstrates the effects of higher susceptibility specimens in which depositional-controlled AMS fabrics dominate.

In the Galataria region, non-standardized specimens exhibit an $L \approx S$ fabric, which appears nearly isotropic from its large, overlapping confidence cones (Fig. 6a, sub-area III). Nevertheless, the mean tensor axes are similar

to the other two preceding localities in this region.

How are these low- κ samples affected by relatively high- κ specimens? Standardizing the specimen AMS to κ reveals similar susceptibility directions overall but demonstrate progressively different confidence cone shapes (Fig. 6b, sub-areas I-III). All show $L \gg S$ ODs. The progressive increase in size of the confidence cones from west to east may be due to the smaller

sample sizes ($n = 152$ to $n = 25$). The NE-trending $k_{\max}L \gg S$ fabric agrees with the crustal tension axis required for the paired normal faults defining the Polis Graben and the normal fault zone defining the Pegia fault system (Payne & Robertson 2000). The $L \gg S$ fabric of the AMS data are also symmetrically compatible with the current tectonic stress regime deduced from earthquake data (Borradaile & Hamilton 2004, Fig. 2).

Localized sampling: Southern slopes of Troodos (sub-areas IV, V, VI)

The three easternmost detailed sub-areas show little difference between standardized and non-standardized samples (Fig. 6, sub-areas IV–VI). The Omodhos-Pakhna sub-area (IV) displays an $L \approx S$ OD fabric with a shallow northward dipping ‘foliation’. The Lefkara and Lymbia (sub-areas V and VI) localities display an $S > L$ OD fabric as shown by the elongate confidence cones k_{\max} and k_{int} and a tight k_{\min} confidence cone with a shallow NNE dipping foliation. These OD fabrics in the eastern localities represent a dominant sedimentary fabric with some secondary tectonic control. However, all are compatible with a south-directed movement (southerly *vergence*) within the limestone cover.

Regional-scale AMS

Non-standardized AMS data of the five regional-scale domains (Fig. 7a, sub-areas I–V) exhibit similar ODs for all areas. All five groups exhibit an $S \gg L$ fabric as shown by the elongate confidence cones for k_{\max} and k_{int} and a tight k_{\min} confidence cone near vertical (Borradaile 2001). This OD is similar to the results exhibited in the density-contoured data in Lagroix and Borradaile (2000). The S -component of the fabric is bedding controlled and k_{\max} is kinematically compatible with N–S extension, parallel to the aligned phyllosilicates caused by the stretching of the sedimentary cover (Lagroix & Borradaile 2000).

But how are these low susceptibility samples affected by relatively high susceptibility samples that may be considered as statistical outliers? Standardizing the specimen ellipsoids to κ . AMS data of the five regional-scale groups (Fig. 7b) reveals similar overall AMS axes but different confidence-cone shapes and, thus, different fabric ODs in the L – S range. These differences change progressively from $L \approx S$ in the east to

$L > S$ in the west. This corresponds to the increasing tectonic strain from east to west, inferred from earthquake data (Ben-Avraham *et al.* 1988; Arvidsson *et al.* 1998; Papazachos & Papaioannou 1999; Borradaile & Hamilton 2004) and overall structural trends (Robertson 2000; Borradaile & Hamilton 2004). In contrast, raw data (non-standardized) are weighted by higher susceptibility depositional subfabrics rather than the weak tectonic ones compatible with supra-subduction SW-directed shortening (Lagroix & Borradaile 2000).

Regional scale AARM

Only standardized data are presented for AARM to avoid the spurious effects due to the large variance in remanence intensity. Domains I, II & V (Fig. 7c) show similar overall AARM axes to standardized AMS (Fig. 7b). This verifies the important contribution of magnetite to some AMS fabrics. They show an $L \approx S$ OD similar to the easternmost standardized AMS, perhaps due to a near-uniaxial shape of magnetite, which when arranged in a weak planar fabric has a strong A_{\min} zone-axis girdle. Thus, the N–S extensional trend (seen in the AMS) is less effectively expressed but the fabric axes are kinematically compatible with movement directed toward the SW (or subduction to the NE). AARM fabrics for the other two sub-areas (Fig. 7c, sub-areas III & IV) exhibit $S \gg L$ fabrics; AARM axes indicate a more southerly directed movement. The AARM fabric may be a composite of the stylonitic cleavage incompletely overprinting the bedding fabric (Lagroix & Borradaile 2000).

Conclusions

- Low- κ rocks such as limestone commonly show unstable AMS axes due to sub-equal competition from subfabrics of diamagnetic calcite and paramagnetic clays, with traces of magnetite. These subfabrics commonly represent weak tectonic overprints on depositional fabrics, as in the limestone cover of the Troodos terrane.
- Standardizing AMS principal values of specimens to their κ equalizes the contributions of subfabrics/specimens with different κ in the overall sample mean tensor. Thus, one sub-fabric may be emphasized or neutralized. This has a similar effect to determining a PSD magnetite subfabric with AARM (Lagroix & Borradaile 2000), although it is not a satisfactory substitute for AARM.

- Applying this methodology to the limestone cover of Troodos, standardized and non-standardized AMS reveal depositional fabrics, neotectonic fabrics associated with NNE subduction, neotectonic fabrics associated with rifting and composite fabrics from feeble stylolitic foliation imprints on bedding.
- Standardizing AMS data for petrofabrically homogenous sub-areas or domains reveals fabrics compatible with neotectonic stress trajectories in post-Paleogene strata. This is well shown in the Polis basin (<5 Ma) and the Galataria sub-area (43–62 Ma) (Figure 6b, sub-areas II and III respectively), which show nearly identical fabrics in rocks with 40 million years age difference, but relatively little geographic difference.
- Examination of AMS tensors for sub-areas, and even larger regions may reveal tectonically significant axes, related to stress rather than finite strain. The orientation distribution of the mean tensor has an ellipsoid shape that may reveal the relative magnitudes of the principal stresses.

The Natural Sciences and Engineering Research Council of Canada (NSERC) funded G. J. Borradaile for this work at the Lakehead University Rock Magnetism Laboratory. The authors were greatly assisted and encouraged by the Geological Survey Department of Cyprus, in particular through G. Petrides and I. Panayides. D. Czeck, P. Kelso and M. Jackson provided helpful, constructive reviews and editorial comments.

References

- ARVIDSSON, R., BEN-AVRAHAM, Z., EKSTRÖM, G. & WDWINSKI, S. 1998. Plate tectonic framework for the October 9, 1996 Cyprus earthquake. *Geophysical Research Letters*, **25**, 2241–2244.
- BEN-AVRAHAM, Z., KEMPLER, D. & GINZBURG, A. 1988. Plate convergence in the Cyprean Arc. *Tectonophysics*, **146**, 231–240.
- BORRADAILE, G. J. 1988. Magnetic susceptibility, petrofabrics and strain. *Tectonophysics*, **156**, 1–20.
- BORRADAILE, G. J. 2001. Magnetic fabrics and petrofabrics: their orientation-distributions and anisotropies. *Journal of Structural Geology*, **23**, 1581–1596.
- BORRADAILE, G. J. 2003. *Statistics of Earth Science Data: Their Distribution in Space, Time, and Orientation*. Springer-Verlag, New York, 293–326.
- BORRADAILE, G. J. & HAMILTON, T. 2003. Limestones distinguished by magnetic hysteresis in three-dimensional projections. *Geophysical Research Letters*, **30**(18), 1973. 10.1029/2003GL017892.
- BORRADAILE, G. J. & HAMILTON, T. D. 2004. Magnetic fabrics may proxy as neotectonic stress trajectories, Polis Rift, Cyprus. *Tectonics*, **23**, TC1001. doi:10.1029/2002TC001434.
- BORRADAILE, G. J. & HENRY, B. 1997. Tectonic applications of magnetic susceptibility and its anisotropy. *Earth Science Reviews*, **42**, 49–93.
- BORRADAILE, G. J. & KEHLENBECK, M. M. 1996. Possible cryptic tectono-magnetic fabrics in 'post-tectonic' granitoid plutons of the Canadian Shield. *Earth and Planetary Science Letters*, **137**, 119–127.
- BORRADAILE, G. J. & LAGROIX, F. 2000. Magnetic characterization of limestones using a new hysteresis projection. *Geophysics Journal International*, **141**, 213–226.
- BORRADAILE, G. J. & LAGROIX, F. 2001. Magnetic fabrics reveal Upper Mantle flow fabrics in the Troodos Ophiolite Complex, Cyprus. *Journal of Structural Geology*, **23**, 1299–1317.
- BORRADAILE, G. J. & STUPAVSKY, M. 1995. Anisotropy of magnetic susceptibility: measurement schemes. *Geophysical Research Letters*, **15**, 1957–1960.
- BORRADAILE, G. J., TELLA, S. & MCARTHUR, J. 1989. Magnetic fabric as a kinematic indicator of faults: a test case. *Annals de Tectonicae*, **3**, 3–11.
- CIFELLI, F., ROSSETTI, F., MATTEI, M., HIRT, A. M., FUNICIELLO, R. & TORTORICI, L. 2004. An AMS, structural and paleomagnetic study of quaternary deformation in eastern Sicily. *Journal of Structural Geology*, **26**, 29–46.
- DE WALL, H., BESTMANN, M. & ULLEMEYER, K. 2000. Anisotropy of susceptibility in Thassos marble: a comparison between measured and modelled data. *Journal of Structural Geology*, **22**, 1761–1771.
- FLINN, D. 1965. On the symmetry principle and the deformation ellipsoid. *Geology Magazine*, **102**, 36–45.
- GIRDLER, R. W. 1961. The measurement and computation of anisotropy of magnetic susceptibility in rocks. *Geophysical Journal of the Royal Astronomical Society*, **5**, 34–44.
- HENRY, B. 1983. Interprétation quantitative de l'anisotropie de susceptibilité magnétique: *Tectonophysics*, **91**, 165–177.
- HENRY, B. 1989. Magnetic fabric and orientation tensor of minerals in rocks: *Tectonophysics*, **165**, 21–28.
- HENRY, B. 1990. Magnetic fabric implications for the relationships between deformation mode and grain growth in slates from the Borrowdale Volcanic Group in the English Lake District. *Tectonophysics*, **178**, 225–230.
- HENRY, B. 1992. Modelling the relationship between magnetic fabric and strain in polymineralic rocks. *Physics of Earth and Planetary Science International*, **70**, 214–218.
- HELLWEGE, K. H. & HELLWEGE, M. 1967. Magnetic properties, II. In: VON BORCHERS, H., HAUSEN, H., HELLWEGE, K. H., SCHAFER, K. & SCHMIDT, E. (eds). *Landolt-Bornstein: Zahlenwerte und Funktionen aus Physik, Chemie, Astronomie, Geophysik und Technik, II/10*. Springer, Berlin, 143.
- HUNT, C. P., MOSKOWITZ, B. M. & BANERJEE, S. K. 1995. Magnetic properties of rocks and minerals. In: AHRENS, T. J. (ed.) *A Handbook of Physical Constants*. American Geophysical Union, Washington DC, 189–204.

- IHMLÉ, P. F., HIRT, A. M., LOWRIE, W. & DIETRICH, D. 1989. Inverse fabric in deformed limestones of the Morcles Nappe, Switzerland. *Geophysical Research Letters*, **16**, 1383–1386.
- JACKSON, M. J., CRADDOCK, J. P., BALLARD, M., VAN DER VOO, R. & MCCABE, C. 1989. An hysteretic remanent magnetic anisotropy and calcite strains in Devonian carbonates from the Appalachian Plateau, New York. *Tectonophysics*, **161**, 43–53.
- JELÍNEK, V. 1978. Statistical processing of anisotropy of magnetic susceptibility measured on groups of specimens. *Studia Geophysica et Geodetica*, **22**, 50–62.
- JELÍNEK, V. 1981. Characterization of the magnetic fabric of rocks. *Tectonophysics*, **79**, 63–67.
- KISSEL, C., BARRIER, E., LAJ, C. & LEE, T. Q. 1986. Magnetic fabric in 'undeformed' marine clays from compressional zones. *Tectonics*, **5**, 769–781.
- KRISHNAN, K. S., GUHA, B. C. & BANERJEE, S. K. 1933. Investigation on magneto-crystallic action, Part I. Diamagnetics. *Philosophical Transactions of the Royal Society London, Serial A*, **231**, 235–262.
- LAGROIX, F. & BORRADAILE, G. J. 2000. Tectonics of the Circum-Troodos Sedimentary Cover of Cyprus, from Rock Magnetic and Structural Observations. *Journal of Structural Geology*, **22**, 453–469.
- LORD, A. R., PANAYIDES, I., URQUHART, E. & XENOPHONTOS, C. 2000. A biochronostratigraphical framework for the Late Cretaceous–Recent circum-Troodos sedimentary sequence, Cyprus. In: PANAYIDES, I., XENOPHONTOS, C. & MALPAS, J. (eds) *Proceedings of the Third International Conference on the Geology of the Eastern Mediterranean*. Cyprus Geological Survey Department, Nicosia, Cyprus, 289–297.
- MALPAS, J., MOORES, E., PANAYIOTOU, A. & XENOPHONTOS, C. (eds). *Ophiolites: Oceanic Crustal Analogues. Proceedings of the Symposium 'Troodos 1987'*. Cyprus Geological Survey Department, Nicosia, Cyprus.
- MATTEI, M., SPERANZA, F., ARGENTIERI, A., ROSETTI, F., SAGNOTTI, L. & FUNICIELLO, R. 1999. Extensional tectonics in the Amantea Basin (Calabria, Italy): a comparison between structural and magnetic anisotropy data. *Tectonophysics*, **307**, 33–49.
- NAKAMURA, N. & BORRADAILE, G. J. 2001. Strain, anisotropy of anhysteretic remanence, and anisotropy of magnetic susceptibility in a slaty tuff. *Physics of Earth and Planetary Science International*, **125**, 85–93.
- OWENS, W. H. & BAMFORD, D. 1976. Magnetic, seismic, and other anisotropic properties of rock fabrics. *Philosophical Transactions of the Royal Society London*, **A283**, 55–68.
- OWENS, W. H. & RUTTER, E. H. 1978. The development of magnetic susceptibility anisotropy through crystallographic preferred orientation in a calcite rock. *Physics of the Earth and Planetary Interiors*, **16**, 215–222.
- PAPAZACHOS, B. C. & PAPAIOANNOU, Ch. A. 1999. Lithospheric boundaries and plate motions in the Cyprus area. *Tectonophysics*, **308**, 193–204.
- PAYNE, A. S. & ROBERTSON, A. H. F. 2000. Structural evolution and regional significance of the Polis graben system, western Cyprus. In: PANAYIDES, I., XENOPHONTOS, C. & MALPAS, J. (eds) *Proceedings of the Third International Conference on the Geology of the Eastern Mediterranean*. Cyprus Geological Survey Department, Nicosia, Cyprus, 45–59.
- REILINGER, R. E., MCCLUSKY, S. C., ORAL, M. B., KING, R. W., TOKSOZ, M. N., BARKA, A. A., KINIK, I., LENK, O. & SANLI, I. 1997. Global position system measurements of present-day crustal movements in the Arabia–Africa–Eurasia plate collision zone. *Journal of Geophysical Research*, **102**, 9983–9999.
- ROBERTSON, A. H. F. 1990. Tectonic evolution of Cyprus. In: MALPAS, J., MOORES, E., PANAYIOTOU, A. & XENOPHONTOS, C. (eds) *Ophiolites: Oceanic Crustal Analogues. Proceedings of the Symposium 'Troodos 1987'*. Cyprus Geological Survey Department, Nicosia, Cyprus, 235–250.
- ROBERTSON, A. H. F. 2000. Tectonic evolution of Cyprus in its Easternmost Mediterranean setting. In: PANAYIDES, I., XENOPHONTOS, C. & MALPAS, J. (eds) *Proceedings of the Third International Conference on the Geology of the Eastern Mediterranean*. Cyprus Geological Survey Department, Nicosia, Cyprus, 11–44.
- ROBERTSON, A. H. F., KIDD, R. B., IVANOV, M. K., LIMONOV, A. F., WOODSIDE, J. M., GALINDO-ZALDICAR, J. & NIETO, L. 1995. Eratosthenes seamount: collisional processes in the easternmost Mediterranean in relation to the Plio-Quaternary uplift of southern Cyprus. *Terra Nova*, **7**, 254–264.
- ROCHETTE, P. 1988. Inverse magnetic fabric in carbonate-bearing rocks. *Earth & Planetary Science Letters*, **90**, 229–237.
- ROCHETTE, P., JACKSON, M. J. & AUBOURG, C. 1992. Rock magnetism and the interpretation of anisotropy of magnetic susceptibility. *Reviews of Geophysics*, **30**, 209–226.
- SAGNOTTI, L., FACENNA, C., FUNICIELLO, R. & MATTEI, M. 1994. Magnetic fabric and structural setting of Plio-Pleistocene clayey units in an extensional regime: the Tyrrhenian margin of central Italy. *Journal of Structural Geology*, **16**, 1243–1257.
- SAGNOTTI, L., SPERANZA, F., WINKLER, W., MATTEI, M. & FUNICIELLO, R. 1998. Magnetic fabric of clay sediments from the external northern Apennines (Italy). *Physics of the Earth and Planetary Interiors*, **105**, 73–93.
- TARLING, D. H. & HROUDA, F. 1993. *The Magnetic Anisotropy of Rocks*. Chapman and Hall, London.
- VOIGHT, W. & KINOSHITA, S. 1907. Bestimmung absoluter Werte von Magnetisierungszahlen, insbesondere für Kristalle. *Annals of Physics*, **24**, 492–514.
- WERNER, T. & BORRADAILE, G. J. 1996. Paleoremanence dispersal across a transpressed Archaean Terrain: Deflection by anisotropy or by late compression? *Journal of Geophysical Research*, **101**, 5531–554.